

申 报	系列：教师系列教 学科研并重型
	专业：生物学
	职称：副教授

业绩成果材料

（申报人的业绩成果材料包括论文、科研项目、获奖以及其他成果等）

单 位（二级单位） 生命科学学院

姓 名 衡月芹

材料核对人：

单位盖章：

核对时间：

华南农业大学制

目 录（模板）

一、科研项目

- 1.主持：关于国家自然面上项目“生物钟调控水稻花时的分子机制研究”的立项通知（合同）及有关佐证材料1
- 2.主持：关于国家自然青年项目“拟南芥 COP1 SUPPRESSOR 6 调控光形态建成的分子机理研究”的立项通知（合同）及有关佐证材料10
- 3.主持：关于广东省自然科学基金面上项目“茉莉酸信号通路关键因子 OsMYB21 调控水稻抽穗期的分子机制” 的立项通知（合同）及有关佐证材料16
- 4.主参：农业生物育种重大项目“适宜复合种植的玉米新品种设计与培育”立项通知（合同）及有关佐证材料27

二、论文、著作等

- 1.检索证明60
- 2.以第一作者发表本专业论文情况
 - 2.1. Natural variation in *OsMYB8* confers diurnal floret opening time divergence between *indica* and *japonica* subspecies63
 - 2.2. A jasmonate-mediated regulatory network modulates diurnal floret opening time in rice79
 - 2.3. Targeted manipulation of grain shape genes effectively improves outcrossing rate and hybrid seed production in rice99
 - 2.4. BBX4, a phyB-interacting and modulated regulator, directly interacts with PIF3 to fine tune red lightmediated photomorphogenesis.....110
 - 2.5. B-Box Containing Proteins BBX30 and BBX31, Acting Downstream of HY5, Negatively Regulate Photomorphogenesis in

Arabidopsis	125
2.6. COP1 SUPPRESSOR 6 represses the PIF4 and PIF5 action to promote light-inhibited hypocotyl growth	143
2.7. A Positive Feedback Loop of BBX11–BBX21–HY5 Promotes Photomorphogenic Development in Arabidopsis	158

三、其他业绩

1. 指导学生学科竞赛

1. 1. 第九届全国大学生生命科学竞赛（科学探究奖）广东省赛区三等奖“水稻茉莉酸抑制因子 JAZs 响应高温调控花时的分子机理与应用研究”.....	170
---	-----

【佐证材料切记与目录页所列页码对应，不要用图片格式的材料进行打印。】



项目批准号	32470375
申请代码	C0207
归口管理部门	
依托单位代码	51064208A0499-0932



国家自然科学基金 资助项目计划书 (预算制项目)

资助类别：面上项目

亚类说明：

附注说明：

项目名称：生物钟调控水稻花时的分子机制研究

直接费用：50万元 执行年限：2025.01-2028.12

负责人：衡月芹 BRID：07183.00.17195

通讯地址：广东省广州市天河区五山路483号

邮政编码：510642 电 话：020-85282180

电子邮件：hengyueqin@scau.edu.cn

依托单位：华南农业大学

联系人：唐家林 电 话：020-85280070

填表日期：2024年08月26日

国家自然科学基金委员会制



国家自然科学基金资助项目计划书填报说明 （预算制项目）

- 一、项目负责人收到《国家自然科学基金资助项目批准通知》（以下简称《批准通知》）后，请认真阅读本填报说明，参照国家自然科学基金相关项目管理办​​法和新修订的《国家自然科学基金资助项目资金管理办法》（以下简称《资金管理办法》，请查阅国家自然科学基金委员会官方网站首页“政策法规”栏目），按《批准通知》的要求认真填写和提交《国家自然科学基金资助项目计划书》（以下简称《计划书》）。
- 二、填写《计划书》时要科学严谨、实事求是、表述清晰、准确。《计划书》经国家自然科学基金委员会相关项目管理部门审核批准后，将作为项目研究计划执行、检查和验收的依据。
- 三、《计划书》各部分填写要求如下：
 - （一）简表：由系统自动生成。
 - （二）摘要及关键词：各类获资助项目都应当填写中、英文摘要及关键词。
 - （三）项目组主要成员：计划书中列出姓名的项目组主要成员由系统自动生成，与申请书原成员保持一致，不可随意调整。如果《批准通知》所附“项目评审意见及修改意见表”中“修改意见”栏目有调整项目组成员相关要求的，待项目开始执行后，按照项目成员变更程序另行办理。
 - （四）资金预算表：根据批准的项目资助额度，按规定调整项目预算，并按照《国家自然科学基金项目计划书预算表编制说明》填报资金预算表和预算说明书。
 - （五）正文：
 1. 面上项目、地区科学基金项目：如果《批准通知》所附“项目评审意见及修改意见表”中“修改意见”栏目没有修改要求的，只需选择“研究内容和研究目标按照申请书执行”即可；如果《批准通知》中上述栏目明确要求调整研究期限或研究内容等的，须选择“根据研究方案修改意见更改”并填报相关修改内容。
 2. 重点项目、重点国际（地区）合作研究项目、重大项目、重大研究计划重点支持项目、重大研究计划集成项目、国家重大科研仪器研制项目、联合基金项目、原创探索计划项目：须选择“根据研究方案修改意见更改”，根据《批准通知》的要求填写研究（研制）内容，不得自行降低、更改研究目标（或仪器研制的技术性能与主要技术指标、验收技术指标等）或缩减研究（研制）内容。此外，还要突出以下几点：
 - （1）研究的难点和在实施过程中可能遇到的问题（或仪器研制风险），拟采用的研究（研制）方案和技术路线；
 - （2）项目主要参与者分工，合作研究单位（如有）之间的关系与分工，重大项目还需说明课题之间的关联；
 - （3）详细的年度研究（研制）计划。
 3. 创新研究群体项目：须选择“根据研究方案修改意见更改”，按下列提纲撰写：



- (1) 研究方向；
 - (2) 结合国内外研究现状，说明研究工作的学术思想和科学意义（限两个页面）；
 - (3) 研究内容、研究方案及预期目标（限两个页面）；
 - (4) 年度研究计划；
 - (5) 研究队伍的组成情况。
4. 基础科学中心项目：须选择“根据研究方案修改意见更改”，根据《批准通知》的要求和现场考察专家组的意见和建议，进一步完善并细化研究计划，按下列提纲撰写：
- (1) 五年拟开展的研究工作（包括主要研究方向、关键科学问题与研究内容）；
 - (2) 研究方案（包括骨干成员之间的分工及合作方式、学科交叉融合研究计划等）；
 - (3) 年度研究计划；
 - (4) 五年预期目标和可能取得的重大突破等；
 - (5) 研究队伍的组成情况。
5. 数学天元基金项目：天元前沿重点专项项目和数学与其他学科交叉联合资助项目，参照重点项目的方式进行选择和填写；其他类型项目，参照面上项目的方式进行选择和填写。
6. 对于其他类型项目，参照面上项目的方式进行选择和填写。



简表

项目负责人信息	姓 名	衡月芹	性 别	女	出生年月	1988年05月	民 族	汉族
	学 位	博士			职称	副教授		
	是否在站博士后	否			电子邮件	hengyueqin@scau.edu.cn		
	电 话	020-85282180			个人网页			
	工 作 单 位	华南农业大学						
	所 在 院 系 所	生命科学学院						
依托单位信息	名 称	华南农业大学					代码	51064208A0499
	联 系 人	唐家林			电子邮件	kyc.jhk@scau.edu.cn		
	电 话	020-85280070			网站地址	http://kjc.scau.edu.cn/		
合作单位信息	单 位 名 称							
项目基本信息	项 目 名 称	生物钟调控水稻花时的分子机制研究						
	资 助 类 别	面上项目				亚 类 说 明		
	附 注 说 明							
	申 请 代 码	C0207:植物生殖与发育						
	基 地 类 别							
	执 行 年 限	2025.01-2028.12						
	直 接 费 用	50万元						



项目摘要

中文摘要:

水稻每日开花时间 (Diurnal floret opening time, DFOT) 是影响授粉率和产量的重要农艺性状, 父母本花时相遇也是杂交制种产量的关键决定因素之一。然而, 由于水稻花时性状难以调查, 其调控机理研究还很匮乏。水稻花时受到生物钟的调控, 但是其具体的调控机制尚不明确。浆片是控制水稻花时性状的关键器官, 而茉莉酸 (JA) 是调控水稻花时最重要内源激素。本项目前期研究发现浆片中JA水平呈现节律性的变化, 并发现花时受到水稻生物钟核心组分OsCCA1基因的调控。本项目将综合利用分子遗传学、生物化学以及生物信息学等手段验证OsCCA1通过直接调控JA合成酶OsAOC基因的表达, 介导浆片中JA水平的节律性变化, 从而调控水稻花时节律性的工作模型。预期结果将揭示生物钟调控水稻花时的分子网络, 为水稻花时的精准改良提供理论依据和新基因资源。

Abstract:

Diurnal floret opening time (DFOT) is a pivotal agronomic trait that influences fertilization and grain yield in rice, and the synchronization of DFOT between parental lines is also a critical determinat of hybrid seed production. However, the regulatory mechanisms of DFOT are still poorly understood, due to the difficulty in precise phenotyping. Rice DFOT can be regulated by the circadian clock, yet its underlying mechanism remains elusive. It has been known that lodicule is a key organ controlling the rice DFOT trait, and jasmonic acid (JA) is the most important endogenous hormone involved in this process. In this study, we found that JA levels in lodicules exhibited diurnal rhythm fluctuations, and OsCCA1, a core clock component in rice, could regulate rice DFOT. In this project, we will utilize a combination of genetics, biochemistry, and bioinformatics approaches to substantiate the working model in which OsCCA1 mediates rhythmic fluctuations of endogenous JA levels in lodicules by orchestrating the expression of the JA biosynthesis enzyme OsAOC, thereby regulating the rice floret opening time. The expected results will reveal the molecular network of the circadian clock in regulating rice DFOT, and provide theoretical basis and new gene resources for precise improvement of rice DFOT in agricultural production.

关键词(用分号分开): 水稻; 激素调控; 花时; 生物钟; 转录调控

Keywords(用分号分开): Rice; Hormone regulation; Diurnal floret opening time; Circadian clock; Transcriptional regulation



项目组主要成员

编号	姓名	出生年月	性别	职称	学位	单位名称	电话	证件号码	项目分工	每年工作 时间 (月)
1	衡月芹	1988.05	女	副教授	博士	华南农业大学	020-85282180	320826198805163068	项目负责人	10
2	李俊娇	1988.05	女	无	博士	华南农业大学		14030219880503044X	负责分子生物学实验	5
3	丁文燕	1996.09	女	助理实验师	硕士	华南农业大学		440223199609032749	组学数据分析	5
总人数				高级	中级	初级		博士后	博士生	硕士生
9				1		1		1	3	3



国家自然科学基金预算制项目预算表

项目批准号： 32470375

项目负责人：衡月芹

金额单位：万元

序号	科目名称	金额
1	一、科学基金资助项目直接费用合计	50.0000
2	1、设备费	0.0000
3	其中：设备购置费	0.0000
4	2、业务费	40.4000
5	3、劳务费	9.6000
6	二、其他来源资金	0.0000
7	三、合计	50.0000

注：请按照项目研究实际需要合理填写各科目预算金额。

国家自然科学基金资助项目批准通知

（预算制项目）

衡月芹 先生/女士：

根据《国家自然科学基金条例》、相关项目管理办法规定和专家评审意见，国家自然科学基金委员会（以下简称自然科学基金委）决定资助您申请的项目。项目批准号：32470375，项目名称：生物钟调控水稻花时的分子机制研究，直接费用：50.00万元，项目起止年月：2025年01月至2028年12月，有关项目的评审意见及修改意见附后。

请您尽快登录科学基金网络信息系统（<https://grants.nsfc.gov.cn>），**认真阅读《国家自然科学基金资助项目计划书填报说明》并按要求填写《国家自然科学基金资助项目计划书》（以下简称计划书）**。对于有修改意见的项目，请您按修改意见及时调整计划书相关内容；如您对修改意见有异议，须在电子版计划书报送截止日期前向相关科学处提出。

请您将电子版计划书通过科学基金网络信息系统（<https://grants.nsfc.gov.cn>）提交，由依托单位审核后提交至自然科学基金委。自然科学基金委审核未通过者，将退回的电子版计划书修改后再行提交；审核通过者，打印纸质版计划书（一式两份，双面打印）并在项目负责人承诺栏签字，由依托单位科研、财务管理等部门审核、签章并在承诺栏加盖依托单位公章，且将申请书纸质签字盖章页订在其中一份计划书之后，一并报送至自然科学基金委项目材料接收工作组。纸质版计划书应当保证与审核通过的电子版计划书内容一致。**自然科学基金委将对申请书纸质签字盖章页进行审核，对存在问题的，允许依托单位进行一次修改或补齐。**

向自然科学基金委提交电子版计划书、报送纸质版计划书并补交申请书纸质签字盖章页截止时间节点如下：

1. **2024年9月9日16点**：提交电子版计划书的截止时间；
2. **2024年9月16日16点**：提交修改后电子版计划书的截止时间；
3. **2024年9月23日**：报送纸质版计划书（一式两份，其中一份包含申请书纸质签字盖章页）的截止时间。
4. **2024年10月8日**：报送修改后的申请书纸质签字盖章页的截止时间。

请按照以上规定及时提交电子版计划书，并报送纸质版计划书和申请书纸质签字盖章页，逾期不报计划书或申请书纸质签字盖章页且未说明理由的，视为自动放弃接受资助；未按要求修改或逾期提交申请书纸质签字盖章页者，将视情况给予暂缓拨付经费等处理。

附件：项目评审意见及修改意见表

国家自然科学基金委员会
2024年8月23日



项目批准号	32100199
申请代码	C0203
归口管理部门	
依托单位代码	51805512A0094-1234



国家自然科学基金 资助项目计划书 (包干制项目)

资助类别：青年科学基金项目

亚类说明：

附注说明：

项目名称：拟南芥COP1 SUPPRESSOR 6调控光形态建成的的分子机理研究

资助经费：30万元 执行年限：2022.01-2024.12

负责人：衡月芹

通讯地址：深圳市南山区学苑大道1088号

邮政编码：518055 电 话：0755-88018462

电子邮件：hengyq@mail.sustech.edu.cn

依托单位：南方科技大学

联系人：詹凯莹 电 话：0755-88010322

填表日期：2021年10月20日

国家自然科学基金委员会制

Version: 1.001.519



国家自然科学基金资助项目计划书填报说明 (包干制项目)

- 一、项目负责人收到《国家自然科学基金资助项目批准通知》（以下简称《批准通知》）后，请认真阅读本填报说明，参照国家自然科学基金相关项目管理办​​法和新修订的《国家自然科学基金资助项目资金管理办法》（以下简称《资金管理办法》，请查阅国家自然科学基金委员会官方网站首页“政策法规”栏目），按《批准通知》的要求认真填写和提交《国家自然科学基金资助项目计划书》（以下简称《计划书》）。
- 二、填写《计划书》时要科学严谨、实事求是、表述清晰、准确。《计划书》经国家自然科学基金委员会相关项目管理部门审核批准后，将作为项目研究计划执行、检查和验收的依据。
- 三、《计划书》各部分填写要求如下：
 - （一）简表：由系统自动生成。
 - （二）摘要及关键词：各类获资助项目都应当填写中、英文摘要及关键词。
 - （三）正文：
 1. 青年科学基金项目：如果《批准通知》所附“项目评审意见及修改意见表”中“修改意见”栏目没有修改要求的，只需选择“研究内容和研究目标按照申请书执行”即可；如果《批准通知》中上述栏目明确要求调整研究期限或研究内容等的，须选择“根据研究方案修改意见更改”并填报相关修改内容。
 2. 国家杰出青年科学基金和优秀青年科学基金，按下列提纲撰写：
 - （1）研究方向；
 - （2）结合国内外研究现状，说明研究工作的学术思想和科学意义（限两个页面）；
 - （3）研究内容、研究方案及预期目标（限两个页面）；
 - （4）年度研究计划；
- 四、资助经费相关要求：
 1. 资助经费批准时不再区分直接费用和间接费用。
 2. 项目负责人在提交计划书时需签署承诺书，承诺尊重科研规律，弘扬科学家精神，遵守科研伦理道德和作风学风诚信要求，认真开展科学研究工作；承诺项目经费全部用于与本项目研究工作相关的支出，不得用于与本项目研究无关的支出。
 3. 项目负责人提交计划书时，无需编制项目预算。项目资金由项目负责人自主决定使用，按照《资金管理办法》第九条规定的开支范围列支。有关管理费用的补助支出，由依托单位根据实际管理需要，在充分征求项目负责人意见基础上合理确定。绩效支出由项目负责人根据实际科研需要和相关薪酬标准自主确定，依托单位按照工资制度进行管理。其余用途经费无额度限制，由项目负责人根据实际需要自主决定使用。
 4. 项目结题时，项目负责人根据实际使用情况编制项目经费决算，经依托单位财



务、科研管理部门审核后，报自然科学基金委。依托单位应当在单位内部公开非涉密项目立项、主要研究人员、资金使用（重点是间接费用、外拨资金、结余资金使用等）、决算、大型仪器设备购置以及项目研究成果等情况，接受内部监督。

5. 自然科学基金委结合项目管理，对经费使用情况和依托单位管理情况定期开展抽查。



简表

项目负责人信息	姓 名	衡月芹	性 别	女	出生年月	1988年05月	民 族	汉族
	学 位	博士			职称	副研究员		
	是否在站博士后	否			电子邮件	hengyq@mail.sustech.edu.cn		
	电 话	0755-88018462			个人网页			
	工 作 单 位	南方科技大学						
	所 在 院 系 所	生物系						
依托单位信息	名 称	南方科技大学					代码	51805512A0094
	联 系 人	詹凯莹			电子邮件	zhanky@sustech.edu.cn		
	电 话	0755-88010322			网站地址	www.sustech.edu.cn		
合作单位信息	单 位 名 称							
项目基本信息	项 目 名 称	拟南芥COP1 SUPPRESSOR 6调控光形态建成的的分子机理研究						
	资 助 类 别	青年科学基金项目				亚 类 说 明		
	附 注 说 明							
	申 请 代 码	C0203:植物光合与固氮						
	基 地 类 别							
	执 行 年 限	2022. 01-2024. 12						
	资 助 经 费	30万元						



项目摘要

中文摘要:

C2H2型锌指蛋白是植物中最大的转录因子家族之一，在植物生长发育、逆境响应等生物学过程中发挥重要作用，然而C2H2型锌指蛋白是否参与调控植物光形态建成尚不清楚。本项目前期通过正向遗传筛选到CSU6（COP1 SUPPRESSOR 6），其编码一个C2H2型锌指蛋白。研究发现CSU6是光形态建成的正调控因子，光促进CSU6的蛋白积累，同时发现CSU6具有转录抑制活性，且与光信号负调控子PIF4/PIF5互作。本项目拟通过解析光信号调控CSU6蛋白稳定性的分子机制，CSU6与PIF4/PIF5互作的生理生化机制以及对下游靶基因的调控机制，构建CSU6调控光形态建成的分子信号通路，阐明CSU6发挥功能的分子机理。该项研究将揭示CSU6在光形态建成中的重要作用，完善对C2H2型锌指蛋白这一重要转录因子家族的生物学功能及作用机理的认识，并为光生物学研究服务于作物分子育种提供分子生物学信息和基因资源。

Abstract:

C2H2-type zinc finger proteins are one of the largest transcription factor families in plants. Recent studies have revealed that C2H2-type zinc finger proteins play vital roles in plant development and stress responses, but their involvement in photomorphogenesis, as well as regulatory mechanisms, remain largely unclear. In this study, we used forward genetic screen to identify COP1 SUPPRESSOR 6 (CSU6), which encodes a C2H2 zinc finger protein. We found that CSU6 is a positive regulator of photomorphogenesis, and CSU6 protein accumulation is induced by light. Further studies showed that CSU6 protein has transcriptional repression activity and interacts with PIF4 and PIF5, which are key negative regulators in light signaling. In this project, we propose to determine how CSU6 protein accumulation is regulated by light and reveal the physiological and biochemical mechanism underlying the interactions between CSU6 and PIF4/PIF5, we also propose to investigate the transcriptional regulation mechanism of CSU6 to downstream genes, thereby further elucidating the molecular mechanism of CSU6 in seedling photomorphogenesis. Our studies will reveal the essential role of CSU6 in light signaling, which can expand the knowledge of C2H2 zinc finger family in plants, and also provide molecular biological information and gene resources for integrating photobiology studies into crop molecular breeding.

关键词(用分号分开): 光形态建成; 光信号转导; C2H2锌指蛋白; 蛋白互作; 转录调控

Keywords(用分号分开): Photomorphogenesis; Light signal transduction; C2H2 zinc finger protein; Protein-protein interaction; Transcriptional regulation

证明

南方科技大学生命科学学院衡月芹承担科研情况：

主持国家自然科学基金青年项目“拟南芥 COP1 SUPPRESSOR 6 调控光形态建成的分子机理研究”（项目批准号：32100199）；立项时间：2021.10.12；资助经费：30 万；执行年限：2022.01-2024.12。

特此证明！



受理编号: c23140500001861

项目编号: 2023A1515012564

文件编号: 粤基金字(2023)2号

广东省基础与应用基础研究基金项目 任务书

项目名称: 茉莉酸信号通路关键因子OsMYB21调控水稻抽穗期的分子机制

项目类别: 广东省自然科学基金-面上项目

项目起止时间: 2023-01-01 至 2025-12-31

管理单位(甲方): 广东省基础与应用基础研究基金委员会

依托单位(乙方): 华南农业大学

通讯地址: 广东省广州市天河区五山路483号

邮政编码: 510642

单位电话: 020-85283435

项目负责人: 衡月芹

联系电话: 13699766834



(广东科技微信公众号)



(查看任务书信息)



(受理纸质材料二维码)

广东省基础与应用基础研究
基金委员会
二〇二〇年制

填写说明

一、项目任务书内容原则上要求与申报书相关内容保持一致，不得无故修改。

二、项目承担单位通过广东省科技业务管理阳光政务平台下载项目任务书，按要求完成签名盖章后扫描上传到广东省科技业务管理阳光政务平台。

三、签名盖章说明。请分别在单位工作分工及经费分配情况页、人员信息页、签约各方页等地方按要求签字或盖章，签章不合规或错漏将不予受理。其中，人员信息页要求所有参与人员本人亲笔签名，代签或印章无效，漏签将不予受理。

四、本任务书自签字并加盖公章之日起生效，各方均应负本任务书的法律责任，不应受机构、人事变动影响。

五、根据《广东省科学技术厅广东省财政厅关于深入推进省基础与应用基础研究基金项目经费使用“负面清单+包干制”改革试点工作的通知》（粤科规范字[2022]2号），2022年度及以后立项资助的全部省基金项目（包括省自然科学基金、省市联合基金、省企联合基金项目等）均适用“负面清单+包干制”，项目提交申请书和任务书时无需编制费用明细科目预算。

一、主要研究内容和要达到的目标

本项目拟通过遗传和生物化学等手段，解析OsMYB21对已知光周期途径开花因子OsCOL4的调控机制以及与OsMYC2互作的遗传和生化机制，阐明OsMYB21发挥功能的分子机理，构建茉莉酸信号途径调控水稻抽穗的分子网络。具体研究内容如下：

（1）分析OsMYB21促进OsCOL4表达的调控机制

我们前期通过对OsMYB21的功能缺失突变体和过表达转基因植株进行表型分析，发现OsMYB21负调控水稻抽穗，并且对其调控机制进行了初步的探索。利用DAP-seq技术，在全基因组水平上鉴定到OsMYB21转录因子富集最显著的两个结合位点（CCWAA和ACCWAMC），并通过酵母单杂交（Y1H）实验证实了OsMYB21直接结合到已知的水稻开花抑制因子OsCOL4启动子区域，qRT-PCR分析发现OsMYB21可以促进OsCOL4的表达。本项目将进一步利用凝胶迁移电泳（EMSA）和染色质免疫共沉淀（ChIP-qPCR）验证OsMYB21能否结合到OsCOL4的启动子区域，以及利用水稻原生质体瞬时表达Dual-LUC实验检测OsMYB21对OsCOL4的转录调控作用。此外，利用qRT-PCR技术验证OsMYB21对OsCOL4下游关键开花基因Ehd1、Hd3a和RFT1的调控作用。

（2）OsMYB21与OsCOL4的遗传关系分析

构建osmyb21 oscol4双突变体以及osmyb21背景过表达OsCOL4株系，分析osmyb21 oscol4双突变体、OsCOL4-OE/osmyb21在自然长短日照条件下的抽穗期表型差异，从而明确OsMYB21与OsCOL4之间在调控水稻抽穗过程中的遗传上下游关系。

（3）OsMYB21与OsMYC2的互作关系分析

MYC2是茉莉酸信号通路的核心转录因子，调控茉莉酸介导的诸多生物学过程。已有报道发现MYC2在水稻中的同源基因OsMYC2的RNAi突变体表现早抽穗的表型，但是具体的机制仍不清楚（Bao et al., 2019）。我们前期通过酵母双杂交（Y2H）、双分子荧光互补（BiFC）实验发现OsMYC2与OsMYB21存在相互作用。本项目将进一步利用体外共沉淀（Pull-down）和体内共沉淀（Co-IP）实验进一步明确OsMYC2与OsMYB21的互作关系。

（4）OsMYB21与OsMYC2互作的生化机制与遗传分析

本项目拟通过凝胶迁移电泳（EMSA）和水稻原生质体瞬时表达Dual-LUC实验分析OsMYC2是否影响OsMYB21对下游靶基因OsCOL4的转录活性，以及进一步利用qRT-PCR检测OsMYC2突变体植株中OsMYB21下游调控基因的表达水平变化，验证OsMYC2与OsMYB21的互作对OsMYB21下游基因的转录调控作用。另外，构建osmyc2 osmyb21双突变体，分析比较双突变体及单突变体在长日与短日照下的抽穗期表型差异，从而明确OsMYC2与OsMYB21之间在水稻开花通路中的遗传上下游关系。

本项目的研究目标：

- （1）解析OsMYB21与OsCOL4之间的功能关系，揭示OsMYB21在水稻抽穗期途径中的位置。
- （2）解析OsMYB21与OsMYC2互作的遗传和生化机制。
- （3）阐明OsMYB21参与调控水稻抽穗的作用机理，建立OsMYB21介导的茉莉酸途径和光周期途径协同调控水稻开花的分子遗传网络。

二、项目预期获得的科研成果及形式

论文及专著情况	国家统计源刊物以上刊物 发表论文（篇）		1		科技报告（篇）		1	
	其中被SCI/EI/ISTP收录 论文数（篇）		1		培养人才（人）			
	专著（册）				引进人才（人）			
专利情况(项)	发明专利		实用新型专利		外观设计专利		国外专利	
	申请	授权	申请	授权	申请	授权	申请	授权

三、项目进度和阶段目标

(一) 项目起止时间： 2023-01-01 至 2025-12-31		
(二) 项目实施进度及阶段主要目标：		
开始日期	结束日期	主要工作内容
2023-01-01	2023-12-31	<p>(1) 将osmyb21单突变体与oscol4单突变体杂交，筛选鉴定杂交后代，获得osmyb21 oscol4双突变体纯合植株。</p> <p>(2) 构建0sCOL4-0E/osmyb21转基因纯合株系。</p> <p>(3) 将osmyb21单突变体与osmyc2-RNAi突变体杂交，筛选鉴定杂交后代，获得osmyb21 osmyc2双突变体纯合植株。</p> <p>(4) qRT-PCR分析ZH11、osmyb21以及0sMYB21过表达株系中0sCOL4下游开花基因Ehd1、Hd3a和RFT1等基因的表达情况。</p> <p>(5) 凝胶迁移电泳（EMSA）实验验证0sMYB21是否结合0sCOL4的启动子区。</p> <p>(6) 染色质免疫共沉淀（ChIP-qPCR）验证0sMYB21在水稻体内是否与0sCOL4的启动子区结合。</p>
2024-01-01	2024-12-31	<p>(1) Pull-down实验验证0sMYB21与0sMYC2是否相互作用。</p> <p>(2) 体内共沉淀（Co-IP）实验验证0sMYB21与0sMYC2是否在体内相互作用。</p> <p>(3) 凝胶迁移电泳（EMSA）实验分析0sMYC2蛋白是否影响0sMYB21对下游靶基因0sCOL4启动子的结合能力。</p> <p>(4) 水稻原生质体瞬时转化Dual-LUC实验分析0sMYC2是否影响0sMYB21对下游靶基因0sCOL4的转录调控。</p> <p>(5) 参加作物学相关会议一次。</p>
2025-01-01	2025-12-31	<p>(1) 利用qRT-PCR 检测ZH11及osmyc2突变体中0sMYB21下游调控基因的表达情况。</p> <p>(2) 将ZH11、osmyb21 oscol4双突变体、0sCOL4/osmyb2转基因株系以及对应的osmyb21和oscol4单突变体在自然长日照条件下进行种植，统计每份材料之间的抽穗期差异，分析0sMYB21与0sCOL4之间的遗传关系。</p> <p>(3) 将ZH11、osmyb21 osmyc2-RNAi双突变体以及对应的osmyb21和osmyc2-RNAi单突变体在自然长日照条件下进行种植，统计分析每份材料之间的抽穗期差异，明确0sMYB21与0sMYC2之间的遗传关系。</p> <p>(4) 对数据进行整理和分析，并进行论文的撰写和投稿。</p>

四、项目总经费及省基金委经费预算

1. 省基金委经费下达总额： （大写）壹拾万圆整；（小写 ）10万元；					
2. 省基金委经费年度下达计划：					
年度	2023 年	年	年	年	年
经费(万元)	10.00				

五、人员信息

项目负责人								
姓名	证件号码	年龄	性别	职称	学历	在项目中承担的任务	所在单位	签名
衡月芹	320826198805163068	35	女	副教授	博士研究生	项目负责人	华南农业大学	衡月芹

项目组主要成员								
姓名	证件号码	年龄	性别	职称	学历	在项目中承担的任务	所在单位	签名
苟亚军	511324199405030865	29	女	未取得	硕士研究生	负责载体构建和转基因材料的创制	华南农业大学	苟亚军
黎晓晴	440105199806245729	25	女	未取得	本科	负责分子生物学和生化实验	华南农业大学	黎晓晴
房裕东	441324199312282336	30	男	未取得	硕士研究生	负责各种遗传材料的基因型鉴定，种植与管理	华南农业大学	房裕东
李亚静	411403199508091222	28	女	未取得	硕士研究生	负责原核表达纯化蛋白及互作验证实验	华南农业大学	李亚静
朱新宇	440183199610312837	27	男	未取得	本科	负责田间抽穗期表型观察与统计	华南农业大学	朱新宇

六、工作分工及财政经费分配

承担/参与单位名称 (盖章)	工作分工	省级财政科技资金分配 (万元)
华南农业大学	本项目无其他参与单位，由华南农业大学独立完成。	10.00
	合计	10.00

七、任务书条款

第一条 甲方与乙方根据《中华人民共和国民法典》及国家有关法规和规定，按照《广东省科学技术厅关于广东省基础与应用基础研究基金（省自然科学基金、联合基金等）项目管理的实施细则（试行）》《广东省省级科技计划项目验收结题工作规程（试行）》等规定，为顺利完成（2023）年茉莉酸信号通路关键因子OsMYB21调控水稻抽穗期的分子机制专项项目（文件编号：粤基金字〔2023〕2号）经协商一致，特订立本任务书，作为甲乙双方在项目实施管理过程中共同遵守的依据。

第二条 甲方的权利义务：

1. 按任务书规定进行经费核拨的有关工作协调。
2. 根据甲方需要，在不影响乙方工作的前提下，定期或不定期对乙方项目的实施情况和经费使用情况进行检查或抽查。
3. 根据《广东省科研诚信管理办法(试行)》等规定对乙方进行科技计划信用管理。

第三条 乙方的权利义务：

1. 确保落实自筹经费及有关保障条件。
2. 按任务书规定，对甲方核拨的经费实行专款专用，单独列账，并随时配合甲方进行监督检查。
3. 经费使用按照广东省级财政科研项目经费使用等有关规定进行管理。
4. 项目依托单位应制定经费使用“负面清单+包干制”内部管理制度并报甲方备案。
5. 使用财政资金采购设备、原材料等，按照《广东省实施〈中华人民共和国招标投标法〉办法》有关规定，符合招标条件的须进行招标。
6. 项目任务书任务完成后，或任务书规定的任务、指标及经费投入等提前完成的，乙方可提出验收结题申请，并按甲方要求做好项目验收结题工作。
7. 若项目发生需要终止结题的情况，乙方须提出终止结题申请，并按甲方要求做好项目终止结题工作。
8. 在每年规定时间内向甲方如实提交上年度工作情况报告，报告内容包含上年度项目进展情况、经费决算和取得的成果等。
9. 按照国家和省有关规定，提交科技报告及其他材料。
10. 利用甲方的经费获得的研究成果，项目负责人和参与者应当注明获得“广东省基础与应用基础研究基金（英文：Guangdong Basic and Applied Basic Research Foundation）（项目编号）”资助或作有关说明。
11. 乙方要恪守科学道德准则，遵守科研活动规范，践行科研诚信要求，不得抄袭、剽窃他人科研成果或者伪造、篡改研究数据、研究结论；不得购买、代写、代投论文，虚构同行评议专家及评议意见；不得违反论文署名规范，擅自标注或虚假标注获得科技计划（专项、基金等）等资助；不得弄虚作假，骗取科技计划（专项、基金等）项目、科研经费以及奖励、荣誉等；不得有其他违背科研诚信要求的行为。
12. 确保本项目开展的研究工作符合我国科技伦理管理相关规定。

第四条 在履行本任务书的过程中，如出现广东省相关政策法规重大改变等不可抗力情况，甲方有权对所核拨经费的数量和时间进行相应调整。

第五条 在履行本任务书的过程中，当事人一方发现可能导致项目整体或部分失败的情形时，应及时通知另一方，并采取适当措施减少损失，没有及时通知并采取适当措施，致使损失扩大的，应当就扩大的损失承担责任。

第六条 本项目技术成果的归属、转让和实施技术成果所产生的经济利益的分享，除双方另有约定外，按国家和广东省有关法规执行。

第七条 根据项目具体情况，经双方另行协商订立的附加条款，作为本任务书正式内容的一部分，与本任务书具有同等效力。

第八条 本任务书一式三份，各份具有同等效力。甲、乙方及项目负责人各执一份，三方签字、盖章后即生效，有效期至项目结题后一年内。各方均应负任务书的法律责任，不应受机构、人事变动的影响。

第九条 乙方必须接受甲方聘请的本项目任务书监理单位的监督和管理。监理单位按照甲方赋予的权利对本项目任务书的履行进行审核、进度调查，对项目任务书变更、经费使用情况进行监督管理及组织项目验收。

说明：1. 本任务书中，凡是当事人约定无需填写的内容，应在空白处划（/）。

2. 委托代理人签订本任务书的，应出具合法、有效的委托书。

八、本任务书签约各方

管理单位（甲方）：

广东省基础与应用基础研究基金委员会（盖章）

法定代表人（或法人代理）：

曾路

（签章）

2023 年 02 月 14 日

依托单位（乙方）：华南农业大学

（盖章）

法定代表人（或法人代理）：刘雅红

（签章）

联系人（项目主管）姓名：倪慧群

Email: kjcgxk@scau.edu.cn

电话：020-85283435 / 15920301530

开户单位名称：华南农业大学

开户银行名称：广东广州工行五山支行

开户银行帐号：3602002609000310520

2023 年 3 月 8 日

联系人（项目负责人）姓名：衡月芹

（签名）

Email: hengyueqin@163.com

电话：13699766834

2023 年 3 月 8 日

农业生物育种重大专项 课题任务书

课 题 名 称	玉米生物技术研发与种质资源创新
所 属 项 目 名 称	适宜复合种植的玉米新品种设计与培育
专 业 机 构	农业农村部科技发展中心
课题牵头承担单位	浙江大学（公章）
课 题 负 责 人	林朝阳
执 行 期 限	2024 年 1 月 至 2025 年 12 月

2024 年 1 月

填 写 说 明

- 一、任务书甲方即项目牵头承担单位，乙方即课题承担单位。
- 二、任务书通过“国家科技计划管理信息系统公共服务平台”，按照系统提示在线填写。
- 三、任务书中的单位名称，请按规范全称填写，并与单位公章一致。
- 四、任务书要求提供乙方与所有参加单位的合作协议，需对原件进行扫描后在线提交。
- 五、任务书中文字须用宋体小四号字填写。
- 六、凡不填写内容的栏目，请用“无”表示。
- 七、乙方完成任务书的在线填写，提交甲方审核确认后，用 A4 纸在线打印、签章后上传电子扫描件。
- 八、如项目下仅设一个课题，课题任务书只需填报课题基本信息表与课题预算部分。
- 九、涉密课题请在“国家科技计划管理信息系统公共服务平台”下载任务书的电子版模板，按保密要求离线填写、报送。一式八份报项目牵头承担单位签章，其中课题承担单位一份，课题负责人一份，作为项目任务书附件六份。
- 十、《项目申报书》和《项目任务书》是本任务书填报的重要依据，任务书填报不得降低考核指标，不得自行对主要研究内容作大的调整。《项目申报书》和《项目任务书》和本任务书将共同作为课题过程管理、综合绩效评价（验收）和监督评估的重要依据。

课题基本信息表

课题名称		玉米生物技术研发与种质资源创新										
课题编号		2022ZD0400501										
所属项目名称		适宜复合种植的玉米新品种设计与培育										
项目编号		2022ZD04005										
所属重大项目		农业生物新品种培育										
密级		<input checked="" type="checkbox"/> 公开 <input type="checkbox"/> 秘密 <input type="checkbox"/> 机密		单位总数		4						
课题成果技术就绪度		<div><input type="checkbox"/> 1.发现基本原理<input type="checkbox"/> 2.形成技术方案<input type="checkbox"/> 3.方案通过验证 <input type="checkbox"/> 4.形成单元并验证<input type="checkbox"/> 5.形成分系统并验证<input type="checkbox"/> 6.形成原型并验证 <input checked="" type="checkbox"/> 7.现实环境的应用验证<input type="checkbox"/> 8.用户验证认可<input type="checkbox"/> 9.得到推广应用</div>										
课题成果应用的主要国民经济行业		农业种植业										
课题的社会经济目标		一级目标 农林牧渔业发展 二级目标 农作物种植及培育										
经费预算		课题总经费根据概算批复结果核定，课题年度经费按照项目任务书约定下达。配套经费不得低于项目任务书约定要求。										
课题周期节点		起始时间		2022 年 12 月		结束时间		2025 年 12 月				
		实施周期		共 37 个月		预计中期时间点		2023 年 12 月				
课题承担单位	单位名称		浙江大学			单位法定代表人姓名		杜江峰				
	单位性质		高等学校			组织机构代码		12100000470095016Q				
	单位主管部门		教育部			隶属关系		中央				
	单位所属地区		浙江省杭州市			地市（市、自治州、盟）		西湖区				
	通信地址		浙江杭州西湖区浙江大学余杭塘路 866 号			邮政编码		310058				
	单位开户名称		浙江大学									
	开户银行（全称）		浙江省农行杭州市浙大支行紫金港支行			汇入地点		浙江 省杭州 市				
	银行账号		19042201040000014			银行机构代码		103331004223				
课题负责人	姓 名		林朝阳		性 别		<input checked="" type="checkbox"/> 男 <input type="checkbox"/> 女		出生日期		1979. 04. 12	
	证件类型		身份证		证件号码		350623197904120056					
	所在单位		浙江大学新农村发展研究院									

	最高学位	<input checked="" type="checkbox"/> 博士 <input type="checkbox"/> 硕士 <input type="checkbox"/> 学士 <input type="checkbox"/> 其他		
	职 称	<input type="checkbox"/> 正高级 <input checked="" type="checkbox"/> 副高级 <input type="checkbox"/> 中级 <input type="checkbox"/> 初级 <input type="checkbox"/> 其他		职务 无
	电子邮箱	chylin@zju.edu.cn	移动电话	13221800591
课题 联系 人	姓 名	林朝阳	电子邮箱	chylin@zju.edu.cn
	固定电话	057188982349	移动电话	13221800591
	证件类型	身份证	证件号码	350623197904120056
课题 财务 负责 人	姓 名	蒋珊珊	电子邮箱	jss200823@126.com
	固定电话	057188982349	移动电话	15888806082
	证件类型	身份证	证件号码	330522198610290622
其他 参与 单位	序号	单位名称	单位性质	组织机构代码
	1	华南农业大学	高等学校	124400004554165634
	2	杭州瑞丰生物科技有限公司	民营企业	9133011069980858X4
	3	杨凌秦丰种业股份有限公司	国有企业	91610403MAB2N7JH3A
课题参 加人数	12 人。其中：		高级职称 6 人，中级职称 6 人，初级职称 0 人，其他 0 人；	
			博士学位 9 人，硕士学位 1 人，学士学位 2 人，其他 0 人。	
课题 简介 (限 500 字以内)	玉米与大豆复合种植对玉米品种特性和除草剂耐受性提出了新的要求。课题组拟以转基因耐除草剂玉米、基因编辑玉米为基础，结合全基因组选择、多基因聚合、诱变等生物育种技术和常规育种技术，建立玉米设计育种技术体系，创制耐除草剂、耐密植、抗倒伏、边际效应强、籽粒脱水速率快的玉米新种质。本课题在转基因耐除草剂技术方面，重点创制与耐除草剂大豆具有同样特性的耐除草剂玉米；并应用基因编辑技术创制耐高密度、改变株高等性状的玉米育种材料。研发适于玉米杂草防治的一季喷一次除草剂的复合除草剂，提高杂草防治效率、降低杂草防治成本。在前期研究中，课题组已利用新型耐除草剂基因 CdP450 培育了高抗草甘膦、烟嘧磺隆、啶嘧磺隆、二甲四氯等多种除草剂的耐除草剂玉米和大豆。耐新型除草剂的玉米大豆复合种植可以为杂草防治提供更为多样化的除草剂方案，能够提高杂草防治效率，延缓抗性杂草的产生。同时，课题组还挖掘了调控玉米耐密株型、穗型、杂交优势、籽粒发育、脱水速率的关键基因，并创制了一批优秀种质资源，为本项目的顺利实施奠定了坚实基础。			

填表说明：1. 组织机构代码指企事业单位国家标准代码，单位若已三证合一请填写单位统一社会信用代码，无组织机构代码的单位填写“0000000000”；
2. 单位公章名称必须与单位名称一致；
3. 单位开户名称应与单位名称一致，如有开户名称不一致等特殊情况，必须提供证明文件。

一、课题目标及考核指标、评测方式/方法

（一）课题目标

1) 获得广谱耐除草剂的转基因玉米，并进行安全评价；2) 筛选出成本比较低，除草效果好，适宜不同玉米生态区的二元复配除草剂；3) 研究适宜复合种植使用的复合除草剂；4) 创制矮秆的转基因或基因编辑玉米，并进行安全评价；5) 聚合转基因广谱耐除草剂、矮秆性状玉米，对其进行功能效率和安全评价。

（二）考核指标

1. 2022-2025 年考核指标

1) 研发适宜复合种植的玉米生物育种技术 3 项。

评测手段/方法：行业专家评审。

2) 申报耐新型除草剂玉米转化体中间试验 100 个以上，转化体环境释放试验 35 个以上，申报生产性试验 6 个以上，最终获得生产应用安全证书 1-2 项。

评测手段/方法：受理通知书或相关批文。

3) 申请或获得发明专利和新品种权 3 件以上。

评测手段/方法：受理通知书或授权公告、证书。

2. 2024 年考核指标

1) 申报转化体环境释放试验 5 个以上，申报生产性试验 2 个；

评测手段/方法：受理通知书或相关批文。

2) 获得含有新型耐除草剂性状指纹图谱没有位点差异的自交系 20 个以上；

评测手段/方法：测试报告；

3) 申请或获得发明专利和新品种权 2 件以上。

评测手段/方法：受理通知书或授权公告、证书。

4) 研发复合种植模式除草方案 1 套。

评测手段/方法：专家现场验收。

3. 2025 年考核指标

1) 申报转化体环境释放试验 10 个以上，申报生产性试验 4 个；

评测手段/方法：受理通知书或相关批文。

2) 申请或获得发明专利和新品种权 2 件以上。

评测手段/方法：受理通知书或授权公告、证书。

3) 研发适宜复合种植的转基因玉米制种技术 1 套。

评测手段/方法：专家现场验收。

(三) 评测方式/方法

安全评价以农业农村部受理通知书或相关批文为准；新品种、专利和新品种权以受理通知书或授权公告、证书为准；自交系材料以试验报告、测试报告为准；技术方案以专家现场验收为准。

课题目标、成果与考核指标表

课题目标 ¹	成果名称	成果简述	成果类型	考核指标 ²					考核方式(方法)及评价手段 ⁴
				指标名称	立项时有指标值/状态	立项时重点国别指标值/状态	中期指标值/状态 ³	完成时指标值/状态	
针对我国西南及南方区、黄淮海区等生产上玉米品种与大豆等作物复合种植存在的耐密抗倒性差、除草难、产量优势弱, 以及东北区、黄淮海区、西北区等玉米宜机收性差、抗逆弱等问题, 综合利用现代生物育种技术与常规技术相结合建立高效玉米设计育种技术体系; 设计与培育耐密植、抗倒伏、边际效应强, 并可与大豆等作物共用相同除草剂的玉米新品种和宜机收高产玉米新品种, 实现推广应用, 提升玉米生产能力。	1: 新型耐除草剂转基因玉米	新型耐除草剂转基因玉米新品种高抗草甘膦、烟嘧磺隆、啶嘧磺隆和二甲四氯等多种除草剂。国内外目前没有相似的产品, 是原始创新的新性状。为复合种植提供高效和多样化的杂草防治方案。	<input type="checkbox"/> 新理论 <input type="checkbox"/> 新原理 <input checked="" type="checkbox"/> 新产品 <input type="checkbox"/> 新技术 <input type="checkbox"/> 新方法 <input type="checkbox"/> 关键部件 <input type="checkbox"/> 数据库 <input type="checkbox"/> 软件 <input type="checkbox"/> 平台 <input type="checkbox"/> 应用解决方案 <input type="checkbox"/> 实验装置/系统 <input type="checkbox"/> 临床指南/规范 <input type="checkbox"/> 工程工艺 <input type="checkbox"/> 标准 <input type="checkbox"/> 论文 <input checked="" type="checkbox"/> 发明专利 <input type="checkbox"/> 其他	转化体中间试验	/	/	100	100	相关部门通知书或批文
				转化体环境释放	/	/	20	35	相关部门通知书或批文
				生产性试验			/	5	相关部门通知书或批文
				安全证书	/	/	/	1-2	相关部门证书
				专利	/	/	1	1	相关部门通知书或批文
				耐受 ⁴ 倍除草剂指标	/	/	/	1	测试报告

科技报告考核指标	2: 耐密抗倒伏基因编辑玉米种质新材料	利用单倍体介导的基因编辑技术创制耐密抗倒伏性状的玉米种质新材料。	<input type="checkbox"/> 新理论 <input checked="" type="checkbox"/> 新产品 <input type="checkbox"/> 新方法 <input type="checkbox"/> 数据库 平台 案 <input type="checkbox"/> 实验装置/系统 <input type="checkbox"/> 临床指南/规范 工程工艺 <input type="checkbox"/> 论文 <input type="checkbox"/> 其他	专利	/	/	1	2	受理或 知书权 授公告
			<input type="checkbox"/> 新原理 <input type="checkbox"/> 新技术 <input type="checkbox"/> 关键部件 <input type="checkbox"/> 软件 <input type="checkbox"/> 应用解决方案 <input type="checkbox"/> 倒伏新种质	1-2	/	测试报告			
	3: 适宜复合种植生物育种技术	多种现代生物育种技术与常规育种相结合的高效玉米设计育种技术。	<input type="checkbox"/> 新理论 <input type="checkbox"/> 新产品 <input type="checkbox"/> 新方法 <input type="checkbox"/> 数据库 平台 案 <input type="checkbox"/> 实验装置/系统 <input type="checkbox"/> 临床指南/规范 工程工艺 <input type="checkbox"/> 论文 <input type="checkbox"/> 其他	技术体系	/	/	3	4	专家 评审
			<input type="checkbox"/> 新原理 <input checked="" type="checkbox"/> 新技术 <input type="checkbox"/> 关键部件 <input type="checkbox"/> 软件 <input type="checkbox"/> 应用解决方案 <input type="checkbox"/> 倒伏新种质	数量	提交时间	公开类别及 时限 ⁶			
		序号	报告类型 ⁶	数量	提交时间			公开类别及 时限 ⁶	
	1	2024 年度技术进展报告	1	2024 年 11 月	延期公开 (5 年)				
	2	2025 年度技术进展报告	1	2025 年 11 月	延期公开 (5 年)				
	3	最终科技报告	1	2025 年 11 月	延期公开 (5 年)				
其他目标与考核指标完成情况									

备注：

- 1.“**课题目标**”，应从以下方面明确描述：（1）研发主要针对什么问题和需求；（2）将要解决哪些科学问题、突破哪些核心/共性/关键技术；（3）预期成果；（4）成果将以何种方式应用在哪些领域/行业/重大工程等，并拟在科技、经济、社会、环境或国防安全等方面发挥何种的作用和影响。（5）所列主要成果原则上不超过 5 项，如有其他重要成果放在“其他”成果中表述。
- 2.“**考核指标**”，指相应成果的数量指标、技术指标、质量指标、应用指标和产业化指标等，其中，数量指标可以为论文、专利、产品等的数量，论文代表作应注重质量，不以数量作为评价标准；技术指标可以为关键技术、产品的性能参数等；质量指标可以为产品的耐震动、高低温、无故障运行时间等；应用指标可以为成果应用的对象、范围和效果等；产业化指标可以为成果产业化的数量、经济效益等。同时，对各项考核指标需填写立项时已有的指标值/状态、课题完成时要到达的指标值/状态，以及立项时重点国别指标值/状态。同时，考核指标也应包括支撑和服务其他重大科研、经济、社会发展、生态环境、科学普及需求等方面的直接和间接效益。如对国家重大工程、社会民生发展等提供了关键技术支撑，成果转让并带动了环境改善、实现了销售收入等。若某项成果属于开创性的成果，立项时已有指标值/状态可填写“无”，若某项成果在立项时已有指标值/状态难以界定，则可填写“/”。
- 3.“**中期指标**”，各重大项目根据管理特点，确定是否填写，阶段目标明确的项目课题应填写中期指标。
- 4.“**考核方式方法**”，应提出符合相关研究成果与指标的具体考核技术方法、测算方法等。
- 5.“**科技报告类型**”，包括课题综合绩效评价（验收）前撰写的全面描述研究过程和技术内容的最终科技报告、课题年度或中期检查时撰写的描述本年度研究过程和进展的年度技术进展报告以及在课题实施过程中撰写的包含科研活动细节及基础数据的专题科技报告（如实验报告、试验报告、调研报告、技术考察报告、设计报告、测试报告等）。其中，每个课题在综合绩效评价（验收）前应撰写一份最终科技报告；研究期限超过 2 年（含 2 年）的项目，应根据管理要求，每年撰写一份年度技术进展报告；每个课题可根据研究内容、期限和经费强度，撰写数量不等的专题科技报告。科技报告应按国家标准规定的格式撰写。
- 6.“**公开类别及时限**”，公开课题科技报告分为公开或延期公开，内容需要发表论文、申请专利、出版专著或涉及技术诀窍的，可标注为“延期公开”。需要发表论文的，延期公开时限原则上在 2 年（含 2 年）以内；需要申请专利、出版专著的，延期公开时限原则上在 3 年（含 3 年）以内；涉及技术诀窍的，延期公开时限原则上在 5 年（含 5 年）以内。涉密课题科技报告按照有关规定管理。

二、课题研究成果、研究方法及技术路线

（一）课题的主要研究内容

拟解决的关键科学问题、关键技术问题，针对这些问题拟开展的主要研究内容，限1000字以内。

1. 2022-2025 年研究内容

1) 获得耐草甘膦、啶嘧磺隆、烟嘧磺隆和二甲四氯的转基因玉米与其他性状的转基因性状叠加的材料，鉴定性状叠加材料的耐除草剂能力，并且测定其对产量、抗病性等其他农艺性状的影响。同时将这个叠加转基因性状导入到各育种单位的玉米骨干自交系中，并且通过 SNP 标记加快回交转育的速度。2) 利用草甘膦、啶嘧磺隆、烟嘧磺隆和二甲四氯等除草剂原料配制复合除草剂，并且在大田中测试这些复合除草剂的杀草效果。特别重视这些复合除草剂的大田有效控草的时间长短、杀草活性以及是否具有增效作用。筛选出成本比较低、除草效果好的至少二种二元复配除草剂。3) 设计新的耐除草剂基因遗传转化载体，通过大规模遗传转化获得耐除草剂转化体，并且分析和鉴定转化体。选择优良转化体，开展转基因玉米材料的安全评价工作，申请安全证书。重点研发耐多种除草剂的转基因玉米，特别是同时包含专利过期耐除草剂基因和新型耐除草剂基因的转基因玉米。此外，利用基因编辑技术，获得一批不同程度降低株高的基因编辑育种材料，重点测定这些材料的抗倒伏能力和耐高密度能力。

2. 2024 年研究内容

1) 开展复合耐除草剂性状的回交转育，综合应用分子标记辅助育种和单倍体技术获得和优良骨干自交系指纹图谱没有位点差异的新型耐除草剂自交系；

2) 将复合耐除草剂性状转育到人工雄性不育系中；

3) 综合评价新型复配除草剂在玉米大豆复合种植和轮作中的杂草防治效率和除草剂残留风险；

4) 挖掘耐PPO 抑制剂类的新抗除草剂基因，研发新一代耐除草剂转基因玉米，筛选优良转化体并开展安全评价；

5) 综合应用基因编辑和转基因技术创制矮秆新种质，聚合矮秆、高产和耐除草剂性状，综合评价矮秆高产玉米的抗倒伏和耐密能力。

3. 2025 年研究内容

- 1) 开展多性状转基因玉米复合种植示范种植，展示新型耐除草剂玉米与新型耐除草剂大豆XP-2、耐草甘膦大豆和常规大豆的除草剂一体化除草；
- 2) 在不同生态区开展玉米高效杂草防治新技术，评估新型复配除草剂对小麦、大豆和水稻等后茬作物的药害风险；
- 3) 综合应用分子标记辅助育种和单倍体技术将广谱耐除草剂、矮秆和高产性状等性状进行聚合并转入到优良自交系；
- 4) 开展矮秆耐除草剂复合性状转基因玉米的区域试验，筛选耐密、抗倒伏和高产的优良自交系和组合；
- 5) 开展适宜复合种植转基因玉米雄性不育制种技术的研究和示范；
- 6) 开展耐PPO 抑制剂类除草剂转基因玉米的性状聚合、回交转育和安全评价。

（二）课题采取的研究方法

针对课题研究拟解决的问题，拟采用的方法、原理、机理、算法、模型等，限 1000 字以内。

本课题拟采用的方法是：1) 利用转基因方法获得抗除草剂玉米，特别是在抗草甘膦和草铵膦基础上，进一步培育抗啶嘧磺隆、二甲四氯、烟嘧磺隆等除草剂的转基因玉米性状；2) 利用转基因技术、基因编辑技术研发改良玉米抗倒伏、耐高密度等方面的性状；3) 利用分子标记技术，加快回交转育和多性状叠加速度。

1) 利用转基因技术创制多抗除草剂转基因玉米新品种。在玉米中过表达多抗除草剂基因*CdP450*，同时聚合抗草甘膦基因*cp4 epsps*、抗草铵膦基因*pat*，创制可同时高抗草甘膦、草铵膦、2,4-D、二甲四氯、啶嘧磺隆、烟嘧磺隆等除草剂的转基因玉米。将*CdP450*基因与其他已经广泛使用的抗除草剂基因聚合使用，创制得到的抗广谱除草剂的转基因玉米新种质。

2) 挖掘抗倒伏、耐密植、边际效应强的基因编辑或转基因玉米新品种。前期研究发现了玉米*phyB*、*phyC*、*PIFs*、*SPL12*、*SPL28*、*YUC2/4* 等基因具有调控玉米株高、穗位高、叶夹角、根系夹角的功能，而对其他农艺性状没有明显负面影响。利用转基因或基因编辑将相关基因通过遗传转化方法导入到玉米中，适当降低玉米转化体的株高，创制具有抗倒伏、耐密植、边际效应强等性状的转基因玉米新品种。

3) 玉米大豆复合种植一体化除草技术。项目团队成员前期研究已经将*CdP450* 基因导入大豆中, 获得了高抗草甘膦、烟嘧磺隆、啶嘧磺隆、二甲四氯等多种除草剂的抗广谱除草剂转基因大豆。在玉米中采用相同技术, 创制得到可与大豆共用的耐广谱除草剂、抗倒伏、耐密植、边际效应强的转基因玉米, 提高杂草防治效率和耕地利用效率, 实现玉米大豆一体化复合种植。

4) 基因组学与转录组学分析。对抗性杂草狗牙根进行基因组学和转录组学分析, 筛选并克隆获得潜在的抗除草剂基因*CdP450*; 对矮秆玉米进行基因组学和转录组学分析, 克隆并验证了与玉米株高和叶夹角密切相关的*ZmSPL12*、*ZmSPL28* 等基因。

5) 基因编辑技术改良植物性状。CRISPR-Cas9 技术是成熟的基因编辑方法, 可以精确实现玉米基因组中特定基因的编辑。对候选的靶标基因进行突变、敲除或修改, 鉴定经基因编辑的玉米的表现性状, 验证候选基因的功能。

6) 分子标记辅助育种。利用分子标记与目标性状基因紧密连锁的特点, 通过分析目标基因紧密连锁的分子标记的基因型, 借助分子标记对目标性状基因型进行选择, 能够缩短育种年限、提高育种效率, 克服常规育种方法中的困难。

三、主要创新点(可选填)

围绕基础前沿、共性关键技术或应用示范等层面, 简述课题的主要创新点。具体内容应包括该项创新的基本形态及其前沿性、时效性等, 并说明是否具备方法、理论和知识产权特征。每项创新点的描述限 500 字以内。

1、创新点 1: 本课题利用杭州瑞丰挖掘的多抗除草剂 *CdP450* 基因, 聚合抗草甘膦基因 *cp4 epsps*、抗草铵膦基因 *pat*, 创制可同时高抗草甘膦、草铵膦、2,4-D、二甲四氯、啶嘧磺隆、烟嘧磺隆的转基因玉米。这是目前国际上耐除草剂种类最多的转基因玉米材料。课题组拥有抗除草剂 *CdP450* 基因在美国、巴西和加拿大的专利权, 覆盖南美和北美主要玉米大豆种植区域。

2、创新点 2: 本课题创制的耐除草剂玉米与课题参加单位杭州瑞丰利用相同技术开发转基因大豆配套种植, 可使用相同的多种除草剂, 为玉米大豆带状复合种植体系提供更多种类的可使用的除草剂。目前市场上的技术主要是草甘膦解决方案, 而国际上的经验是草甘膦抗性杂草在推广耐草甘膦大豆和玉米以后迅速发生的发展。美国目前已经有超过 30 种杂草出现了抗草甘膦的能力。

3、创新点3：本课题利用华南农大王海洋团队挖掘的抗倒伏、耐密基因 *SPL28*，创制抗倒伏、耐密的转基因玉米，该创新技术处于国际领先水平。同时本课题还利用基因编辑技术，调控玉米赤霉素合成，为创制耐密、抗倒伏玉米新品种提供底层技术支撑。

四、预期经济社会效益

课题的科学、技术、产业预期指标及科学价值、社会、经济、生态效益。限 500 字以内。

玉米大豆带状复合种植模式是当前全国重点推广的一项农业增产增效技术，是对传统间作套种模式的创新和发展，可实现在保证玉米基本不减产的情况下，增收一季大豆，对提高复种指数和土地产出率、扩大大豆生产、实现玉米大豆双丰收意义重大。本课题将创制转基因耐除草剂玉米新种质，并与常规育种技术相结合，研究建立高效玉米设计育种技术体系，从而设计和创制多基因聚合的耐除草剂、耐密植、抗倒伏、边际效应强、籽粒脱水快的玉米育种新材料，促进与大豆等作物复合种植创新模式的推进，创造更高科学价值、社会、经济、生态效益。

课题研发的新型耐除草剂转基因玉米使用了具有自主知识产权的耐除草剂基因，对草甘膦、啶嘧磺隆、烟嘧磺隆、2,4-D 和二甲四氯等多种除草剂有高度耐受性，极大扩展了玉米的除草谱，从而为农民提供一个高效、广谱、低成本的杂草防治方案。且这些耐除草剂性状可同时应用于大豆，使玉米与大豆共用相同除草剂，最大限度提高了复合种植模式的除草效率。

推动新型杂草防治方案，科学价值显著。草害是长期制约我国农作物生产的一个重要因素，我国每年因草害造成农作物产量的损失为1000万吨左右。除草剂的使用，为减少杂草而提高农作物产量提供了重要保障。转基因耐除草剂玉米、大豆在国外得到了广泛的应用，极大地简化了杂草防治方法，降低了杂草防治成本。此外，利用除草剂防治杂草也更加有利于推广免耕技术，减少土壤和肥料的流失。本课题研发的新型耐除草剂转基因玉米使用了具有自主知识产权的耐除草剂基因，对草甘膦、啶嘧磺隆、烟嘧磺隆、2,4-D 和二甲四氯等多种除草剂有高度耐受性，极大扩展了玉米的除草谱，从而为农民提供一个高效、广谱、低成本的杂草防治方案。且这些耐除草剂性状可同时应用于大豆，使玉米与大豆共用相同除草剂，最大限度提高了复合种植模式的除草效率。

五、课题年度计划

按每 6 个月制定形成课题的计划进度，应将课题的考核指标分解落实到年度计划中。

1、2024 年 1 月—2024 年 6 月

任务：挖掘耐PPO 抑制剂类新耐除草剂基因，创制矮秆、高产、抗倒伏和耐新型除草剂玉米；开展转基因性状回交转育；创制耐密植、抗倒伏、边际效应强等多基因聚合育种新材料。

考核指标：获得环境释放批文5 个以上，申报生产性试验1 个，获得含有新型耐除草剂性状指纹图谱位点没有差异的自交系10 个以上。

成果形式：农业农村部受理通知书或相关批文，科技报告、鉴定报告或专家鉴定意见等。

2、2024 年 7 月—2024 年 12 月

任务：获得耐PPO 抑制剂类新耐除草剂转基因玉米，对新创制的转基因和基因编辑材料进行安全评价，开展适宜玉米大豆复合种植一体化的复合除草剂配方和除草方案研究，规模化开展玉米大豆复合种植的一体化除草试验；开展耐密植、抗倒伏、边际效应强等多基因聚合育种新材料创制与鉴定。

考核指标：申报生产性试验1 个，获得含有新型耐除草剂性状指纹图谱没有位点差异的自交系10 个以上，集成适宜复合种植新品种配套栽培技术1 套，申请或获得发明专利和新品种权2件以上。

成果形式：受理通知书或相关批文，鉴定报告或专家鉴定意见。

3、2025 年 1 月—2025 年 6 月

任务：开展多性状转基因玉米复合种植示范种植，聚合广谱耐除草剂、矮秆和高产性状并开展回交转育，开展适宜复合种植转基因玉米雄性不育制种技术的研究和示范。

考核指标：申请转化体环境释放试验5 个以上，申报生产性试验2 个以上。

成果形式：农业农村部受理通知书或相关批文，鉴定报告或专家鉴定意见。

4、2025 年 7 月—2025 年 12 月

任务：开展新型耐除草剂玉米与新型耐除草剂大豆XP-2、耐草甘膦大豆和常规大豆的

除草剂一体化除草，聚合广谱耐除草剂、矮秆和高产性状并开展回交转育，完成安全评价。开展适宜复合种植转基因玉米雄性不育制种技术的研究和示范。

考核指标：申请转化体环境释放试验5 个以上，申报生产性试验2 个以上，申请或获得发明专利或新品种权2件以上。

成果形式：农业农村部受理通知书或相关批文，鉴定报告或专家鉴定意见。

六、课题组织实施机制及保障措施

1、课题的内部组织管理方式、协调机制等，限 500 字以内。

本课题由浙江大学牵头，华南农业大学、杭州瑞丰生物科技有限公司和秦丰种业参与。

（1）课题实行主持单位负责和主持人负责制，课题主持单位负责课题组织协调工作，根据项目要求的整体框架，组织制定课题实施方案和检查监督，协调并处理课题执行过程中出现的有关问题。课题承担单位严格按照课题联合实施协议书要求，执行并落实项目规定的课题各项任务，根据责权利相结合的基本原则进行综合管理，并接受有关管理部门的管理和监督。

（2）加强课题内资源共享和交流。建立课题技术实施小组，进行种质创新，育种关键技术攻关，新品种联合测试。

（3）在课题实施过程中严格把控关键节点，落实年度工作落实会、中期田间考察交流，课题年度总结汇报和学术交流汇报制度。加强与项目主持单位的联系，及时向项目主持单位汇报研究进展。

（4）规范经费开支，加强财务管理。课题承担单位指定财务部门专人进行资金管理。

2、课题实施的相关政策，已有的组织、技术基础，支撑保障条件，限 500 字以内。

本课题主持单位为浙江大学，具有组织申报和承担国家重点研发计划、国家自然科学基金等项目的经验，在课题任务分解与完成、财务管理与专款专用落实上均积累了丰富的经验。

课题参加单位华南农业大学在十三五期间参与国家重点研发计划“七大农作物育种”重点专项。十四五期间，承担“玉米高产优质性状形成的分子调控网络及其协同改良机

制”国家重点研发项目。在现代玉米耐密遗传育种改良规律和分子育种指纹鉴定、玉米避荫反应分子调控机理和玉米耐密株型调控基因克隆方面做出了国际领先的研究成果。

课题参加单位杭州瑞丰生物科技有限公司是国内生物育种头部企业，研发了一系列具有自主知识产权的基因和转化体，已经获得多个转基因作物生产应用安全证书。

在项目的统筹下，将严格遵照国家制定的各项法律法规政策，保障课题能够高效实施，通过课题定期的交流规范课题管理，在坚持自主创新的同时，加强参与单位之间的合作交流，为课题的技术创新和推广应用提供有效保障。

3、对实现项目总目标的支撑作用，及与项目内其他课题的协同机制，限 500 字以内。

本课题由具有基因挖掘、转化体创制、安全评价、分子检测经验的浙江大学、杭州瑞丰、华南农业大学和秦丰种业承担。主要应用各自团队已经挖掘的新基因、新性状，集成应用转基因、基因编辑、全基因组选择和多基因聚合等生物育种技术建立高效玉米设计育种技术体系，创制新型广谱耐除草剂、耐密、抗倒伏、籽粒脱水快等新育种材料。并对获得的新育种材料进行分子鉴定、遗传稳定性分析、环境安全、食品营养安全和功能性状评价。建立分子精准鉴定和快速检测技术，为性状转育提供技术支撑。本课题将为课题 2-5 提供创新型种质和现代生物技术育种相关的技术支撑。课题组还将深入研究玉米大豆复合种植一体化除草技术，研发适于玉米杂草防治的一季喷一次除草剂的复合除草剂，提高杂草防治效果、降低杂草防治成本。本课题为实现项目的总目标提供了优质种质，也和大豆复合种植项目有很好的协同性，项目完成后能够为我国大豆玉米复合种植提供适宜的品种和丰富的杂草防治方案。

按照重大项目整体部署，项目实施过程中产生的新种质、新品系以及新品种等，在横向支撑平台体系中开展基因型鉴定、测试测定以及验证评价，实现标准化数据汇集。鉴定、测试、验证评价结果作为后续考核验收依据。

4、生物安全管理与科普宣传。

课题需严格遵守《农业转基因生物安全管理条例》及其配套规章制度，按要求进行试验审批或报备。课题单位需建立生物安全管理责任制，做到分工明确、责任到人，对违反相关规定的，接受相关责任追究和取消相关人员及团队承担有关农业科研项目资格等处罚。

为营造生物育种产业化良好的社会氛围，课题单位需积极参与科普宣传工作，制定

年度科普宣传工作计划。课题单位通过举办专题报告会、讲座、培训、开放日，发表科普文章，参与集体科普活动等方式积极开展生物技术科普宣传，让大众更好了解生物技术，科学引导大众认识生物技术研发与应用。每个课题需推荐 1 名正式工作人员担任网络科普员，每人每月在网上发布 1-2 篇生物技术科普信息（含转发和评论），并在农业农村部科学技术司统一组织下开展科普宣传活动。

七、知识产权对策、成果管理及合作权益分配

本课题多抗除草剂基因 *CdP450* 是浙江大学与杭州瑞丰生物科技有限公司共同研发获得的，课题的基因的知识产权属于杭州瑞丰生物科技有限公司，杭州瑞丰获得了 *CdP450* 基因在美国、加拿大、巴西等国的专利授权。矮秆基因 *SPL28* 是由华南农大王海洋教授团队克隆，该基因已经申请了中国专利，国际专利正在申请中。育种材料、育种新技术由课题承担单位共享；自交系、杂交种等研究成果除承担单位内部协议外的部分归完成单位所有，参与单位在申请本课题之前各自所获得的知识产权及相应权益均归各自所有。非知识产权和成果可在项目承担单位之间进行交流。

课题执行期向对方提供的未公开的、或在提供之前已告知不能向第三方提供的与本课题相关的技术资料、数据等所有信息，未经提供方同意，不得提供给第三方。也不构成向对方授予任何关于专利、著作权、商标权等知识产权的许可行为。

各方独立完成的科技成果及其形成的知识产权归各方独自所有；由双方共同完成的科技成果及其形成的知识产权归双方共有。科技成果和技术实施许可、转让而获得的经济收益由双方另行约定。

八、需要约定的其他内容

无。

九、课题参加人员基本情况表

填表说明：1、专业技术职称：A、正高级 B、副高级 C、中级 D、初级 E、其他； 2、投入本课题的全时工作时间（人月）是指在课题实施期间该人总共为课题工作的满月度工作量；累计是指课题组所有人员投入人月之和； 3、课题固定研究人员需填写人员明细； 4、是否有工资性收入：Y、是 N、否； 5、人员分类代码：B、课题负责人 C、项目/课题骨干 D、其他研究人员； 6、工作单位：填写单位全称，其中高校要具体填写到所在院系。														
序 号	姓 名	性 别	出 生 日 期	证 件 类 型	证 件 号 码	专 业 技 术 职 称	职 务	最 高 学 位	专 业	投 入 本 课 题 的 全 时 工 作 时 间 （人月）	人 员 分 类 代 码	在 课 题 中 分 担 的 任 务	是 否 有 工 资 性 收 入	工 作 单 位
1	王海洋	男	1965. 12. 14	护照	561962265	A	国家重点 实验室副主 任	博士	作物遗传 育种	6	C	项目首席专 家，新种质 创制	Y	华南农业大学 农业生物资源保护与利用国 家重点实验室
2	林朝阳	男	1979. 04. 12	身份证	350623197904120056	B	无	博士	农业昆虫 与害虫防 治	12	B	耐除草剂玉 米创制	Y	浙江大学新农村发展研究院
3	叶雨轩	男	1990. 03. 07	身份证	3302261990030762	C	无	博士	生物化学 与分子生 物学	6	C	耐除草剂玉 米创制	Y	浙江大学新农村发展研究院
4	赵宇	女	1992. 04. 29	身份证	532526199204291442	C	无	博士	农业昆虫 与害虫防 治	6	C	耐除草剂玉 米创制	Y	浙江大学农学院
5	王鹏飞	男	1987. 01. 24	身份证	211322198701247278	C	安评总 监	博士	农业昆虫 与害虫防 治	6	C	安全评价	Y	杭州瑞丰生物科技有限公司
6	于小星	女	1991. 04. 02	身份证	411122199104028043	C	无	博士	农业昆虫 与害虫防 治	6	C	抗性功能评 价	Y	杭州瑞丰生物科技有限公司
7	林海燕	女	1994. 09. 03	身份证	332624199409034226	C	无	博士	农业昆虫 与害虫防 治	6	C	抗性功能评 价	Y	杭州瑞丰生物科技有限公司

8	孔德鑫	男	1980.05.05	身份证	413029198005052415	B	无	博士	作物遗传 育种	6	C	基因编辑	Y	华南农业大学农业生物资源 保护与利用国家重点实验室
9	衡月芹	女	1988.05.16	身份证	320826198805163068	B	无	博士	作物遗传 育种	6	C	基因编辑	Y	华南农业大学农业生物资源 保护与利用国家重点实验室
10	谈宏斌	男	1971.11.06	身份证	1101081971111069355	B	秦丰研 究院院 长	学士	植物遗传 育种	6	C	性状叠加	Y	杨凌秦丰种业股份有限公司
11	安红卫	男	1967.01.30	身份证	610403196701300076	B	秦丰研 究院玉 米研究 室主任	学士	植物遗传 育种	6	C	性状叠加	Y	杨凌秦丰种业股份有限公司
12	王轩	男	1988.06.22	身份证	610104198806223432	C	秦丰研 究院副 院长	硕士	作物遗传 育种	6	C	抗性功能评 价	Y	杨凌秦丰种业股份有限公司
固定研究人员合计										78	/	/	/	/
流动人员或临时聘用人员合计										0	/	/	/	/
累计										78	/	/	/	/

十、课题信息表

序号：1—1 课题编号：2022ZD0400501 课题名称：玉米生物技术研发与种质资源创新

填表说明：单位类型为课题牵头单位或课题参与单位。						
序号	单位名称	纳税人识别号（统一社会信用代码）	单位类型	任务分工	研究任务负责人	
	(1)	(2)	(3)	(4)	(5)	
1	浙江大学	12100000470095016Q	课题牵头单位	耐除草剂育种材料安全评价、鉴定	林朝阳	
2	华南农业大学	124400004554165634	课题参与单位	耐密抗倒伏育种材料创制	王海洋	
3	杭州瑞丰生物科技有限公司	9133011069980858X4	课题参与单位	耐除草剂育种材料创制	于小星	
4	杨凌秦丰种业股份有限公司	91610403MAB2N7JH3A	课题参与单位	耐除草剂功能性状评价	谈宏斌	

项目联合申报协议

项目牵头单位（甲方）：山东登海种业股份有限公司

项目参与单位（乙方）：浙江大学

甲乙双方共同申报农业生物育种重大项目“适宜复合种植的玉米新品种设计与培育”项目，经友好协商，达成如下协议：

1. 双方合作申请该项目，甲方主持并组织项目申报，乙方作为项目参与单位之一，积极配合甲方完成各项申报事宜。

2. 乙方完全理解和接受农业生物育种重大项目的一切规定和要求。乙方承诺对本单位提供的申报内容或材料的真实性予以负责，并满足申报指南所规定的其他申报条件。

3. 甲方负责材料保密，并保证材料仅用于此项目的申报。

4. 若项目申报成功，甲乙双方将按照农业生物育种重大项目管理办法的要求和相关规定开展相关研究，并且严格履行相应义务。

5. 双方在申请本项目之前各自所获得的知识产权及相应权益均归各自所有，不因共同申请本项目而改变。

6. 双方承诺本项目产生的所有科学数据无条件、按期递交到农业生物育种重大项目指定的平台，在约定条件下对农业生物育种重大项目各承担单位，乃至今后面向所有的科技工作者和公众开放共享。

7. 双方负有为对方技术保密的责任。

8. 本协议一式四份，均具有同等法律效力。

甲方（单位公章）：

乙方（单位公章）：

法人或委托代理人（签章）：



法人或委托代理人（签章）：

项目负责人（签章）：

课题（任务）负责人（签章）：

2022年12月6日

项目联合申报协议

项目牵头单位（甲方）：山东登海种业股份有限公司

项目参与单位（乙方）：华南农业大学

甲乙双方共同申报农业生物育种重大项目“适宜复合种植的玉米新品种设计与培育”项目，经友好协商，达成如下协议：

1. 双方合作申请该项目，甲方主持并组织项目申报，乙方作为项目参与单位之一，积极配合甲方完成各项申报事宜。

2. 乙方完全理解和接受农业生物育种重大项目的一切规定和要求。乙方承诺对本单位提供的申报内容或材料的真实性予以负责，并满足申报指南所规定的其他申报条件。

3. 甲方负责材料保密，并保证材料仅用于此项目的申报。

4. 若项目申报成功，甲乙双方将按照农业生物育种重大项目管理办法的要求和相关规定开展相关研究，并且严格履行相应义务。

5. 双方在申请本项目之前各自所获得的知识产权及相应权益均归各自所有，不因共同申请本项目而改变。

6. 双方承诺本项目产生的所有科学数据无条件、按期递交到农业生物育种重大项目指定的平台，在约定条件下对农业生物育种重大项目各承担单位，乃至今后面向所有的科技工作者和公众开放共享。

7. 双方负有为对方技术保密的责任。

8. 本协议一式四份，均具有同等法律效力。



甲方（单位公章）：

法人或委托代理人（签章）：



项目负责人（签章）：王祥



乙方（单位公章）：

法人或委托代理人（签章）：

课题（任务）负责人（签章）：王海洋

孔德亮 衡月新

2022年12月6日

项目联合申报协议

项目牵头单位（甲方）：山东登海种业股份有限公司

项目参与单位（乙方）：杭州瑞丰生物科技有限公司

甲乙双方共同申报农业生物育种重大项目“适宜复合种植的玉米新品种设计与培育”项目，经友好协商，达成如下协议：

1. 双方合作申请该项目，甲方主持并组织项目申报，乙方作为项目参与单位之一，积极配合甲方完成各项申报事宜。

2. 乙方完全理解和接受农业生物育种重大项目的一切规定和要求。乙方承诺对本单位提供的申报内容或材料的真实性予以负责，并满足申报指南所规定的其他申报条件。

3. 甲方负责材料保密，并保证材料仅用于此项目的申报。

4. 若项目申报成功，甲乙双方将按照农业生物育种重大项目管理办法的要求和相关规定开展相关研究，并且严格履行相应义务。

5. 双方在申请本项目之前各自所获得的知识产权及相应权益均归各自所有，不因共同申请本项目而改变。

6. 双方承诺本项目产生的所有科学数据无条件、按期递交到农业生物育种重大项目指定的平台，在约定条件下对农业生物育种重大项目各承担单位，乃至今后面向所有的科技工作者和公众开放共享。

7. 双方负有为对方技术保密的责任。

8. 本协议一式四份，均具有同等法律效力。



甲方（单位公章）

法人或委托代理人（签章）：

项目负责人（签章）：



乙方（单位公章）：

法人或委托代理人（签章）：

课题（任务）负责人（签章）：



2022 年 12 月 6 日

项目联合申报协议

项目牵头单位（甲方）：山东登海种业股份有限公司

项目参与单位（乙方）：杨凌秦丰种业股份有限公司

甲乙双方共同申报农业生物育种重大项目“适宜复合种植的玉米新品种设计与培育”项目，经友好协商，达成如下协议：

1. 双方合作申请该项目，甲方主持并组织项目申报，乙方作为项目参与单位之一，积极配合甲方完成各项申报事宜。

2. 乙方完全理解和接受农业生物育种重大项目的一切规定和要求。乙方承诺对本单位提供的申报内容或材料的真实性予以负责，并满足申报指南所规定的其他申报条件。

3. 甲方负责材料保密，并保证材料仅用于此项目的申报。

4. 若项目申报成功，甲乙双方将按照农业生物育种重大项目管理办法的要求和相关规定开展相关研究，并且严格履行相应义务。

5. 双方在申请本项目之前各自所获得的知识产权及相应权益均归各自所有，不因共同申请本项目而改变。

6. 双方承诺本项目产生的所有科学数据无条件、按期递交到农业生物育种重大项目指定的平台，在约定条件下对农业生物育种重大项目各承担单位，乃至今后面向所有的科技工作者和公众开放共享。

7. 双方负有为对方技术保密的责任。

8. 本协议一式四份，均具有同等法律效力。

甲方（单位公章）：

法人或委托代理人（签章）：

项目负责人（签章）：

乙方（单位公章）：

法人或委托代理人（签章）：

课题（任务）负责人（签章）：

2022年12月6日

用于生物育种专项



事业单位法人证书

统一社会信用代码 121000004700950160

名称 浙江大学

法定代表人 吴朝晖

宗旨和

经费来源 财政补助、上级补助、事业、附属单位上缴收入

业务范围

开办资金 ¥192923万元

住所

举办单位 教育部

登记管理机关

有效期 自2021年07月28日至2026年07月28日

请于每年3月31日前向登记管理机关报送上一年度的年度报告



国家事业单位登记管理局监制

中华人民共和国 事业单位法人证书 (副本)

统一社会信用代码 124400004554165634



有效期 自2021年06月02日至2026年06月01日

名称 华南农业大学

宗旨和 承担普通高等学历教育、成人学历教育、承担科技人员函授和自考继续教育和培训、相关科学研究与技术开发、科技成果推广与科技咨询服务、国内外校际教育合作和学术交流

业务范围

住所 广东省广州市天河区五山

法定代表人 刘雅红

经费来源 财政核拨

开办资金 ¥311733万元

举办单位 广东省教育厅

登记管理机关



124400004554165634-02

国家事业单位登记管理局监制

统一社会信用代码 9133011069980858X4 (1/1)		营业执照 (副本)		 扫描二维码登录“国家企业信用信息公示系统”了解更多登记、备案、许可、监管信息	
名称	杭州瑞丰生物科技有限公司	注册资本	叁仟陆佰零肆万捌仟陆玖拾贰元		
类型	有限责任公司(自然人投资或控股)	成立日期	2009年12月28日		
法定代表人	沈志成	营业期限	2009年12月28日至2029年12月27日		
经营范围	生物技术、生物制品、食品的技术开发;销售:生物制品;食品经营;货物进出口(法律、行政法规禁止经营的项目除外,法律、行政法规限制经营的项目取得许可证后方可经营)。(依法须经批准的项目,经相关部门批准后方可开展经营活动)				
		住所	浙江省杭州市余杭区仓前街道文一西路1500号1号楼103室		
		登记机关			
			2022年04月22日		

国家企业信用信息公示系统网址: <http://www.gsxt.gov.cn>

市场主体应当于每年1月1日至6月30日通过国家信用信息公示系统报送公示年度报告。

国家市场监督管理总局监制

统一社会信用代码 91610403MAB2N7JH3A		营业执照 (副本)2-1		 扫描二维码登录“国家企业信用信息公示系统”了解更多登记、备案、许可、监管信息	
名称	杨凌泰丰种业股份有限公司	注册资本	叁亿陆仟万元人民币		
类型	其他股份有限公司(非上市)	成立日期	2021年05月07日		
法定代表人	李晓锋	营业期限	长期		
经营范围	一般项目:农作物种子经营(仅限不再分装的包装种子);非主要农作物种子生产;谷物种植;谷物销售;农产品的生产、销售、加工、运输、贮藏及其他相关服务;初级农产品收购;农作物病虫害防治服务;农作物栽培服务;豆类种植;蔬菜种植;食用菌种植;豆及薯类销售;农副产品销售;肥料销售;农用薄膜销售;互联网销售(除销售需要许可的商品);食用农产品初加工;农业科学研究和试验发展;技术服务、技术开发、技术咨询、技术交流、技术转让、技术推广;生物有机肥料研发;农业专业及辅助性活动(除依法须经批准的项目外,凭营业执照依法自主开展经营活动)。许可项目:农作物种子经营;主要农作物种子生产;农作物种子进出口;农作物种子质量检验;粮食收购;粮油仓储服务;农药零售(依法须经批准的项目,经相关部门批准后方可开展经营活动,具体经营项目以审批结果为准)。				
		住所	陕西省杨凌示范区杨凌大道种业国际大厦5层		
		登记机关			
			2021年06月18日		

国家企业信用信息公示系统网址: <http://www.gsxt.gov.cn/>

市场主体应当于每年1月1日至6月30日通过国家信用信息公示系统报送公示年度报告。

国家市场监督管理总局监制

任务书签署

甲乙双方根据《国务院印发关于深化中央财政科技计划（专项、基金）管理改革方案的通知》（国发〔2014〕64号）、《国务院关于优化科研管理提升科研绩效若干措施的通知》（国发〔2018〕25号）、《国务院办公厅关于改革完善中央财政科研经费管理的若干意见》（国办发〔2021〕32号）、《科学技术活动违规行为处理暂行规定》（科学技术部令第19号）、《科技部 财政部关于印发<中央财政科技计划（专项、基金等）监督工作暂行规定>的通知》（国科发政〔2015〕471号）、《科技部 自然科学基金委关于进一步压实国家科技计划（专项、基金等）任务承担单位科研作风学风和科研诚信主体责任的通知》（国科发监〔2020〕203号）、《科技部、财政部、自然科学基金委关于进一步加强统筹国家科技计划项目立项管理工作的通知》（国科办资〔2022〕107号）等有关文件规定，以及有关法律、政策和管理要求，依据项目立项通知，签署本任务书。

同时，本单位和课题负责人郑重承诺：对本课题所有成果产出（包括但不限于新产品、新技术、标准、论文、专利等）的真实性、与项目（课题）的关联性等负责，将按要求落实科研作风学风和科研诚信主体责任；课题经费全部用于与本课题研究工作相关的支出，不截留、挪用、侵占，不用于与科学研究无关的支出；接受并积极配合相关部门的监督检查。如有违反，本单位和课题负责人以及相关成果产出者愿接受项目管理专业机构和相关部门做出的各项处理决定，包括但不限于终止课题执行、追回课题经费，取消一定期限国家科技计划项目（课题）申报资格，记入科研诚信严重失信行为数据库以及主要负责人接受相应党纪政纪处理等。

项目牵头承担单位（甲方）：

法定代表人签字（签章）：



（公章）

2024年7月28日

项目负责人签字（签章）：

唐世伟

2024年7月28日

课题牵头承担单位（乙方）：

法定代表人签字（签章）：



（公章）

2024年7月22日

课题负责人签字（签章）：

林朝付

2024年7月22日

项目预算表（2022-2023 年）

表 A2 项目编号：2022ZD04005

项目名称：适宜复合种植的玉米新品种设计与培育

金额单位：万元

课题预算															
资金来源												经费支出			
课题 编号	课题名称	课题承担单 位	课 题 负 责 人	中央 财政 资金	其他来源资金				合计	中央财政资金			其他 来源 资金	合计	
					地方财 政资金	单位自筹 资金	其他 渠道 获得 资金	小计		直接 费用	间接 费用	小计			
(1)	(2)	(3)	(4)	(5)	(6)	(7)	(8)	(9)	(10)	(11)	(12)	(13)	(14)	(15)	
2022Z D0400 501	玉米生物技术 研发与种质资 源创新	浙江大学	林朝 阳	1021.00	0	6000.00	0	6000.00	7021.00	850.00	171.00	1021.00	6000.00	7021.00	
2022Z D0400 502	黄淮海区适宜 复合种植和宜 机收玉米品种 设计与培育	山东登海种 业股份有限 公司	李旭 华	1000.40	0	3200.00	0	3200.00	4200.40	829.17	171.23	1000.40	3200.00	4200.40	
2022Z D0400 503	西南区适宜复 合种植玉米新 品种设计与培 育	四川省农业 科学院作物 研究所	何文 铸	391.60	200.00	800.00	0	1000.00	1391.60	348.00	43.60	391.60	1000.00	1391.60	
2022Z D0400 504	东北区宜机收 玉米新品种设 计与培育	黑龙江省农 业科学院玉 米研究所	张建 国	513.90	0	3000.00	0	3000.00	3513.90	432.00	81.90	513.90	3000.00	3513.90	
2022Z D0400 505	西北区适宜复 合种植宜机收 高产玉米新品 种设计与培育	西北农林科 技大学	徐淑 兔	291.60	0	0	0	0	291.60	234.00	57.60	291.60	0	291.60	
累计				3218.50	200.00	13000.00	0	13200.00	16418.50	2693.17	525.33	3218.50	13200.00	16418.50	

课题单位经费预算明细表（2022-2023 年）

金额单位：万元

表 B3 课题序号：2022ZD0400501 课题名称：玉米生物技术研发与种质资源创新

填表说明：1.单位类型分课题承担单位、课题参与单位； 2.组织机构代码指企事业单位国家标准代码，单位若已三证合一请填写单位统一社会信用代码，无组织机构代码的单位填写“0000000000”。										
序 号	单位名称	组织机构代码-统一社会信用代码		单位类型	任务分工	研究任务负责人	合计	中央财政专项资金		
		(2)	(3)					小计	其中：间接费用	其他来源资金
课题 1	浙江大学		91610403MAB2N7JH3A	高等学校	耐除草剂育种材料安全评价、鉴定	林朝阳	194.00	194.00	34.00	
课题 1	华南农业大学		124400004554165634	高等学校	耐密抗倒伏育种材料创制	王海洋	244.00	244.00	34.00	
课题 1	杭州瑞丰生物科技有限公司		9133011069980858X4	民营企业	耐除草剂育种材料创制	于小星	3389.00	389.00	69.00	3000.00
课题 1	杨凌秦丰种业股份有限公司		91610403MAB2N7JH3A	国有企业	耐除草剂功能性状评价	谈宏斌	3194.00	194.00	34.00	3000.00
累计							7021.00	1021.00	171.00	6000.00

课题编号： 2022ZD0400501

密级：公开

农业生物育种重大专项 课题年度预算书

课 题 名 称 :	玉米生物技术研发与种质资源创新
所 属 项 目 名 称 :	农业生物新品种培育
专 业 机 构 :	农业农村部科技发展中心
课题牵头承担单位:	浙江大学 (公章)
课 题 负 责 人 :	林朝阳
课 题 预 算 期 间 :	2024 年 1 月 至 2024 年 12 月

2024 年 1 月

课题预算表（2024 年）

表 B1 课题编号：2022ZD0400501 课题名称：玉米生物技术研发与种质资源创新 金额单位：万元

序号	预算科目名称	金额
	(1)	(2)
1	一、中央财政专项资金	1120.00
2	（一）直接费用	950.00
3	1. 设备费	50.00
4	其中：购置设备费	50.00
5	2. 业务费	700.00
6	3. 劳务费	200.00
7	（二）间接费用	170.00
8	二、其他来源资金	6200.00
9	三、合计	7320.00

注：1、间接费用无需编制预算说明；2、绩效支出在间接费用中无比例限制。承担单位在统筹安排间接费用时，要处理好合理分摊间接成本和对科研人员激励的关系，绩效支出安排与科研人员在课题工作中的实际贡献挂钩。

课题单位经费预算明细表（2024 年）

表 B3		课题编号：		课题名称：		金额单位：万元				
填表说明：1.单位类型分课题承担单位、课题参与单位； 2.组织机构代码指企事业单位国家标准代码，单位若已三证合一请填写单位统一社会信用代码，无组织机构代码的单位填写“0000000000”。										
序 号	单位名称	组织机构代码-统一社会信用代码		单位类型	任务分工	研究任务负责人	合计	中央财政资金		其他来源资金
		(2)	(3)					小计	其中：间接费用	
1	浙江大学	统一社会信用代码	91610403MAB2N7JH3A	课题承担单位	耐除草剂育种材料安全评价、鉴定	林朝阳	200.00	200.00	35.00	0.00
2	华南农业大学	统一社会信用代码	124400004554165634	课题参与单位	耐密抗倒伏育种材料创制	王海洋	270.00	270.00	45.00	0.00
3	杭州瑞丰生物科技有限公司	统一社会信用代码	9133011069980858X4	课题参与单位	耐除草剂育种材料创制	于小星	1850.00	450.00	55.00	1400.00
4	杨凌秦丰种业股份有限公司	统一社会信用代码	91610403MAB2N7JH3A	课题参与单位	耐除草剂功能性状评价	谈宏斌	5000.00	200.00	35.00	4800.00
累计							7320.00	1120.00	170.00	6200.00

检索证明

根据委托人提供的论文材料，委托人华南农业大学生命科学学院 衡月芹 7 篇论文收录情况如下表。

序号	论文名称	发表刊物及发表的年月卷期/页码等	作者排名	论文等级	作者工作单位	收录情况	影响因子	中科院大分类区
1	Natural variation in OsMYB8 confers diurnal floret opening time divergence between indica and japonica subspecies	NATURE COMMUNICATIONS 出版年: 2024 出版日期: MAR 13 卷期: 15 1 页码: - 文献号: 2262 文献类型: Article	并列第一作者 (排名第三)	T2 类	华南农业大学 生命科学学院	SCI	IF2-year=15.7 IF5-year=17.2 (2024)	综合性期刊 1 区 Top 期刊: 是 (2025)
2	A jasmonate-mediated regulatory network modulates diurnal floret opening time in rice	NEW PHYTOLOGIST 出版年: 2024 出版日期: OCT 卷期: 244 1 页码: 176-191 文献类型: Article	共同通讯作者 (倒数第三)	T2 类	华南农业大学 生命科学学院	SCI	IF2-year=8.1 IF5-year=10.3 (2024)	生物学 1 区 Top 期刊: 是 (2025)
3	Targeted manipulation of grain shape genes effectively improves outcrossing rate and hybrid seed production in rice	PLANT BIOTECHNOLOGY JOURNAL 出版年: 2023 出版日期: FEB 卷期: 21 2 页码: 381-390 文献类型: Article	并列第一作者 (排名第三)	T2 类	华南农业大学 生命科学学院	SCI	IF2-year=11.2 IF5-year=12.1 (2023)	生物学 1 区 Top 期刊: 是 (2023)

4	BBX4, a phyB-interacting and modulated regulator, directly interacts with PIF3 to fine tune red light-mediated photomorphogenesis	PROCEEDINGS OF THE NATIONAL ACADEMY OF SCIENCES OF THE UNITED STATES OF AMERICA 出版年: 2019 出版日期: DEC 17 卷期: 116 51 页码: 26049-26056 文献类型: Article	第一作者	T2 类	南方科技大学 生命科学学院	SCI	IF2-year=9.412 IF5-year=10.62 (2019)	综合性期刊 1 区 Top 期刊: 是 (2019)
5	B-Box Containing Proteins BBX30 and BBX31, Acting Downstream of HY5, Negatively Regulate Photomorphogenesis in Arabidopsis	PLANT PHYSIOLOGY 出版年: 2019 出版日期: MAY 卷期: 180 页码: 497-508 文献类型: Article	第一作者	T2 类	南方科技大学 生命科学学院	SCI	IF2-year=6.902 IF5-year=7.52 (2019)	生物学 1 区 Top 期刊: 是 (2019)
6	COP1 SUPPRESSOR 6 represses the PIF4 and PIF5 action to promote light-inhibited hypocotyl growth	JOURNAL OF INTEGRATIVE PLANT BIOLOGY 出版年: 2022 出版日期: NOV 卷期: 64 11 页码: 2097-2110 文献类型: Article	并列第一作者 (排名第二)	T2 类	南方科技大学 生命科学学院	SCI	IF2-year=11.4 IF5-year=10.1 (2022)	生物学 1 区 Top 期刊: 是 (2022)

7	A Positive Feedback Loop of BBX11-BBX21-HY5 Promotes Photomorphogenic Development in Arabidopsis	PLANT COMMUNICATIONS 出版年: 2020 出版日期: SEP 14 卷期: 1 5 页码: - 文献号: 100045 文献类型: Article	并列第一作者(排名第二)	南方科技大学 生命科学学院	SCI	无	无
---	--	--	--------------	------------------	-----	---	---

说明: 论文等级和中科院大类分区按《华南农业大学学术论文评价方案(试行)》划分。

报告免责声明: 如未盖章, 报告无效

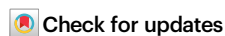


Natural variation in *OsMYB8* confers diurnal floret opening time divergence between *indica* and *japonica* subspecies

Received: 26 July 2023

Accepted: 1 March 2024

Published online: 13 March 2024



Yajun Gou^{1,4}, Yueqin Heng^{1,4}, Wenyan Ding¹, Canhong Xu¹, Qiushuang Tan¹, Yajing Li¹, Yudong Fang¹, Xiaoqing Li¹, Degui Zhou², Xinyu Zhu¹, Mingyue Zhang¹, Rongjian Ye³, Haiyang Wang¹✉ & Rongxin Shen¹✉

The inter-subspecific *indica-japonica* hybrid rice confer potential higher yield than the widely used *indica-indica* intra-subspecific hybrid rice. Nevertheless, the utilization of this strong heterosis is currently hindered by asynchronous diurnal floret opening time (DFOT) of *indica* and *japonica* parental lines. Here, we identify *OsMYB8* as a key regulator of rice DFOT. *OsMYB8* induces the transcription of JA-Ile synthetase *OsJAR1*, thereby regulating the expression of genes related to cell osmolality and cell wall remodeling in lodicules to promote floret opening. Natural variations of *OsMYB8* promoter contribute to its differential expression, thus differential transcription of *OsJAR1* and accumulation of JA-Ile in lodicules of *indica* and *japonica* subspecies. Furthermore, introgression of the *indica* haplotype of *OsMYB8* into *japonica* effectively promotes DFOT in *japonica*. Our findings reveal an *OsMYB8-OsJAR1* module that regulates differential DFOT in *indica* and *japonica*, and provide a strategy for breeding early DFOT *japonica* to facilitate breeding of *indica-japonica* hybrids.

Rice (*Oryza sativa* L.) is the preferred major staple crop for over half of the world population (FAO statistical databases, 2022). Historically, several major leaps in rice yield per unit land area have occurred due to improvement of breeding technologies and utilization of advanced cultivars. A major landmark in rice breeding is the utilization of the semi-dwarf gene *sd1* (encoding an enzyme essential for gibberellin biosynthesis) and breeding of lodging-resistant rice cultivars in the 1950s, leading to the “first-green revolution” in rice production (average rice yield increased from ~150 kg/mu to 300 kg/mu)¹. The second landmark in rice breeding is development of hybrid rice in China in the 1970s, led by a group of scientists headed by professor Longping Yuan. Two-hybrid rice breeding technologies, the “three-line” (based on CMS-WA cytoplasmic male sterility) and the “two-line” (based on photoperiod- or

thermo-sensitive male sterility) hybrid systems, were developed sequentially in China in the 1970s and 1980s respectively, and are still widely used nowadays^{2–4}. Three-line hybrid rice has a yield advantage of ~20–30% over the traditional inbred varieties, and two-line hybrid rice could confer ~5–10% additional yield increase over three-line hybrid rice⁵. To date, the large-scale application of commercial hybrid rice has increased total accumulated rice yield by over 0.6 billion tons, contributing significantly to securing global food supply^{6,7}.

Indica and *japonica* are two major genetically differentiated ecotypes of Asian cultivated rice. Currently, the majority of hybrid rice is intra-subspecific hybrid rice produced from crosses between *indica* varieties, with few inter-subspecific hybrid rice produced from crosses between *indica* and *japonica* subspecies (China Rice

¹State Key Laboratory for Conservation and Utilization of Subtropical Agro-Bioresources, Guangdong Laboratory for Lingnan Modern Agriculture, South China Agricultural University, Guangzhou 510642, China. ²Guangdong Key Laboratory of New Technology in Rice Breeding, Rice Research Institute, Guangdong Academy of Agricultural Sciences, Guangzhou 510640, China. ³Life Science and Technology Center, China National Seed Group Co., LTD, Wuhan 430073, China. ⁴These authors contributed equally: Yajun Gou, Yueqin Heng. ✉e-mail: whyang@scau.edu.cn; shenrongxin@scau.edu.cn

Data Center, <https://www.ricedata.cn>). Over the past few decades, yield of intra-subspecific *indica* hybrid rice has reached a plateau due to the limited genetic diversity of the parental lines⁸. As *indica-japonica* inter-subspecific hybrid rice has a yield advantage of ~15–30% over the intra-subspecific *indica/indica* hybrid rice, it is believed that developing more *indica-japonica* inter-subspecific hybrid rice is an essential route to boost rice production in the future. Nevertheless, production of *indica-japonica* hybrid rice is currently hindered by several technical bottlenecks, such as hybrid male sterility, prolonged life span, prone to lodging of the hybrids due to exaggerated plant height, and low yield of hybrid seed production. A major reason for low yield of hybrid seed production is asynchronous diurnal floret opening time (DFOT) of the *indica* and *japonica* parental lines. During production of *indica-japonica* inter-subspecific hybrid rice, *japonica* varieties are often used as the male sterile lines (maternal parent), whereas *indica* varieties are often used as the pollen donors (parental line). In general, *indica* rice has an earlier DFOT than *japonica* rice (average 1–3 h)⁹. This asynchronous DFOT of *indica* and *japonica* would severely reduce the efficiency of cross-pollination and large-scale hybrid seed production¹⁰. Therefore, genetic improvement and synchronization of DFOT of the *indica* and *japonica* parental lines are urgently needed for successful commercial production of *indica-japonica* inter-subspecific hybrid rice seeds.

Previous studies have revealed that lodicule, a small scale-like organ lying between the lemma/palea and stamens within the base of florets, plays an important role in controlling DFOT in rice. During floret opening, the lodicule cells absorb water and expand, pushing the lemma and palea apart to drive floret opening. After pollination, lodicule loses water and undergoes programmed cell death, leading to closure of the glumes^{10–12}. The opening and closing processes of rice spikelets entail a dynamic change of turgor and osmotic pressure in the parenchymatous cells of the lodicule^{13–15}. Mounting evidence indicated that the plant hormone jasmonic acid (JA) plays a key role in regulating floret opening and closure in rice and other monocotyledonous plant species such as wheat and rye^{16–19}. In addition, several recent studies have reported that *Diurnal Flower Opening Time 1 (DFOT1) / Early Morning Flowering1 (EMF1)*, which encodes a DUF642 domain-containing protein, negatively regulates rice DFOT through modulating methylesterification of lodicule cell wall pectin^{11,20}. Despite the progress made in this field, the genetic basis and molecular mechanisms regulating DFOT in rice, especially the differentiation of DFOT in *indica* and *japonica*, have remained essentially unknown.

In this study, we identify an R2R3-MYB transcription factor OsMYB8 as a key regulator of asynchronous DFOT by performing a comparative time-course transcriptome analysis of lodicules in *indica* and *japonica*. We find that *OsMYB8* promotes floret opening in both *indica* and *japonica* rice through directly activating the expression of a JA biosynthesis gene *OsARI*, leading to elevated JA-Ile accumulation and thus altered expression of genes related to cell osmolality and cell wall remodeling in the lodicules. We also reveal that natural variation in the promoter sequences of *OsMYB8* confers higher expression level of *OsMYB8* in *indica*, thus higher accumulation of JA-Ile and earlier DFOT in *indica* as compared to *japonica*. Finally, we demonstrate that introgression of the *indica* *OsMYB8* allele into *japonica* rice could confer earlier DFOT in *japonica* rice. Our study not only provides a significant breakthrough into the understanding of the genetic network regulating asynchronous DFOT of *indica* and *japonica* rice but also provides effective genetic resources for genetic improvement of rice DFOT to facilitate hybrid breeding between *indica* and *japonica* subspecies.

Results

Diurnal floret opening time divergence in rice subspecies

To investigate the genetic variation for the DFOT trait in rice, we collected a rice diversity panel, including 12 *japonica* and 28 *indica* cultivars (Supplementary Data 1), and compared their DFOT in October 2019 in Guangzhou (Longitude, 113.27°; Latitude, 23.13°). The results showed that the *indica* cultivars exhibited the peak opening time at around 10:00–11:00 am, whereas the *japonica* cultivars had peak opening time at approximately 12:00–12:30 noon, indicating that the DFOT of *indica* cultivars was significantly earlier than that of *japonica* cultivars (Fig. 1a, Supplementary Data 1). Subsequently, the DFOT trait of a typical *indica* cultivar TianFengB (TFB) and a typical *japonica* cultivar ZhongHua11 (ZH11) was further analyzed in the early (June) and late (October) growing seasons of 2020 in Guangzhou. As expected, the DFOT of TFB was 1–2 h earlier than that of ZH11 in both the early and late seasons (Fig. 1b–e). Meanwhile, we carefully recorded the size and morphology of the lodicules of TFB and ZH11 at different time points under a stereomicroscope. The results showed that the lodicules of TFB swelled and reached the maximum size by 10:00 am, while the lodicules of ZH11 displayed a delay in swelling and did not reach the maximum size until 12:00 noon (Fig. 1f–h). Measurement of water content in the lodicules of TFB and ZH11 at different time points revealed a gradual increase of water content as the floret opening time approaching. Water content reached the highest at 10:00 am in the lodicules of TFB, but did not reach the highest until 12:00 noon in ZH11 (Fig. 1i). Taken together, these results indicate that the *indica* cultivars exhibit earlier DFOT than *japonica* cultivars, which could be attributed to advanced swelling of the lodicules in *indica* cultivars.

Identification of *OsMYB8* as a key regulator of differential DFOT in *indica* and *japonica*

To explore the molecular basis underlying the differential lodicule swelling in *indica* and *japonica*, we performed a comprehensive comparative RNA-seq analysis of the lodicules of TFB and ZH11 at different time points, including 18:00 the day before floret opening (T18 in TFB, Z18 in ZH11), 3 h before opening in ZH11 (Z9, -9:00 am), 1 h before opening (T9, -9:00 am in TFB; Z11, -11:00 am in ZH11) and undergoing peak floret opening time (TF, -10:00 am in TFB; ZF, -12:00 noon in ZH11) (Supplementary Fig. 1a, b). Correlation analysis of biological replicates from each time point showed very high correlation coefficients ($R^2 \geq 0.90$; Supplementary Fig. 1c). Thus, we calculated the average FPKM value of the replicates as the gene expression level for each sample. We further performed pairwise differential gene expression analyses between two consecutive time points and identified 6102 differentially expressed genes (DEGs) between T9 vs. T18, 6326 DEGs between TF vs. T9, 7164 DEGs between Z9 vs. Z18, 2972 DEGs between Z11 vs. Z9, 7012 DEGs between ZF vs. Z11 and 7430 DEGs between T9 vs. Z9 (P -value < 0.05, absolute \log_2FC (fold change) ≥ 1 ; Supplementary Fig. 1d; Supplementary Data 2). Gene Ontology (GO) term enrichment analysis revealed that biological processes and molecular pathways related to cell osmolality and cell wall remodeling, such as sugar transport, water channel activity, JA synthesis and signaling, calcium signaling and ethylene signaling were enriched in one or more datasets (Supplementary Fig. 2). Principal component analysis (PCA) showed that the dataset of T18 was grouped together with that of Z18. Likewise, the dataset of TF was grouped together with that of ZF (Fig. 2a). In congruent with earlier DFOT in TFB, the T9 time point was grouped together with Z11 but not Z9, suggesting that transcriptional activities related to floret opening process are advanced in TFB, compared to ZH11 (Fig. 2a).

Considering that the time point of 1 h before opening is the crucial stage for floret opening^{10,21}, we speculated that genes responsible for differentiated DFOT in *indica* and *japonica* might show characteristic expressional changes in T9 and Z11, and likely be up-regulated in the

datasets of T9 vs. Z9. Therefore, we first performed k-means clustering analysis of all expressed genes and identified a total of 20 clusters with distinct gene expression patterns (Supplementary Fig. 1e). Among them, the Cluster18 genes showing peak expression at T9 and Z11 were selected for further detailed analyses. Next, we performed an overlap analysis of Cluster18 genes with up-regulated DEGs of T9 vs. Z9. A total of 251 overlapping genes were identified (Fig. 2b). GO term analysis revealed an enrichment of DNA binding and transcription factor activity (Fig. 2c). We further noted that among the 11 overlapping genes encoding transcription factors, *LOC_Os01g45090* (*OsMYB8*), encoding an R2R3-MYB transcription factor, exhibited the highest expression level and was gradually up-regulated in the lodicules before floret opening (Fig. 2d). Neighbor-joining tree analysis showed that *OsMYB8* is homologous to *AtMYB21/24*, which are involved in JA signaling and regulating stamen development in *Arabidopsis*²² (Supplementary Fig. 3). The RiceXPro data and reverse transcriptional quantitative PCR (RT-qPCR) analyses showed that *OsMYB8* was preferentially expressed in lemma, palea, stamen, stigma, and lodicule, but with low expression level in root, stem, leaf, and young panicle (Supplementary Fig. 4a, b). Histochemical staining analysis of transgenic lines expressing the *pOsMYB8::GUS* (β -glucuronidase) reporter gene also revealed a similar expression pattern (Supplementary Fig. 4c). RT-qPCR analysis showed that the expression level of *OsMYB8* was lower in the lodicules of TFB and ZH11 at the day before floret

opening, and then gradually increased towards opening time, and decreased thereafter. Additionally, we found that the expression level of *OsMYB8* in *indica* lodicules was significantly higher than that in *japonica* lodicules before floret opening (Supplementary Fig. 5). Moreover, RT-qPCR analysis verified that the expression levels of *OsMYB8* in the lodicules of TFB at 9:00 am (the time before floret opening) were about 2-fold of that in ZH11 at the same time points (Fig. 2e). These observations together suggest that the elevated expression level and an earlier peak expression time of *OsMYB8* in TFB compared with that in ZH11 may contribute to the earlier floret opening time in *indica* varieties. Thus, we selected *OsMYB8* as a candidate gene regulating the differentiated DFOT in *indica* and *japonica* subspecies.

OsMYB8 promotes floret opening in rice

To explore the role of *OsMYB8* in DFOT regulation, we knocked out the *OsMYB8* gene in both ZH11 and TFB backgrounds using the CRISPR/Cas9 technology. Two verified independent *OsMYB8* knockout lines in ZH11 (*Osmyb8^{ZH1}#1* and *Osmyb8^{ZH1}#2*) and TFB background (*Osmyb8^{TF}#1* and *Osmyb8^{TF}#2*) were selected for detailed phenotypic analysis (Fig. 3a, Supplementary Fig. 6). The florets of ZH11 started opening at around 10:30 am, and achieved peak opening time by 11:30 am, whereas the *Osmyb8^{ZH1}* mutants did not achieve peak opening time until 12:00 noon, about 0.5 h later than ZH11 (Fig. 3b, c). Similarly, the

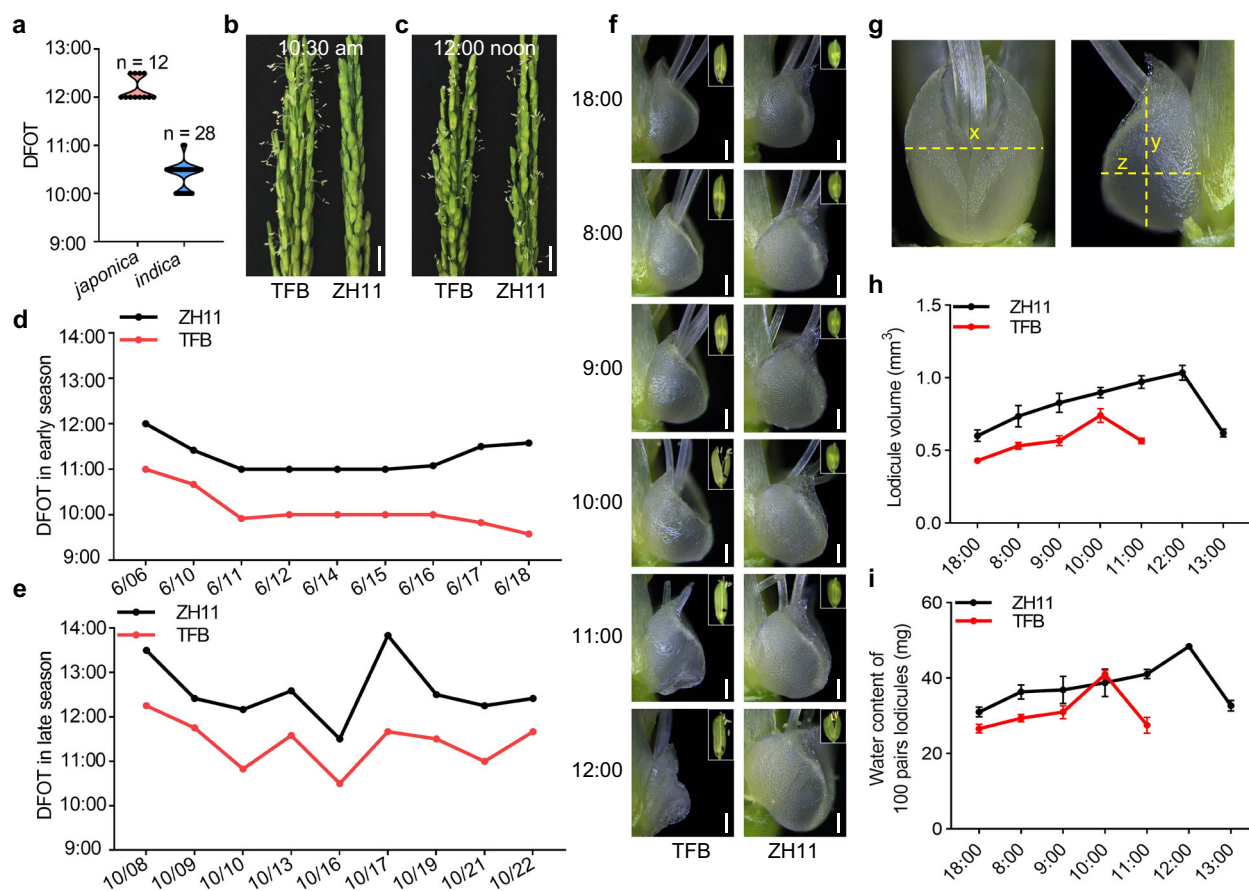


Fig. 1 | DFOT divergence in rice subspecies. **a** Diurnal floret opening time (DFOT) of *japonica* cultivars ($n = 12$ accessions) and *indica* cultivars ($n = 28$ accessions) in October 2019 in Guangzhou. **b, c** Comparison of panicles undergoing floret opening in the *indica* cultivar TFB and *japonica* cultivar ZH11 at 10:30 am (**b**) and 12:00 noon in October 2020 in Guangzhou (**c**). Scale bars, 1 cm. **d, e** The DFOT of TFB and ZH11 in June 2020 in Guangzhou (**d**) and October 2020 in Guangzhou (**e**). **f** Lodicule morphology of TFB and ZH11 at different time points in October 2020 in Guangzhou. Scale bars, 250 μ m. The boxed areas indicate the corresponding

florets. ($n = 10$ lodicules). **g** Viewing the lodicule as an ellipsoid, its x, y, and z-axes are shown in the diagram. **h** Quantitative comparison of lodicules volume in ZH11 and TFB at different time points. Lodicule volume was calculated using the ellipsoid volume formula ($V = 4\pi abc/3$). **a, b, c** correspond to the semi-axes along the x, y, and z-axes shown in **g**. Values are means \pm SEM. ($n = 10$ lodicules). **i** Analysis of the water content of 100 pairs lodicules of ZH11 and TFB at different time points. Values are means \pm SEM. ($n = 3$ biological replicates). Source data are provided as a Source Data file.

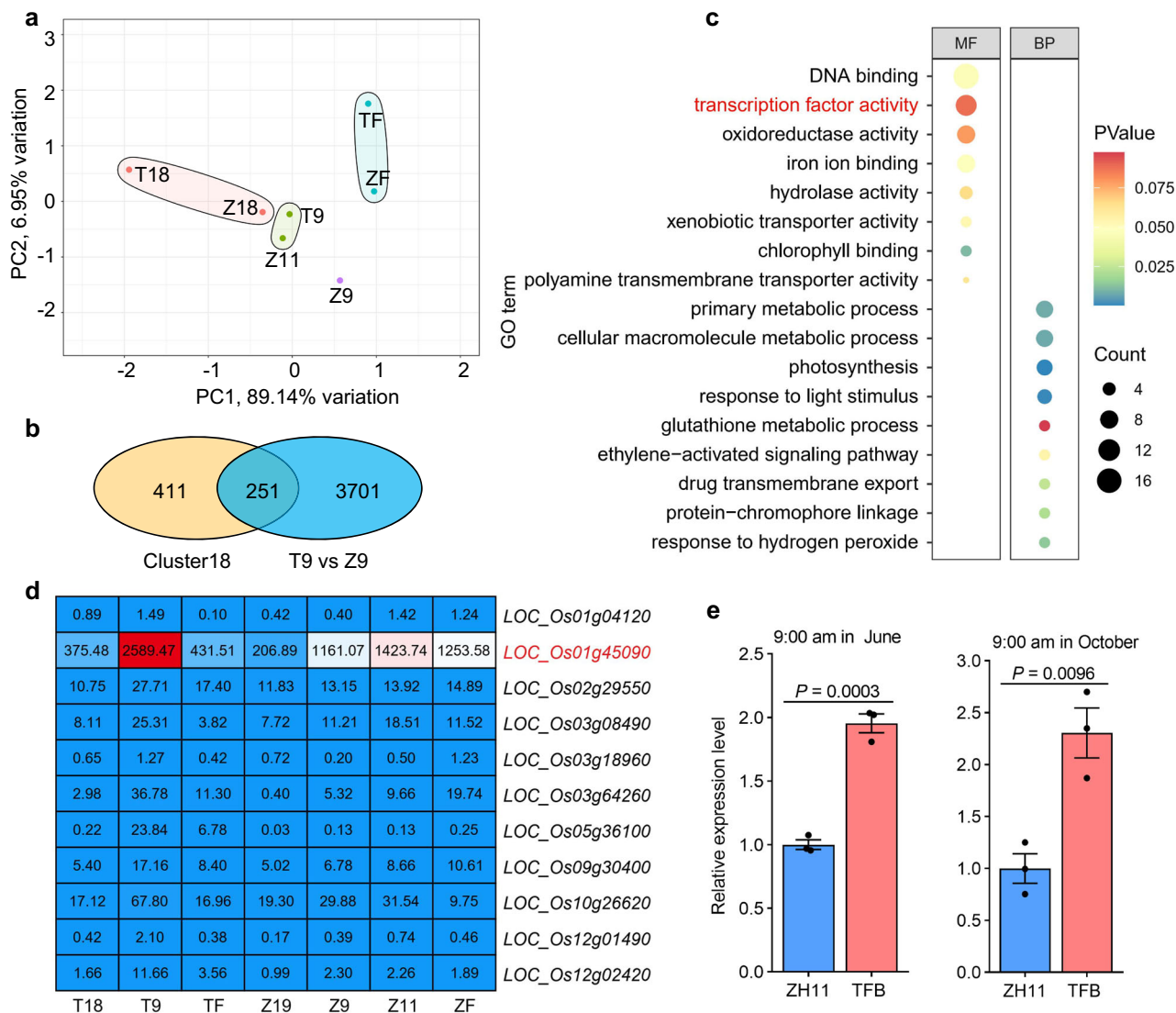


Fig. 2 | Identification of *OsMYB8* by comparative transcriptomic analysis of lodicules between *indica* and *japonica*. **a** Principal component analysis (PCA) of the transcriptome datasets of lodicules between TFB and ZH11 at different time points. T18 and Z18 indicate 18:00 the day before floret opening; T9 and Z9 indicate 9:00 am (1 h and 3 h before floret opening in TFB and ZH11, respectively); Z11 indicate 11:00 am (1 h before opening in ZH11); TF and ZF indicate the time undergoing peak floret opening time (~10:00 am in TFB; ~12:00 noon in ZH11). **b** Venn Diagram showing the number of overlapping genes between the Cluster18 genes and up-regulated DEGs from T9 vs Z9. **c** Gene Ontology (GO) enrichment

analysis of 251 overlap genes in (b). MF indicates molecular function, BP indicates biological process. The term of "transcription factor activity" is highlighted in red. **d** Expression analysis of 11 transcription factors selected through GO analysis in (c). The numbers in the heatmap represent the average FPKM values. **e** Reverse transcriptional quantitative PCR (RT-qPCR) analysis of *OsMYB8* expression level in the lodicules of TFB and ZH11 at 9:00 am in June and October in 2021. Values are mean \pm SEM. ($n = 3$ biological replicates). Significance is evaluated by the two-sided Student's *t*-test at each time point, and *P* values are indicated. Source data are provided as a Source Data file.

peak opening time of the *Osmyb8^{TF}* mutants was about 1 h later than TFB (Fig. 3e, f). In addition, given that *OsMYB8* showed higher expression level in TFB than in ZH11, we also generated two transgenic lines expressing *OsMYB8* of TFB (including the coding sequence and 2-kb upstream promoter sequence) in the ZH11 background (*OsMYB8^{TF}/ZH11#1* and *OsMYB8^{TF}/ZH11#2*) (Fig. 3h, i). As shown in Fig. 3j, the peak opening time of the *OsMYB8^{TF}/ZH11* plants occurred ~0.5–1 h earlier than ZH11 (Fig. 3j, k). The daily number of opening florets of both the *Osmyb8* mutants and *OsMYB8^{TF}/ZH11* lines was comparable to that of the wild-type plants (Fig. 3d, g, l). Additionally, both the *OsMYB8* knockout lines in ZH11 and TFB backgrounds exhibited normal spikelet and stamen development, and their anthers also dehiscence normally (Supplementary Fig. 7a–c). Besides, I₂-KI (potassium iodide) solution staining experiments showed that the pollen fertility of the *Osmyb8* mutants were comparable to that of the WT plants (Supplementary Fig. 7d, e). Moreover, seed setting rates of

Osmyb8^{ZH1}#1 and *Osmyb8^{ZH1}#2* were comparable to ZH11, while *Osmyb8^{TF}#1* and *Osmyb8^{TF}#2* showed slightly lower seed setting rates compared to TFB (Supplementary Fig. 7f). These results demonstrated that *OsMYB8* primarily acts to promote rice floret opening but confer minimal influence on the pollen development and spikelet fertility.

Identification of the genome-wide direct targets of *OsMYB8*
Consistent with *OsMYB8* encoding an R2R3-MYB transcription factor, the *OsMYB8*-GFP fusion protein was localized to the nucleus in rice protoplasts (Fig. 4a). Moreover, transcriptional activity analysis of *OsMYB8* in yeast revealed that *OsMYB8* is a transcriptional activator and the activation domain is located at its C-terminus (Fig. 4b).

To identify the direct downstream targets of *OsMYB8*, we first performed DNA affinity purification sequencing (DAP-seq) to unravel its genome-wide binding sites. Purified recombinant GST-*OsMYB8* fusion protein (expressed in *E. coli*) was used to affinity purify the

sheared genomic DNA of 14-day old ZH11 seedlings, followed by deep sequencing (Supplementary Fig. 8a). In total, 27,764 binding peaks located within the regulatory regions of 20,832 genes were detected

(Supplementary Data 3), 70.74% of which were distributed in the promoter or intergenic regions, 13.26% and 11.82% were in the exon and the intron regions respectively, while 4.18% was in the 5'UTR and 3'

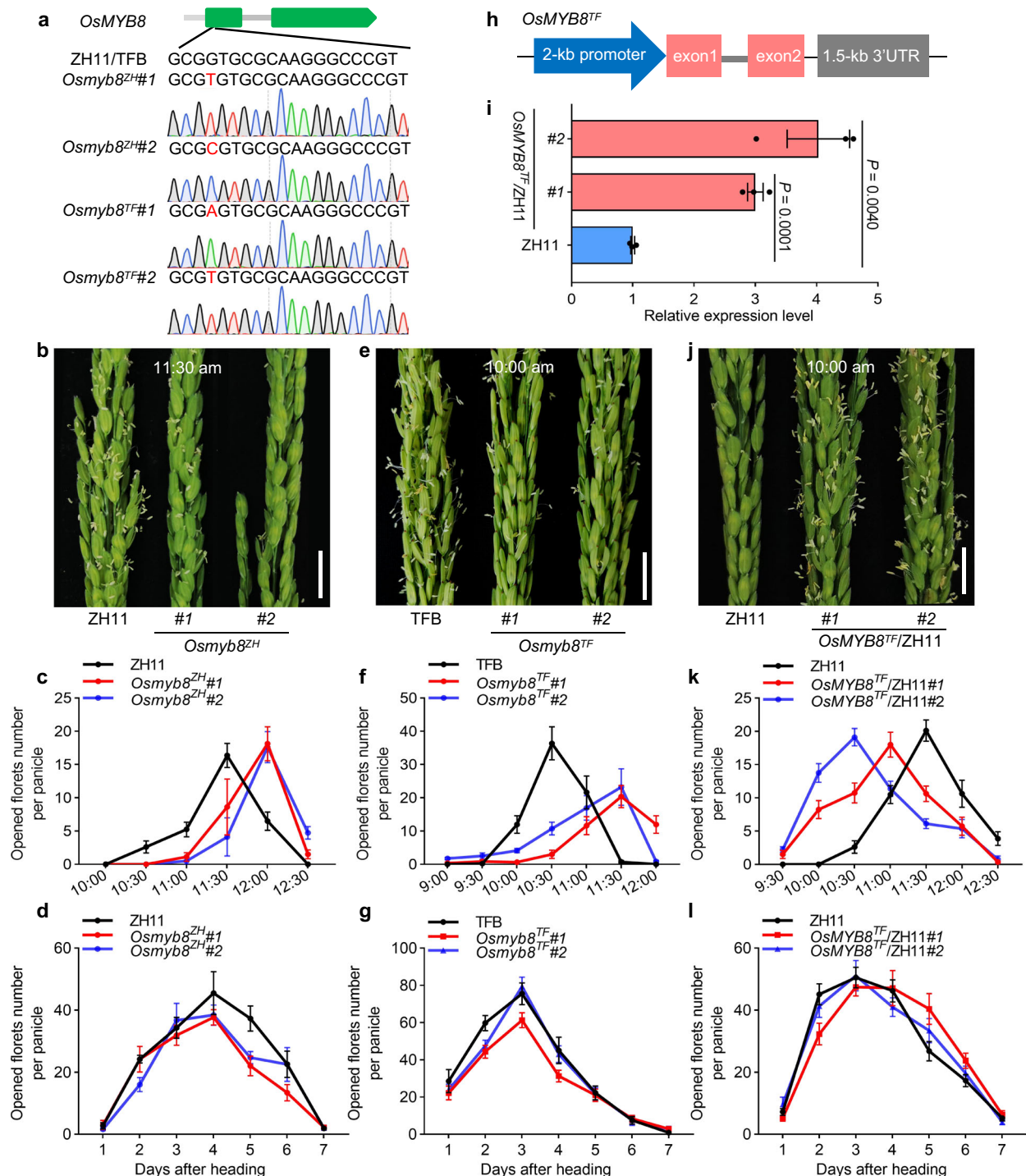


Fig. 3 | *OsMYB8* positively regulates rice DFOT. **a** Creation of the *Osmby8* mutants using the CRISPR/Cas9 genome editing approach. *Osmby8* mutants in ZH11 and TFB backgrounds were named as *Osmby8^{ZH}* and *Osmby8^{TF}* respectively. The upper panel shows a schematic diagram of the *OsMYB8* gene bearing the CRISPR/Cas9 target site. The mutation site was indicated in red. **b, e, j** Comparison of panicles in ZH11 and *Osmby8^{ZH}* mutants at 11:30 am (**b**) TFB and *Osmby8^{TF}* mutants at 10:00 am (**e**) ZH11 and *OsMYB8^{TF}*/ZH11 lines at 10:00 am in June 2021 in Guangzhou (**j**). Scale bars, 1 cm. **c, f, k** Number of opened florets per panicle in ZH11 and *Osmby8^{ZH}* mutants (**c**), TFB and *Osmby8^{TF}* mutants (**f**), and ZH11 and *OsMYB8^{TF}*/ZH11 lines (**k**) at different time points of the day in June 2021 in Guangzhou. Values are means \pm SEM. ($n = 8$

panicles). **d, g, i** Number of opened florets in ZH11 and *Osmby8^{ZH}* mutants (**d**), TFB and *Osmby8^{TF}* mutants (**g**), and ZH11 and *OsMYB8^{TF}*/ZH11 lines (**i**) at different days after heading in June 2021 in Guangzhou. Values are means \pm SEM. ($n = 10$ panicles). **h** Schematic diagram of the vector structure used for constructing *OsMYB8^{TF}*/ZH11 transgenic plants. **i** RT-qPCR analysis of *OsMYB8* transcripts levels in the lodicules of the *OsMYB8^{TF}*/ZH11 transgenic lines. ZH11 was used as a negative control. Values are means \pm SEM. ($n = 3$ biological replicates). Significance is evaluated by the two-sided Student's *t*-test, and *P* values are indicated. Source data are provided as a Source Data file.

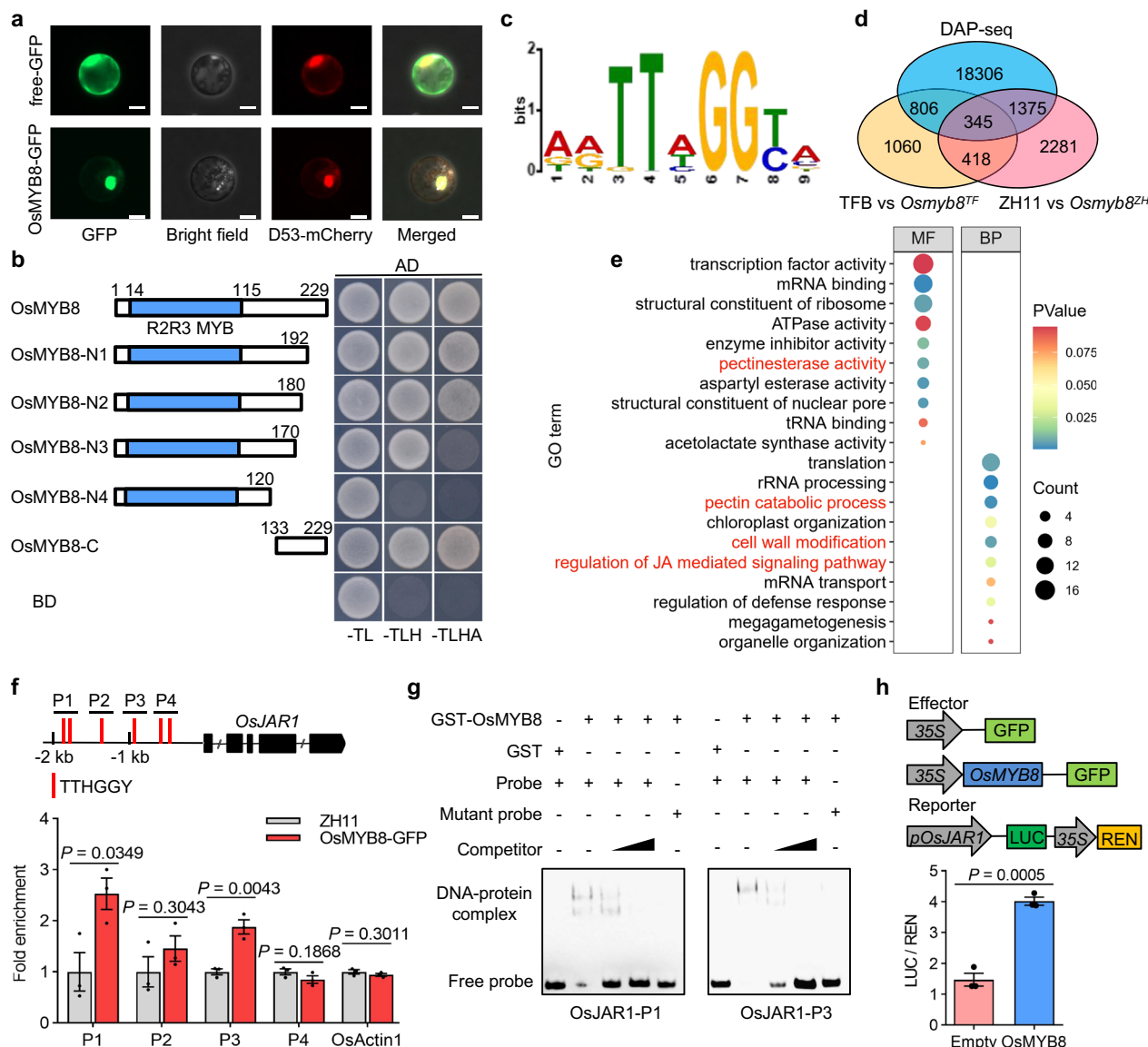


Fig. 4 | Identification of the genome-wide direct targets of OsMYB8. **a** Nuclear localization of OsMYB8-GFP in rice protoplasts. D53-mCherry was used as a nuclear marker. Scale bars, 20 μ m. **b** Yeast two-hybrid assay showing the transcriptional activity of OsMYB8. Left is the diagrams of full-length and truncated OsMYB8 proteins, which were fused with the DNA-binding domain (BD). **c** The core binding motif of OsMYB8 protein identified using MEME-ChIP. **d** Venn diagrams showing a comparison of DAP-seq binding genes with the identified DEGs in *Osmyb8* mutants by RNA-seq. **e** GO enrichment analysis of 345 overlap genes in (d). MF indicates molecular function, BP indicates biological process. **f** ChIP-qPCR analysis showing that OsMYB8 binds to the *OsJAR1* promoter in vivo. The upper panel is a diagram of *OsJAR1* promoter with the indicated regions used for detection by ChIP-qPCR. The red lines indicate the position of “TTHGGY” motifs in the *OsJAR1* promoter regions. Immunoprecipitation was performed with anti-GFP antibody, ZH11 was used as a

negative control. ($n = 3$ technical replicates). **g** EMSA assay showing that GST-OsMYB8 recombinant protein directly binds to the “TTHGGY” motif-containing regions of the *OsJAR1* promoter. Unlabeled probes were used as competitors. GST was used as a negative control. **h** Transient dual-LUC assay showing that OsMYB8 induces the transcriptions of *OsJAR1* promoter in rice protoplasts. The upper panel is diagrams of various constructs used in the transient expression assay. The expression level of REN was used as an internal control. The LUC/REN ratio represents the relative activity of the *OsJAR1* promoter. ($n = 3$ technical replicates). The Values in (f) and (h) are means \pm SEM. Significance is evaluated by the two-sided Student’s *t*-test, and *P* values are indicated. The subcellular localization experiments in (a) and the EMSA experiments in (g) were independently repeated three times with similar results. Source data are provided as a Source Data file.

UTR regions (Supplementary Fig. 8b). By using the MEME Suite, a representative DNA binding motif of MYB proteins with a core sequence of “TTHGGY” (H indicates A/T/G, Y indicates T/C) was significantly enriched among the OsMYB8 binding regions²³ (Fig. 4c). To verify the reliability of our DAP-seq result, we randomly selected 3 putative target genes, and further carried out electrophoretic mobility shift assays (EMSAs) using native promoter probes harboring the wild-type “TTHGGY” motif or its mutated forms “TTHAAY”. The results showed that OsMYB8 could directly bind to the native promoter probes, whereas mutations in the “TTHGGY” motif largely abolished

the binding of OsMYB8 (Supplementary Fig. 8c), thus confirming that OsMYB8 could directly bind to the “TTHGGY” motif.

To narrow down the potential direct targets of OsMYB8 for regulating rice DFOT, we performed RNA-seq of the lodicules of TFB and *Osmyb8^{TF}* collected at 9:00 am or lodicules of ZH11 and *Osmyb8^{ZH}* collected at 10:00 am. Correlation analysis showed very high correlation coefficients within three biological replicates for each group (Supplementary Fig. 8d). Among them, 2629 DEGs were identified between TFB vs. *Osmyb8^{TF}*, and 4419 DEGs were identified between ZH11 vs. *Osmyb8^{ZH}*, respectively (*P*-value < 0.05, absolute \log_2 FC ≥ 1 ;

Supplementary Fig. 8e, Supplementary Data 4, 5). By overlapping analysis of the DEGs and the OsMYB8 binding genes, we identified 345 potential genes that were differentially expressed in *Osmyb8* lodicules and directly bound by OsMYB8 (Fig. 4d). GO term analysis revealed significant enrichment of several molecular functions known to be related to lodicule swelling and closure, such as cell wall modification and regulation of JA-mediated signaling pathway (Fig. 4e, Supplementary Data 6). Among them, the *OsJARI* gene, which encodes an enzyme essential for the conversion of JA to active JA (JA-Ile)²⁴, was down-regulated in the lodicules of the *Osmyb8* mutants, but up-regulated in the lodicules of the *OsMYB8^{TF}/ZH11* lines (Supplementary Fig. 9a–c). RT-qPCR analysis revealed that similar to *OsMYB8*, the expression level of *OsJARI* in the lodicules of TFB and ZH11 increases as the floret opening time approaches (Supplementary Fig. 9d).

To verify that *OsJARI* is a direct target of OsMYB8, we analyzed the promoter region of *OsJARI*, and identified a set of OsMYB8 binding motifs (TTHGGY) in the 2-kb region upstream of the transcription start site (Fig. 4f). To examine the binding capacity of OsMYB8 to the *OsJARI* promoter in vivo, we generated two transgenic lines with stable expression of *OsMYB8-GFP* driven by the native *OsMYB8* promoter of TFB (Supplementary Fig. 10a–c). We also found that the *OsMYB8-GFP* lines exhibited about 1 h earlier DFOT than ZH11 (Supplementary Fig. 10d, e), suggesting that the OsMYB8-GFP fusion protein is biologically functional. ChIP-qPCR assays using florets of the *OsMYB8-GFP#2* transgenic line showed that anti-GFP antibody could specifically precipitate the P1 and P3 fragments containing the OsMYB8 binding motif in the *OsJARI* promoter (Fig. 4f). EMSAs also demonstrated that GST-OsMYB8 could directly bind to the P1 and P3 fragments of the *OsJARI* promoter (Fig. 4g). In addition, transient expression assay in rice protoplasts showed that *LUC* expression driven by the native *OsJARI* promoter was increased significantly when the reporter was co-transformed with the OsMYB8 effector in rice protoplasts (Fig. 4h). Taken together, our findings suggest that OsMYB8 directly activates *OsJARI* transcription.

OsMYB8 genetically acts upstream of *OsJARI* to regulate rice DFOT

To test whether *OsJARI* regulates rice DFOT, we performed targeted mutagenesis of *OsJARI* in the ZH11 background using the CRISPR/Cas9 technology. Two independent knockout lines (*Osjar1#1* and *Osjar1#2*) were obtained for phenotypic analysis (Fig. 5a). We counted the number of opened florets at different time points of ZH11 and *Osjar1* mutants in June 2022 in Guangzhou, and found that in contrast to ZH11, which had a peak DFOT at around 11:30 am, the *Osjar1* mutants displayed a scattered floret opening phenotype (random floret opening throughout the day), indicating that *OsJARI* is required for proper floret opening (Fig. 5b, c). As expected, measurement of JA-Ile in the lodicules of ZH11, *Osjar1* mutant and *Osmyb8^{zh}* showed that the JA-Ile content in the lodicules of *Osjar1* and *Osmyb8^{zh}* mutant was significantly lower than that of ZH11 (Fig. 5d). In contrast, the JA-Ile content of *OsMYB8^{TF}/ZH11* was significantly higher than that of ZH11 (Fig. 5e). These data together suggest that *OsMYB8* regulates JA-Ile content in lodicules to promote floret opening in rice.

To further determine the genetic relationship between *OsJARI* and *OsMYB8*, we introduced the *OsJARI* coding sequence driven by the *OsMYB8* promoter of TFB (which possesses high transcriptional activity in lodicules, Fig. 2d) into the *Osmyb8^{zh}* mutant background (Fig. 5f). Two independent transgenic lines (*OsJARI^{com}#1* and *OsJARI^{com}#2*) with higher *OsJARI* expression level in lodicules than that of ZH11 and *Osmyb8^{zh}* exhibited an intermediate peak DFOT between ZH11 and *Osmyb8^{zh}* (Fig. 5g–i), suggesting that up-regulation of *OsJARI* expression could partially complement the delayed DFOT of *Osmyb8^{zh}*. Moreover, we generated *OsMYB8^{TF}/Osjar1* line by crossing *OsMYB8^{TF}/ZH11* with an *Osjar1* line and found that the *OsMYB8^{TF}/Osjar1* line displayed a scattered floret opening phenotype, similar to *Osjar1*

(Fig. 5j, k). These observations support the placement of *OsJARI* downstream of *OsMYB8* to regulate DFOT in rice.

As genes related to cell osmolality and cell wall remodeling play a predominant role in DFOT regulation^{10,21} (Supplementary Fig. 2), we next tested whether dysfunction of *OsJARI* could influence their expressions. As expected, we found that a series of differentially expressed genes associated with carbohydrate metabolic process, sugar transport, cell wall organization, and water channel activity showed altered expression in the transcriptome data of TFB vs. *Osmyb8^{TF}* and ZH11 vs. *Osmyb8^{zh}* (Supplementary Fig. 11a), and most of the DEGs were down-regulated in lodicules of both *Osmyb8^{TF}* and *Osmyb8^{zh}*. Remarkably, four *Pectin Methylesterase* genes (*OsPME12/22/23/29*) were up-regulated, in line with the potential negative role of this gene family in DFOT regulation¹¹. We further performed RT-qPCR analyses to examine the expression changes of these genes in the lodicules of the *Osjar1* mutants. As expected, a large portion of genes exhibited similar changes to that of the *Osmyb8* mutants. For example, expression of *OsAmy2*, *Os4BGLU*, *OsSWEET11/15*, *OsEXPB7*, *OsXTH16*, *OsPG17* and *OsNIP1;1* was significantly decreased, while expression of *OsPME23/29* was significantly increased (Supplementary Fig. 11b, c). We further analyzed soluble sugar content in the lodicules of ZH11 and *Osmyb8^{zh}* collected at 10:00 am, and the result showed that the levels of sucrose, fructose and total soluble sugars were decreased in the lodicules of *Osmyb8^{zh}* (Supplementary Fig. 12). These results suggest that *OsMYB8-OsJARI* module likely influence floret opening by modulating the expression of genes related to lodicule hydration and expansion.

Natural variation in *OsMYB8* promoter confers DFOT divergence in *japonica* and *indica*

To look for the natural variation underlying differential expression of *OsMYB8* in *indica* and *japonica* rice, we conducted sequence analysis of the coding region and 2-kb promoter sequences of *OsMYB8* between TFB and ZH11. The results showed that there are six SNPs (−1176, −1244, −1286, −1469, −1550 and −1871) in the promoter and one synonymous SNP in the coding region (Fig. 6a). Based on the six SNPs, we performed haplotype analysis of the *OsMYB8* 2-kb promoter using 1973 *indica* (*Ind*), 767 *temperate japonica* (*Tej*), 504 *tropical japonica* (*Trj*), and 269 *Aus*²⁵ (Supplementary Data 7). A total of three haplotypes (Hap1–3) was identified in these rice accessions. Hap1 and Hap2 differed in six SNPs, while Hap3 differed from Hap1 at four SNPs (−1286, −1469, −1550, and −1871), and Hap2 at two SNPs (−1176 and −1244) (Fig. 6a). Hap1 was mainly present in the *Ind* accessions (including TFB). In contrast, 671 out of 767 (−88.0%) *Tej* accessions (including ZH11) carried Hap2. Hap3 was mostly detected in *Ind*, *Trj*, and *Aus* (Fig. 6b). To investigate whether *OsMYB8* has undergone selection during rice domestication, we surveyed the nucleotide diversity (π) across the *OsMYB8* genomic region using 295 *Ind* and 91 *Tej* from a rice core collection²⁶ and 185 *O. rufipogon* (*Ruf*)²⁷ (Supplementary Data 8). The nucleotide diversity of the *OsMYB8* 2-kb promoter region was extremely low in *Ind* ($\pi = 0.00074$) and *Tej* ($\pi = 0.00076$), as compared with that of *Ruf* ($\pi = 0.0053$), and was also much lower than that of the whole genome of *O. sativa* ($\pi = 0.0024$)²⁸ (Fig. 6c, Supplementary Data 9). Meanwhile, the fixation index (F_{ST}) value around *OsMYB8* exhibited a higher level of differentiation between the *Ind* and *Tej* populations (*Ind_Tej*) (Fig. 6d, Supplementary Data 10). These results indicate that *OsMYB8* has undergone divergent selection in the *indica* and *japonica* subspecies.

To further evaluate the functional difference between *OsMYB8^{Hap1}* and *OsMYB8^{Hap2}*, we analyzed dozens of accessions with Hap1 and Hap2, respectively (Supplementary Data 8). We found that the Hap1-carrying accessions exhibited earlier DOFT compared to the Hap2-carrying accessions (Fig. 6e). Furthermore, the Hap1-carrying accessions showed higher levels of *OsMYB8* gene expression and JA-Ile level

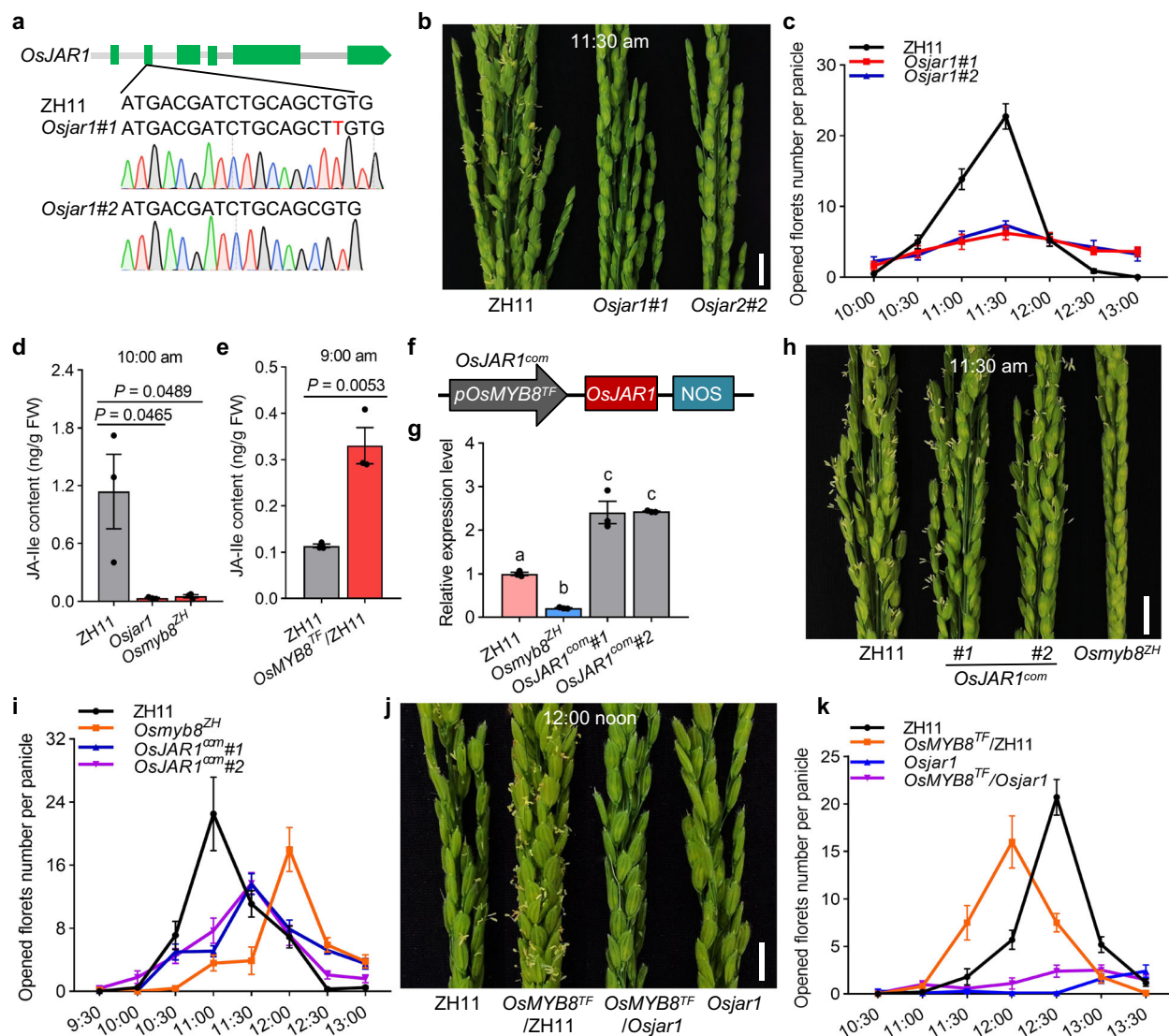


Fig. 5 | *OsJAR1* influences JA-Ile content in lodicule to regulate rice DFOT.

a Creation of the *Osjar1* mutants in ZH11 background using the CRISPR/Cas9 genome editing approach. The mutation site was indicated in red. **b** Comparison of panicles in ZH11 and *Osjar1* mutants at 11:30 am in June 2022 in Guangzhou. Scale bars, 1 cm. **c** Number of opened florets per panicle in ZH11 and *Osjar1* mutants at different time points of the day. Values are mean \pm SEM. ($n = 10$ panicles). **d, e** JA-Ile content in lodicules at 10:00 am of ZH11, *Osjar1*, and *Osmysb8^{zh}* (**d**) at 9:00 am of ZH11 and *Osmysb8^{TF}/ZH11* (**e**). Values are mean \pm SEM. ($n = 3$ biological replicates). Significance is evaluated by the two-sided Student's *t*-test, and *P* values are indicated. **f** Schematic diagram of the vector structure used for constructing *OsJAR1^{com}* materials. The *pOsMYB8^{TF}* means the promoter was amplified from TFB. **g** Relative

expression level of *OsJAR1* in the lodicules of ZH11, *OsJAR1^{com}* and *Osmysb8^{zh}*. Values are mean \pm SEM. ($n = 3$ biological replicates). Letters above the bars indicate significant differences ($P < 0.05$), as evaluated by one-way ANOVA with Tukey's multiple comparisons test. **h, j** Comparison of panicles in ZH11, *OsJAR1^{com}* and *Osmysb8^{zh}* at 11:30 am in June 2022 in Guangzhou (**h**) and in ZH11, *OsMYB8^{TF}/ZH11*, *OsMYB8^{TF}/Osjar1* and *Osjar1* at 12:00 noon in October 2022 in Guangzhou (**j**). Scale bars, 1 cm. **i** Number of opened florets in ZH11, *OsJAR1^{com}*, and *Osmysb8^{zh}* at different time points of the day in June 2022 in Guangzhou. Values are mean \pm SEM. ($n = 10$ panicles). **k** Number of opened florets in ZH11, *OsMYB8^{TF}/ZH11*, *OsMYB8^{TF}/Osjar1*, and *Osjar1* at different time points of the day in October 2022 in Guangzhou. Values are mean \pm SEM. ($n = 10$ panicles). Source data are provided as a Source Data file.

(Fig. 6f, g). Moreover, transient transcriptional activation experiments showed that the *OsMYB8^{Hap1}* promoter possessed higher transcriptional activity than the *OsMYB8^{Hap2}* promoter in rice protoplast (Fig. 6h). These findings suggest that the sequence variations between Hap1 and Hap2 might cause differential expression of the *OsMYB8*, thus conferring earlier DFOT in the Hap1-carrying varieties as compared to the Hap2-carrying varieties. To consolidate this notion, we introduced the TFB *OsMYB8* allele (*OsMYB8^{TF}*) containing the 2-kb promoter and intact coding region into the *Osmysb8^{zh}* mutant to generate complementary plants. Two independent transgenic lines with single copy insertion of *OsMYB8^{TF}* (*OsMYB8^{TF}/Osmysb8^{zh}#1*, *OsMYB8^{TF}/Osmysb8^{zh}#2*) were selected to be further analyzed (Supplementary Fig. 13). RT-qPCR analysis showed that the expression levels of *OsMYB8*

in lodicules of *OsMYB8^{TF}/Osmysb8^{zh}* plants were about 2-fold that of ZH11 and *Osmysb8^{zh}* mutant (Fig. 6i), similar to the expression difference of *OsMYB8* between TFB and ZH11 (Fig. 2d, e). Consistently, the expression level of *OsJAR1* was higher in *OsMYB8^{TF}/Osmysb8^{zh}* than in ZH11 and the *Osmysb8^{zh}* mutant, and the JA-Ile content in the lodicules of *OsMYB8^{TF}/Osmysb8^{zh}* was significantly higher than that of ZH11 (Supplementary Fig. 14). Phenotypic analysis showed that the *OsMYB8^{TF}/Osmysb8^{zh}* plants exhibited about 0.5 and 1 h earlier DFOT than ZH11 and the *Osmysb8^{zh}* mutant, respectively (Fig. 6j, k). These results together support the notion that the natural variation in the *OsMYB8* promoter contributes to the differential expression of *OsMYB8*, and thus divergence of DFOT in *indica* and *japonica* subspecies.

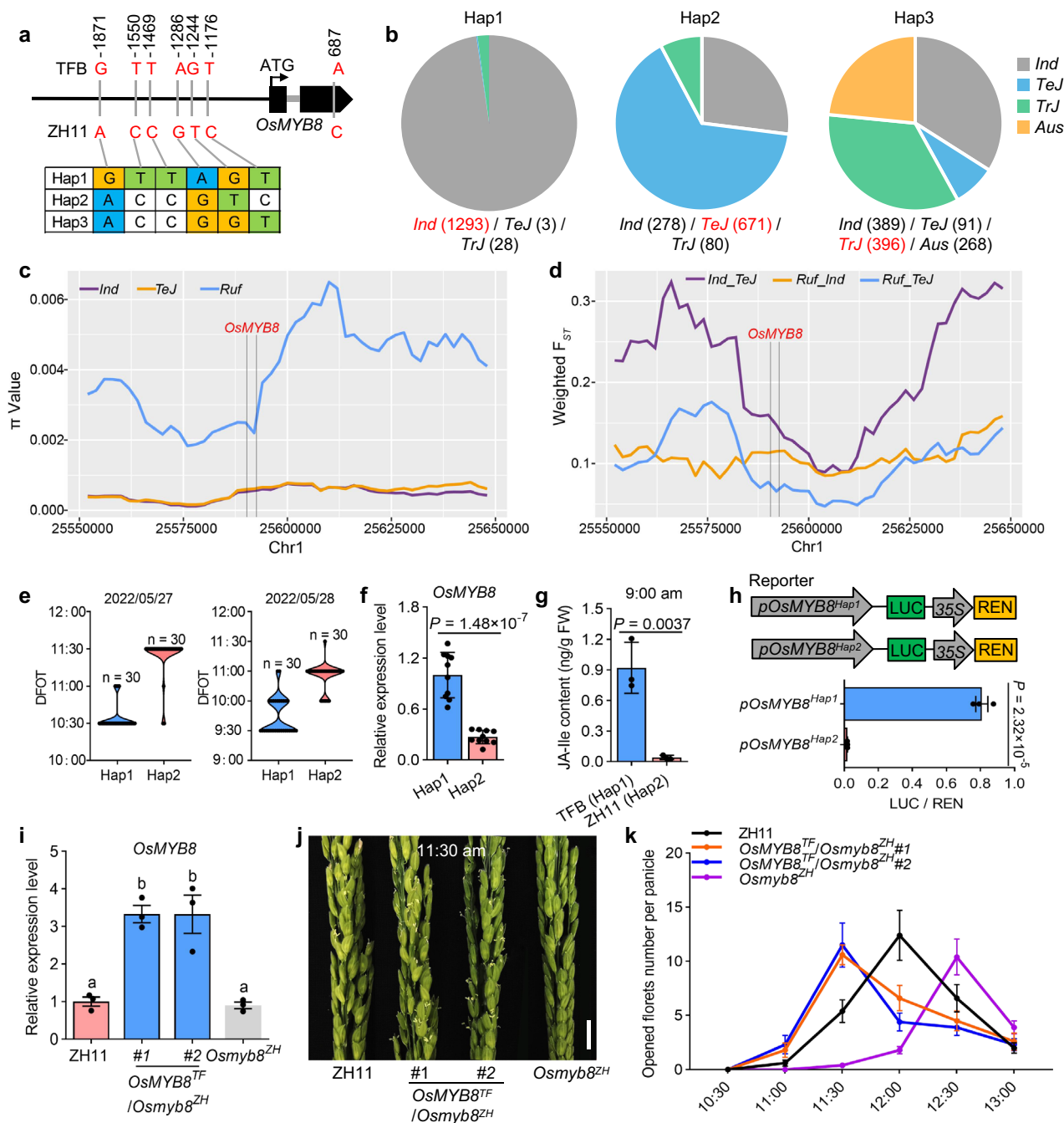


Fig. 6 | Natural variation in *OsMYB8* promoter confers DFOT divergence in japonica and indica. **a** Haplotype analysis of *OsMYB8* promoter in the 3513 rice germplasms. Nucleotide variations in the 2-kb promoter of *OsMYB8* were shown. **b** Distribution frequency of the three *OsMYB8* haplotypes in diverse Asian cultivated rice accession. The haplotype with the largest number was highlighted in red. **c** Nucleotide diversity (π) of a 100-kb genomic region surrounding *OsMYB8* in the *indica* (*Ind*), *temperate japonica* (*TeJ*) and *O. rufipogon* (*Ruf*). The regions (Chr1: 25,590,725–25,592,725) between two black vertical lines indicates the position of *OsMYB8* promoter. **d** F_{ST} values of *TeJ_Ind*, *Ruf_TeJ*, and *Ruf_Ind* in a 100-kb genomic region surrounding *OsMYB8*. The region (Chr1: 25,590,725–25,592,725) between two black vertical lines indicates the position of *OsMYB8* promoter. **e** The DFOT of the rice accessions with Hap1 and Hap2 in May 2022 in Guangzhou. ($n = 30$ accessions). **f** Relative expression levels of *OsMYB8* in lodicules of the rice accessions with Hap1 and Hap2, respectively. ($n = 10$ accessions). **g** JA-Ile content in TFB and ZH11

lodicules at 9:00 am. ($n = 3$ biological replicates). **h** Transient dual-luciferase assays showing the transcriptional activity of *pOsMYB8^{Hap1}* and *pOsMYB8^{Hap2}* in rice protoplasts. ($n = 3$ technical replicates). The values in **f–h** are shown as mean \pm SEM. Significance is evaluated by the two-sided Student's *t*-test, and *P* values are indicated. **i** Relative expression levels of *OsMYB8* in lodicules of ZH11, *OsMYB8^{TF}/Osmby8^{ZH}* transgenic lines and the *Osmby8^{ZH}* mutant. Values are mean \pm SEM. ($n = 3$ biological replicates). Letters above the bars indicate significant differences ($P < 0.05$), as evaluated by one-way ANOVA with Tukey's multiple comparisons test. **j** Comparison of panicles in ZH11, *OsMYB8^{TF}/Osmby8^{ZH}* transgenic lines and the *Osmby8^{ZH}* mutant at 11:30 am in October 2022 in Guangzhou. Scale bars, 1 cm. **k** Number of opened florets in ZH11, *OsMYB8^{TF}/Osmby8^{ZH}* transgenic lines, and the *Osmby8^{ZH}* mutant at different time points of the day in October 2022 in Guangzhou. Values are mean \pm SEM. ($n = 10$ panicles). Source data are provided as a Source Data file.

Potential breeding utilization of *OsMYB8*^{Hap1} in DFOT improvement of *japonica* varieties

The asynchronous DFOT of *indica* and *japonica* could severely reduce the efficiency of cross-pollination and large-scale hybrid seed production, causing high price of the hybrid seeds. To evaluate the breeding potential of the *OsMYB8*^{Hap1} allele in DFOT improvement of *japonica* varieties, we introduced the TFB allele of *OsMYB8* into ZH11 through backcrossing and marker-assisted selection. The near-isogenic line (NIL) NIL^{TFB} with the introgressed *OsMYB8*^{TFB} allele in ZH11 background was selected from BC₄F₃ plants. We also acquired a chromosome segment substitution line CSSL⁹³¹¹ that carries a 13 Mb genome segment containing *OsMYB8* from the donor parent 9311 (an *indica* variety) in the *japonica* variety XiuShui134 (XS134) background²⁹. Under field conditions, NIL^{TFB} and CSSL⁹³¹¹ plants exhibited about 0.5 h earlier DFOT than their recurrent parents (Fig. 7a, b, d, e), without obvious impacts on the tiller number, plant height, heading date, panicle traits, and seed setting rate (Supplementary Fig. 15). In addition, RT-qPCR results showed that the expression levels of *OsMYB8* and *OsJARI* in NIL^{TFB} and CSSL⁹³¹¹ lodicules were higher than that in ZH11 and XS134, respectively (Fig. 7c, f). Therefore, the *OsMYB8*^{Hap1} allele could promote floret opening in *japonica* varieties, conferring great potential to improve *japonica* DFOT and hybrid seed production.

Discussion

Indica and *japonica* are two subspecies of Asian cultivated rice domesticated from the wild rice *O. rufipogon*²⁸. Due to long-term adaptation to different ecological niches, *indica* and *japonica* rice have evolved to exhibit a differentiated DFOT, which might be beneficial for promoting prezygotic reproductive isolation by preventing mating and hybridization, thus facilitating divergence of these two subspecies. However, the asynchronised DFOT of the *indica* and *japonica* parental lines hindered the utilization of the strong heterosis of *indica-japonica* hybrid rice. DFOT is a complex quantitative trait and is easily affected by environmental factors (such as light, temperature and humidity)^{30–33}. Although a number of quantitative trait loci (QTL) for DFOT has been previously mapped to different chromosomes of rice, none of them has been molecularly cloned, largely due to the difficulty in precise phenotyping and the small additive effects of the individual locus (typically less than 10% phenotypic variance)^{34–38}. In this study, we identified *OsMYB8* as a key regulator of DFOT in both *indica* and *japonica* rice through comprehensive comparative, time-course transcriptome analyses of the lodicules of a representative *indica* TFB and a representative *japonica* ZH11. We showed that expression of *OsMYB8* is up-regulated in the lodicules before floret opening and reaches a plateau at the peak opening time, then gradually declines (Fig. 2d, Supplementary Fig. 5). We further identified *OsJARI* as a direct target gene of *OsMYB8*, which acts to promote the conversion of JA into biologically active JA-Ile and regulate the expression of genes related to cell osmolality and cell wall remodeling in the lodicules, thus promoting floret opening. Strikingly, we demonstrated that natural variation (6 SNPs) in the 2-kb promoter region of *OsMYB8* confers higher expression of *OsMYB8*, and thus higher expression of *OsJARI* and higher accumulation of JA-Ile in lodicule cells, ultimately leading to earlier DFOT in *indica* rice compared to *japonica* rice (Fig. 7g). Thus, our results provided insights into the genetic and molecular regulation of DFOT in rice.

Previous studies have documented ample evidence that jasmonate is a vital hormone regulating multiple reproductive processes including flower opening time, and stamen/female organ development, and fertility^{39,40}. MYB transcription factors, especially R2R3-MYB members, have been shown to function as key regulators in JA-mediated flower opening and floral organ development in different plant species^{41,42}. For example, AtMYB21/24, two homologs of *OsMYB8*,

are targets of JAZ repressors and could interact with MYC2/3/4/5 to regulate petal elongation (thus leading to petal opening), stamen development, and pollen fertility in *Arabidopsis*^{43,44}. The tomato homolog SIMYB21 regulates floret opening as well as carpel and ovule development, through promoting JA biosynthesis in a positive-feedback manner⁴⁵. Previous studies have also reported that the rice mutants deficient in JA biosynthesis and signaling, such as *allene oxide cyclase* (*Osaoc*), *oxophytodienoate reductase 7* (*Osopr7*), *jasmonate resistant 1* (*Osjar1*) and *coronatine insensitive* (*Oscoi1a*, *Oscoi1b* and *Oscoi2*) mutants, usually exhibit defects in spikelet morphology, anther dehiscence, flower opening and spikelet fertility^{46–49}. In this study, we showed that *OsMYB8* acts upstream of *OsJARI* to promote JA synthesis, and the *Osmyb8* mutant exhibits delayed DFOT, but normal spikelet morphology, pollen maturation, and fertility (Supplementary Fig. 7), suggesting that *OsMYB8* mainly functions in controlling the floret opening time, and it represents an elite gene resource for improving DFOT in rice, with minimal negative pleiotropic effect on stamen development. Notably, phylogenetic analysis identified an *OsMYB8-like* gene in the rice genome that shares 45.2% homology with *OsMYB8* (Supplementary Fig. 3, Supplementary Fig. 16a), and it was preferentially expressed in stamen (Supplementary Fig. 16b), hinting a possible role in regulating stamen development. Further studies are required to elucidate the biological function of the *OsMYB8-like* gene in the future.

Earlier studies have shown that the lodicule undergoes dramatic changes in multiple physiological processes during floret opening and closure, including an increase in soluble sugar content, which leads to a rise in cell osmotic pressure to drive water uptake by the lodicules¹³. An earlier study has demonstrated a critical role of auxin signaling cascade in regulating floret opening. The authors demonstrated that *OsARF2* and *OsARF18* antagonistically regulate the expression of *OsSUT1* (a sucrose transporter gene) to regulate sucrose transport from the source tissues (vegetative organs) into the sink tissues (reproductive organs) and floret opening⁵⁰. It will be worthy to investigate how the *OsMYB8*-mediated JA signaling pathway cross-talks with the auxin signaling pathway to coordinately regulate DFOT in future studies. In addition, recent studies have demonstrated that *DFOT1/EMF1* negatively regulate DFOT through modulating the activity of pectin methylesterases (PMEs), thus loosening the stiffness of cell walls of lodicules cells^{11,20}. In this study, our transcriptome and RT-qPCR analyses indicated that *OsMYB8* regulates the expression levels of various genes related to the cell wall modification. In addition, we also observed that the expression of these genes was altered in the lodicules of the *Osjar1* mutants. Thus, we speculate that *OsMYB8-OsJARI* module likely regulates floret opening through regulating cell wall relaxation and expansion. It is also worth noting that DFOT is easily affected by environmental factors, such as light, temperature, and humidity^{30–33}. We found that the *OsMYB8* promoters of *japonica* and *indica* varieties contain various cis-elements responsive to light, temperature, and hormones based on sequence analysis with PLANTCARE. How these external factors influence the expression of *OsMYB8*, and thus DFOT will be an interesting avenue for future research.

Inter-subspecific *indica-japonica* hybrid rice was proposed to be an important direction of future rice breeding due to its superior heterosis. Nevertheless, current breeding and utilization of *indica-japonica* hybrid rice is still hampered by asynchronised DFOT (and thus low yield of hybrid seed production) in the *indica* and *japonica* parental lines. In this study, we showed that elevating expression level of *OsMYB8* in the *japonica* background or introgression of the Hap1 allele of *OsMYB8* from *indica* varieties into *japonica* varieties could promote DFOT over half an hour, thus effectively reducing the interval between the DFOT of *indica* and *japonica* varieties (Fig. 7a, b, d, e). Importantly, we did not find any significant negative impact of the introgression of *OsMYB8*^{Hap1} allele on other agronomic

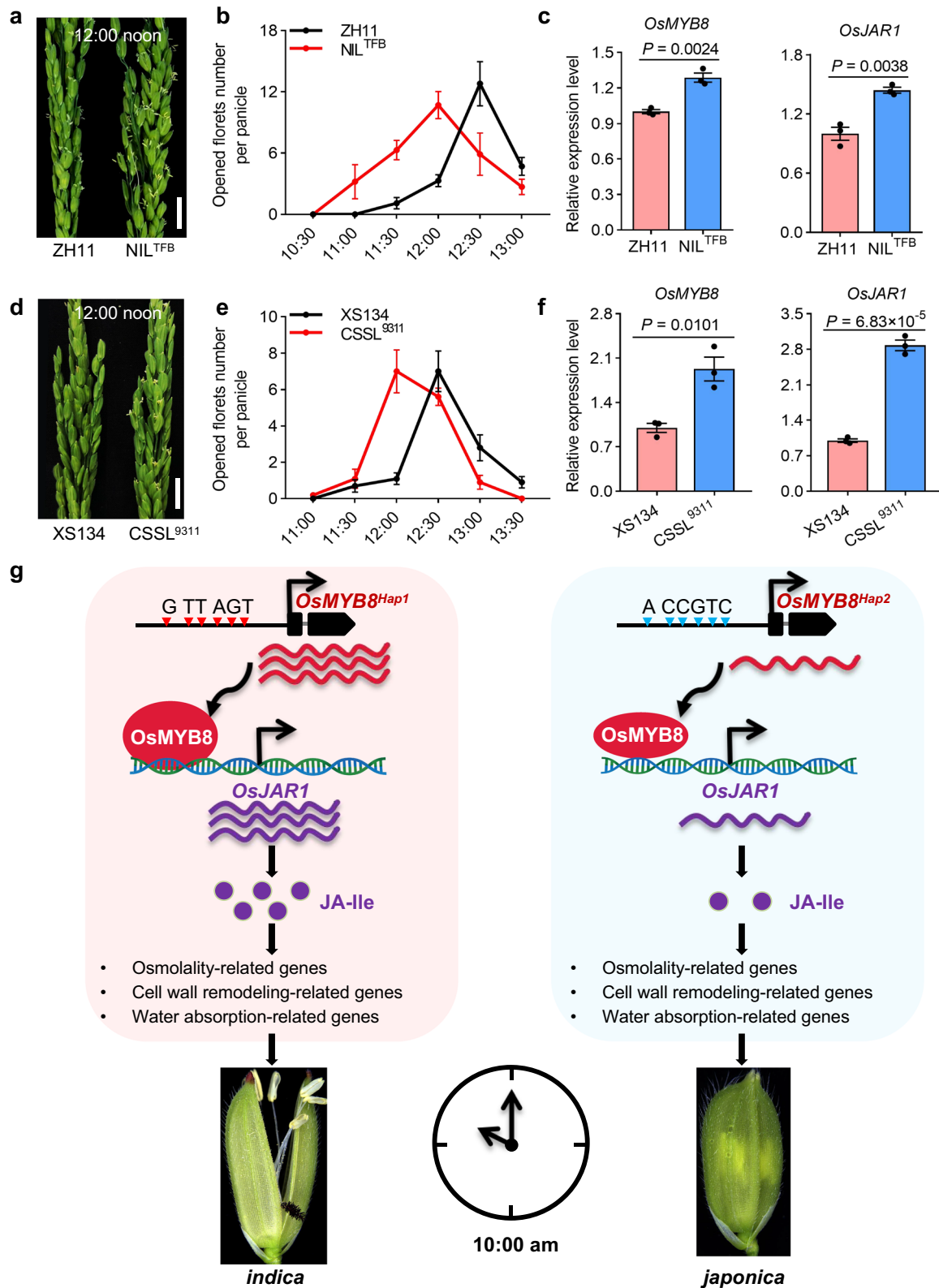


Fig. 7 | The *indica* allele of *OsMYB8* promotes *japonica* DFOT. a, d Comparison of panicles in ZH11 and NIL^{TFB} (a) XS134 and CSSL⁹³¹¹ (d) at 12:00 noon in October 2022 in Guangzhou. Scale bars, 1 cm. **b, e** Number of opened florets in ZH11 and NIL^{TFB} (b) XS134 and CSSL⁹³¹¹ (e) at different time points of the day in October 2022 in Guangzhou. Values are mean \pm SEM. ($n = 10$ panicles). **c, f** Relative expression levels of *OsMYB8* and *OsJAR1* in lodicules of ZH11 and NIL^{TFB} (c) XS134 and CSSL⁹³¹¹ (f).

Values are mean \pm SEM. ($n = 3$ biological replicates). Significance is evaluated by the two-sided Student's *t*-test, and *P* values are indicated. **g** A model depicting an *OsMYB8*-*OsJAR1* module regulating differential DFOT in *indica* and *japonica* rice. Natural variation in the promoter sequences of *OsMYB8* confers higher expression level of *OsMYB8* in *indica*, thus higher accumulation of JA-Ile and earlier DFOT in *indica* as compared to *japonica*. Source data are provided as a Source Data file.

traits (plant architecture and heading date, Supplementary Fig. 14). Thus, further manipulation of *OsMYB8* expression levels may offer a feasible approach to facilitate hybrid seed production and utilization of inter-subspecific *indica-japonica* hybrid rice.

Methods

Plant materials and growth conditions

Rice cultivar ZhongHua11 (ZH11) (*Oryza sativa* cv. *Japonica*) and TianFengB (TFB) (*Oryza sativa* cv. *Indica*) were used as wild-type controls for mutation or transgenic analyses. The 529 core rice germplasm resources were supplied by National Key Laboratory of Crop Genetic Improvement, Huazhong Agricultural University²⁶ (Supplementary Data 8). A total of 40 elite rice varieties, including 12 *japonica* varieties and 28 *indica* varieties, were kindly supplied by D. Zhou and were used for DFOT investigation (Supplementary Data 1). XiuShui134 (XS134) and the CSSL line carrying *OsMYB8^{zh}* were kindly provided by B. Hu and C. Chu. For NIL^{TFB} construction, F₁ of ZH11 and TFB plants were backcrossed with ZH11, and NIL^{TFB} were selected in the BC₄F₃ generation with molecular markers. All rice plants were grown in the experimental field of the South China Agricultural University in Guangzhou (23°7' N, 113°15' E) from March to November in 2019 to 2023, and in Lingshui, Hainan (18°22' N, 109°45' E) from November to April in 2019 to 2023.

Transgene construct preparation and rice transformation

To generate the *Osmyb8* and *Osjar1* knockout lines, gene-specific guide RNA sequences were designed with an online software toolkit CRISPR-GE⁵¹ and cloned into the CRISPR/Cas9 binary vector *pYLCRISPR/Cas9-Pubi-H²*. To generate the *OsMYB8^{TF}/ZH11* and *OsMYB8^{TF}/Osmyb8^{zh}* transgenic lines, the *OsMYB8* genomic fragment (including 2-kb promoter, coding region, and 1.5 kb 3'UTR) was amplified from TFB gDNA and inserted into the *pCAMBIA1300* vector, forming a recombinant plasmid *p1300-OsMYB8*. To generate the *proOsMYB8::GUS* construct, the 2-kb promoter sequence of *OsMYB8* was amplified from TFB gDNA and cloned into *pCAMBIA1305.1* for plant transformation. To construct the *proOsMYB8::JAR1* plasmid, the *OsJAR1* coding sequence was amplified from ZH11 cDNA and cloned into the *pCAMBIA1300* vector driven by the 2-kb promoter sequence of *OsMYB8* from TFB gDNA. To generate the *proOsMYB8::OsMYB8-GFP* construct, the *OsMYB8* coding sequence (without stop codon) was amplified from ZH11 cDNA and cloned into the *pOx-eGFP* vector driven by the 2-kb promoter sequence of *OsMYB8* from TFB gDNA. The above constructs were transformed into indicated background by Agrobacterium-mediated transformation (Bioneer Biological Company, China). Hygromycin (hyg) was used for screening the positive transgenic lines. The mutation sites or gene expression levels were examined by DNA sequencing or RT-qPCR analysis. The primers used for vector constructions are listed in Supplementary Data 11.

Measurement of the water content in lodicules

100 pairs of lodicules were carefully extracted from the florets and collected as one sample. The fresh weight of each sample was firstly measured using an analytical balance. Then, the samples were dried at 65 °C overnight, and the dry weight of each sample was measured again. The water content of the lodicules was determined by subtracting the dry weight from the fresh weight. Three biological replicates were performed for each sample.

RNA extraction and RT-qPCR analysis

Total RNAs were extracted from lodicules and other tissues using TRIzol reagent (Thermo Fisher, USA). The complementary DNAs (cDNAs) were synthesized by reverse-transcription according to the manufacturer's instructions (Yeasen, China). RT-qPCR was performed using the LightCycler96 real-time PCR system (Roche, Switzerland) with the qPCR SYBR Green Master Mix (Yeasen, China) according to

the manufacturer's instructions. The *OsActin1* gene (*LOC_Os03g50885*) was used as the internal control. The expression level of genes was calculated using the 2^{-ΔCt} method. All the primers used for RT-qPCR above are shown in Supplementary Data 11.

RNA-seq analysis

The lodicules of rice were separated by tweezers and were frozen immediately in liquid nitrogen for RNA-seq analysis. Three biological replicates were performed for each sample, except for the samples of TF with two biological replicates. RNA sequencing was performed at the Azenta company using the Illumina HiSeq platform. For data analysis, the processed reads were compared with Hisat2 v2.0.1⁵³ to the reference genome MSU Release 7.0⁵⁴. HTSeq v0.6.1⁵⁵ was used for quantitative analysis of genes. DESeq2⁵⁶ was used for differential expression analysis, and *P*-value < 0.05, absolute log₂FC ≥ 1 were used for screening of the differentially expressed genes. The Gene Ontology (GO) analysis was conducted with the David database (<https://david.ncifcrf.gov/home>).

GUS staining and histological observation

For histochemical analysis, the florets about 1–2 h before opening from *proOsMYB8::GUS* transgenic lines were collected for staining using the GUS stain Kit (Coolaber, China) according to the manufacturer's protocol. After staining, the florets were decolorized with 70% (v/v) ethanol and photographed under a Zeiss dissecting microscope.

Subcellular localization

To determine the subcellular localization of *OsMYB8*, the coding sequence of *OsMYB8* without the stop codon was amplified from cDNA of the ZH11 and cloned into the *pCAMBIA1305-35S::GFP* vector, resulting in the *35S::OsMYB8-GFP* construct. The nuclear-localized protein D53 fused with mCherry was used as a nuclear marker⁵⁷. The *35S::OsMYB8-GFP* and *p35S::D53-mCherry* fusion constructs were transiently co-transformed into rice protoplasts. The GFP and mCherry fluorescence in protoplasts were observed with a confocal microscope (Zeiss LSM780, Germany).

Droplet digital PCR

Droplet digital PCR (ddPCR) was performed to select single copy transgene of *OsMYB8^{TF}* in the *Osmyb8^{zh}* background⁵⁸. The ddPCR reaction mixture consists of 10 μL of 2 × ddPCR super mix for probes (Bio-Rad, USA), 50–100 ng DNA, 900 nM *OsMYB8* primers/250 nM probe (5' FAM, 3' BHQ1), 900 nM *OsActin1* primers/250 nM probe (5' HEX, 3' BHQ1) and variable ddH₂O in a final volume of 20 μL. The entire reaction mixture was loaded into a disposable plastic cartridge (Bio-Rad, USA) together with 60 μL of droplet generation oil (Bio-Rad, USA) and placed into the droplet generator (Bio-Rad, USA). After processing, the droplets generated from each sample were transferred to a 96-well PCR plate (Eppendorf, Germany). PCR amplification was carried out on a T100 Touch thermal cycler (Bio-Rad, USA) using a thermal profile beginning at 95 °C for 10 min, followed by 45 cycles of 94 °C for 10 s, and 58 °C for 60 s, and ending of 98 °C for 10 min at a ramp rate of 2 °C/s. After PCR, the plate was loaded on the droplet reader (Bio-Rad, USA). The Data were analyzed using the QuantaSoft Analysis Pro software (Bio-Rad, USA).

DAP-seq analysis

DAP-seq (DNA affinity purification sequencing) is a method used to identify DNA-binding sites of transcription factors⁵⁹. Briefly, 10 μg of ZH11 genomic DNA was broken into 200-bp fragments, fragmented gDNA were constructed into libraries using the VAHTS Universal Pro DNA Library Prep Kit for Illumina (Vazyme, China). The coding sequence of *OsMYB8* was cloned into the *pGEX-4T1* vector to generate the *GST-OsMYB8* recombinant construct. GST-

OsMYB8 recombinant protein or GST protein were purified from *E. coli* strain (DE3) with Glutathione Sepharose Beads (Sangon, China). The production of GST-OsMYB8 recombinant protein was induced by the addition of 0.4 mM isopropyl β-D-thiogalactopyranoside and grown at 16 °C overnight, and then were purified with GST 4FF Sefinose (TM) Resin Kit (Sangon Biotech, China) according to the manufacturer's protocol. The purified protein was incubated with 500 ng adaptor-ligated gDNA library at room temperature for 2 h before washing away the unbound DNA fragments. The GST proteins were used as the controls. The eluted DNAs were then sequenced using the Illumina HiSeq sequencing platform with two technical replicates.

The clean reads were aligned to the reference genome MSU Release 7.0 using Bowtie2 v2.3.5.1⁶⁰. Aligned reads were sorted and duplicated reads were removed by SAMtools v1.12⁶¹. Peaks were called using MACS2 v2.1.0⁶² ($P < 0.01$). Peaks were identified using the MEME-ChIP online software (<https://meme-suite.org/meme/>). Putative genes associated with peaks were annotated using ChIP-seeker v1.32.1⁶³.

Yeast two-hybrid assay

For Y2H assay, the full-length or truncated CDS of *OsMYB8* were amplified and cloned into the vector *pGBKT7*, and then the recombinant plasmid and *pGADT7* were co-transformed into AH109 yeast cells mediated by PEG4000. The positive transformants were first selected on the (SD)/-Leu/-Trp medium and then transferred to (SD)/-His/-Leu/-Trp and (SD)/-Ade/-His/-Leu/-Trp selection medium (Coolaber, China). The empty vector *pGBKT7* and *pGADT7* were co-transformed as negative controls.

Electrophoretic mobility shift assay

Native and mutated probes were synthesized and labeled with biotin using the electrophoretic mobility shift assay (EMSA) Probe Biotin Labeling Kit (Beyotime, China). EMSAs were carried out using a Chemiluminescent EMSA Kit (Beyotime, China). Briefly, biotin-labeled probes were incubated for 20 min with the GST or GST-OsMYB8 protein in the binding buffer at room temperature. For competition reaction, 5× and 20× unlabeled cold probes were mixed with the labeled probes. The DNA-protein complex was separated by 5% native polyacrylamide gel electrophoresis and the signal of biotin was photographed using the Biostep Celvin S420 system (Biostep, German). The probes used in this study are listed in Supplementary Data 11.

Transient transcription dual-LUC assay

For dual-LUC assay, the -2-kb *OsARI* promoter was amplified and inserted into the *pGreenII0800-LUC* vector to generate the reporter plasmid. The *OsMYB8* coding sequence without stop codon was amplified and inserted into the *pUC19* vector to generate the effector plasmid. The effector and reporter plasmids were co-transformed into rice protoplasts and incubated in darkness at 28 °C for 12 h. The protoplasts were collected and disintegrated in passive lysis buffer provided in Dual-Luciferase Reporter Gene Assay Kit (Yeasen, 11402ES60). Luciferase activity was also measured using GloMax2020 (Promega) following the manufacturer's instructions. Renilla luciferase (REN) driven by 35S promoter in *pGreenII0800-LUC* was used as the internal control. The relative firefly luciferase activity was counted as the ratio of LUC/REN for each sample.

Chromatin immunoprecipitation assay

For ChIP assays, rice florets of the ZHI1 and transgenic *pOsMYB8::OsMYB8-GFP* plants were harvested and cross-linked in a fixation buffer with 1% (v/v) formaldehyde under vacuum for 20 min. Glycine was added to terminate the cross-linking reaction. The prepared

chromatin complexes were sonicated into 200–500 bp fragments and then precleared with protein A magnetic beads (Merck Millipore, USA)⁶⁴. For immunoprecipitations, Anti-GFP (Nanobody) Magnetic beads (ABclonal, China) were added into samples and incubated overnight at 4 °C. DNA was precipitated with magnetic beads. For the real-time-qPCR reaction, the precipitated DNA was recovered and dissolved in water as the template. The enrichment was standardized to the input DNA to obtain the fold enrichment. An unrelated DNA sequence from the rice *OsActin1* gene was used as an internal control. All relevant primers used in the ChIP assay are listed in Supplementary Data 11.

Measurement of JA-Ile concentration

The quantification of JA-Ile was conducted by Wuhan Metware Biotechnology Co., Ltd, located in Wuhan, China. Approximately 50 mg of lodicules sample was frozen in liquid nitrogen and ground into a fine powder. The sample extracts were analyzed using an LC-ESI-MS/MS system (HPLC: Shim-pack UFLC SHI-MADZU CBM30A system; Shimadzu MS, Applied Biosystems 6500 Triple Quadrupole). The analytical conditions of HPLC were as follows, LC: column, Waters ACQUITY UPLC HSS T3 C18 (100 mm × 2.1 mm, 1.8 μm); solvent system, water with 0.04% acetic acid (A), acetonitrile with 0.04% acetic acid (B); gradient program, started at 5% B (0–1 min), increased to 95% B (1–8 min), 95% B (8–9 min), finally ramped back to 5% B (9.1–12 min); flow rate, 0.35 mL/min; temperature, 40 °C; injection volume: 2 μL. The ESI source operation parameters were as follows: ion source, ESI±; source temperature 550 °C; ion spray voltage (IS) 5.5 kV (positive), -4.5 kV (negative); curtain gas (CUR) was set at 35 psi, respectively. The contents of JA-Ile were determined using an internal standard method, with three biological replications performed for each sample.

Measurement of sugar concentration

The quantification of sugar in the lodicules was conducted by Wuhan Metware Biotechnology Co., Ltd, Wuhan, China. The freeze-dried materials were crushed using a mixer mill (MM 400, Retsch) with a zirconia bead for 1.5 min at 30 Hz. 20 mg of powder was diluted to 500 μL with methanol: isopropanol: water (3:3:2 V/V/V), vortexed for 3 min and ultrasound for 30 min. The extract was centrifuged at 13,188 × *g* under 4 °C for 3 min. 50 μL of the supernatant was mixed with 20 μL internal standard (ribitol, 100 μg/mL) and evaporated under nitrogen gas stream. The evaporated sample was transferred to the lyophilizer for freeze-drying. The residue was used for further derivatization. The derivatization method was as follows: the sample was mixed with 100 μL solution of methoxyamine hydrochloride in pyridine (15 mg/mL). The mixture was incubated at 37 °C for 2 h. Then 100 μL of BSTFA was added into the mixture and kept at 37 °C for 30 min after vortex-mixing. The mixture was analyzed using GC-MS after being diluted to an appropriate concentration. Agilent 7890B gas chromatograph coupled to a 7000 D mass spectrometer with a DB-5MS column (30 m length × 0.25 mm i.d. × 0.25 μm film thickness, J&W Scientific, USA) was employed for GC-MS analysis of sugars. Helium was used as carrier gas, at a flow rate of 1 mL/min. Injections were made in the split mode with a split ratio 3:1 and the injection volume was 3 μL. The oven temperature was held at 170 °C for 2 min, and then raised to 240 °C at 10 °C/min, raised to 280 °C at 5 °C/min, raised to 310 °C at 25 °C/min, and held at the temperature for 4 min. All samples were analyzed in selective ion monitoring mode. The ion source and transfer line temperature were 230 °C and 240 °C, respectively. Three biological replicates were performed for each sample.

Phylogenetic analysis of R2R3-MYB transcription factors

There are 89 and 124 R2R3-MYB transcription factors in rice and *Ara-bidopsis* respectively⁶⁵. The full-length protein sequences of R2R3-MYB

transcription factors from both the rice and *Aarabidopsis* genomes were obtained from Ensembl database (<http://plants.ensembl.org/index.html>). These sequences were then aligned using ClustalW in MEGA7⁶⁶. A neighbor-joining phylogenetic tree was constructed based on the alignment, using the poisson correction method and pairwise deletion of gaps. The reliability of the tree was assessed by bootstrap analysis with 1000 replicates.

Haplotype analysis

The 2-kb promoter sequence of *OsMYB8* in 3513 cultivated rice accessions were retrieved from the RiceVarMap2.0 database (<http://ricevarmap.ncpgr.cn/v2/>), and haplotype analysis was carried out using the method in the database. Only haplotypes found in ≥ 10 rice accessions were recorded.

Nucleotide diversity and fixation index calculation

The raw sequencing data of the 386 cultivated rice were downloaded from NCBI with BioProject PRJNA171289 ($>2.5\times$ per genome)²⁶. The raw sequencing data of the 185 wild rice were downloaded from NCBI with BioProject accession number PRJNA658215 ($>5\times$ per genome)²⁷. We mapped the reads to the reference genome MSU Release 7.0 using BWA v0.7.12⁶⁷, sorted and indexed the resulting BAM files using SAMtools v1.12⁶¹. The SNPs were identified using GATK v4.2.0.0⁶⁸, the GVCfs of each sample were generated with HaplotypeCaller. We then used CombineGVCfs and GenotypeGVCfs to generate VCF file, the variations were further filtered by VariantFiltration. Nucleotide diversity (π) and fixation index (F_{ST}) of *OsMYB8* in wild rice and cultivated rice were calculated using VCFtools v0.1.16⁶⁹ with 20-kb windows and 2-kb steps on the 100-kb region.

Statistical analysis

We used GraphPad Prism 8 for statistical analysis. Data are mean \pm SEM. Two-sided unpaired Student's *t*-test was used to test the significant difference between two groups. Three groups and more were analyzed by one-way analysis of variance (ANOVA) with Tukey's multiple comparisons test.

Reporting summary

Further information on research design is available in the Nature Portfolio Reporting Summary linked to this article.

Data availability

DAP-seq and RNA-seq data generated in this study have been deposited in the NCBI Sequence Read Archive database under the accession number [PRJNA1000954](#) and [PRJNA1000956](#), respectively. Source data are provided with this paper.

References

- Sasaki, A. et al. Green revolution: a mutant gibberellin-synthesis gene in rice. *Nature* **416**, 701–702 (2002).
- Fan, Y. & Zhang, Q. Genetic and molecular characterization of photoperiod and thermo-sensitive male sterility in rice. *Plant Reprod.* **31**, 3–14 (2018).
- Wang, H. & Deng, X. Development of the “third-generation” hybrid rice in China. *Genom. Proteom. Bioinf.* **16**, 393–396 (2018).
- Qian, Q., Zhang, F. & Xin, Y. Yuan Longping and hybrid rice research. *Rice* **14**, 101 (2021).
- Ma, G. & Yuan, L. Hybrid rice achievements, development and prospect in China. *J. Integr. Agr.* **14**, 197–205 (2015).
- Peng, S. et al. Yield potential trends of tropical rice since the release of IR8 and the challenge of increasing rice yield potential. *Crop Sci.* **39**, 1552–1559 (1999).
- Zhu, Y. Fifty years of hybrid rice research in China. *Chin. Sci. Bull.* **61**, 3740–3745 (2016).
- Lv, Q. et al. Resequencing of 1,143 indica rice accessions reveals important genetic variations and different heterosis patterns. *Nat. Commun.* **11**, 4778 (2020).
- Li, J. et al. Comparative experiment of flower opening time in different rice cultivars. *J. Zhejiang Agric. Sci.* **1**, 63–66 (2007).
- Yan, Z., Deng, R., Zhang, H., Li, J. & Zhu, S. Transcriptome analysis of floret opening and closure both *Indica* and *Japonica* rice. *3 Biotech.* **12**, 188 (2022).
- Wang, M. et al. Methylesterification of cell-wall pectin controls the diurnal flower-opening times in rice. *Mol. Plant* **15**, 956–972 (2022).
- Li, X. et al. OPEN GLUME1: a key enzyme reducing the precursor of JA, participates in carbohydrate transport of lodicules during anthesis in rice. *Plant Cell Rep.* **37**, 329–346 (2018).
- Wang, Z., Gu, Y. & Gao, Y. Studies on the mechanism of the anthesis of rice III. structure of the lodicule and changes of its contents during flowering. *Acta Agron. Sin.* **17**, 96–101 (1991).
- Heslop-Harrison, Y. & Heslop-Harrison, J. S. Lodicule function and filament extension in the grasses: potassium ion movement and tissue specialization. *Ann. Bot.* **77**, 573–582 (1996).
- Qin, Y., Yang, J. & Zhao, J. Calcium changes and the response to methyl jasmonate in rice lodicules during anthesis. *Protoplasma* **225**, 103–112 (2005).
- Zeng, X. et al. Opening of rice floret in rapid response to methyl jasmonate. *J. Plant Growth Regul.* **18**, 153–158 (1999).
- Yan, Z. et al. Inducing effect of coronatine and methyl jasmonate on the opening of spikelets in wheat, rye and mildew. *Sci. Agric. Sin.* **34**, 334–337 (2001).
- Liu, L. et al. Jasmonic acid deficiency leads to scattered floret opening time in cytoplasmic male sterile rice Zhenshan 97A. *J. Exp. Bot.* **68**, 4613–4625 (2017).
- Ming, H. et al. Dynamic changes of jasmonic acid biosynthesis in rice florets during natural anthesis. *Acta Agron. Sin.* **38**, 1891–1899 (2012).
- Xu, P. et al. *EARLY MORNING FLOWERING1 (EMF1)* regulates the floret opening time by mediating lodicule cell wall formation in rice. *Plant Biotechnol. J.* **20**, 1441–1443 (2022).
- Fu, Y., Xiang, M., Jiang, H., He, Y. & Zeng, X. Transcriptome profiling of lodicules before floret opening in *Oryza sativa* L. *Sci. Agric. Sin.* **49**, 1017–1033 (2016).
- Song, S. et al. The jasmonate-ZIM domain proteins interact with the R2R3-MYB transcription factors MYB21 and MYB24 to affect jasmonate-regulated stamen development in *Arabidopsis*. *Plant Cell* **23**, 1000–1013 (2011).
- Franco-Zorrilla, J. M. et al. DNA-binding specificities of plant transcription factors and their potential to define target genes. *Proc. Natl Acad. Sci. USA* **111**, 2367–2372 (2014).
- Xiao, Y. et al. *OsJAR1* is required for JA-regulated floret opening and anther dehiscence in rice. *Plant Mol. Biol.* **86**, 19–33 (2014).
- Zhao, H. et al. An inferred functional impact map of genetic variants in rice. *Mol. Plant* **14**, 1584–1599 (2021).
- Chen, W. et al. Genome-wide association analyses provide genetic and biochemical insights into natural variation in rice metabolism. *Nat. Genet.* **46**, 714–721 (2014).
- Zheng, X. et al. Genomic signatures of domestication and adaptation during geographical expansions of rice cultivation. *Plant Biotechnol. J.* **20**, 16–18 (2022).
- Huang, X. et al. A map of rice genome variation reveals the origin of cultivated rice. *Nature* **490**, 497–501 (2012).
- Liu, Y. et al. Genomic basis of geographical adaptation to soil nitrogen in rice. *Nature* **590**, 600–605 (2021).
- Kobayashi, K. et al. Effects of temperature, solar radiation, and vapor-pressure deficit on flower opening time in rice. *Plant Prod. Sci.* **13**, 21–28 (2010).

31. Zhang, M. et al. Advances on the study of flowering time trait in hybrid rice. *Acta Agric. Nucl. Sin.* **30**, 267–274 (2016).
32. Ishimaru, T. et al. Effect of the light and dark conditions on flower opening time between cultivated rice (*Oryza sativa*) and a near-isogenic early-morning flowering line. *AoB Plants* **4**, plab040 (2021).
33. Ma, Z., Zhan, Z. & Cheng, X. Flowering time in filial generations of cross between *indica* and *japonica* rice and its response to external environment. *Hybrid Rice* **26**, 70–76 (2011).
34. Ma, Z. et al. QTL analysis on flowering time in filial generations of cross between *indica* and *japonica* rice. *Acta Phytophysiol. Sin.* **47**, 799–802 (2011).
35. Wan, G. et al. QTL mapping of floret opening time in rice. *Acta Agric. Nucl. Sin.* **27**, 52–56 (2013).
36. Thanh, P. T. et al. QTL analysis for flowering time using backcross population between *Oryza sativa* Nipponbare and *O. rufipogon*. *Genes Genet. Syst.* **85**, 273 (2010).
37. Hirabayashi, H. et al. *qEMF3*, a novel QTL for the early-morning flowering trait from wild rice, *Oryza officinalis*, to mitigate heat stress damage at flowering in rice, *O. sativa*. *J. Exp. Bot.* **66**, 1227–1236 (2015).
38. Zhang, M. et al. Identification of QTLs for rice flower opening time in two environments. *Euphytica* **213**, 181 (2017).
39. Ghorbel, M., Brini, F., Sharma, A. & Landi, M. Role of jasmonic acid in plants: the molecular point of view. *Plant Cell Rep.* **40**, 1471–1494 (2021).
40. Huang, H., Chen, Y., Wang, S., Qi, T. & Song, S. Jasmonate action and crosstalk in flower development and fertility. *J. Exp. Bot.* **74**, 1186–1197 (2023).
41. Chopy, M. et al. A single MYB transcription factor with multiple functions during flower development. *N. Phytol.* **239**, 2007–2025 (2023).
42. Wang, Y. et al. MYB transcription factors and their roles in the male reproductive development of flowering plants. *Plant Sci.* **335**, 111811 (2023).
43. Reeves, P. H. et al. A regulatory network for coordinated flower maturation. *PLoS Genet.* **8**, e1002506 (2012).
44. Huang, H., Liu, B., Liu, L. & Song, S. Jasmonate action in plant growth and development. *J. Exp. Bot.* **68**, 1349–1359 (2017).
45. Schubert, R. et al. Tomato MYB21 acts in ovules to mediate jasmonate-regulated fertility. *Plant Cell* **31**, 1043–1062 (2019).
46. Riemann, M., Riemann, M. & Takano, M. Rice *JASMONATE RESISTANT 1* is involved in phytochrome and jasmonate signalling. *Plant Cell Environ.* **31**, 783–792 (2010).
47. Riemann, M., Haga, K., Shimizu, T., Okada, K. & Iino, M. Identification of rice *ALLENE OXIDE CYCLASE* mutants and the function of jasmonate for defence against *Magnaporthe oryzae*. *Plant J.* **74**, 226–238 (2013).
48. Inagaki, H. et al. Genome editing reveals both the crucial role of *OsCOI2* in jasmonate signaling and the functional diversity of *COI1* homologs in rice. *Plant Cell Physiol.* **64**, 405–421 (2023).
49. Svyatyna, K. et al. Light induces jasmonate-isoleucine conjugation via *OsJAR1*-dependent and -independent pathways in rice. *Plant Cell Environ.* **37**, 827–839 (2014).
50. Zhao, Z. et al. Auxin regulates source-sink carbohydrate partitioning and reproductive organ development in rice. *Proc. Natl Acad. Sci. USA* **119**, e2121671119 (2022).
51. Xie, X. et al. CRISPR-GE: a convenient software toolkit for CRISPR-Based genome editing. *Mol. Plant* **10**, 1246–1249 (2017).
52. Ma, X. et al. A robust CRISPR/Cas9 system for convenient, high-efficiency multiplex genome editing in monocot and dicot Plants. *Mol. Plant* **8**, 1274–1284 (2015).
53. Kim, D., Langmead, B. & Salzberg, S. L. HISAT: a fast spliced aligner with low memory requirements. *Nat. Methods* **12**, 357–360 (2015).
54. Kawahara, Y. et al. Improvement of the *Oryza sativa* Nipponbare reference genome using next generation sequence and optical map data. *Rice* **6**, 4 (2013).
55. Simon, A., Theodor, P. P. & Wolfgang, H. HTSeq—a Python framework to work with high-throughput sequencing data. *Bioinformatics* **31**, 166–169 (2015).
56. Love, M. I., Huber, W. & Anders, S. Moderated estimation of fold change and dispersion for RNA-seq data with DESeq2. *Genome Biology* **15**, 550 (2014).
57. Jiang, L. et al. DWARF 53 acts as a repressor of strigolactone signalling in rice. *Nature* **504**, 401–405 (2013).
58. Mazaika, E. & Homsy, J. Digital droplet PCR: CNV analysis and other applications. *Curr. Protoc. Hum. Genet.* **82**, 7–24 (2014).
59. Anna, B. et al. Mapping genome-wide transcription factor binding sites using DAP-seq. *Nat. Protoc.* **12**, 1659–1672 (2017).
60. Langmead, B. & Salzberg, S. L. Fast gapped-read alignment with Bowtie 2. *Nat. Methods* **9**, 357–359 (2012).
61. Li, H. et al. The sequence alignment/map format and SAMtools. *Bioinformatics* **16**, 2078–2079 (2009).
62. Zhang, Y. et al. Model-based analysis of ChIP-Seq (MACS). *Genome Biol.* **9**, 137 (2008).
63. Yu, G., Wang, L. & He, Q. ChIPseeker: an R/Bioconductor package for ChIP peak annotation, comparison and visualization. *Bioinformatics* **31**, 2382–2383 (2015).
64. You, X. et al. OsPEX5 regulates rice spikelet development through modulating jasmonic acid biosynthesis. *N. Phytol.* **224**, 712–724 (2019).
65. Katiyar, A. et al. Genome-wide classification and expression analysis of MYB transcription factor families in rice and *Arabidopsis*. *BMC Genom.* **13**, 544 (2012).
66. Kumar, S., Stecher, G. & Tamura, K. MEGA7: molecular evolutionary genetics analysis version 7.0 for bigger datasets. *Mol. Biol. Evol.* **33**, 1870–1874 (2016).
67. Li, H. & Durbin, R. Fast and accurate short read alignment with Burrows-Wheeler transform. *Bioinformatics* **14**, 1754–1760 (2009).
68. McKenna, A. et al. The Genome Analysis Toolkit: a MapReduce framework for analyzing next-generation DNA sequencing data. *Genome Res.* **20**, 1297–1303 (2010).
69. Danecek, P. et al. The variant call format and VCFtools. *Bioinformatics* **27**, 2156–2158 (2011).

Acknowledgements

We thank B. Hu and C. Chu (South China Agricultural University, SCAU) for providing Xiushui134 (XS134) and the CSSL line carrying *OsMYB8^{gsm}*. This work was supported by the National Natural Science Foundation of China (No. 31921004 to H.H.; No. 31991222 to H.H.; No. 32172056 to R.S.), Hainan Yazhou Bay Seed Laboratory (No. B23YQ1515 to R.S.; No. B23CQ15FP to R.S.), the Natural Science Foundation of Guangdong Province-Guangzhou City Collaborative Key Project (No. 2019B1515120061 to R.S.) and the Double First-class Discipline Promotion Project (No. 2021B10564001 to R.S.).

Author contributions

H.W. and R.S. conceived and designed experiments. Y.G. performed most of the experiments, W.D., Y.H. and M.Z. analyzed the data. C.X. and Q.T. characterized the genotypes and phenotypes of the edited lines. Y.L., Y.F. and R.Y. designed the CRISPR target and constructed the plasmid library. D.Z., X.L. and X.Z. carried out the phenotype investigation of transgenic rice and other rice germplasms. Y.G., Y.H., H.W. and R.S. wrote the manuscript. H.W. revised the article.

Competing interests

The authors declare no competing interests.

Additional information

Supplementary information The online version contains supplementary material available at <https://doi.org/10.1038/s41467-024-46579-z>.

Correspondence and requests for materials should be addressed to Haiyang Wang or Rongxin Shen.

Peer review information *Nature Communications* thanks Shinsuke Kutsuna, Michael Riemann, Zheng Yuan, and the other, anonymous, reviewer(s) for their contribution to the peer review of this work. A peer review file is available.

Reprints and permissions information is available at <http://www.nature.com/reprints>

Publisher's note Springer Nature remains neutral with regard to jurisdictional claims in published maps and institutional affiliations.

Open Access This article is licensed under a Creative Commons Attribution 4.0 International License, which permits use, sharing, adaptation, distribution and reproduction in any medium or format, as long as you give appropriate credit to the original author(s) and the source, provide a link to the Creative Commons licence, and indicate if changes were made. The images or other third party material in this article are included in the article's Creative Commons licence, unless indicated otherwise in a credit line to the material. If material is not included in the article's Creative Commons licence and your intended use is not permitted by statutory regulation or exceeds the permitted use, you will need to obtain permission directly from the copyright holder. To view a copy of this licence, visit <http://creativecommons.org/licenses/by/4.0/>.

© The Author(s) 2024

New Phytologist

October 2024
Vol. 244
No. 1

ISSN 0028-646X
eISSN 1469-8137

www.newphytologist.com

International Journal of Plant Science



CONTENTS

Forum

Commentary

- 5 New insights into the regulation of ethylene biosynthesis during leaf senescence in *Arabidopsis*
- 7 You can't always get what you want from pollinators

Letter

- 10 Oxidative burst causes loss of tapetal Ubisch body and male sterility in rice
C. Shi, S. Yang, Y. Cui, Z. Xu, B. Zhang, M. Guo, Y. Zhu, Y. Yang, F. Wang, H. Liu, Y. Zhang, Q. Qian & L. Shang
- 16 Hurricane-induced pollinator shifts in a tightly coadapted plant–hummingbird mutualism
T. S. O. Schröder, F. Gonçalves, M. G. R. Vollstädt, T. Zhang, R. D. Jensen, F. L. Tarazona-Tubens, S. Kim, M. Galetti, B. I. Simmons, C. N. Kaiser-Bunbury, E. J. Temeles & B. Dalsgaard

Viewpoint

- 21 The marriage between stable isotope ecology and plant metabolomics – new perspectives for metabolic flux analysis and the interpretation of ecological archives
A. Gessler, T. Wieloch, M. Saurer, M. M. Lehmann, R. A. Werner & B. Kammerer
- 32 Local adaptation, recombination, and the fate of neopolyploids
S. F. McDaniel

Meeting report

- 39 Can we harmonize the monitoring of plants and pollinators?
E. Porcher, P. Bonnet, C. Damgaard, P. De Frenne, N. Deguines, B. K. Ehlers, J. Frei, M. B. García, C. Gros, U. Jandt, A. Joly, G. Martin, D. Michez, O. L. Pescott, T. Roth & D. Waller

Profile

- 43 David L. Des Marais

Review

Tansley insight

- 46 Insights into a functional synthetic plant genome
F. Du, J. Dai & Y. Jiao

Research review

- 51 Heat stress transcription factors as the central molecular rheostat to optimize plant survival and recovery from heat stress
A. Bakery, S. Vraggalas, B. Shalha, H. Chauchan, M. Benhamed & S. Fragkostefanakis
- 65 Revisiting plant cuticle biophysics
A. Heredia, J. J. Benítez, A. González Moreno & E. Domínguez

Research

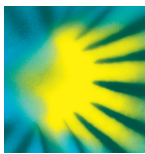
Full paper

- 74 Life at the conservative end of the leaf economics spectrum: intergeneric variation in the allocation of phosphorus to biochemical fractions in species of *Banksia* (Proteaceae) and *Hakea* (Proteaceae)
C. E. Gille, P. E. Hayes, K. Ranathunge, S. T. Liu, R. P. G. Newman, F. de Tombour, H. Lambers & P. M. Finnegan
- 91 From tree to plot: investigating stem CO₂ efflux and its drivers along a logging gradient in Sabah, Malaysian Borneo
M. B. Mills, S. Both, P. Jotan, W. Huaraca Huasco, R. Cruz, M. M. Pillco, D. F. R. P. Burslem, C. Maycock, Y. Malhi, R. M. Ewers, J. C. Berrio, J. Kaduk, S. Page, R. Robert, Y. A. Teh & T. Riutta
- 104 The auxin efflux carrier PIN1a regulates vascular patterning in cereal roots
R. Fusi, S. G. Milner, S. Rosignoli, R. Bovina, C. De Jesus Vieira Teixeira, H. Lou, B. S. Atkinson, A. N. Borkar, L. M. York, D. H. Jones, C. J. Sturrock, N. Stein, M. Mascher, R. Tuberosa, D. O'Connor, M. J. Bennett, A. Bishopp, S. Salvi & R. Bhosale

- 116 Casein kinase 1 AELs promote senescence by enhancing ethylene biosynthesis through phosphorylating WRKY22 transcription factor
G.-Q. Zhu, L. Qu & H.-W. Xue
- **Commentary p 5**
- 131 The transcription factor LBD10 sustains pollen tube growth and integrity by modulating reactive oxygen species homeostasis via the regulation of flavonol biosynthesis in *Arabidopsis*
T.-H. Nguyen, M. J. Kim & J. Kim
- 147 Dynamic soil hydraulic resistance regulates stomata
A. Manandhar, I. M. Rimer, T. Soares Pereira, J. Pichaco, F. E. Rockwell & S. A. M. McAdam
- 159 Metabolic modelling identifies mitochondrial Pi uptake and pyruvate efflux as key aspects of daytime metabolism and proton homeostasis in crassulacean acid metabolism leaves
S. Daems, S. Shameer, N. Ceusters, L. Sweetlove & J. Ceusters
- 176 A jasmonate-mediated regulatory network modulates diurnal fleret opening time in rice
W. Ding, Y. Gou, Y. Li, J. Li, Y. Fang, X. Liu, X. Zhu, R. Ye, Y. Heng, H. Wang & R. Shen
- 192 Plant infection by the necrotrophic fungus *Botrytis* requires actin-dependent generation of high invasive turgor pressure
T. Müller, J. Bronkhorst, J. Müller, N. Safari, M. Hahn, J. Sprakel & D. Scheuring
- 202 The StPti5 ethylene response factor acts as a susceptibility factor by negatively regulating the potato immune response to pathogens
A. Coll, T. Lukan, K. Stare, M. Zagorščak, T. Mahkovec Povalej, Š. Baebler, S. Prat, N. S. Coll, M. Valls, M. Petek & K. Gruden
- 219 High rate of gene family evolution in proximity to the origin of ectomycorrhizal symbiosis in Inocybaceae
F. K. Khan, M. Sánchez-García, H. Johannesson & M. Ryberg
- 235 Accumulation of pathogens in soil microbiome can explain long-term fluctuations of legumes in a grassland community
P. Kohout, R. Sudová, I. Odriozola, J. Kvasničková, M. Petružálková, V. Hadincová, F. Krahulec, S. Pecháčková, H. Skálová & T. Herben
- 249 Integration of attractive and defensive phytochemicals is unlikely to constrain chemical diversification in a perennial herb
H. E. Thosteman, K. Eisen, H. Petrén, S. Boutsis, L. Pace, J. M. Halley, C. M. De Moraes, M. C. Mescher, J. Buckley & M. Friberg
- 265 Climatic variation allows montane willows to escape an adaptive trade-off
K. C. Rosenblad & D. D. Ackerly
- 277 The 'queen of the Andes' (*Puya raimondii*) is genetically fragile and fragmented: a consequence of long generation time and semelparity?
L. Liu, J. James, Y.-Q. Zhang, Z.-F. Wang, M. Arakaki, G. Vellido, Q.-J. Zhou, M. Lascoux & X.-J. Ge
- 292 Diversity and functional differentiation of renewal buds in temperate herbaceous plants
R. Schnablová, A. Bartušková, E. Horčíčková, P. Šmarda, J. Klimešová & T. Herben
- 307 Strong habitat and seasonal phenology effects on the evolution of self-compatibility, clonality and pollinator shifts in *Lachenalia* (Asparagaceae: Scilloideae)
G. D. Duncan, A. G. Ellis, F. Forest & G. A. Verboom
- **Commentary p 7**
- **Methods**
- 318 Development of a tightly regulated copper-inducible transient gene expression system in *Nicotiana benthamiana* incorporating a suicide exon and Cre recombinase
B.-J. Chiang, K.-Y. Lin, Y.-F. Chen, C.-Y. Huang, F.-J. Goh, L.-T. Huang, L.-H. Chen & C.-H. Wu

Cover Legend

Vascular patterning phenotype of young barley roots with altered PIN activity. Radial cross sections were obtained by vibratome sectioning, cleared using the ClearSee method, and stained with Calcofluor White (blue) and Fuchsin (yellow). Image courtesy of Riccardo Fusi (Fusi *et al.*, pp. 104–115).



Editor-in-Chief

Alistair M Hetherington, Bristol, UK

Tansley Reviews Editor

Liam Dolan FRS, Vienna, Austria

Section Editors

Physiology & Development

John M Christie, Glasgow, UK

Environment

Amy T Austin, Buenos Aires, Argentina

Interaction

Ralph Panstruga, Aachen, Germany

Evolution

Elena M Kramer, Cambridge, MA, USA

Transformative Plant Biotechnology

Claire Halpin, Dundee, UK

Central Office

Executive Editor

Sarah Lennox

Managing Editor

Helen Pinfield-Wells

Senior Commissioning Editor

Holly Slater

Peer Review Manager

Fiona Tooke

Production Manager

Sarah J Gibbons

Events and Promotions Manager

Christine Phillips

Development Coordinator

Mike G Whitfield

Assistant Forum Editor

Zoë Irwin

Senior Editorial Assistant

Lauren Colwell

Editorial Assistants

Jennifer Brunning, Glyndwr Jones, Clódagh McSweeney,

Ruth Mordue, Tom Williams

Finance and Operations Manager

Gena Etta Shew

Executive Officer

Samantha Smyth

Illustration

Debbie Maizels

New Phytologist Central Office

np-centraloffice@lancaster.ac.uk

Editors

Owen K Atkin, Canberra, Australia

Carlos L Ballaré, Buenos Aires, Argentina

Jeanine Cavender-Bares, Cambridge, MA, USA

Ian A Dickie, Canterbury, New Zealand

Teresa B Fitzpatrick, Geneva, Switzerland

Andrew Groover, Davis, CA, USA

Gwyneth Ingram, Lyon, France

Colleen M Iversen, Oak Ridge, TN, USA

André Kessler, Ithaca, NY, USA

Hongzhi Kong, Beijing, China

Jörg Kudla, Münster, Germany

Anna-Liisa Laine, Zürich, Switzerland

Tracy Lawson, Colchester, UK

Björn D Lindahl, Uppsala, Sweden

Keith Lindsey, Durham, UK

Jian Feng Ma, Okayama, Japan

Wenbo Ma, Norwich, UK

Susana Magallón, Mexico City, Mexico

Francis M Martin, Nancy, France

Martin R McAtinsh, Lancaster, UK

Nathan G McDowell, Richland, WA, USA

Jennifer McElwain, Dublin, Ireland

Belinda E Medlyn, Sydney, Australia

Carl Ng, Dublin, Ireland

Richard J Norby, Knoxville, TN, USA

Maarja Opik, Tartu, Estonia

Anne E Osbourn FRS, Norwich, UK

Andrea Polle, Göttingen, Germany

Mark D Rausher, Durham, NC, USA

Sasha C Reed, Moab, UT, USA

Hardy Rolltschek, Gatersleben, Germany

Marc-André Selosse, Paris, France

P Spanu, London, UK

Steve Strauss, Corvallis, OR, USA

Nathalie Verbruggen, Brussels, Belgium

Pengwei Wang, Wuhan, China

Lizhong Xiong, Wuhan, China

Shuhua Yang, Beijing, China

Weicai Yang, Beijing, China

Amy Zanne, Millbrook, NY, USA

Associate Editors

TJ Brodribb, Tasmania, Australia

JP Carr, Cambridge, UK

LA Cernusak, Cairns, Australia

SM Coelho, Tübingen, Germany

MG De Kauwe, Bristol, UK

AN Dodd, Norwich, UK

PJ Franks, Sydney, Australia

A Genre, Turin, Italy

S Hacquard, Cologne, Germany

DR Kelley, Ames, IA, USA

DL Des Marais, Cambridge, MA, USA

AJ McCormick, Edinburgh, UK

MG Mitchum, Athens, GA, USA

N Nakayama, London, UK

D Ortiz-Barrientos, Brisbane, Australia

J Pittermann, Santa Cruz, CA, USA

MRG Roelfsema, Würzburg, Germany

A Sadanandom, Durham, UK

E Shani, Tel Aviv, Israel

DA Smales, Plymouth, UK

AG Smith, Cambridge, UK

C-P Song, Henan, China

J Vamori, Calgary, Canada

E Wang, Shanghai, China

Co-Editors

HP Comes, Salzburg, Austria

H Ougham, Aberystwyth, UK

JR Stinchcombe, Toronto, Canada

MG Tjoelker, Penrith, Australia

Board of Advisors

G van den Akerke, Utrecht, the Netherlands

KL Adams, Vancouver, Canada

ME Afkhami, Miami, FL, USA

EA Ainsworth, Urbana, IL, USA

DK Allen, St Louis, MO, USA

WS Armbruster, Portsmouth, UK

T-L Ashman, Pittsburgh, PA, USA

BA Atkinson, Lawrence, KS, USA

Y Bai, Beijing, China

BO Bargmann, Blacksburg, VA, USA

MM Barbour, Hamilton, New Zealand

ME Bartlett, Amherst, MA, USA

GTS Beemster, Antwerp, Belgium

DJ Beerling FRS, Sheffield, UK

C Bell, New Orleans, LA, USA

Y Benitez-Alfonso, Leeds, UK

CA Beveridge, Brisbane, Australia

H de Boer, Utrecht, the Netherlands

M Bogdziewicz, Poznań, Poland

P Bonfante, Torino, Italy

P Borrell, Norwich, UK

O Bozkurt, London, UK

CG Bueno, Jaca, Spain

TM Burch-Smith, St Louis, MO, USA

LT Burghardt, University Park, PA, USA

JF Cahill, Edmonton, Canada

E Cahoon, Lincoln, NE, USA

SA Casson, Sheffield, UK

M Charpentier, Norwich, UK

VB Chaudhary, Hanover, NH, USA

LQ Chen, Urbana, IL, USA

G Chomicki, Durham, UK

JW Clark, Bath, UK

K Clay, New Orleans, LA, USA

KE Clemmensen, Uppsala, Sweden

A Costa, Milan, Italy

G Cott, Dublin, Ireland

JM Coughlan, New Haven, CT, USA

P-E Courty, Dijon, France

KY Crous, Penrith, Australia

KC Cushman, Balboa, Panama

J Davison, Tartu, Estonia

SP DiFazio, Morgantown, WV, USA

Z Ding, Shandong, China

MR Dudash, Brookings, SD, USA

AJ Eckert, Richmond, VA, USA

C Eckert, Kingston, Canada

P Edgar, East Lansing, MI, USA

JM Estévez, Buenos Aires, Argentina

C Fankhauser, Lausanne, Switzerland

A Feechan, Edinburgh, UK

N Ferrol, Granada, Spain

RA Fisher, Oslo, Norway

L Fishman, Missoula, MT, USA

A Fleming, Sheffield, UK

J Flexas, Palma de Mallorca, Spain

E Foo, Hobart, Tasmania, Australia

KA Franklin, Bristol, UK

F Frugier, Paris, France

Y Fu, Beijing, China

C Gachon, Paris, France

D Gasperini, Halle, Germany

KB Gedan, Washington, DC, USA

C-M Geilfus, Berlin, Germany

BJ Glover, Cambridge, UK

C Goodwillie, Greenville, NC, USA

J Gray, Sheffield, UK

JJ Grossman, Northfield, MN, USA

M Grube, Graz, Austria

KJ Gupta, Delhi, India

B Hause, Halle, Germany

M Haydon, Melbourne, Australia

M van der Heijden, Zürich, Switzerland

T Helgason, Edinburgh, UK

BR Helliker, Philadelphia, PA, USA

I Henry, Davis, CA, USA

M Heskell, St Paul, MN, USA

AJ Hetherington, Edinburgh, UK

K Hikosaka, Sendai, Japan

LC Hilleman, Lawrence, KS, USA

SR Hind, Urbana, IL, USA

SJ Hiscock, Oxford, UK

EA Hobbie, Durham, NH, USA

A Hodge, York, UK

R Hopkins, Boston, MA, USA

H Hörak, Tartu, Estonia

T Ischebeck, Münster, Germany

KJ Jardine, Berkeley, CA, USA

M Jasiński, Poznań, Poland

X Jin, Beijing, China

D Johnson, Manchester, UK

LJ Johnson, Palmerston North, New Zealand

AM Jones, Cambridge, UK

M Jones, Glasgow, UK

T Jucker, Bristol, UK

RR Junker, Marburg, Germany

NC Kane, Boulder, CO, USA

S Kangasjärvi, Helsinki, Finland

K Kanyuka, Cambridge, UK

P Kardol, Umeå, Sweden

F Katagiri, St Paul, MN, USA

PG Kennedy, St Paul, MN, USA

C Kidner, Edinburgh, UK

NG King, Plymouth, UK

P Kohout, Prague, Czech Republic

D Kong, Zhengzhou, China

S Kothari, Montreal, Canada

KV Krasileva, Berkeley, CA, USA

H Kudoh, Kyoto, Japan

S Kusch, Aachen, Germany

TW Kuyper, Wageningen, the Netherlands

T Lahaye, Tübingen, Germany

E Laliberté, Montreal, Canada

E Lamb, Saskatoon, Canada

L Lanfranco, Torino, Italy

M Lascoux, Uppsala, Sweden

OS Lau, Singapore, Republic of Singapore

J Leake, Sheffield, UK

D Leister, Munich, Germany

Y Lekberg, Missoula, MT, USA

F Lens, Leiden, the Netherlands

Y-K Liang, Wuhan, China

Y Li-Beisson, Saint-Paul-lès-Durance, France

NS Lin, Taipei, Taiwan

CW Locke, Cambridge, UK

X Lu, Wuhan, China

J Lundberg-Felten, Umeå, Sweden

ZB Luo, Beijing, China

L Mackinder, York, UK

PA Manavella, Sante Fe, Argentina

S Mathews, Baton Rouge, LA, USA

I Mayrose, Tel Aviv, Israel

AA Meharg, Belfast, UK

JE Meireles, Orono, ME, USA

DNL Menge, New York, NY, USA

S Michaelitz, Vancouver, Canada

MV Mickelbart, West Lafayette, IN, USA

E Moyroud, Cambridge, UK

LM Mueller, La Jolla, CA, USA

E Murchie, Nottingham, UK

J Murray, Norwich, UK

K Nara, Tokyo, Japan

A Nardini, Trieste, Italy

G Newcombe, Moscow, ID, USA

I Nishida, Saitama, Japan

ME Olson, Mexico City, Mexico

JG Onyenedum, New York, NY, USA

NL Pabón-Mora, Medellín, Colombia

J Pannell, Lausanne, Switzerland

K Papadopoulou, Thessaly, Greece

C Parisod, Fribourg, Switzerland

U Paszkowski, Cambridge, UK

KG Peay, Stanford, CA, USA

WA Peer, College Park, MS, USA

R Pena, Reading, UK

S Penfield, Norwich, UK

J Peñuelas, Barcelona, Spain

NAL Pilon, Campinas, Brazil

J Pitther, Kelowna, Canada

JM Plett, Richmond, Australia

JR Powell, Sydney, Australia

S Pujalon, Lyon, France

H Qiao, Austin, TX, USA

L Ragni, Freiburg, Germany

G-Y Rao, Beijing, China

KS Ramirez, El Paso, TX, USA

R Ree, Chicago, IL, USA

V Resco de Dios, Lleida, Spain

S Robatzek, Munich, Germany

CAM Robert, Bern, Switzerland

JA Rosell, Mexico City, Mexico

R Roth, Oxford, UK

MA Rúa, Dayton, USA

JA Rudgers, Albuquerque, NM, USA

A Sala, Missoula, MT, USA

A Satake, Fukuoka, Japan

S Savaldi-Goldstein, Haifa, Israel

S Schmidt, Brisbane, Australia

M Schwarzländer, Münster, Germany

AK Schweiger, Bozeman, MT, USA

D Seung, Norwich, UK

SA Sevanto, Los

Aims and Scope

New Phytologist offers rapid publication of high quality, original research in plant science. Falling within five sections – Physiology & Development, Environment, Interaction, Evolution and Transformative Plant Biotechnology – articles cover topics that range from intracellular processes through to global environmental change. Cross-disciplinary approaches are particularly encouraged but for guidance the journal is organized as follows and recognizes that techniques from molecular and cell biology, and functional genomics through to modelling and system-based approaches will be applied across the whole spectrum of plant science:

- **Physiology & Development:** intra/inter-cellular signalling, long-distance signalling, physiology, development, eco-devo – phenotypic plasticity, transport, biochemistry.
- **Environment:** global change and Earth system functioning, environmental stress, ecophysiology, plant–soil interactions, heavy metals.
- **Interaction:** plant–biotic interactions (including viruses, prokaryotes, oomycetes, fungi/mycorrhizas, viruses, nematodes and insects), symbionts, endophytes, pathogens, plant microbiome, fungal genomics, multitrophic systems, plant–microbe–soil interactions.
- **Evolution:** molecular evolution, population or quantitative genetics, mating systems, phylogenetics, speciation, plant–enemy coevolution, evo-devo.
- **Transformative Plant Biotechnology:** plant bioengineering, plant biotechnology, plant gene editing, genetic manipulation or engineering of plant biosynthetic pathways or regulatory circuits or signalling cascades, plant synthetic biology.

All papers must focus on timely research that provides new insights into the broad principles of plant science. The topic should be original, addressing clear hypotheses or questions and of general interest to our readers. In addition to original research articles, short Letters, and other submissions to the Forum section, Research reviews, Rapid reports, Modelling/Theory and Methods papers, as well as Viewpoints are encouraged. Please refer to the full Author Guidelines for further information (www.newphytologist.com).

About *New Phytologist*

- *New Phytologist* is owned by the New Phytologist Foundation, a not-for-profit organization dedicated to the promotion of plant science, facilitating projects from symposia to free access for our Tansley reviews and Tansley insights.
- We are committed to rapid processing, from online submission through to publication 'as ready' via *Early View* – our average time to decision is <23 days.
- There are no page or colour charges and a PDF version will be provided for each article. Authors may opt to make their article Open Access.
- The journal is available online at Wiley Online Library. Visit www.newphytologist.com to search the articles and register for table of contents email alerts.
- If you have any questions, do get in touch with Central Office (np-centraloffice@lancaster.ac.uk)
- For submission instructions, subscription and all the latest information visit www.newphytologist.com.

Publisher

New Phytologist is published by John Wiley & Sons Ltd, 9600 Garsington Road, Oxford, OX4 2DQ, UK. Tel: +44 1865 776868

Production Editor

Aishwarya Chandramouli, nph@wiley.com

Journal Customer Services: For ordering information, claims and any enquiry concerning your journal subscription please

visit our Online Customer Help at <https://wolsupport.wiley.com/s/contactsupport> or contact your nearest office.

Americas: email: cs-journals@wiley.com; Tel: +1 877 762 2974

Europe, Middle East and Africa: email: cs-journals@wiley.com; tel: +44 (0) 1243 684083

Asia Pacific: email: cs-journals@wiley.com; tel: +65 3165 0890.

Japan: for Japanese speaking support, email: cs-japan@wiley.com.

For a full list of frequently asked questions, please visit <https://wolsupport.wiley.com/s/>

Information for subscribers

New Phytologist is an electronic (online-only) journal published as 24 issues per year. Six parts form a volume and four volumes are published annually. Institutional subscription prices for 2024 are US\$5344 (Americas), €3675 (Europe), £2897 (UK), US\$6233 (Rest of World). Prices are exclusive of tax and include access to the current and all online back files, where available. For other pricing options and further information visit [http://ordering.onlinelibrary.wiley.com/subs.asp?ref=1469-8137&doi=10.1111/\(ISSN\)1469-8137](http://ordering.onlinelibrary.wiley.com/subs.asp?ref=1469-8137&doi=10.1111/(ISSN)1469-8137)

Copyright and Photocopying

Copyright © 2024 New Phytologist Foundation. All rights reserved. No part of this publication may be reproduced, stored or transmitted in any form or by any means without the prior permission in writing from the copyright holder. Authorization to copy items for internal and personal use is granted by the copyright holder for libraries and other users registered with their local Reproduction Rights Organisation (RRO), e.g. Copyright Clearance Center (CCC), 222 Rosewood Drive, Danvers, MA 01923, USA (www.copyright.com), provided the appropriate fee is paid directly to the RRO. This consent does not extend to other kinds of copying or use such as copying for general distribution, for advertising or promotional purposes, for republication, for creating new collective works, for resale, or for artificial intelligence tools or technologies. Permissions for such reuse can be obtained using the RightsLink "Request Permissions" link on Wiley Online Library. Special requests should be addressed to: permissions@wiley.com

Disclaimer: The Publisher, New Phytologist Foundation and Editors cannot be held responsible for any errors in or any consequences arising from the use of information contained in this journal. The views and opinions expressed do not necessarily reflect those of the Publisher, New Phytologist Foundation or Editors, neither does the publication of advertisements constitute any endorsement by the Publisher, New Phytologist Foundation, Editors, or Authors of the products advertised.

Typeset in India by Straive

ISSN 1469-8137 (online)

For submission instructions, subscription and all the latest information visit www.newphytologist.com

A jasmonate-mediated regulatory network modulates diurnal floret opening time in rice

Wenyan Ding^{1*} , Yajun Gou^{1*} , Yajing Li^{1*}, Juanjuan Li¹, Yudong Fang¹, Xupeng Liu¹, Xinyu Zhu¹, Rongjian Ye², Yueqin Heng¹ , Haiyang Wang¹  and Rongxin Shen¹ 

¹State Key Laboratory for Conservation and Utilization of Subtropical Agro-Bioresources, Guangdong Laboratory for Lingnan Modern Agriculture, College of Life Sciences, South China Agricultural University, Guangzhou, 510642, China; ²Life Science and Technology Center, China National Seed Group Co. Ltd, Wuhan, 430073, China

Authors for correspondence:

Haiyang Wang

Email: whyang@scau.edu.cn

Rongxin Shen

Email: shenrongxin@scau.edu.cn

Yueqin Heng

Email: hengyueqin@scau.edu.cn

Received: 26 July 2023

Accepted: 17 July 2024

New Phytologist (2024) 244: 176–191

doi: 10.1111/nph.20039

Key words: diurnal floret opening time, jasmonic acid, OsAOS1, OsMYC2, OsSWEET4, rice.

Summary

- Diurnal floret opening time (DFOT) is a pivotal trait for successful fertilization and hybrid breeding in rice. However, the molecular mechanism underlying this trait is poorly understood in rice.
- In this study, we combined the cytological, genetic and molecular studies to demonstrate that jasmonic acid (JA) regulates DFOT in rice through modulating the turgor and osmotic pressure of the lodicules.
- We show that lodicules undergo dramatic morphologic changes, accompanied by changes in water and sugar contents during the process of floret opening. Consistently, a large set of genes associated with cell osmolality and cell wall remodeling exhibits distinct expression profiles at different time points in our time-course transcriptomes of lodicules. Notably, a group of JA biosynthesis and signaling genes is continuously upregulated, accompanied by a gradual increase in JA accumulation as floret opening approaching. Furthermore, we demonstrate that the JA biosynthesis gene *OsAOS1* is required for endogenous JA biosynthesis in lodicules and promoting rice DFOT. Moreover, *OsMYC2*, a master regulator of JA signaling, regulates rice DFOT by directly activating *OsAOS1*, *OsSWEET4*, *OsPIP2;2* and *OsXTH9*.
- Collectively, our findings establish a core regulatory network mediated by JA for modulating rice DFOT and provide effective gene targets for the genetic improvement of DFOT in rice.

Introduction

Anthesis, a flowering period between diurnal floret opening and closure in plants, embodies multiple tempo- and spatially coordinated reproductive activities, including stamen filament elongation, anther dehiscence and pollen release, which are critical for plant fertilization and seed setting (Van Doorn & Kamdee, 2014). Flowering plants have evolved to flexibly adjust their diurnal floret opening time (DFOT) for adaptation to the fluctuating environments and attracting pollinators, thus enhancing plant fitness (Van Doorn & Van Meeteren, 2003; Baack *et al.*, 2015; Soufflet-Freslon *et al.*, 2021).

Earlier studies have documented that in dicot plants, floret opening is generally controlled by differential expansion of the two sides of petal (Rolland-Lagan *et al.*, 2003). Petal movement is achieved by a gradual loosening of the cell wall and an increase in osmotic pressure inside the petal cells, followed by water uptake (Zonia & Munnik, 2007; Kunio *et al.*, 2009). In contrast to that controlled by petals in dicots, floret opening in the grasses such as rice is controlled by the lodicule, a small scale-like organ

lying between the lemma/palea and stamens at the base of florets. At the beginning of floret opening in rice, the lodicule cells absorb water and expand, pushing the lemma and palea apart to drive floret opening. After that, the lodicule cells lose water and shrink, thus closing the glume (Wang *et al.*, 1991; Heslop-Harrison & Heslop-Harrison, 1996). Thus, the alterations of cell turgor and osmotic pressure are important driving forces of floret opening and closure in both dicots and monocots (Wang *et al.*, 1991; Fu *et al.*, 2016).

Previous studies have also documented ample evidence suggesting that floret opening is regulated by multiple classes of phytohormones. For example, it was reported that ethylene, auxin and gibberellins (GA) could promote floret opening in many ornamental plants (Li *et al.*, 2015; Ke *et al.*, 2018; Cheng *et al.*, 2021), and mutants in genes related to ethylene, auxin and jasmonic acid (JA) signaling pathways in *Arabidopsis* are defective in petal expansion and floret opening (Ishiguro *et al.*, 2001; Irish, 2008; Varaud *et al.*, 2011). JA was considered as a stress hormone implicated in plant response to both the biotic and abiotic stresses (Turner *et al.*, 2002; Trang Nguyen *et al.*, 2019). Moreover, JA could serve as an important endogenous developmental signal to regulate various growth and development events,

*These authors contributed equally to this work.

such as seed size, root growth, stamen and floret organ development (Cai *et al.*, 2014; Huang *et al.*, 2017; Cao *et al.*, 2021). Previous studies have revealed that JA and its derivative jasmonates (JAs) could effectively stimulate DFOT in rice and other grasses (Zeng *et al.*, 1999; Song *et al.*, 2001; Gao *et al.*, 2003), and that DFOT is seriously impaired in several reported JA-deficient mutants (such as *Oscpm1*, *Osjar1* and *Osopr7*; Xiao *et al.*, 2014; Hibara *et al.*, 2016; Li *et al.*, 2018). However, the detailed molecular mechanisms regulating JA biosynthesis and signaling in the lodicules and DFOT in rice have remained unexplored.

In this study, we establish a JA-mediated regulatory network regulating DFOT in rice. Our time-course transcriptome analysis of the lodicule cells at four consecutive time points of anthesis identifies a group of genes associated with cell wall modification, sugar transport and water channel activity being downstream targets of JA signaling. Functional analyses of the JA synthetic gene *OsAOS1* and the key JA signaling transcription factor *OsMYC2* validate our working hypothesis. This work provides comprehensive insights into regulation of DFOT in rice and strategies for molecular breeding of rice with optimized DFOT.

Materials and Methods

Plant materials and growth conditions

Rice cultivar ZhongHua 11 (ZH11) (*Oryza sativa* L ssp. *Japonica*) was used as the wild-type (WT) control for mutation or transgenic analyses in this study. The transgenic 35S::*OsMYC2-Flag* materials were kindly provided by professor Jianmin Wan (Institute of Crop Sciences, Chinese Academy of Agricultural Sciences; You *et al.*, 2019). All plants were grown in the experimental fields of South China Agricultural University in Guangzhou (23°7'N, 113°15'E) and Lingshui, Hainan (18°22'N, 109°45'E).

Vector construction and rice transformation

To generate the *Osaos1* and *Ossweet4* knockout constructs, gene-specific guide RNA sequences were designed with an online software toolkit CRISPR-GE (Xie *et al.*, 2017) and cloned into the binary vector *pYLCRISPR/Cas9Pubi-H* (Ma *et al.*, 2015). To generate the *OsMYC2-RNAi* construct, a 244-bp specific fragment of the *OsMYC2* CDS was amplified and inserted into the vector *pEGRNAI-Pubi-H-M2-RNAi*. To analyze the expression pattern of *OsAOS1*, the 3.5-kb promoter sequence of *OsAOS1* was amplified and inserted into *pCAMBIA1305*, resulting in the *proOsAOS1::GUS* construct. To generate the *OsAOS1* complementation construct, the *OsAOS1* genomic fragment (including 2-kb promoter, coding region and 1-kb 3' downstream region) was amplified from ZH11 gDNA and inserted into the *pCAMBIA2300* vector. To generate the *OsAOS1* overexpression construct, the full-length CDS of *OsAOS1* was amplified and cloned into the *pCAMBIA2300* vector under the control of maize *Ubi-quitin* promoter.

The above constructs were transformed into the *agrobacterium tumefaciens* strain EHA105 by electroporation and used to

transform relevant rice calli with indicated background by *agrobacterium*-mediated transformation. Hygromycin (hyg) was used for screening the positive transgenic lines. The mutation sites or gene expression levels were examined by DNA sequencing or reverse transcription quantitative polymerase chain reaction (RT-qPCR) analysis. The primers used for vector construction are listed in Supporting Information Table S1.

Characterization of the DFOT phenotype

The dynamic statistics of the DFOT phenotype were determined by the point spikelet method (Zhang *et al.*, 2016). During anthesis, the number of opened florets was counted at different time points of the day. More than 10 individual panicles per plant were used for statistical analysis. The morphology of the spikelets and lodicules at different time points was photographed under a stereomicroscope Leica M205 FA (Leica, Wetzlar, Germany). The length, width and height of the lodicule were measured using the IMAGEJ software.

MeJA treatment

The hormone treatments were conducted according to the previously described method (Song *et al.*, 2001). Two mmol l⁻¹ MeJA (CAS: 39924-52-2; Mackin, Shanghai, China) solution was sprayed on the panicles with similar growth status until all panicles were wet. The number of opened florets was counted at different time points after MeJA treatment. More than eight individual panicles per plant were used for statistical analysis.

Histological analysis and electron microscopy

For semi-thin section analysis, the lodicules at different time points of the day were first fixed in the FAA solution (17.5% formaldehyde, 45% alcohol, 5% acetic and 32.5% water) for more than 4 h. Semi-thin sections (2 µm) were stained with 1% toluidine blue for 30 s, critically dried and subsequently observed under the bright field of fluorescence microscope Y-TV55 (Nikon, Germany). The scanning electron microscopy (SEM) examination was performed as described by Juarez *et al.* (2004) with some modifications. Briefly, the lodicules at different time points were collected and fixed in a 0.1 M phosphate buffer (pH 7.0) containing 4% glutaraldehyde and 2% paraformaldehyde overnight. The samples were washed in the 0.1 M phosphate buffer (pH 7.0) three times (15 min for each step) and were then incubated in a 0.1 M phosphate buffer (pH 7.0) containing 1% osmic acid for 1–2 h. After being dehydrated by a graded series of ethanol (30%, 50%, 70%, 85%, 95% and 100%; 20 min for each step), the samples were incubated twice in the absolute acetone and then transferred into in 3 : 1, 1 : 1 and 1 : 3 mixtures of absolute acetone and spurr resin, respectively, at room temperature (more than 4 h in each mixture), and finally incubated in pure spurr resin mixture for 24 h. After being baked at 70°C for 24 h, the samples embedded in Spurr resin were sliced with ultra-thin microtome Leica EM UC7 (Leica) to obtain 70–90 nm slices. These slices were sequentially stained by

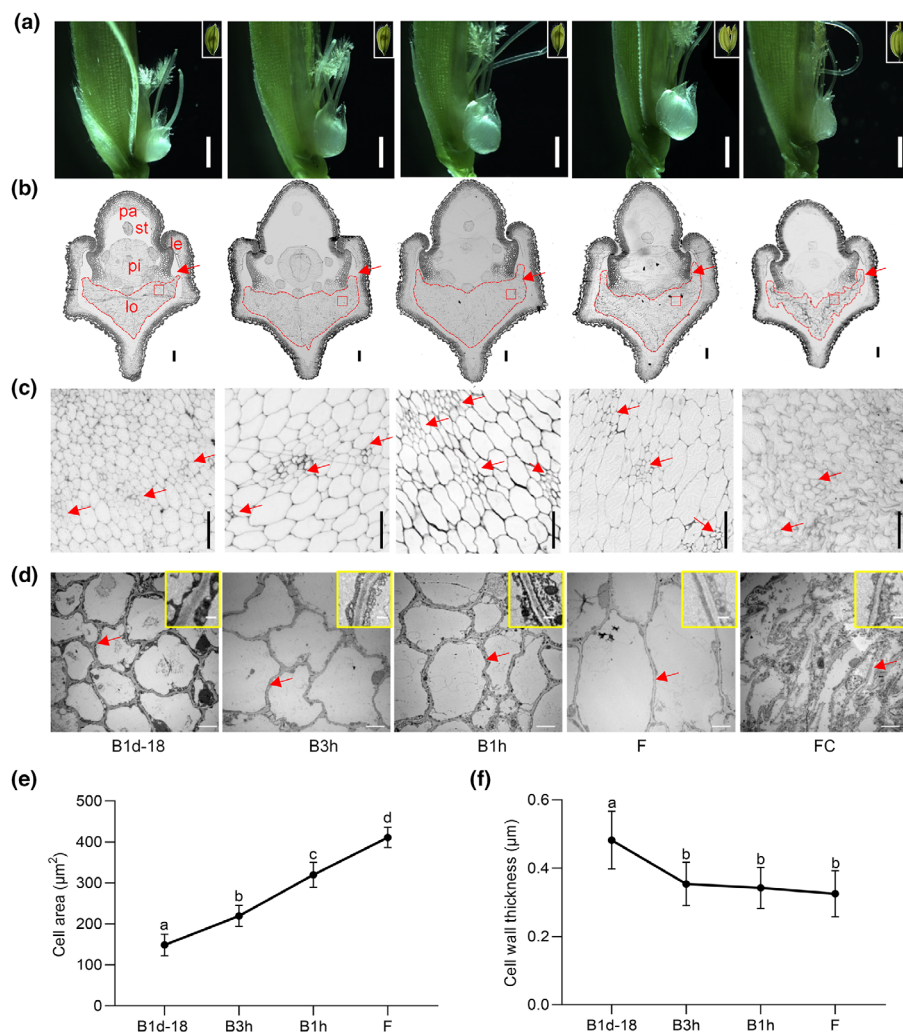


Fig. 1 Dynamic morphological changes in the lodicule during rice anthesis. (a) Lodicule morphology of wild-type (ZH11) at different time points of anthesis, including B1d-18 (18:00 h at the day before floret opening), B3h (3 h before floret opening), B1h (1 h before floret opening), F (floret opening time) and FC (floret closure after opening). Bars, 1 mm. (b) Transverse semi-thin sections of the corresponding florets in (a). Lodicules are highlighted by red dashed line. The red arrows indicate the gap between the lemma and palea, stamen, pistil, lodicule, lemma, palea. Bars, 100 μm. (c) Transverse semi-thin sections of ZH11 lodicules at the corresponding time points in red box (b). The red arrows denote the vascular bundle. Bars, 20 μm. (d) Transmission electron microscopic images of the ZH11 lodicule cells at the corresponding time points in (a). The red arrowheads indicate the cell wall of parenchyma cells. Bars, 5 μm. (e) The average area of the ZH11 lodicule cells at different time points of B1d-18, B3h, B1h and F. Data are shown as means ± SD ($n = 3$). Different letters above the bars indicate significant differences at $P < 0.05$ determined by Duncan's multiple range test. (f) The cell wall thickness of the ZH11 lodicule cells at different time points of B1d-18, B3h, B1h and F. Data are shown as means ± SD ($n = 15$). Different letters above the bars indicate significant differences at $P < 0.05$ determined by Duncan's multiple range test.

uranyl acetate and alkaline lead citrate, each step for 30 min, and then were scanned under the Model Talos L120C TEM (FEI, Hillsboro, OR, USA).

For calculating the average size of lodicules cells, the area (N) of all intact thin-walled cells in the field of each view shown in Fig. 1(c) was measured using IMAGEJ, with exclusion of the vascular bundle and incomplete cells, and the average size of lodicule cells was re-calculated using the following formula: S/N , in which N indicates the total number of all intact thin-walled cells in the field of each view. Three slices from three independent lodicules at each stage were used in this analysis, and the data were shown as means ± SD ($n = 3$). We used ImageJ to measure the thickness of parenchyma cell walls, and the data were shown as means ± SD ($n = 15$).

Measurement of the water and sugar contents in the lodicules

For measurement of the water content in the lodicules, 50 pairs of lodicules were carefully extracted from the florets and collected as one sample. The fresh weight of each sample was first measured using an analytical balance. Then, the samples were dried

at 65°C overnight, and the dry weight of each sample was measured again. The water content of the lodicules was determined by subtracting the dry weight from the fresh weight. Three biological replicates were performed for each sample.

The quantification of sugar in the lodicules was conducted by Wuhan Metware Biotechnology Co. Ltd, Wuhan, China. The freeze-dried materials were crushed using a mixer mill (MM 400; Retsch, Haan, Germany) with a zirconia bead for 1.5 min at 30 Hz. Twenty milligrams of powder was diluted to a 500 μl with methanol : isopropanol : water (3 : 3 : 2 v/v/v), vortexed for 3 min and ultrasound for 30 min. The extract was centrifuged at 13 188 g under 4°C for 3 min. Fifty microliters of the supernatant was mixed with 20 μl internal standard (ribitol, 100 μg ml⁻¹) and evaporated under nitrogen gas stream. The evaporated sample was transferred to the lyophilizer for freeze-drying. The residue was used for further derivatization. The derivatization method was as follows: the sample was mixed with 100 μl solution of methoxyamine hydrochloride in pyridine (15 mg ml⁻¹). The mixture was incubated at 37°C for 2 h. Then, 100 μl of BSTFA was added to the mixture and kept at 37°C for 30 min after vortex-mixing. The mixture was analyzed by GC-MS after being diluted to an appropriate concentration.

Agilent 7890B gas chromatograph coupled to a 7000 D mass spectrometer with a DB-5MS column (30 m length \times 0.25 mm i.d. \times 0.25 μ m film thickness; J&W Scientific, Folsom, CA, USA) was employed for GC-MS analysis of sugars. Helium was used as carrier gas, at a flow rate of 1 ml min⁻¹. Injections were made in the split mode with a split ratio 3 : 1, and the injection volume was 3 μ l. The oven temperature was held at 170°C for 2 min, then raised to 240°C at 10°C min⁻¹, raised to 280°C at 5°C min⁻¹, raised to 310°C at 25°C min⁻¹ and held at the temperature for 4 min. All samples were analyzed in selective ion monitoring mode. The ion source and transfer line temperature were 230°C and 240°C, respectively. Three biological replicates were performed for each sample.

Measurement of JAs in the lodicules

The quantification of JAs was conducted by Wuhan Metware Biotechnology Co. Ltd, Wuhan, China. Approximately 50 mg of lodicules sample was frozen in liquid nitrogen and ground into a fine powder. The sample extracts were analyzed using an LC-ESI-MS/MS system (HPLC: Shim-pack UFLC SHI-MADZU CBM30A system; Shimadzu MS, Applied Biosystems 6500 Triple Quadrupole). The analytical conditions of HPLC were as follows: LC: column, Waters ACQUITY UPLC HSS T3 C18 (100 mm \times 2.1 mm, 1.8 μ m); solvent system, water with 0.04% acetic acid (A), acetonitrile with 0.04% acetic acid (B); gradient program, started at 5% B (0–1 min), increased to 95% B (1–8 min), 95% B (8–9 min), finally ramped back to 5% B (9.1–12 min); flow rate, 0.35 ml min⁻¹; temperature, 40°C; injection volume: 2 μ l. The ESI source operation parameters were as follows: ion source, ESI +/-; source temperature 550°C; ion spray voltage (IS) 5.5 kV (positive), -4.5 kV (negative); curtain gas (CUR) was set at 35 psi, respectively. The contents of JAs were determined using an internal standard method, and three biological replicates were performed for samples of each time point.

RNA extraction and RT-qPCR

Total RNA was extracted from the samples and purified using the TRIzol reagent (TransGen Biotech, Beijing, China) according to the manufacturer's protocol. For RT-qPCR, the total RNA was reversely transcribed to cDNA according to the manufacturer's instructions (Yeasten, Shanghai, China). The RT-qPCR assay was performed using the LightCycler96 real-time PCR system (Roche, Switzerland) with the qPCR SYBR Green Master Mix (Yeasten) according to the manufacturer's instructions. The *OsActin1* gene (*LOC_Os03g50885*) was used as an internal normalization control. The expression levels of genes were calculated using the 2^{- Δ Ct} method. The primers used for RT-qPCR above are listed in Table S1.

RNA-seq and transcriptome data analysis

The lodicules of rice were separated by tweezers and were frozen immediately in liquid nitrogen for RNA-seq analysis. Three biological replicates were performed for each sample. RNA

sequencing was performed at the Azenta Co. using the Illumina HiSeq platform. For data analysis, FASTP v.0.20.1 (Chen *et al.*, 2018) was used to filter out the connectors and low-quality reads. The processed reads were compared with HISAT2 v.2.2.1 (Kim *et al.*, 2015) to the reference genome MSU Release v.7.0 (Ouyang *et al.*, 2007). HTSEQ v.0.13.5 (Putri *et al.*, 2022) was used for quantitative analysis of genes. The EDGER package (Robinson *et al.*, 2010) was used for differential expression analysis, and false discovery rate (FDR) < 0.05, absolute log₂FC (FoldChange) \geq 1 were used for screening of the significantly different genes. The Gene Ontology (GO) analysis was conducted with the David database (<https://david.ncifcrf.gov/home>) with *P*-value < 0.05 as the threshold to screen for significantly different GO terms, and the enrichment results were plotted using the ggplot2 (Wickham, 2016). Principal component analysis (PCA) was analyzed using the 'PCATOOLS' with default settings. *K*-means clustering was applied to all differentially expressed genes (DEGs) in four time points and 30 clusters were identified by the R software. The expression heatmaps were generated using the R package PHEATMAP, and the expression levels of genes were normalized by calling the parameter scale as 'row'.

Weighted gene co-expression network analysis

Weighted gene co-expression network analysis (WGCNA) was performed to construct co-expression networks using the R Bioconductor package (Langfelder & Horvath, 2008, 2012). A matrix of all genes with their fragments per kilobase of transcript per million mapped reads (FPKM) values in all individual biological replicates was used as the input. To determine the similarity between genes, the adjacency matrixes were generated through a soft thresholding procedure using the 'pickSoftThreshold' with a soft power of 20. The adjacency matrixes were then incorporated into a topological overlap measure (TOM) to estimate network interconnectedness. Module eigengenes (MEs), the first principal component of a given module, was used as a representative gene expression profile for that module. Modules were further merged based on their MEs (using cut-Height = 0.25) and the module membership (MM) for each gene indicates the degree of similarity between its expression profile and each ME. The gene co-expression networks were visualized using CYTOSCAPE v.3.8.1 (Shannon *et al.*, 2003).

GUS staining assay

The florets from the *proOsAOS1:GUS* transgenic lines were collected and incubated in the GUS staining solution at 37°C for 12 h. After staining, the florets were destained and fixed in 70% (v/v) ethanol, and finally photographed under a stereomicroscope M205 FA (Leica). The GUS staining kit was obtained from Beijing Coolaber Technology Co. Ltd (Beijing, China).

Subcellular localization

The coding sequences of *OsAOS1* from ZH11 were amplified and inserted into the *pAN580* vector to generate the *p35S::*

OsAOS1-GFP construct. The fusion plasmid was transfected into rice protoplasts using the polyethylene glycol (PEG) mediated transformation method as described previously (Zhang *et al.*, 2011). Chloroplast autofluorescence was used as a chloroplast localization marker. After culturing at 28°C for 12 h in the dark, the fluorescence signals were captured using a confocal laser-scanning microscope (Zeiss LSM780, Germany). Primers used for amplification are shown in Table S1.

Yeast one-hybrid assay

For yeast one-hybrid (Y1H) assay, the coding region of *OsMYC2* was amplified and cloned into the *pJG4-5* vector (Clontech, USA), while the promoter regions of *OsAOS1*, *OsSWEET4*, *OsXTH9* and *OsPIP2;2* were cloned into the *pLacZi2μ* vector (Lin *et al.*, 2007). Various combinations of plasmids were co-transformed into the yeast strain EGY48 using the PEG method. Transformants were cultured on the SD/-Trp/-Ura selective medium (Clontech, USA) for 2–3 d and then transferred to the SD/-Trp/-Ura selective medium (Clontech, USA) containing X-gal (Amresco, Solon, OH, USA) for 1–2 d. The empty vector *pLacZi2μ* was co-transformed as a negative control.

Electrophoretic mobility shift assay

The coding region of *OsMYC2* was cloned into the *pGEX-4 T1* vector and expressed in the *E. coli* strain DE3 to produce the recombinant protein GST-*OsMYC2*. The probes containing G-box motif were synthesized and labeled with biotin using the EMSA Probe Biotin Labeling Kit (Beyotime, Nantong, China). Electrophoretic mobility shift assays (EMSAs) were carried out using a Chemiluminescent EMSA Kit (Beyotime). Briefly, biotin-labeled probes were mixed with the GST or GST-*OsMYC2* protein in the binding buffer and incubated at room temperature for 20 min. For competition reaction, unlabeled cold probes were mixed with the labeled probes and added to the reactions. The probes used in this study are listed in Table S1.

CUT&Tag assay

The protoplasts were harvested from 14-d-old seedlings of 35S::*OsMYC2-Flag* plants and treated according to the manufacturer's instructions using the Hyperactive Universal CUT&Tag Assay Kit for Illumina (TD903-01; Vazyme, Nanjing, China). The DNAs were extracted and subjected to RT-qPCR and the DNA spike-in was used as a reference.

Transient transcription dual-LUC assay

For dual-LUC assay, the *c.* 2-kb promoter regions of *OsAOS1*, *OsSWEET4*, *OsXTH9* and *OsPIP2;2* upstream of the ATG starting codon were amplified and inserted into the *pGreenII0800-LUC* vector to generate the reporter plasmids. The *OsMYC2* coding sequence without stop codon was amplified and inserted into the *pAN580* vector to generate the effector plasmid. The effector and reporter plasmids were co-transformed into rice

protoplasts in different combinations and incubated in darkness at 28°C for 12 h. The protoplasts were collected and disintegrated by PLB in the Dual Luciferase Reporter Gene Assay Kit (Yeasen, 11402ES60). Luciferase activity was also determined using GloMax2020 (Promega) according to the manufacturer's instructions. Renilla luciferase (REN) under the control of 35S promoter in *pGreenII0800-LUC* was used as the internal control. The relative firefly luciferase activity was counted as the ratio of LUC/REN for each sample.

Statistical analysis

Statistical analysis was performed using GRAPHPAD PRISM 6. All experimental data were shown as mean \pm SE or \pm SD, and the differences between different groups or treatments were analyzed using two-side Student's *t*-test.

Accession numbers

The genes studied in this work are under the following accession nos.: *OsAOS1* (LOC_Os03g55800), *OsMYC2* (LOC_Os10g42430), *OsSWEET4* (LOC_Os02g19820), *OsPIP2;2* (LOC_Os02g41860), *OsXTH9* (LOC_Os04g51460) and *OsActin1* (LOC_Os03g50885).

Results

The dynamic morphological changes in the lodicule during rice anthesis

To survey the dynamic morphological changes in the lodicules during rice anthesis, we first carefully recorded the size and morphology of the lodicules of ZH11 at seven time points, including 14:00 h, 16:00 h and 18:00 h at the day before floret opening (B1d-14, B1d-16 and B1d-18), 3 h before opening (B3h, *c.* 09:00 h), 1 h before opening (B1h, *c.* 11:00 h), the time undergoing floret opening (F, *c.* 12:00 h) and the time at floret closure (FC, *c.* 12:30 h), under a stereomicroscope. The results showed that before the day of floret opening, the lodicules had no significant change in size, whereas on the day of opening, they rapidly expanded, and reached the maximum size by the F time point. After then, the lodicules lost water and became shrunk (Figs 1a, S1). We next carried on semi-thin transection analysis to examine the cellular change in the lodicules at five time points (B1d-18, B3h, B1h, F and FC). In line with the expansion process of the lodicules, the size of parenchyma cells in the lodicules gradually increased from the B1d-18 stage to the F stage (Fig. 1b–e). Notably, we found that during anthesis, the lodicules expanded and inserted into the conjunction region between the lemma and palea, pushing them apart to drive floret opening (Fig. 1b–e). Furthermore, transmission electron microscope (TEM) examination revealed that the thickness of parenchyma cell walls was significantly reduced from the B1d-18 stage to the F stage (Fig. 1d,f). Taken together, these results suggest that dynamic changes in cell size and cell wall thickness of parenchyma cells of the lodicules are essential for triggering floret opening and closure at anthesis.

Determination of water and sugar contents in the lodicules during rice anthesis

To further examine the physiological changes in the lodicules during rice anthesis, we first measured the water content in the lodicules at four time points of anthesis: B1d-18, B3h, B1h and F. The results showed that the water content was gradually increased, accompanied by the lodicule expansion during anthesis (Fig. S2a). As the osmolality of the lodicule cell might be regulated by the soluble sugars (Wang *et al.*, 1991), we investigated the dynamic change in soluble sugar content in the lodicules during anthesis using the metabolome technology. A total of 13 soluble sugars were detected in the lodicules, c. 99.0% of which were sucrose, glucose and fructose (Fig. S2b; Table S2). Noteworthy, we found that the glucose and fructose contents gradually increased while the sucrose content slightly declined, leading to a gradual increase in total soluble sugar in the lodicules as the opening time approaching (Fig. S2b). These results indicate that glucose, fructose and sucrose likely constitute the major osmotic substances in the lodicules.

A comprehensive transcriptome analysis of the lodicules across anthesis

To explore the molecular basis underlying the lodicule expansion, we performed a comprehensive comparative RNA-seq analysis of the lodicules at four time points during anthesis: B1d-18, B3h, B1h and F (Fig. S3a). Principal component analysis showed that samples from different time points are well separated (Fig. S3b), and the correlation analysis showed high correlation coefficients within three biological replicates from each time point ($R^2 \geq 0.90$; Fig. S3c), indicating the reliability of our RNA-seq results. Thus, we calculated the average FPKM value of three biological replicates, and identified 20 994 genes with FPKM ≥ 1 in 12 datasets (Table S3). Next, we performed pairwise differential gene expression analyses between two consecutive time points, and identified 7152 DEGs between B1d-18 and B3h, 6268 DEGs between B1h and B3h and 5279 DEGs between F and B1h (FDR < 0.05, absolute $\log_2FC \geq 1$; Fig. S3d; Tables S4–S6). Notably, these DEGs exhibited distinct expression profiles at different time points (Fig. 2a), suggesting that expansion and closure of the lodicules are subject to stage-specific transcriptional regulation.

To further identify these time point-specific genes, we performed a k-means clustering analysis of all DEGs (Table S7) and identified six representative clusters (Cluster 1–6) displaying time point-specific expression profiles (Fig. 2b). Of which, Cluster 1 genes showed highest expression at B1d-18 and the expression was sharply reduced at B3h. The expression of Cluster 2 genes was gradually reduced from B1d-18 to F. By contrast, the transcript levels of Cluster 3 genes prominently increased from B1d-18 to B3h and maintained relatively stable thereafter. The Cluster 4 and Cluster 6 genes showed peaked expression at B1h and F, respectively. The Cluster 5 genes showed opposite expression patterns to the Cluster 2 (Fig. 2b). Gene Ontology enrichment analysis of each cluster showed that DEGs related to circadian

rhythm, cell wall modification, carbohydrate metabolism and sugar transport, water channel activity, and phytohormone and calcium signaling pathways were significantly enriched in one or more clusters (Fig. 2c). For example, several circadian clock-related genes, such as *OsTOC1*, *OsLUC* and *OsGI*, were detected in Cluster 1, hinting a potential negative role of circadian clock in regulating DFOT (Fig. S4). Several *Pectin Methylesterase* (*OsPME*) genes (*OsPME33/34/35*) related to cell wall modifications were identified in Cluster 2 and were largely downregulated along with anthesis progression (Fig. S4), consistent with a negative role of *OsPMEs* on rice DFOT (Wang *et al.*, 2022; Xu *et al.*, 2022), whereas several *Xyloglucan Endotransglucosylase/Hydrolases* genes (*OsXTH3/16/22*) responsible for cell wall relaxation were sharply upregulated at the F time point (Fig. S4), in agreement with the proposed role of cell wall relaxation for DFOT regulation (Ochiai *et al.*, 2013).

Additionally, enrichment of a series of transporter genes was also detected. The water transporter genes *AQUAPORINs* (*OsPIP1;3*, *OsPIP2;1*, *OsPIP2;2*, etc.) were enriched in Cluster 3, while other transmembrane transporters, such as the sugar transporter genes (*OsSWEET4/6a/16*), K^+ transporters and channel-associated genes (*OsHAK9* and *OsGORK*), were identified in Cluster 3 and Cluster 4 (Fig. S4). The increased expression of these genes would elevate the osmotic pressure and facilitate water transport into the lodicule cells. Moreover, we detected enrichment of a group of JA biosynthesis and signaling-related genes in both Cluster 5 and Cluster 6 (Fig. 3a,b). Besides, numerous genes related to signaling pathways of calcium and other phytohormones (such as auxin, abscisic acid and ethylene) were also identified in the Cluster 5 or Cluster 6 gene sets (Fig. S4), implying that these signaling pathways might also be involved in DFOT regulation. In short, our transcriptome analysis identified 337 time point-specific genes (referred to the molecular processes highlighted with red arrows in Fig. 2) related to cell osmolality and cell wall remodeling for regulating DFOT in rice, therefore termed DFOT-related genes in this study (Table S8). RT-qPCR analysis of eight DFOT-related genes revealed similar expression patterns to the RNA-seq dataset (Fig. S5), thus validating the reliability of our RNA-seq data.

Dynamic changes in JA accumulation and signaling in the lodicules during anthesis

Considering the key role of JA in DFOT regulation (Zeng *et al.*, 1999), we carefully analyzed the expression profiles of genes involved in JA biosynthesis and signaling identified in the DEG datasets. We showed that a number of JA biosynthesis-related genes, such as *OsAOS1* and *OsDADI-1*, were upregulated as early as at the B3h time point, while more genes, such as *OsAOC*, *OsDADs* and *OsOPRs*, did not exhibited elevated expressions until the F time point. Strikingly, the expression of a group of JA repressor genes *OsJAZs* (Chico *et al.*, 2008) was also elevated, probably due to a feedback response to JA signaling activation (Fig. 3a,b). RT-qPCR analyses further confirmed the RNA-seq data (Fig. 3c,d). We next performed a metabolome analysis to examine the content of endogenous JAs in the lodicules. The

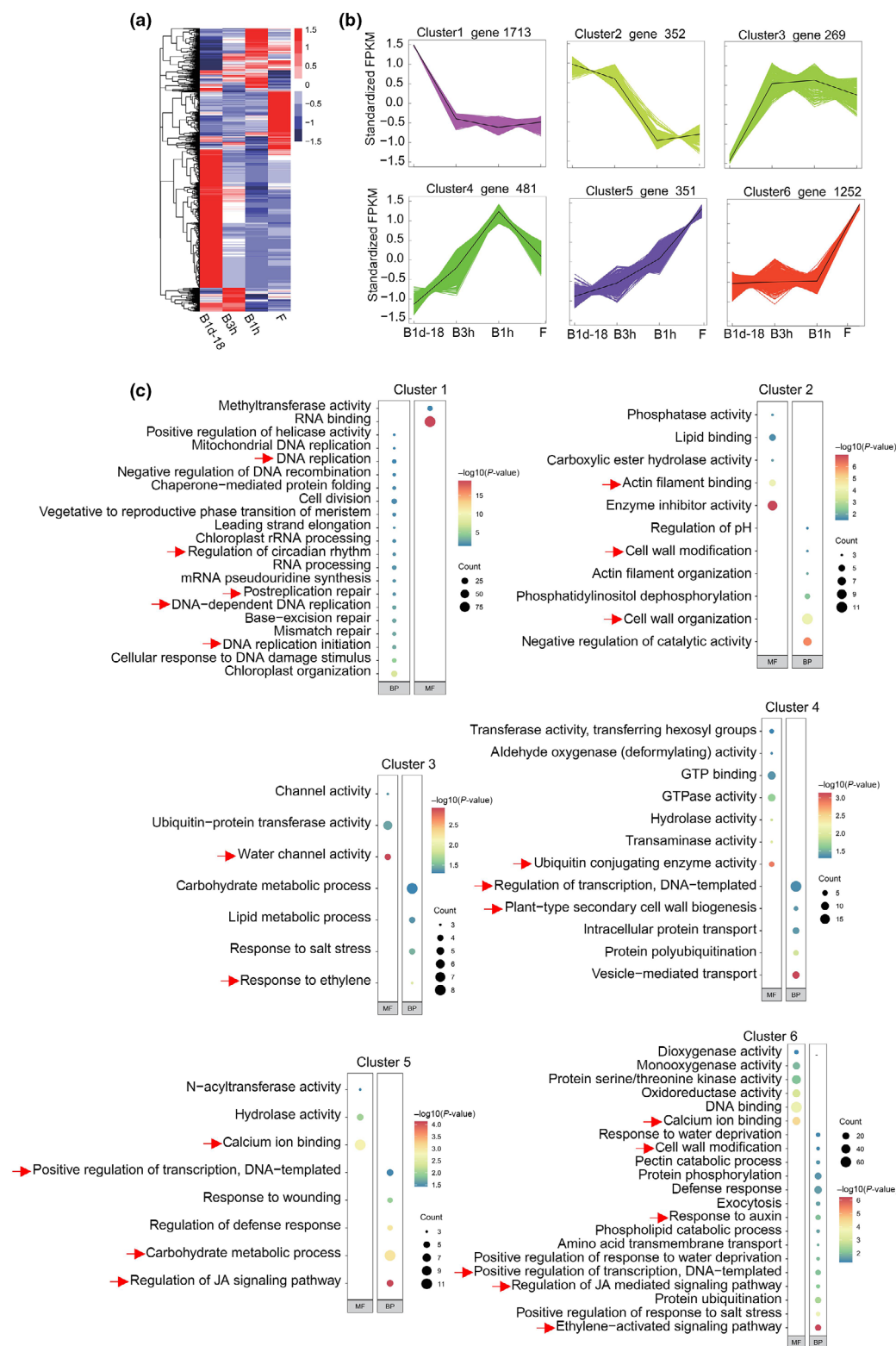


Fig. 2 Transcriptome profiles of the lodicules during rice anthesis progression. (a) Expression profiles of all differentially expressed genes (DEGs) between two consecutive time points (B3h and B1d-18, B1h and B3h and F and B1h). For each gene, the scaled fragments per kilobase of transcript per million mapped reads (FPKM) value is exhibited by the continuous heat scale. The color gradient from blue to red indicates high to low gene expression. (b) *k*-means clustering of normalized gene expression patterns at four time points during anthesis. Six clusters (Cluster 1–Cluster 6) with distinct gene expression patterns were shown. Each line depicts the expression pattern of one gene, and the core values for each cluster are plotted in black. (c) Gene Ontology (GO) enrichment of genes in each cluster. The red arrows indicate the molecular processes related to cell osmolality and cell wall remodeling. BP, biological process; MF, molecular function; B1d-18, 18:00 at the day before floret opening; B3h, 3 h before floret opening; B1h, 1 h before floret opening; F, the time undergoing floret opening.

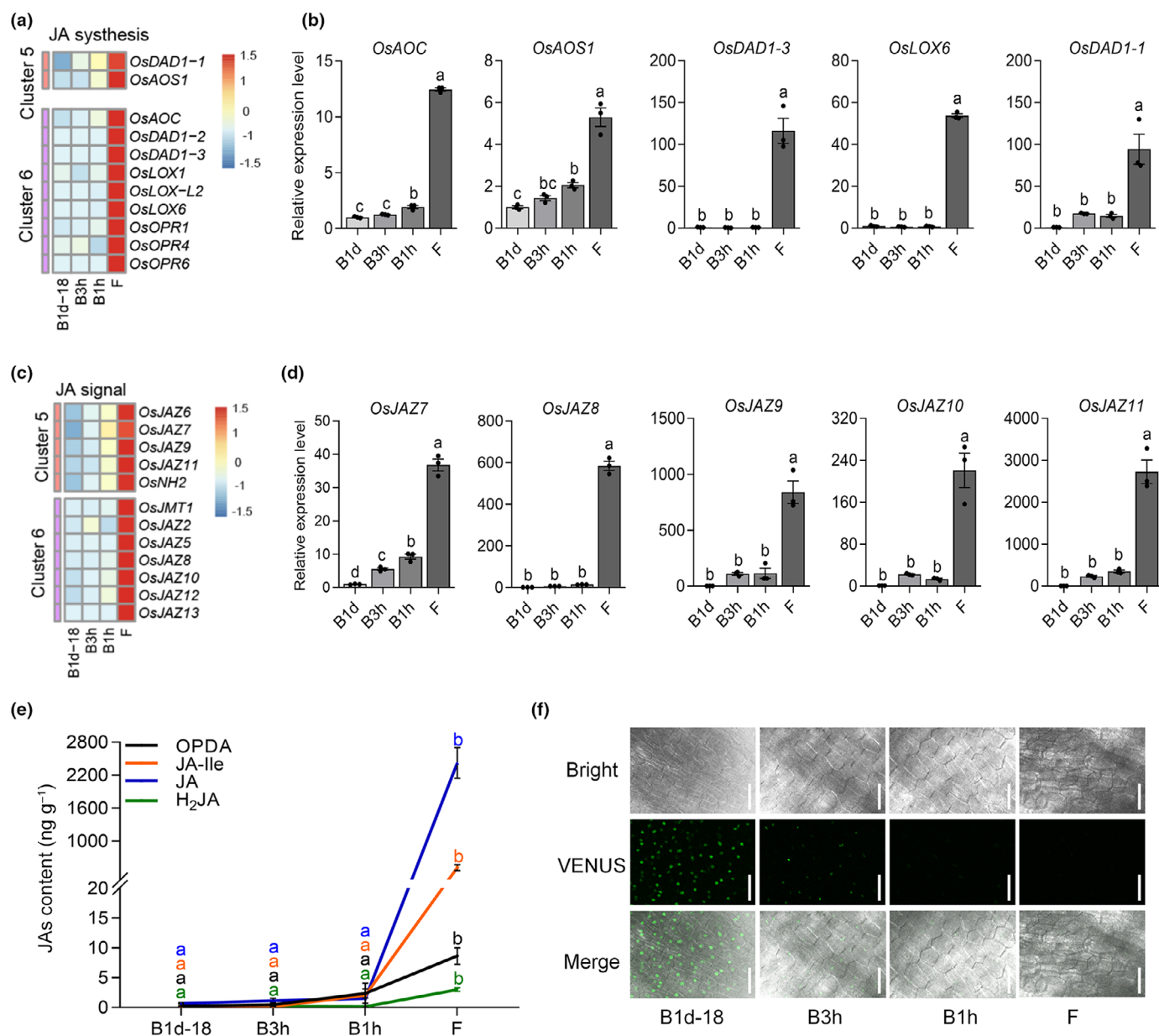


Fig. 3 Dynamic changes in jasmonic acid (JA) accumulation and signaling in the lodicules during rice anthesis. (a, b) The heatmaps show expression patterns of JA biosynthesis and signaling-related genes. For each gene, the scaled fragments per kilobase of transcript per million mapped reads (FPKM) value is exhibited by the continuous heat scale. Different letters above the bars indicate significant differences at $P < 0.05$ determined by Duncan's multiple range test. (c, d) Relative expression levels of JA biosynthesis and signaling genes in ZH11 lodicules at different time points of B1d-18, B3h, B1h and F. Data are shown as means \pm SE ($n = 3$). Different letters above the bars indicate significant differences at $P < 0.05$ determined by Duncan's multiple range test. (e) Measurement of JA, JA-Ile and H₂JA contents in ZH11 lodicules at different time points of B1d-18, B3h, B1h and F. Data are shown as means \pm SE ($n = 3$). Different letters above the bars indicate significant differences at $P < 0.05$ determined by Duncan's multiple range test. (f) VENUS fluorescence of ZH11 lodicule cells at different time points of B1d-18, B3h, B1h and F. Bars, 40 μ m. The color gradient from blue to red in a and c indicates high to low gene expression. B1d-18, 18:00 at the day before floret opening; B3h, 3 h before floret opening; B1h, 1 h before floret opening; F, the time undergoing floret opening.

results showed that the levels of JAs (JA, JA-Ile and H₂JA) and JA biosynthetic precursor 12-oxophytodienoic acid (OPDA) dramatically rose at the F time point, and the content of JA and JA-Ile were much higher than that of H₂JA and OPDA (Fig. 3e). Moreover, we investigated the dynamic change in endogenous JA by analyzing the transgenic rice carrying a JA perception biosensor

OsJAZ6-VENUS (Li *et al.*, 2021), which could sensitively visualize JA content *in vivo*. As shown in Fig. 3(f), the VENUS signals were obviously decreased from B1d-18 to B3h and then vanished at B1h and F. By contrast, the mutated version, mJAZ6-VENUS, was stable in lodicules during the process of floret opening (Fig. S6). These findings indicate endogenous JA had

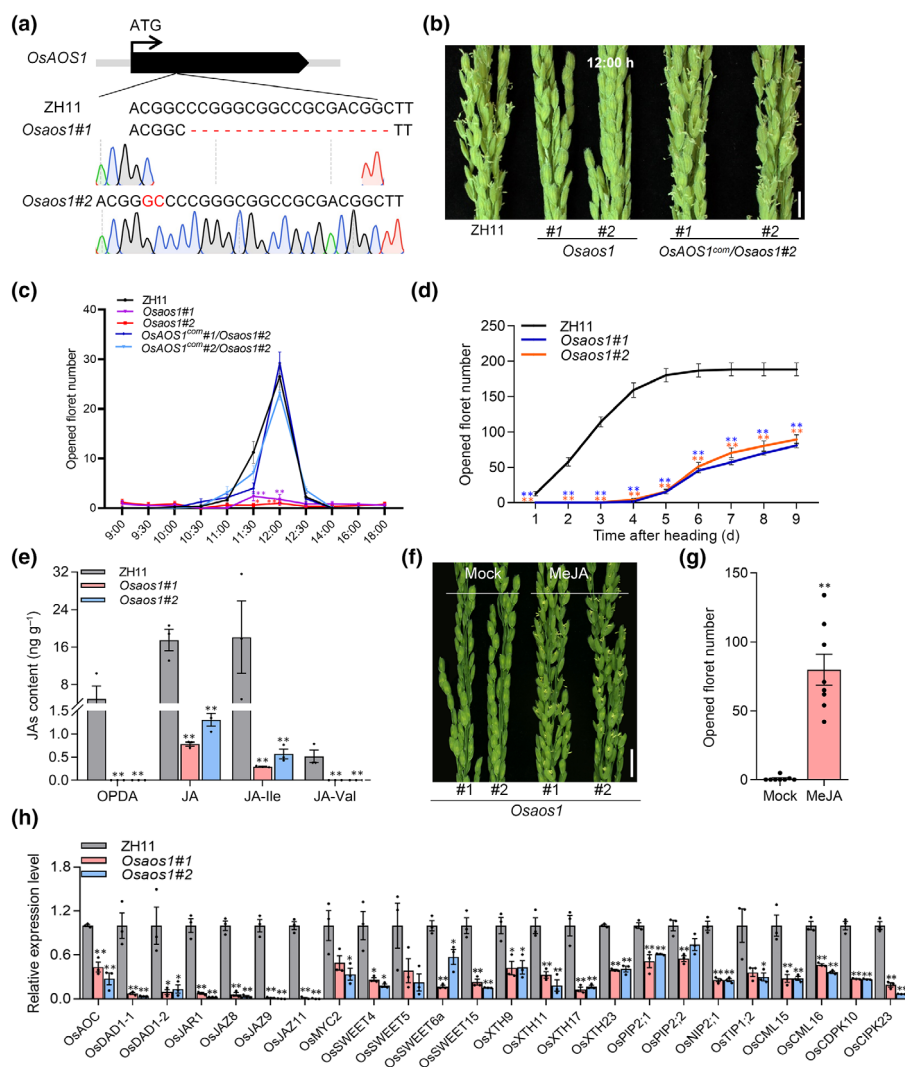


Fig. 4 *OsAOS1* plays a crucial role in regulating rice DFOT. (a) The sequences of two knockout mutant alleles of *Osaos1*#1 and *Osaos1*#2. (b) Comparison of panicles in ZH11, *Osaos1* and the complemented transgenic lines (*OsAOS1^{com}* / *Osaos1*#2) at the floret opening time (12:00 h). Bar, 1 cm. (c) Number of opened florets per panicle of ZH11, *Osaos1* and the *OsAOS1^{com}* / *Osaos1*#2 lines at different time points from 09:00 h to 18:00 h. Data are shown as means \pm SE ($n = 8$). Significance between *Osaos1* mutant and ZH11 is determined by a two-sided Student's *t*-test, *, $P < 0.05$; **, $P < 0.01$. (d) Total number of opened florets per panicle of ZH11 and *Osaos1* mutants on different days after heading. Data are shown as means \pm SE ($n = 10$). Significance between *Osaos1* mutant and ZH11 is determined by a two-sided Student's *t*-test, *, $P < 0.05$; **, $P < 0.01$. (e) Measurement of jasmonic acid (JA), JA-Ile, JA-Val and OPDA contents in ZH11 and *Osaos1* florets. Data are shown as means \pm SE ($n = 3$). Significance is determined by two-sided Student's *t*-test, *, $P < 0.05$; **, $P < 0.01$. (f) Phenotypic observation of *Osaos1* panicles after treatment with 2 mM MeJA for 30 min. Bar, 1 cm. (g) Number of opened florets in *Osaos1*#1 after treatment with 2 mM MeJA for 30 min. Data are shown as means \pm SE ($n = 8$). (h) Relative expression levels of genes related to JA synthesis and signaling, cell wall modification, and transmembrane transport in ZH11 and *Osaos1* mutants. Data are shown as means \pm SE ($n = 3$). Significance is determined by a two-sided Student's *t*-test, *, $P < 0.05$; **, $P < 0.01$. DFOT, diurnal floret opening time.

accumulated as early as at B3h, then continued to increase at B1h and reached its maximum at F. This accumulation pattern was in high accordance with the expression profiles of the JA biosynthesis and signaling genes. Furthermore, our transcriptome analysis showed that genes related to JA signaling pathway and other pathways exhibited similar expression patterns (Fig. S4), we thus conducted a WGCNA of the JA biosynthesis and signaling genes with other DEGs. Intriguingly, we showed that these genes were predicted to be functionally associated with many genes involved in cell wall modification, carbohydrate metabolism and sugar transport, water channel activity, ethylene signaling and calcium signaling pathways (Fig. S7). Collectively, these results suggest that a JA-mediated regulatory network plays a key role in regulating DFOT during anthesis.

OsAOS1 is required for regulating rice DFOT

Although JAs have been known to regulate the DFOT, but the underlying molecular mechanism remains largely unknown. AOSs are a family of allene oxide synthase that convert the hydroperoxide 13-hydroperoxyoctadeca-9,11-dienoic acid (13-HPOT) to 12,13-

epoxylinolenic acid in chloroplast, a key step for JA biosynthesis (Laudert *et al.*, 1997; Kuroda *et al.*, 2005). In our transcriptomic data, *OsAOS1* was greatly upregulated in the lodicules from the B1d-18 stage to the F stage, while the expression levels of other three paralogous genes (*OsAOS2/3/4*) were very low and not significantly altered during this process (Fig. S8a,b). Consistently, our histochemical analysis of *proOsAOS1::GUS* reporter gene transgenic lines also revealed stronger GUS signal in the lodicule at the F stage (Fig. S8c). Moreover, the *OsAOS1*-GFP fusion protein was indeed localized in the chloroplasts of rice protoplasts (Fig. S9). These results implied that *OsAOS1* may be involved in JA biosynthesis in the lodicules.

To further elucidate the biological function of *OsAOS1* in rice lodicules, we generated knockout mutants of *OsAOS1* in the Zhonghua11 (ZH11) background using the CRISPR/Cas9 technology, and two independent mutant lines were selected for detailed phenotypic analysis (*Osaos1*#1 and *Osaos1*#2; Fig. 4a). During anthesis, the florets of ZH11 opened at the period from 11:00 h to 12:30 h. However, the florets of *Osaos1* mutants seldomly opened until 18:00 h (Fig. 4b,c). Introduction of a complementary construct of *OsAOS1* driven by its native promoter

(*OsAOS1^{com}*) successfully rescued the disrupted DFOT phenotype of the *Osaos1* mutants (Fig. 4b,c), thus verifying a critical role of *OsAOS1* in regulating DFOT. Notably, we also found that the initial anthesis time of the *Osaos1* mutants was delayed c. 5 d, compared with ZH11, and the number of opening florets of *Osaos1* was significantly decreased (Fig. 4d). We next examined the contents of JA in the lodicules of ZH11 and *Osaos1*. As expected, we found that the levels of JA, JA-Ile, JA-Val and OPDA in the lodicules of the *Osaos1* mutants were significantly lower than those in ZH11 (Fig. 4e), and exogenous MeJA application could restore the abnormal floret opening phenotype of *Osaos1* to the WT (Fig. 4f,g), indicating that *OsAOS1* is required for JA biosynthesis in the lodicules. Besides, the levels of sucrose, glucose, fructose and the total soluble sugars were also decreased in the lodicules of the *Osaos1* mutants (Fig. S10). In addition, RT-qPCR analysis showed that the expression levels of dozens of DFOT-related genes were significantly downregulated in the *Osaos1* mutants compared with WT at B1h (Fig. 4h), while treatment with exogenous MeJA could obviously elevate these down-regulate genes (Fig. S11). These results collectively indicated that *OsAOS1* could promote JAs accumulation in the lodicules to induce the florets opening through regulating the DFOT-related genes. In further support of this notion, we also generated multiple *OsAOS1* overexpression lines by introducing the full-length CDS of *OsAOS1* under the control of the maize *Ubiquitin* promoter into the ZH11 background. As expected, the T_0 transgenic lines with a significantly elevated *OsAOS1* transcript levels exhibited a peak DFOT at 10:30 am in Lingshui (110°N, 18°5'E), c. 0.5 h earlier than ZH11 (Fig. S12).

An *OsMYC2*-mediated regulatory network is essential for rice floret opening

It was reported that *OsMYC2* is a master regulator involved in JA signaling transduction (Ogawa *et al.*, 2017; You *et al.*, 2019). RT-qPCR analysis revealed that *OsMYC2* was widely expressed in leaf, sheath, root, stem and various flower organs (lemma, palea, stamen, pistil and lodicule), and exhibited comparable expression level in lodicules at different stages of floret opening (Fig. S13). Notably, our results above showed that *OsMYC2* expression is downregulated in the lodicules of the *Osaos1* mutants and could be induced in response to exogenous MeJA treatment (Figs 4h, S11). We thus speculated that *OsMYC2* might function to mediate JA signaling in the lodicules of rice. To study the function of *OsMYC2* in DFOT regulation, we utilized the RNA interference (RNAi) technology to attenuate the expression of *OsMYC2* in rice. Two independent *OsMYC2-RNAi* lines with significant reduction in *OsMYC2* expression were identified (Fig. 5a), and phenotypic analysis showed that almost all the florets from *OsMYC2-RNAi* lines failed to open during the day (Fig. 5b,c). These results suggest that *OsMYC2* is essential for floret opening in rice.

It was known that MYC transcription factors prefer to bind to the G-box and G-box-like motifs (CAYGTK, Y represents T/C, K represents T/G; Fernández-Calvo *et al.*, 2010; López-Vidriero *et al.*, 2021). Our results above also demonstrated that JA

induced the florets opening through regulating the DFOT-related genes (Figs 4h, S11). Thus, we speculated that *OsMYC2* might control rice DFOT through regulating the DFOT-related genes identified above (Table S8). To test this notion, we first analyzed the 2-kb promoter sequences of these DFOT-related genes at the online website PlantCARE (<http://bioinformatics.psb.ugent.be/webtools/plantcare/html/>). A total of 59 different *cis*-acting elements were detected, of which the G-box motif accounted for the largest portion (Fig. S14a). Notably, 332 out of 337 (c. 98.5%) time point-specific genes related to cell osmolality and cell wall remodeling contained one or more G-box motifs in their promoters (Fig. S14b). We next performed RT-qPCR analyses and found that dozens of DFOT-related genes involved in JA biosynthesis, sugar transport, cell wall modification and water channel activity were significantly downregulated in the *OMYC2-RNAi* lines (Fig. S15). Among them, four down-regulated genes belong to different molecular pathways, including *OsAOS1* (regulating JA biosynthesis), *OsSWEET4* (regulating sugar transport), *OsXTH9* (regulating cell wall modification) and *OsPIP2;2* (regulating water channel activity), were selected for further analysis (Fig. 5d). Yeast one-hybrid and EMSA assays confirmed that *OsMYC2* could bind to the G-box-containing promoter fragments of *OsAOS1*, *OsSWEET4*, *OsPIP2;2* and *OsXTH9* (Fig. 5e,f). Moreover, the CUT&Tag-qPCR assay further confirmed the binding of *OsMYC2* to the *OsAOS1*, *OsSWEET4*, *OsPIP2;2* and *OsXTH9* promoters containing G-box motifs *in vivo* (Fig. 5g). Furthermore, dual-LUC assay indicated that LUC activity driven by the *OsAOS1*, *OsSWEET4*, *OsPIP2;2*, *OsXTH9* promoters was transiently induced by *OsMYC2* (Fig. 5h,i).

To examine whether these downstream genes are involved in rice DFOT regulation, we generated knockout mutants of *OsSWEET4* in the ZH11 background through the CRISPR/Cas9 technology (Fig. 6a). As expected, the *Ossweet4* mutants displayed scattered floret opening phenotype (random floret opening throughout the day) and delayed anthesis, similar to the *Osaos1* and *OsMYC2-RNAi* mutants (Fig. 6b–d). Besides, we screened a CRISPR/Cas9 library in ZH11 background (Lu *et al.*, 2017) and identified mutated lines of *OsPIP2;2* and *OsXTH9*. Both *Ospip2;2* and *Osxth9* mutants exhibited normal floret opening phenotype (data not shown), probably due to functional redundancy of their homologous genes. Taken together, these results suggest an *OsMYC2*-mediated regulatory network regulating rice DFOT.

Discussion

Proper DFOT is crucial for successful reproduction in rice and other plants. However, the molecular mechanisms underlying the regulation of DFOT are not well explored in rice. In this study, we collected several lines of evidence supporting the notion that JA acts as a master regulator of the rice DFOT through modulating multiple molecular processes related to cell osmolality and cell wall remodeling. We first found that the lodicules undergo dramatic changes in cytological characteristics and multiple physiological processes during the process of floret opening and

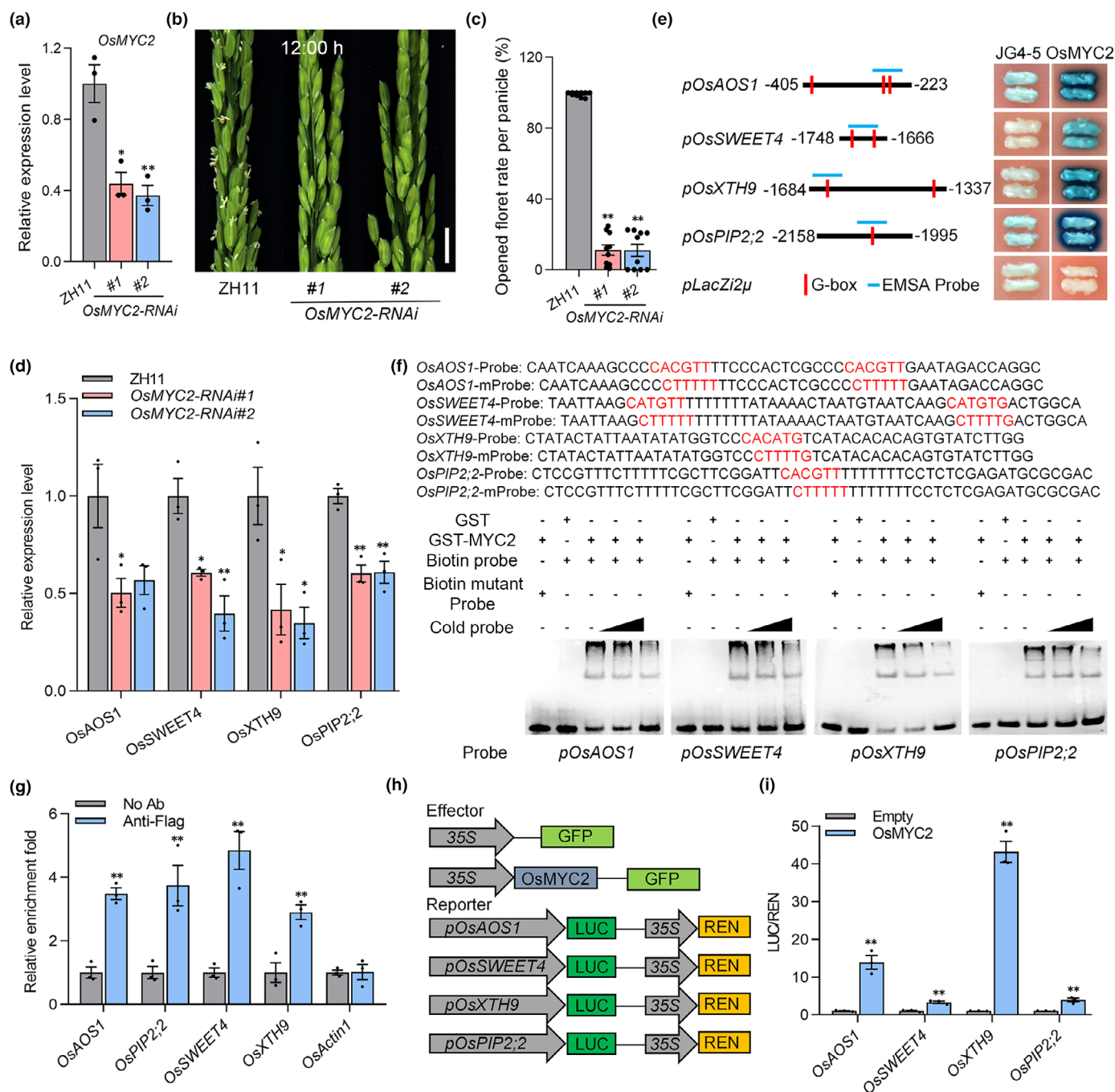


Fig. 5 *OsMYC2*-dependent regulatory network is required for regulating rice DFOT. (a) Relative expression levels of *OsMYC2* in ZH11 and *OsMYC2-RNAi* lodicules. Data are shown as means \pm SE ($n = 3$). Significance is determined by a two-sided Student's t -test: *, $P < 0.05$; **, $P < 0.01$. (b) Comparison of ZH11 and *OsMYC2-RNAi* panicles at the floret opening time (12:00 h). Bar, 1 cm. (c) Comparison of opened floret rate of ZH11 and *OsMYC2-RNAi* lines. Data are shown as means \pm SE ($n = 10$). (d) Relative expression levels of *OsAOS1*, *OsSWEET4*, *OsXTH9* and *OsPIP2;2* in ZH11 and *OsMYC2-RNAi* lodicules. Data are shown as means \pm SE ($n = 3$). Significance is determined by a two-sided Student's t -test: *, $P < 0.05$; **, $P < 0.01$. (e) Yeast one-hybrid assay shows that *OsMYC2* binds to the promoters of *OsAOS1*, *OsSWEET4*, *OsXTH9* and *OsPIP2;2*. The G-box motifs and their mutant versions are shown in red. Probe sequences are marked with blue lines in (e). (f) Electrophoretic mobility shift assays (EMSA) assay shows that *OsMYC2* binds to the promoters of *OsAOS1*, *OsSWEET4*, *OsXTH9* and *OsPIP2;2*. The G-box motifs and their mutant versions are shown in red. Probe sequences are marked with blue lines in (e). (g) CUT&Tag-qPCR assay shows that *OsMYC2* binds to the promoters of *OsAOS1*, *OsSWEET4*, *OsXTH9* and *OsPIP2;2*. The promoter of *OsActin1* without G-box was used as a control. Data are shown as means \pm SE ($n = 3$). Significance is determined by a two-sided Student's t -test: **, $P < 0.01$. (h) Schema of constructs used for transient dual-LUC assay in rice protoplasts. (i) Transient dual-LUC assay shows that *OsMYC2* induces the transcriptions of *pOsAOS1*, *pOsSWEET4*, *pOsXTH9* and *pOsPIP2;2* reporters in rice protoplasts. Data are shown as means \pm SE ($n = 3$). Significance is determined by a two-sided Student's t -test: *, $P < 0.05$; **, $P < 0.01$. DFOT, diurnal floret opening time.

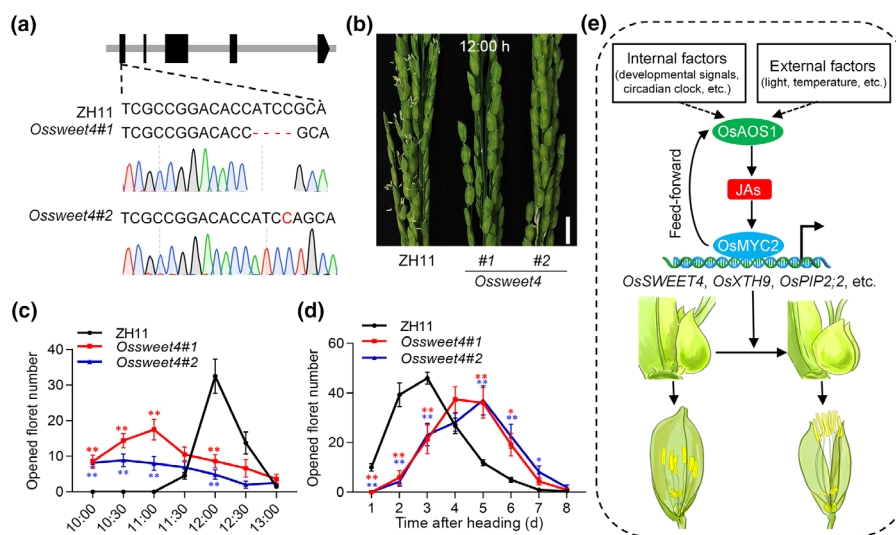


Fig. 6 Jasmonic acid (JA)-mediated feed-forward regulatory model for DFOT regulation in rice. (a) The sequences of two knockout mutant alleles of *Oosweet4#1* and *Oosweet4#2*. (b) Comparison of ZH11 and *Oosweet4* mutant panicles at the floret opening time (12:00 h). Bar, 1 cm. (c) Number of opened florets per panicle of ZH11 and *Oosweet4* mutants at different time points from 10:00 h to 13:00 h. Data are shown as means \pm SE ($n = 8$). Significance is determined by a two-sided Student's *t*-test: *, $P < 0.05$; **, $P < 0.01$. (d) Total number of opened florets per panicle of ZH11 and *Oosweet4* mutants at different days after heading. Data are shown as means \pm SE ($n = 10$). Significance is determined by a two-sided Student's *t*-test: *, $P < 0.05$; **, $P < 0.01$. (e) A working model of JAs in regulating rice floret opening. DFOT, diurnal floret opening time. Dashed arrows represent mechanisms that are still unclear, while solid arrows represent confirmed pathways.

closure, such as cell size, cell wall thickness, water and sugar contents (Fig. 1). In line with these findings, we further identified a large set of DFOT-related genes associated with cell osmolality and cell wall remodeling through the time-course transcriptome analyses of the lodicules (Figs 2, 3, S4). Notably, we found that JA biosynthesis and signaling genes exhibited a trend of continuous upregulation in the lodicules, which was accompanied by a continuous increase in JA accumulation during anthesis progression (Fig. 3). Furthermore, we demonstrated that *OsAOS1* is required for endogenous JA biosynthesis in the lodicules, while *OsMYC2* acts as a master regulator to directly promote expression of genes related to sugar transport (*OsSWEET4*), water transport (*OsPIP2;2*) and cell wall modification (*OsXTH9*), thus promoting DFOT in rice (Figs 4, 5). We also found that *OsMYC2* could directly bind to and promote the expression of *OsAOS1* (Fig. 5d–i), suggesting a positive feedback loop regulating JA biosynthesis and signaling during rice anthesis. Strikingly, we showed that *OsMYC2* exhibited comparable expression levels in lodicules at different stages of floret opening (Fig. S13b), while *OsAOS1*, *OsSWEET4*, *OsPIP2;2* and *OsXTH9* exhibited a continuous upregulation trend, reaching peak expression at the F stage (Fig. S5), consistent with the JA accumulation pattern (Fig. 3e,f). Considering that elevated JA levels lead to the degradation of JAZ proteins, thereby abolishing the inhibitory effects of JAZs on *OsMYC2* (Cai *et al.*, 2014; Wu *et al.*, 2015), we speculate that *OsMYC2*-mediated activation of *OsAOS1*, *OsSWEET4*, *OsPIP2;2* and *OsXTH9* expression during anthesis might be mainly regulated at the posttranscriptional level via JAZ proteins. Thus, we propose a model that JA activates its downstream regulator *OsMYC2* early before floret opening, which in turn promotes the expression of sugar transporters, aquaporins,

cell wall remodeling factor and JA biosynthesis genes respectively, thus promoting DFOT by increasing osmotic pressure, water absorption and cell expansion of the lodicules (Fig. 6e). We speculate that this JA-mediated regulatory model controlling floret opening may also operate in other grasses and dicot plants, as similar changes in cellular osmotic and turgor pressure occur during floret opening in diverse plants (Wang *et al.*, 1991, 2022; Gookin *et al.*, 2003; Van Doorn & Van Meeteren, 2003; Xu *et al.*, 2022).

Besides JA, earlier studies have suggested that auxin, ethylene, calcium and the circadian clock are also involved in regulating DFOT in diverse plant species. For example, a recent study reported a signaling cascade constituted of *OsARF2* and *OsARF18* regulates floret opening in rice by regulating sucrose transport from the source tissues (vegetative organs) into the sink tissues (reproductive organs; Zhao *et al.*, 2022). In addition, the role of ethylene in the flower opening was repeatedly reported in ornamental plants (Cheng *et al.*, 2021; Sun *et al.*, 2021). It was also reported that silencing the core circadian clock genes *NaLHY* and *NaZTL* in *Nicotiana attenuata* could strongly alter the floret movement rhythm thus affecting the DFOT (Yon *et al.*, 2016). Notably, we found that many DEGs related to calcium, circadian clock, auxin and ethylene signaling pathways were also co-regulated with the JA signaling-related genes during anthesis (Figs 2, 3). Therefore, it will be worthy to investigate how the JA signaling pathway cross-talks with other signaling pathways to coordinately regulate DFOT in future studies. Moreover, it has been documented that various environmental factors, such as light, temperature and humidity, could affect DFOT in rice (Gu & Wang, 1993; Jagadish *et al.*, 2007; Kobayasi *et al.*, 2010; Zhou

et al., 2014). However, how these external factors are integrated with the internal regulatory programs to regulate DFOT has not yet been carefully studied. Considering the extensive role of JA in plant responses to environmental conditions (such as heat, cold and drought; An *et al.*, 2021; Zhu *et al.*, 2021; Kong *et al.*, 2023), it will be an interesting avenue to exploit the possible role of JA regulatory networks in adjusting rice DFOT under different environmental conditions in future research.

Due to the escalated global warming effect, heat stress is causing serious impacts on reproductive development and production in rice (Jagadish *et al.*, 2016). Earlier studies reported that rice varieties with early floret opening might help to mitigate heat-induced spikelet sterility at the anthesis stage by escaping heat stress during the daytime, thus enhancing rice thermotolerance (Jagadish *et al.*, 2007; Ishimaru *et al.*, 2010; Das *et al.*, 2014; Zhou *et al.*, 2014). For example, introducing an *early-morning flowering* (EMF) QTL designated as *qEMF3* from the wild rice *O. officinalis* into a popular *indica* variety IR64 shifted the DFOT by c. 2.0 h earlier for the IR64, and effectively reduced heat stress-induced spikelet sterility both under growth chamber and field conditions in the Philippine tropics (Hirabayashi *et al.*, 2015). In this study, we have identified a number of DFOT-related genes, including positive regulators such as *OsAOS1*, *OsMYC2* and *OsSWEET4*, and potential negative regulators such as *OsJAZs*, *OsPMEs* and the circadian clock genes (Fig. S4). We speculate that elevating the expression of the DFOT positive regulators in the lodicules or knocking out the DFOT negative regulators may help to breed rice varieties with earlier DFOT to escape heat stress. Besides, DFOT is also important for hybrid rice seed production. Hybrid rice seeds are produced by crossing the male sterile (MS) line with the restorer (R) line, and a synchronous DFOT of the parental lines is a prerequisite for successful hybrid seed production. However, the average DFOT of MS lines, especially the *japonica* MS lines for producing the inter-subspecific *indica-japonica* hybrid rice, is usually later than the R lines, greatly reducing hybrid seed production (Wang *et al.*, 1994). Recently, a study reported that overexpressing the JA biosynthesis gene *OsOPR7* or knocking out JA inactivation gene *OsHANI* in a *japonica* male lines GAZS significantly advances DFOT and enhances the *indica-japonica* hybrid F₁ seed production (Wang *et al.*, 2024). Additionally, introgressing the *indica* allele of *OsMYB8* (a key regulator of JA biosynthesis) into *japonica* rice could confer earlier DFOT, thus effectively helping to synchronize the DFOT of *indica* and *japonica* varieties (Gou *et al.*, 2024). In this study, we also showed that overexpressing *OsAOS1* promotes DFOT (Fig. S12). Thus, we suggest that further manipulation of JA-related genes may offer an effective approach to overcome asynchronous DFOT and improve hybrid seed production, especially for the inter-subspecific *indica-japonica* hybrid rice.

Acknowledgements

This work was supported by the National Natural Science Foundation of China (31991222, 31921004 and 32172056), Hainan Yazhou Bay Seed Laboratory (B23YQ1515 and B23CQ15FP),

the Natural Science Foundation of Guangdong Province-Guangzhou City Collaborative Key Project (2019B1515120061) and the Double First-class Discipline Promotion Project (2021B10564001).

Competing interests

None declared.

Authors contributions

HW, RS and YH conceived and designed experiments. WD, YG and YL performed most of the experiments, WD analyzed the data. YL and JL characterized the genotypes and phenotypes of the edited lines. YF and XL designed the CRISPR target and constructed the plasmid library. XZ and RY carried out the phenotype investigation of transgenic rice. WD, YG, YH, HW and RS wrote the manuscript. HW revised the article. WD, YG and YL contributed equally to this work.

ORCID

Wenyan Ding  <https://orcid.org/0000-0001-7750-2410>
Yajun Gou  <https://orcid.org/0009-0000-2548-7546>
Yueqin Heng  <https://orcid.org/0000-0001-7209-9714>
Rongxin Shen  <https://orcid.org/0009-0004-0791-0370>
Haiyang Wang  <https://orcid.org/0000-0002-1302-5747>

Data availability

All data needed to evaluate the conclusions in the paper are present in the paper and/or the [Supporting Information](#). RNA-seq data generated in this study have been deposited in the NCBI Sequence Read Archive database under the accession no.: PRJNA1000954. Additional data related to this paper may be requested from the authors.

References

- An JP, Wang XF, Zhang W, Yo CX, Hao YJ. 2021. Apple B-box protein BBX37 regulates jasmonic acid mediated cold tolerance through the JAZ-BBX37-ICE1-CBF pathway and undergoes MIEL1-mediated ubiquitination and degradation. *New Phytologist* 229: 2707–2729.
- Baack E, Melo MC, Rieseberg LH, Ortiz-Barrientos D. 2015. The origins of reproductive isolation in plants. *New Phytologist* 207: 968–984.
- Cai Q, Yuan Z, Chen M, Yin C, Luo Z, Zhao X, Liang W, Hu J, Zhang D. 2014. Jasmonic acid regulates spikelet development in rice. *Nature Communications* 5: 3476.
- Cao L, Tian J, Liu Y, Chen X, Li S, Persson S, Lu D, Chen M, Luo Z, Zhang D *et al.* 2021. Ectopic expression of *OsJAZ6*, which interacts with *OsJAZ1*, alters JA signaling and spikelet development in rice. *The Plant Journal* 8: 1083–1096.
- Chen S, Zhou Y, Chen Y, Gu J. 2018. FASTP: an ultra-fast all-in-one FASTQ preprocessor. *Bioinformatics* 34: 884–890.
- Cheng C, Yu Q, Wang Y, Wang H, Dong Y, Ji Y, Zhou X, Li Y, Jiang C, Gan S *et al.* 2021. Ethylene-regulated asymmetric growth of the petal base promotes flower opening in rose (*Rosa hybrida*). *Plant Cell* 33: 1229–1251.
- Chico JM, Chini A, Fonseca S, Solano R. 2008. JAZ repressors set the rhythm in jasmonate signaling. *Current Opinion in Plant Biology* 11: 486–494.

- Das S, Krishnan P, Nayak M, Ramakrishnan B. 2014. High temperature stress effects on pollens of rice (*Oryza sativa* L.) genotypes. *Environmental and Experimental Botany* 101: 36–46.
- Fernández-Calvo P, Chini A, Fernández-Barbero G, Chico JM, Gimenez-Ibanez S, Geerinck J, Eeckhout D, Schweizer F, Godoy M, Franco-Zorrilla JM *et al.* 2010. The *Arabidopsis* bHLH transcription factors MYC3 and MYC4 are targets of JAZ repressors and act additively with MYC2 in the activation of jasmonate responses. *Plant Cell* 23: 701–715.
- Fu Y, Xiang M, Jiang H, He Y, Zeng X. 2016. Transcriptome profiling of lodicules before floret opening in *Oryza sativa* L. *Scientia Agricultura Sinica* 49: 1017–1033.
- Gao X, Zeng X, Wang S, Lin P, Zhou X. 2003. Effect of methyl jasmonate and salicylic acid on the blossom of spikelets in sorghum and sudanese grass. *Chinese Agricultural Science Bulletin* 16: 7–9.
- Gookin TE, Hunter DA, Reid MS. 2003. Temporal analysis of alpha and beta-expansin expression during floral opening and senescence. *Plant Science* 164: 769–781.
- Gou Y, Heng Y, Ding W, Xu C, Tan Q, Li Y, Fang Y, Li X, Zhou D, Zhu X *et al.* 2024. Natural variation in *OsMYB8* confers diurnal floret opening time divergence between indica and japonica subspecies. *Nature Communications* 15: 2262.
- Gu Y, Wang Z. 1993. An investigation on the effects of environmental factors on the opening and closure of florets in rice. *Acta Physiologica Sinica* 19: 345–352.
- Heslop-Harrison Y, Heslop-Harrison JS. 1996. Lodicule function and filament extension in the grasses: potassium ion movement and tissue specialization. *Annals of Botany* 77: 573–582.
- Hibara K, Isono M, Mimura M, Sentoku N, Kojima M, Sakakibara H, Kitomi Y, Yoshikawa T, Itoh JI, Nagato Y. 2016. Jasmonate regulates juvenile-adult phase transition in rice. *Development* 143: 3407–3416.
- Hirabayashi H, Sasaki K, Kambe T, Gannabani RB, Miras MA, Mendioro MS, Simon EV, Lumanglas PD, Fujita D, Takemoto-Kuno Y *et al.* 2015. *qEMF3*, a novel QTL for the early-morning flowering trait from wild rice, *Oryza officinalis*, to mitigate heat stress damage at flowering in rice, *O. sativa*. *Journal of Experimental Botany* 66: 1227–1236.
- Huang H, Liu B, Liu L, Song S. 2017. Jasmonate action in plant growth and development. *Journal of Experimental Botany* 68: 1349–1359.
- Irish VF. 2008. The *Arabidopsis* petal: a model for plant organogenesis. *Trends in Plant Science* 13: 430–436.
- Ishiguro S, Kawai-Oda A, Ueda J, Nishida K, Okada K. 2001. The *DEFECTIVE IN ANTER DEHISCENCE1* gene encodes a novel phospholipase A1 catalyzing the initial step of jasmonic acid biosynthesis, which synchronizes pollen maturation, anther dehiscence, and flower opening in *Arabidopsis*. *Plant Cell* 13: 2191–2209.
- Ishimaru T, Hirabayashi H, Ida M, Takai T, San-Oh YA, Yoshinaga S, Ando I, Ogawa T, Kondo M. 2010. A genetic resource for early-morning flowering trait of wild rice *Oryza officinalis* to mitigate high temperature-induced spikelet sterility at anthesis. *Annals of Botany* 106: 515–520.
- Jagadeesh SV, Bahuguna RN, Djanaguiraman M, Gamuyao R, Prasad PV, Craufurd PQ. 2016. Implications of high temperature and elevated CO₂ on flowering time in plants. *Frontiers in Plant Science* 7: 913.
- Jagadeesh SV, Craufurd PQ, Wheeler TR. 2007. High temperature stress and spikelet fertility in rice (*Oryza sativa* L.). *Journal of Experimental Botany* 58: 1627–1635.
- Juarez MT, Twigg RW, Timmermans MC. 2004. Specification of adaxial fate during maize leaf development. *Development* 131: 4533–4544.
- Ke M, Gao Z, Chen J, Qiu Y, Zhang L, Chen X. 2018. Auxin controls circadian flower opening and closure in the waterlily. *BMC Plant Biology* 18: 143.
- Kim D, Langmead B, Salzberg SL. 2015. HISAT: a fast spliced aligner with low memory requirements. *Nature Methods* 12: 357–360.
- Kobayashi K, Matsui T, Yoshimoto M, Hasegawa T. 2010. Effects of temperature, solar radiation, and vapor-pressure deficit on flower opening time in rice. *Plant Production Science* 13: 21–28.
- Kong L, Song Q, Wei H, Wang Y, Lin M, Sun K, Zhang Y, Yang J, Li C, Luo K. 2023. The AP2/ERF transcription factor PtoERF15 confers drought tolerance via JA-mediated signaling in *Populus*. *New Phytologist* 240: 1848–1867.
- Kunio Y, Ryo N, Katsumi S, Takaaki N, Hideo I, Kazuo I. 2009. Cell division and expansion growth during rose petal development. *Journal of the Japanese Society for Horticultural Science* 78: 356–362.
- Kuroda H, Oshima T, Kaneda H, Takashio M. 2005. Identification and functional analyses of two cDNAs that encode fatty acid 9–/13-hydroperoxide lyase (CYP74C) in rice. *Bioscience, Biotechnology and Biochemistry* 69: 1545–1554.
- Langfelder P, Horvath S. 2008. WGCNA: an R package for weighted correlation network analysis. *BMC Bioinformatics* 9: 559.
- Langfelder P, Horvath S. 2012. Fast R functions for robust correlations and hierarchical clustering. *Journal of Statistical Software* 46: 1–17.
- Laudert D, Hennig P, Stelmach BA, Müller A, Andert L, Weiler EW. 1997. Analysis of 12-oxo-phytodienoic acid enantiomers in biological samples by capillary gas chromatography-mass spectrometry using cyclodextrin stationary phases. *Analytical Biochemistry* 246: 211–217.
- Li L, Zhang W, Zhang L, Li N, Peng J, Wang Y, Zhong C, Yang Y, Sun S, Liang S *et al.* 2015. Transcriptomic insights into antagonistic effects of gibberellin and abscisic acid on petal growth in *Gerbera hybrida*. *Frontiers in Plant Science* 6: 168.
- Li S, Cao L, Chen X, Liu Y, Persson S, Hu J, Chen M, Chen Z, Zhang D, Yuan Z. 2021. Synthetic biosensor for mapping dynamic responses and spatio-temporal distribution of jasmonate in rice. *Plant Biotechnology Journal* 19: 2392–2394.
- Li X, Wang Y, Duan E, Qi Q, Zhou K, Lin Q, Wang D, Wang Y, Long W, Zhao Z. 2018. OPEN GLUME1: a key enzyme reducing the precursor of JA, participates in carbohydrate transport of lodicules during anthesis in rice. *Plant Cell Reports* 37: 329–346.
- Lin R, Ding L, Casola C, Ripoll DR, Feschotte C, Wang H. 2007. Transposase-derived transcription factors regulate light signaling in *Arabidopsis*. *Science* 318: 1302–1305.
- López-Vidriero I, Godoy M, Grau J, Peñuelas M, Solano R, Franco-Zorrilla JM. 2021. DNA features beyond the transcription factor binding site specify target recognition by plant MYC2-related bHLH proteins. *Plant Communications* 2: 100232.
- Lu Y, Ye X, Guo R, Huang J, Wang W, Tang J, Tan L, Zhu JK, Chu C, Qian Y. 2017. Genome-wide targeted mutagenesis in rice using the CRISPR/Cas9 system. *Molecular Plant* 10: 1242–1245.
- Ma X, Zhang Q, Zhu Q, Liu W, Chen Y, Qiu R, Wang B, Yang Z, Li H, Lin Y *et al.* 2015. A robust CRISPR/Cas9 system for convenient, high-efficiency multiplex genome editing in monocot and dicot plants. *Molecular Plant* 8: 1274–1284.
- Ochiai M, Matsumoto S, Yamada K. 2013. Methyl jasmonate treatment promotes flower opening of cut Eustoma by inducing cell wall loosening proteins in petals. *Postharvest Biology and Technology* 82: 1–5.
- Ogawa S, Miyamoto K, Nemoto K, Sawasaki T, Yamane H, Nojiri H, Okada K. 2017. OsMYC2, an essential factor for JA-inductive sakuranetin production in rice, interacts with MYC2-like proteins that enhance its transactivation ability. *Scientific Reports* 7: 4015.
- Ouyang S, Zhu W, Hamilton J, Lin H, Campbell M, Chids K, Thibaud-Nissen F, Malek RL, Lee Y, Zheng L *et al.* 2007. The TIGR rice genome annotation resource: improvements and new features. *Nucleic Acids Research* 35: D883–D887.
- Putri GH, Anders S, Pyl PT, Pimanda JE, Zanini F. 2022. Analysing high-throughput sequencing data in Python with HTSEQ 2.0. *Bioinformatics* 38: 2943–2945.
- Robinson MD, McCarthy DJ, Smyth GK. 2010. EDGE: a bioconductor package for differential expression analysis of digital gene expression data. *Bioinformatics* 26: 139–140.
- Rolland-Lagan A, Bangham J, Coen E. 2003. Growth dynamics underlying petal shape and asymmetry. *Nature* 422: 161–163.
- Shannon P, Markiel A, Ozier O, Baliga NS, Wang JT, Ramage D, Amin N, Schwikowski B, Ideker T. 2003. CYTOSCAPE: a software environment for integrated models of biomolecular interaction networks. *Genome Research* 13: 2498–2504.
- Song P, Xia K, Wu C, Bao D, Chen L, Zhou X, Cao X. 2001. Differential response of floret opening in male-sterile and male-fertile rices to methyl jasmonate. *Acta Botanica Sinica* 43: 480–485.
- Soufflet-Freslon V, Araou E, Jeaufré J, Thouroude T, Chastellier A, Michel G, Mikanagi Y, Kawamura K, Banfield M, Oghina-Pavie C *et al.* 2021. Diversity

- and selection of the continuous-flowering gene, *RoKSN*, in rose. *Horticulture Research* 8: 76.
- Sun X, Qin M, Yu Q, Huang Z, Xiao Y, Li Y, Ma N, Gao J. 2021. Molecular understanding of postharvest flower opening and senescence. *Molecular Horticulture* 1: 7.
- Trang Nguyen H, Thi Mai To H, Lebrun M, Bellafiore S, Champion A. 2019. Jasmonates-the master regulator of rice development, adaptation and defense. *Plants* 8: 339.
- Turner JG, Ellis C, Devoto A. 2002. The jasmonate signal pathway. *Plant Cell* 14: 153–164.
- Van Doorn WG, Kamdee C. 2014. Flower opening and closure: an update. *Journal of Experimental Botany* 65: 5749–5757.
- Van Doorn WG, Van Meeteren U. 2003. Flower opening and closure: a review. *Journal of Experimental Botany* 54: 1801–1812.
- Varaud E, Brioudes F, Szécsi J, Leroux J, Brown S, Perrot-Rechenmann C, Bendahmane M. 2011. *AUXIN RESPONSE FACTOR8* regulates *Arabidopsis* petal growth by interacting with the bHLH transcription factor BIGPETALp. *Plant Cell* 23: 973–983.
- Wang M, Zhu X, Huang Z, Chen M, Xu P, Liao S, Zhao Y, Gao Y, He J, Luo Y *et al.* 2024. Controlling diurnal flower-opening time by manipulating the jasmonate pathway accelerates development of *indica-japonica* hybrid rice breeding. *Plant Biotechnology Journal* 22: 2267–2281.
- Wang M, Zhu X, Peng G, Liu M, Zhang S, Chen M, Liao S, Wei X, Xu P, Tan X *et al.* 2022. Methylesterification of cell-wall pectin controls the diurnal flower-opening times in rice. *Molecular Plant* 15: 956–972.
- Wang Z, Gu Y, Gao Y. 1991. Studies on the mechanism of the anthesis of rice III. Structures of the lodicule and changes of its contents during flowering. *The Crop Journal* 17: 96–101.
- Wang Z, Gu Y, Gao Y. 1994. Studies on the mechanism of the anthesis of rice: V. Comparison of lodicule and filament structure between sterile line and fertile line. *The Crop Journal* 20: 13–17.
- Wickham H. 2016. *ggplot2: elegant graphics for data analysis*. New York, NY, UK: Springer-Verlag Press.
- Wu H, Ye H, Yao R, Zhang T, Xiong L. 2015. *OsJAZ9* acts as a transcriptional regulator in jasmonate signaling and modulates salt stress tolerance in rice. *Plant Science* 232: 1–12.
- Xiao Y, Chen Y, Charnikhova T, Mulder PJ, Heijmans J, Hoogenboom A, Agalou A, Michel C, Morel J, Dreni L *et al.* 2014. *OsJAZ1* is required for JA-regulated floret opening and anther dehiscence in rice. *Plant Molecular Biology* 86: 19–33.
- Xie X, Ma X, Zhu Q, Zeng D, Li G, Liu Y. 2017. CRISPR-GE: a convenient software toolkit for CRISPR-Based genome editing. *Molecular Plant* 10: 1246–1249.
- Xu P, Wu T, Ali A, Zhang H, Liao Y, Chen X, Tian Y, Wang W, Fu X, Li Y *et al.* 2022. *EARLY MORNING FLOWERING1 (EMF1)* regulates the floret opening time by mediating lodicule cell wall formation in rice. *Plant Biotechnology Journal* 20: 1441–1443.
- Yon F, Joo Y, Llorca LC, Rothe E, Baldwin IT, Kim S. 2016. Silencing *Nicotiana attenuata* *LHY* and *ZTL* alters circadian rhythms in flowers. *New Phytologist* 209: 1058–1066.
- You X, Zhu S, Zhang W, Zhang J, Wang C, Jing R, Chen W, Wu H, Cai Y, Feng Z *et al.* 2019. *OsPEX5* regulates rice spikelet development through modulating jasmonic acid biosynthesis. *New Phytologist* 224: 712–724.
- Zeng X, Zhou X, Zhang W, Murofushi N, Kitahara T, Kamuro Y. 1999. Opening of rice floret in rapid response to methyl jasmonate. *Journal of Plant Growth Regulation* 18: 153–158.
- Zhang M, Dai D, Li X, Zhang H, Ma L. 2016. Advances in the traits of flowering time in rice. *Journal of Nuclear Agricultural Sciences* 30: 267–274.
- Zhang Y, Su J, Duan S, Ao Y, Wang H. 2011. A highly efficient rice green tissue protoplast system for transient gene expression and studying light/chloroplast-related processes. *Plant Methods* 7: 30.
- Zhao Z, Wang C, Yu X, Tian Y, Wang W, Zhang Y, Bai W, Yang N, Zhang T, Zheng H *et al.* 2022. Auxin regulates source-sink carbohydrate partitioning and reproductive organ development in rice. *Proceedings of the National Academy of Sciences, USA* 119: e2121671119.
- Zhou J, Zhang Y, Zhu D, Lin X, Xiang J, Chen H, Hu S. 2014. Influence of flowering characteristic on spikelet fertility under high temperature. *Chinese Journal of Rice Science* 28: 297–303.
- Zhu T, Herrfurth C, Xin M, Savchenko T, Feussner I, Goossens A, De Smet I. 2021. Warm temperature triggers JOX and ST2A-mediated jasmonate catabolism to promote plant growth. *Nature Communications* 12: 4804.
- Zonia L, Munnik T. 2007. Life under pressure: hydrostatic pressure in cell growth and function. *Trends in Plant Science* 12: 90–97.

Supporting Information

Additional Supporting Information may be found online in the Supporting Information section at the end of the article.

Fig. S1. Morphological observations of ZH11 lodicules during rice anthesis.

Fig. S2 Determination of water and sugar contents in the lodicules of ZH11.

Fig. S3 RNA-seq analysis of ZH11 lodicules.

Fig. S4 Heatmaps showing the expression patterns of representative genes related to DFOT regulation in rice.

Fig. S5 RT-qPCR assay verifies the transcriptome data of ZH11 lodicules at different time points.

Fig. S6 VENUS fluorescence of the mJAZ6-VENUS reporter in rice lodicule cells at different time points.

Fig. S7 Co-expression analysis of JA biosynthesis and signaling-related genes with other DEGs across anthesis progression in rice.

Fig. S8 The expression pattern of *OsAOS1* in rice.

Fig. S9 The subcellular localization of *OsAOS1*.

Fig. S10 The sugars content in the lodicules of ZH11 and *Osaos1* mutants.

Fig. S11 Expression analyses of DFOT-related genes in the lodicules of *Osaos1#1* treated by MeJA.

Fig. S12 The phenotype of ZH11 and the *OsAOS1-OE* lines.

Fig. S13 The expression pattern of *OsMYC2* in ZH11.

Fig. S14 *Cis*-acting element analysis of the genes shown in Table S8.

Fig. S15 Expression analyses of DFOT-related genes in the lodicules of ZH11 and the *OsMYC2-RNAi* lines.

Table S1 Primers used in this study.

Table S2 Determination of the soluble sugar content in ZH11 lodicules at different time points.

Table S3 FPKM values of all expressed genes in 12 samples.

Table S4 The differentially expressed genes (DEGs) in the lodicules between B3h and B1d-18.

Table S5 The differentially expressed genes (DEGs) in the lodicules between B1h and B3h.

Table S6 The differentially expressed genes (DEGs) in the lodicules between F and B1h.

Table S7 *k*-means clustering analysis of all differentially expressed genes (DEGs).

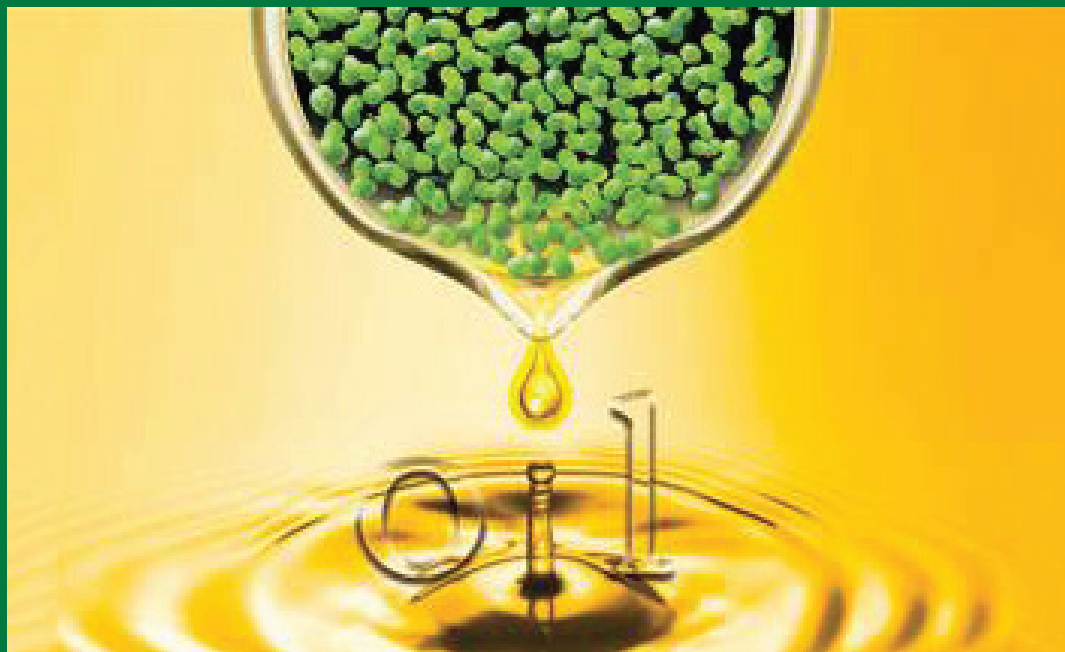
Table S8 List of 337 potential DFOT-related genes associated with cell osmolality and cell wall remodeling.

Please note: Wiley is not responsible for the content or functionality of any Supporting Information supplied by the authors. Any queries (other than missing material) should be directed to the *New Phytologist* Central Office.

Plant Biotechnology Journal

Open Access

Volume 21 • Issue 2 • February 2023



WILEY

www.plantbiotechnologyjournal.com | ISSN 1467-7644

第99页

Editorial Board Information

Editor-in-Chief

Johnathan Napier
Rothamsted Research, Harpenden,
Hertfordshire, UK
EMAIL johnathan.napier@rothamsted.ac.uk

Editorial Office

Plant Biotechnology Journal Editorial Office
Wiley | 9600 | Garsington Road | Oxford | OX4 2DQ | UK
TEL +44 (0) 1865 476 206 | FAX +44 (0) 1865 714591
EMAIL plant-biotechj@wiley.com

Editor Emeritus

Henry Daniell, W.D. Miller Professor and Director of Translational Research,
School of Dental Medicine, University of Pennsylvania, Philadelphia, Pennsylvania, USA
EMAIL hdaniell@upenn.edu

Executive Editor

Shuangxia Jin, National Key Laboratory of Crop Genetic Improvement, Huazhong Agricultural
University, China
EMAIL jsx@mail.hzau.edu.cn

Senior Editors

Dominique Michaud, Department of Plant Sciences Plant Research & Innovation Centre Université
Laval Québec QC, Canada
EMAIL dominique.michaud@fsaa.ulaval.ca
Rajeev Varshney, State Agricultural Biotechnology Centre; Centre of Crop and Food Innovation;
International Chair in Agriculture & Food Security, Murdoch University, Australia
EMAIL Rajeev.Varshney@murdoch.edu.au

Associate Editors

Jacqueline Batley, School of Agriculture & Food Sciences, The University of Queensland, Australia
EMAIL jacqueline.batley@uwa.edu.au
François Belzile, Department of Plant Sciences, Institute for Integrative and Systems Biology, Laval
University, Québec, Canada
EMAIL Francois.Belzile@fsaa.ulaval.ca
Mario Caccamo, NIAB EMR, Kent, UK
EMAIL mario.caccamo@niab.com
Xiao-Ya Chen, Institute of Plant Physiology and Ecology, Shanghai Institutes for Biological Sciences,
Chinese Academy of Sciences, China
EMAIL xychen@sibs.ac.cn
Nigel Halford, Plant Sciences, Rothamsted Research, United Kingdom.
EMAIL nigel.halford@rothamsted.ac.uk
Zuhua He, National Laboratory of Plant Molecular Genetics, Institute of Plant Physiology and
Ecology, Shanghai Institutes for Biological Sciences, Chinese Academy of Sciences, Shanghai, China
EMAIL zhehe@sibs.ac.cn
Xuehui Huang, College of Life Sciences, Shanghai Normal University, Shanghai, China
EMAIL xhhuang@shnu.edu.cn
Thomas Jacobs, VIB-Ugent Center for Plant Systems Biology, VIB-Ghent University, Belgium
EMAIL thomas.jacobs@psb.vib-ugent.be
Yanfei Mau, Shanghai Center for Plant Stress Biology, Chinese Academy of Sciences, Shanghai, China
EMAIL yfmao@sibs.ac.cn
Martin A.J. Parry, Lancaster Environment Centre, Lancaster University, UK
EMAIL m.parry@lancaster.ac.uk
Nicola J. Patron, The Earlham Institute, Norwich Research Park, NR4 7UK
EMAIL nicola.patron@tgac.ac.uk
Yiping Qi, Department of Plant Science and Landscape Architecture University of Maryland, MD, USA
EMAIL yiping@umd.edu
Nils Stein, Leibniz Institute of Plant Genetics and Crop Plant Research (IPK), Gatersleben, Germany
EMAIL stein@ipk-gatersleben.de

Stephen J Streatfield, Fraunhofer USA Center for Molecular Biotechnology, Newark, DE 19348, USA
EMAIL sstreatfield@fraunhofer.org
Neal Stewart, Department of Plant Sciences, The University of Tennessee, Knoxville, TN USA
EMAIL nealstewart@utk.edu
Leena Tripathi, Department of Biosciences, International Institute of Tropical Agriculture (IITA),
Nairobi, Kenya.
EMAIL l.tripathi@cgiar.org
Kan Wang, Plant Transformation Facility, Iowa State University, Ames, Iowa, USA
EMAIL kanwang@iastate.edu
Wolfram Weckworth, Ecogenomics and Systems, University of Vienna, Wien, Austria
EMAIL wolfram.weckworth@univie.ac.at
Bing Yang, Division of Plant Sciences, University of Missouri – Columbia, MO, USA
EMAIL yangbi@missouri.edu

Editorial Board

Kailash Bansal, National Research Centre on Plant Biotechnology, Indian Agricultural Research
Institute, India
Ralph Bock, Max Planck Institute of Molecular Plant Physiology, Germany
Udo Conrad, Leibniz Institute of Plant Genetics and Crop Plant Research, Germany
Luis Herrera Estrella, Langebio, Cinvestav Campus, Mexico
Hui-Shan Guo, Institute of Microbiology, Chinese Academy of Sciences, Chaoyang District, Beijing
100101, China
Tuan-Hua Ho, Academia Sinica Institute of Plant and Microbial Biology, Taipei 115, Taiwan
Elizabeth Hood, College of Agriculture and Technology, Arkansas State University, Arkansas, USA
Dirk Inzé, Department of Plant Genetics, VIB/Universiteit Gent, Belgium
Jizeng Jian, Institute of Crop Sciences, Chinese Academy of Agricultural Sciences, China
Theodore Klein, DuPont Pioneer Agricultural Biotechnology, USA
Sandeep Kumar, Dow AgroSciences LLC, 9330 Zionsville Road, Indianapolis, USA
Shashi Kumar, Metabolic Engineering (Biofuels and Industrial Biotechnology), International Centre
for Genetic Engineering and Biotechnology, Aruna Asaf Ali Marg, New Delhi, India
Prakash Lakshmanan, Sugar Research Australia, Brisbane, Australia
Phil Larkin, Metabolic Engineering of New Plant Products, CSIRO Plant Industry, Canberra, Australia
Xin Liu, BGI Research, Yantian District, Shenzhen 518083, China
Hugh Mason, The Biodesign Institute, Arizona State University, USA
Magdy Mahfouz, King Abdullah University of Science and Technology, Makkah, Saudi Arabia
Sagadevan Mundree, Queensland University of Technology, Australia
Xiaoqun Qi, Institute of Botany, Chinese Academy of Sciences, Beijing, China
Elbio Rech, EMBRAPA Genetic Resources and Biotechnology, University of Brasília, Brazil
Ed Rybicki, University of Cape Town, South Africa
Maria Fátima Grossi de Sá, Embrapa Recursos Genéticos e Biotecnologia, PqEB-Final W5 Norte - CP
02372, Brasília-DF-Brasil
Ming-Che Shih, Agricultural Biotechnology Research Center Academia Sinica Nankang, Taiwan
Vibha Srivastava, University of Arkansas, Crop, Soil & Environmental Sciences, Fayetteville, USA
Herta Steinkellner, Department of Applied Genetics and Cell Biology, University of Agricultural
Sciences, 1190 Vienna, Austria
Eva Stoger, Institute of Applied Genetics and Cell Biology (IAGZ), University of Natural Resources
and Life Sciences, Austria
Fumio Takaïwa, National Institute of Agrobiological Sciences, Japan
Weihsia Tang, Shanghai Institutes for Biological Sciences, Chinese Academy of Science, Institute of
Plant Physiology and Ecology, China
Roberto Tuberosa, Department of Agroenvironmental Science and Technology, Bologna, Italy
Zeng-Yu Wang, The Noble Foundation, Ardmore, USA
Spencer Witney, Australian National Laboratory, Canberra, ACT 2600, Australia
Xianlong Zhang, National Key Laboratory of Crop Genetic Improvement, Huazhong Agricultural
University, China

Aims and Scope

Plant Biotechnology Journal is published by Wiley in association with the Society for Experimental Biology (SEB) and the Association of Applied Biologists (AAB).

Plant Biotechnology Journal aims to publish high-impact original research and incisive reviews by leading researchers in applied plant science, with an emphasis on molecular plant sciences and their applications through plant biotechnology. We aim to provide a forum for the most important advances in this field, including curiosity-driven studies with the potential for application, strategic research in plant biotechnology, scientific analysis of key issues for the beneficial application of plant sciences and scientific analysis of the performance of the products of plant biotechnology in practice.

Plant Biotechnology Journal often receives manuscripts describing research carried out solely in model species. While the *Plant Biotechnology Journal* will continue to accept exceptional manuscripts describing novel and useful procedures carried out in model species, one of the strengths of the *Plant Biotechnology Journal* is its ability to focus on application. Therefore, from January 2011 the *Plant Biotechnology Journal* will immediately reject manuscripts containing high quality, but not exceptional, research relating solely to model species.

To be accepted for publication in *Plant Biotechnology Journal*, original research papers will need to present major new findings with conclusions thoroughly supported by critical experimental evidence and make a substantial contribution to plant biotechnology and/or scientific understanding. Reviews must accordingly provide a high level of insight and synthesis beyond a summary of published work. Sciences underpinning plant biotechnology include functional genomics and proteomics, molecular genetics, physiology, biochemistry and cell biology, with applications through molecular marker, mutant and transgenic approaches. Applications may involve agriculture, horticulture, forestry, biodiversity and conservation, enhanced yield, reduced environmental impact, phytoremediation, environmental sensors, improved foods and food-processing, biofuels and biomaterials including pharmaceuticals from terrestrial, aquatic or marine plant systems including industrial crops and natural systems. Examples of areas covered in *Plant Biotechnology Journal* include:

- Gene, genome, proteome and metabolome analysis: molecular screening technologies; analysis of gene function from nucleotide sequence to phenotype; understanding of gene networks; applications ranging from metabolic engineering to marker assisted breeding.
- Functional genomics, comparative genomics, bioinformatics and their applications in understanding and beneficial use of biodiversity, conservation, introgression, and rational design of improved genes for industrial plant improvement.
- Transgenic technologies: production and analysis of transgenic crops; molecular farming; gene insertion, expression and silencing; field-testing and commercialisation of modified plants for agricultural, health, industrial and environmental benefits, improved foods, biofuels and biomaterials; safety and regulatory affairs.
- Developmental, physiological and biochemical studies relevant to enhanced understanding of plant function, with potential for improvement of plant characteristics important to humans including the adaptation of plants to new environments.

Plant Biotechnology Journal seeks to achieve a balance between a speedy review process and providing authors with rigorous, objective and critical reviews. Submissions are initially reviewed by editors to select only those considered most promising for critical review by at least two independent experts. We promise speedy responses to authors, rigorous scientific review and rapid publication.

Plant Biotechnology Journal provides the opportunity to publish supplementary material, such as large data sets, extra colour illustrations, bibliographies, videos, or any other material for which insufficient space in the journal is available. Please contact the Editor-in-Chief for details.

Open Access and Copyright

All articles published by *Plant Biotechnology Journal* are fully open access: immediately freely available to read, download and share. All *Plant Biotechnology Journal* articles are published under the terms of the Creative Commons Attribution License which permits use, distribution and reproduction in any medium, provided the original work is properly cited, and allows the commercial use of published articles. Copyright on any research article in a journal published by *Plant Biotechnology Journal* is retained by the author(s). Authors grant Wiley a license to publish the article and identify itself as the original publisher. Authors also grant any third party the right to use the article freely as long as its integrity is maintained and its original authors, citation details and publisher are identified. Further information about open access license and copyright can be found on <http://www.wileyopenaccess.com/details/content/12f25db4c87/Copyright-License.html>.

Use by commercial 'for-profit' organisations. Use of Wiley Open Access articles for commercial, promotional, or marketing purposes requires further explicit permission from Wiley (corporatesales@wiley.com) and will be subject to a fee. Commercial purposes include:

- Copying or downloading of articles, or linking to such articles for further redistribution, sale or licensing;
- Copying, downloading or posting by a site or service that incorporates advertising with such content;
- The inclusion or incorporation of article content in other works or services (other than normal quotations with an appropriate citation) that is then available for sale or licensing, for a fee (for example, a compilation produced for marketing purposes, inclusion in a salespack);
- Use of article content (other than normal quotations with appropriate citation) by forprofit t organisations for promotional purposes;
- Linking to article content in e-mails redistributed for promotional, marketing or educational purposes;
- Use for the purposes of monetary reward by means of sale, resale, licence, loan, transfer or other form of commercial exploitation such as marketing products;
- Print reprints of Wiley Open Access articles can be purchased from corporatesales@wiley.com.

This journal is available online at *Wiley Online Library*. Visit wileyonlinelibrary.com/journal/pbi to search the articles and register for table of contents e-mail alerts.

Access to this journal is available free online within institutions in the developing world through the AGORA initiative with the FAO and the OARE initiative with UNEP. For information, visit www.aginternetwork.org and www.oaresciences.org

Disclaimer

The Publisher, the SEB, AAB and Editors cannot be held responsible for errors or any consequences arising from the use of information contained in this journal; the views and opinions expressed do not necessarily reflect those of the Publisher, SEB, AAB or Editors, neither does the publication of advertisements constitute any endorsement by the Publisher, SEB, AAB or Editors of the products advertised. Wiley Open Access articles posted to repositories or websites are without warranty from Wiley of any kind, either express or implied, including, but not limited to, warranties of merchantability, fitness for a particular purpose, or non-infringement. To the fullest extent permitted by law Wiley disclaims all liability for any loss or damage arising out of, or in connection with, the use of or inability to use the content.

Front cover image:

Cover illustration shows duckweed, *Lemma japonica*, engineered to accumulate approximately 10% of its dry weight as triacylglycerols (i.e., oil) in its fronds. This is achieved by expression of an estradiol-inducible WRINKLED1 fusion protein along with strong constitutive expression of mouse diacylglycerol acyl-CoA acyltransferase2 and a sesame oleosin variant. The image graphically represents oil being obtained from induced cells. Cover illustration refers to the article published in this issue (Lang et al., pp. 317–330).

Targeted manipulation of grain shape genes effectively improves outcrossing rate and hybrid seed production in rice

Xinyu Zhu^{1,†}, Yajun Gou^{1,†}, Yueqin Heng^{1,†}, Wenyan Ding¹, Yajing Li¹, Degui Zhou² , Xiaoqing Li¹, Churong Liang¹, Chuanyin Wu³, Haiyang Wang^{1,4,*}  and Rongxin Shen^{1,*}

¹State Key Laboratory for Conservation and Utilization of Subtropical Agro-Bioresources, South China Agricultural University, Guangzhou, 510642, China

²Guangdong Key Laboratory of New Technology in Rice Breeding, Rice Research Institute, Guangdong Academy of Agricultural Sciences, Guangzhou, 510640, China

³Institute of Crop Science, Chinese Academy of Agricultural Sciences, Beijing, 100081, China

⁴Guangdong Laboratory for Lingnan Modern Agriculture, Guangzhou, 510642, China

Received 2 August 2022;

revised 9 October 2022;

accepted 2 November 2022.

*Correspondence (Tel/fax +86 02

85282180; email whyang@scau.edu.cn

(HW) and Tel/fax +86 02 85282180; email

shenrongxin@scau.edu.cn (RS))

[†]These authors have contributed equally to this work.

Summary

Stigma exertion rate (SER) of the male sterile line is a key limiting factor for hybrid seed production in rice. Although a large number of quantitative trait loci associated with SER have been reported, few genes have been molecularly cloned and functionally characterized, severely hindering the genetic improvement of SER of the male sterile line and the breeding efficiency of hybrid rice. In this study, we identified three grain shape regulatory genes, *GS3*, *GW8* and *GS9*, as potential candidate genes for targeted manipulation of grain shape and SER. We show that simultaneously knocking out these three genes could effectively increase SER by increasing the ratio of spikelet length/spikelet width and length of stigma and style, without negative impacts on other agronomic traits. Cellular examination and transcriptomic analyses revealed a role of these genes in coordinated regulation of transverse and longitudinal cell division in the pistils. Moreover, we demonstrate that targeted manipulation of these grain shape genes could significantly improve the outcrossing rate in both the ZH11 (a *japonica* variety) and Zhu6S (an *indica* male sterile line) backgrounds. Our results provide new insights into the mechanisms of rice SER regulation and develop an effective strategy to improve SER and out-crossing rate in rice, thus facilitating hybrid rice production.

Keywords: hybrid rice, stigma exertion rate, *GS3*, *GW8*, *GS9*.

Introduction

Rice is a staple crop for more than half of the world's population (FAO Statistical Databases, 2021). Asian cultivated rice (*Oryza sativa* L.) is domesticated from the wild rice (*Oryza rufipogon* Griff.) and is differentiated into two major ecotypes, *japonica* and *indica* (Huang *et al.*, 2012). Since the 1970s, the development of "three-line" and "two-line" hybrid systems has contributed significantly to increased rice production and securing global food supply (Peng *et al.*, 1999; Yuan and Virmani, 1988; Zhu, 2016). During commercial production of hybrid seeds, plants of the female parent (usually a male sterile line) are planted in rows side-by-side with plants of the male parent (normally 5–6 rows of female parent:1 row of male parent), and pollination is aided by humans or mechanicals (such as unmanned-helicopters). To be commercially profitable, hybrid seed yield should reach no less than 150 kg/mu, and higher yield is desirable for reducing the cost of hybrid seeds for selling to the farmers.

Several characteristics of the female and male parental lines affect the yield of hybrid seed production, including the interval of anthesis between the male and female parents, the stigma exertion rate (SER) and stigma vigour of the female parental lines, and pollen number/vigour of the male parental lines (Marathi and Jena, 2015; Virmani *et al.*, 1982). Among them, SER of the female parental line is believed to be a crucial one. The rice SER is defined as the frequency of exerted stigmas which

stay outside after closing of the lemma and palea, and could be gauged by the single stigma exertion rate (SSE), the dual stigma exertion rate (DSE) and the total stigma exertion rate (TSE) (Rahman *et al.*, 2017b). As the exerted stigmas could stay viable for 4–6 days to be pollinated, the male sterile lines with high SER would extend the cross-pollination opportunity by trapping more pollens and overcome non-synchronous anthesis between the two parental lines, thus elevating the outcrossing ability of the male sterility lines and promoting hybrid rice seed production (Kato and Namai, 1987; Lou *et al.*, 2014; Tian, 1993; Wen *et al.*, 2009; Yan, 1999; Yuan, 2002). Thus, higher SER (normally above 40–50% TSE) is a preferred trait for the development of a commercially viable male sterile line for hybrid seed production. However, the average SER is <25% in *indica*, <15% in tropical *japonica*, and about 5% in temperate *japonica* (Ling and Xu, 1988; Uga *et al.*, 2003; Ying and Zhang, 1989; Zhou *et al.*, 2017). Thus, it is often a laborious and time-consuming process to develop male sterile lines with high SER, which severely limits the breeding efficiency of hybrid rice.

The rice SER is a complex quantitative trait and is easily affected by environmental factors (such as temperature) (Yan *et al.*, 2009). Previous studies have shown that SER is largely determined by stigma length (STL), style length (SYL), and the sum of stigma and style length (TSSL) (Dang *et al.*, 2020), and thus extensive genetic analyses have been performed to identify SER-associated loci through phenotyping STL, SYL and/or TSSL. Although more than

40 quantitative trait loci (QTL) for SER have been reported, none of them has been molecularly cloned and functionally characterized, largely due to the difficulty in precise phenotyping and the small additive effects of the individual locus (typically less than 10%) (Bakti and Tanaka, 2019; Li et al., 2001, 2014; Liu et al., 2015, 2019; Marathi and Jena, 2015; Rahman et al., 2017a,b; Tan et al., 2020; Uga et al., 2003; Zhang et al., 2018). Recently, genome-wide association studies (GWAS) analyses were utilized to identify SER-associated genes. Notably, three rice grain size regulatory genes, *Grain Size 3* (*GS3*, encodes a G-protein γ subunit, Mao et al., 2010), *Grain Width 2* (*GW2*, encodes a RING-type E3 ubiquitin ligase, Song et al., 2007) and *Grain Width 5* (*GW5*, encodes a novel calmodulin-binding protein, Liu et al., 2017), were identified (Dang et al., 2020; Zhou et al., 2017). These observations suggest that SER is tightly linked with grain shape. However, the detailed roles of these genes in regulating SER and whether these genes could be utilized to improve SER of the male parent line for hybrid seed production have not been meticulously evaluated.

In this study, we selected three grain shape regulatory genes, *GS3*, *GW8* and *GS9*, as potential candidate genes for targeted manipulation of grain shape and SER. We show that these genes could act synchronously to modulate the spikelet length, spikelet width, stigma length, and style length. Their individual or double knockout plants exhibit improved SER, but the *gs3/gw8/gs9* triple mutant exhibit the most dramatic improvement in SER (TSE reaching ~60%). Moreover, we show that simultaneously knocking out these three genes could effectively improve the outcrossing rate in both *indica* and *japonica* backgrounds. The potential utility of these genes in boosting hybrid seed production, especially in *indica-japonica* hybrid seed production, is discussed.

Results

Identification of SER regulatory genes by analysing rice grain shape genes

Previous studies have shown that in rice, SER is largely determined by stigma length (STL), style length (SYL), and the sum of stigma and style length (TSSL) (Dang et al., 2020) and tightly associated with grain shape (Uga et al., 2003, 2010; Zhou et al., 2017). Thus, we speculated that these traits might be regulated by a common set of genes. To substantiate this notion, we examined the developmental processes of the spikelet and pistil (containing style and stigma) of ZH11 throughout the S8b ~ S12 stages (Zhang et al., 2006, 2011). We found that the spikelet and pistil exhibited synchronous growth, with a sharp increase from S11a to S12 (Figure 1a,b). Pearson's correlation analysis showed that the sum of stigma and style length was significantly and positively correlated with the spikelet area, spikelet length and width (Figure 1b; Figure S1). We then performed a detail analysis of more than 50 rice grain size regulatory genes according to their functions and their genetic effects on grain shape-related traits (Li et al., 2019) (Table S1). Three genes, *GS3*, *GW8* and *GS9*, were selected as they are negative regulators of grain length and/or positive regulators of grain width, and their loss-of-function alleles could increase grain quality and confer no adverse effect on other agronomic traits in rice (Fan et al., 2006; Wang et al., 2012; Zhao et al., 2018). Reverse-transcription quantitative PCR (RT-qPCR) assay showed that *GS3*, *GW8* and *GS9* displayed similar expression patterns in the developing pistils, with highest expression at the S11b stage (Figure 1c), coinciding with the

maximum growth rate of the spikelet and pistil at this stage. Therefore, we speculated that knocking out these genes may confer increased grain length/width ratio, increased pistil length and consequently increased SER in rice.

GS3, *GW8* and *GS9* synchronously regulate glume shape, pistil growth and the SER in rice

We thus designed a CRISPR/Cas9 construct aimed to generate various single, double and triple knockout mutants of *GS3*, *GW8* and *GS9* in the *japonica* variety Zhonghua11 (ZH11) background (Figure S2). Multiple single, double and triple mutants harbouring base insertions or deletions were identified through sequencing analysis (Figure S2b-d). Next, we examined the phenotype of spikelet and pistil in various knockout mutants. Compared with the wild-type (WT) plant ZH11, all the homozygous mutants exhibited increased spikelet length (except for the *gw8* single mutant) but decreased glume width (except for the *gs3* single mutant) (Figure 2a-h,q,r; Figure S3a-f,m,n). Notably, the spikelet length/width ratio was gradually elevated from the single mutant to the triple mutant, suggesting that *GS3*, *GW8* and *GS9* function additively in regulating grain shape in rice (Figure 2s; Figure S3o). In line with the increased spikelet length/width ratio, all the knockout mutants displayed increased stigma length and style length (except for the style length of the *gw8/gs9* double mutant), thus leading to a gradual increase of the total stigma and style length from the single mutant to the triple mutant (Figure 2i-p,t-v; Figure S3g-l,p-r). Consistently, Pearson's correlation analysis showed that the stigma exertion rate was positively correlated with spikelet length/width ratio and spikelet length, but negatively correlated with spikelet width (Figure S4). As expected, phenotype analysis showed that at anthesis, all the mutated lines exhibited increased SSE, DSE (except for the *gs3* and *gs9* single mutant) and TSE (Figure 2w-y; Figure S3s-u). In comparison to ZH11 with a very low TSE (<5%), the average TSE was increased by 54.92% in *gs3/gw8/gs9*#1 and 64.17% in *gs3/gw8/gs9*#2 (Figure 2w-y; Figure S3s-u). Noteworthy, the triple mutant produced more slender grains than ZH11 with decreased 1000-grain weight (Figure S5a-d), whereas the number of tillers and grains per plants in triple mutant were significantly increased compared to wild-type ZH11 (Figure S5k,l). All the improved traits are beneficial for the hybrid seed production. No significant differences were observed for the panicle architecture (including panicle length, number of primary branches and number of secondary branches) and plant height between the triple mutants and wild-type ZH11 (Figure 5e-j). Together, these findings clearly demonstrate that knocking out these grain shape genes could confer increased SER in rice.

GS3, *GW8* and *GS9* regulate grain and pistil traits by altering cell division

To further examine the cellular changes that occurred in the spikelet and pistil of the *gs3/gw8/gs9* triple mutant, we performed cytological observations in more detail. Scanning electron microscopy (SEM) observations showed that the length of the outer epidermal cells of spikelet glumes in *gs3/gw8/gs9*#1 was decreased by ~10% (Figure 3a-c), but an approximate 13% increase in longitudinal cell number compared with the wild-type ZH11 (Figure 3d), indicating that the increased grain length in *gs3/gw8/gs9*#1 is likely resulted from increased cell division in the longitudinal direction. Additionally, transverse sections of palea and lemma showed that *gs3/gw8/gs9*#1 contained fewer inner parenchyma cells than the wild-type ZH11, which may contribute

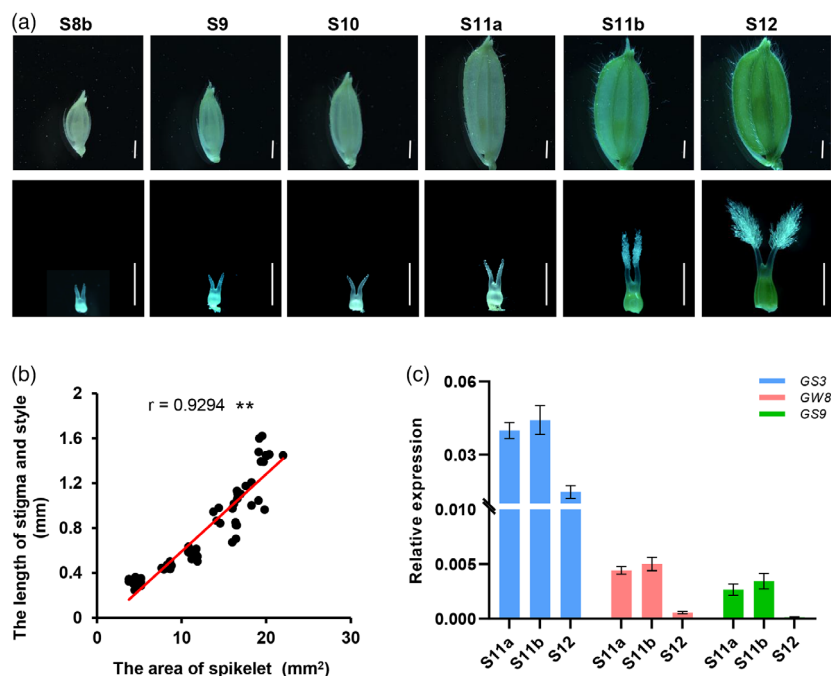


Figure 1 Identification of *GS3*, *GW8* and *GS9* as stigma exsertion regulatory genes in rice. (a) Dynamic change of spikelet and pistil for the ZH11 during spikelet development. S8b–S12 stages represent different developmental stages based on the reference by Zhang *et al.* (2006) and Zhang *et al.* (2011). Bars = 1 mm. (b) Pearson's correlation between the spikelet area and the total length of stigma and style. r , Pearson's correlation coefficient. $**P < 0.01$. (c) RT-qPCR analysis of *GS3*, *GW8* and *GS9* in pistils at S11a, S11b and S12 stages. Data are shown as means \pm SEM ($n = 3$).

to the decreased transverse spikelet perimeter (by 19%) of the *gs3/gw8/gs9#1* hulls (Figure 3e–h).

Next, we compared the cellular changes within pistil between *gs3/gw8/gs9#1* and wild-type ZH11. Transverse section analysis of the joint region between stigma and style showed that the number of inner parenchyma cells in *gs3/gw8/gs9#1* was significantly decreased compared with ZH11 (Figure 4a,b,e), thus leading to an approximate 22% decrease in transverse area of the joint region in *gs3/gw8/gs9#1* (Figure 4f). Additionally, transmission electron microscopy (TEM) analysis showed no significant difference in the average cell length and longitudinal cell number of the style between *gs3/gw8/gs9#1* and ZH11 (Figure 4c,d,g,h), implying that the increased style length in *gs3/gw8/gs9#1* is also likely resulted from increased cell division in the longitudinal direction. These results suggest that *GS3*, *GW8* and *GS9* act together to inhibit cell division in the longitudinal direction and promote cell division in the transverse direction of style in rice.

Transcriptome analysis reveals enrichment of cell proliferation-related genes in the triple mutant

To further probe the molecular mechanism of action of *GS3*, *GW8* and *GS9* in regulating pistil growth, we performed RNA sequencing (RNA-seq) to compare the global gene expression profiling between the *gs3/gw8/gs9* triple mutant and ZH11. As the stigma and style of *gs3/gw8/gs9* triple mutant started to display a differential growth rate with that of ZH11 from the S11b to S12 stages (Figure S6), we used the pistils at the S11b stage for transcriptome analysis. Pearson's correlation analysis showed significant correlation between two biological replicates for each sample (Figure S7a). A total of 1498 differentially expressed genes (DEGs) were identified based on the criteria of a 2-fold change and false discovery rate (FDR) < 0.05 (Dataset S1). Among them,

861 genes were up-regulated and 637 genes were down-regulated in the *gs3/gw8/gs9* mutant when compared to ZH11 (Figure S7b). Gene Ontology (GO) term enrichment analysis and KEGG pathway enrichment analysis showed that these DEGs were mainly enriched in multiple processes (Figure S7c,d; Dataset S1, S3). Notably, a large proportion of the DEGs were clustered into cell proliferation-related terms such as 'cell division', 'microtubule binding', 'microtubule motor activity', and 'cell wall remodeling' (Figure S7c), consistent with the alteration of cell division detected in the *gs3/gw8/gs9* mutant. We further confirmed the expression profiles of several cell division-related genes by RT-qPCR (Figure S7b). Our results suggest that *GS3*, *GW8* and *GS9* cooperatively regulate cell division during pistil development.

Knocking out of *GS3*, *GW8* and *GS9* significantly increase outcrossing rates of ZH11 and Zhu6S

To test whether the increased SER in the *gs3/gw8/gs9* mutants may promote out-crossing, we further carried out a field experiment by crossing ZH11 and *gs3/gw8/gs9* with an orange-red-grained astaxanthin rice (Zhu *et al.*, 2018) as the male parent. The outcrossing rate was evaluated by calculating the percentage of orange-red grain in the F_1 seeds (the self-pollinated seeds are white and the cross-pollinated hybrid seeds are orange-red). As expected, both lines of the *gs3/gw8/gs9* triple mutants exhibited significantly higher outcrossing seed setting rates compared with ZH11, when pollinated by the orange-red-grained astaxanthin rice (Figure 5a,b). To further evaluate the potential application of loss-of-function alleles of *gs3*, *gw8* and *gs9* in hybrid seed production, we selected an elite *indica* male sterile line Zhu6S for genetic improvement. Zhu6S is known to have a low SER (~20%), and thus is not

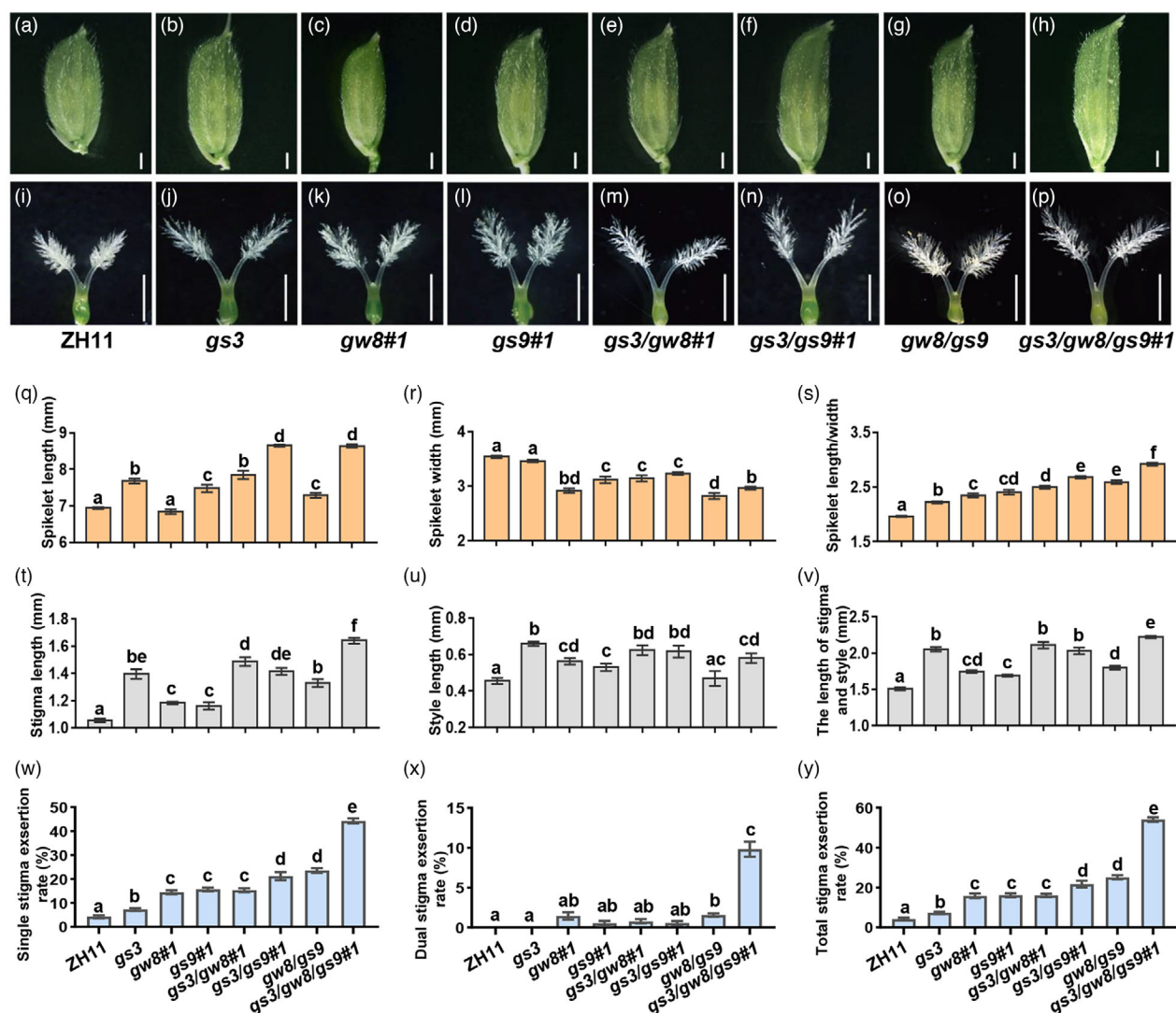


Figure 2 *GS3*, *GW8* and *GS9* synchronously regulate the spikelet, pistil growth and stigma exertion rate in rice. (a–h) Comparison of spikelet shape among ZH11 and its various knockout combinations of *gs3*, *gw8* and *gs9*. Bar = 1 mm. (i–p) Comparison of pistil shape among ZH11 and its various knockout combinations of *gs3*, *gw8* and *gs9*. Bar = 1 mm. (q–v) Statistical analyses of spikelet length (q), spikelet width (r), spikelet length/spikelet width (s), stigma length (t), style length (u), the length of stigma and style (v), single stigma exertion (w), dual stigma exertion (x), total stigma exertion (y) of ZH11 and its various knockout mutants. Letters above the bars indicate significant differences ($P < 0.05$) as determined by one-way ANOVA with Tukey's post-hoc analysis. Data are shown as means \pm SEM ($n = 10$).

suitable for hybrid seed production. As Zhu6S contained a loss-of-function allele of *gs3* (Figure S8a), we simultaneously knocked out *GW8* and *GS9* using the CRISPR/Cas9 technology (Figure S8b). As expected, the edited Zhu6S lines (with *gw8* and *gs9* knockout) exhibited significantly increased SSE, DSE and TSE when compared to the original Zhu6S (Figure 5c,d). The average TSE was increased from 22.87% in the original Zhu6S to 60.65% in the *Edited Zhu6S-1* and 62.62% in *Edited Zhu6S-2* (Figure 5d). We further performed a natural outcrossing test by planting the original Zhu6S and its edited lines together with a male fertile rice variety Tianfeng B. As both the original Zhu6S and the edited Zhu6S are male sterile lines, the seeds produced on these plants were hybrid seeds derived from natural cross-pollination between the sterile lines and Tianfeng B. Notably, the seed setting rate of the edited Zhu6S reached ~50%, which is about two times higher than that of the original Zhu6S

(~25%) (Figure 5e,f). These results indicate that manipulation of *GS3*, *GW8* and *GS9* could effectively improve the outcrossing rate of male sterile lines and thus hybrid rice seed production.

Discussion

The SER trait of the male sterile line is a key limiting factor for hybrid seed production in rice. However, few SER-related genes have so far been cloned and characterized, severely hindering the genetic improvement of rice SER and the efficacy of hybrid rice breeding. In this study, we demonstrate that besides the previously reported *GS3* (Takano-Kai *et al.*, 2009; Zhou *et al.*, 2017), *GW8* and *GS9* are also common regulators of grain shape and SER and that targeted manipulation of these genes could be used to effectively improve SER and out-crossing rate in rice, thus facilitating hybrid rice production. Our phenotypic analysis showed

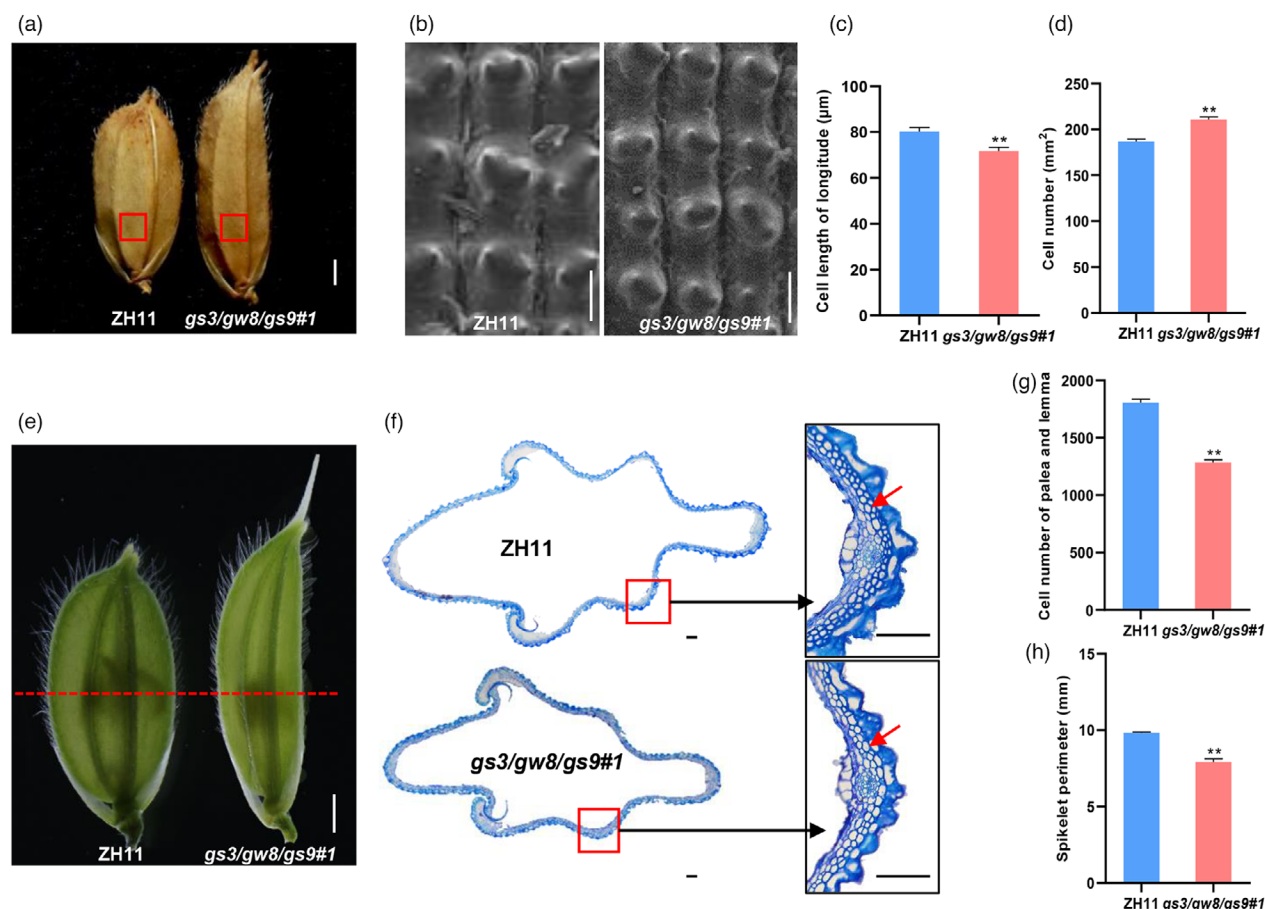


Figure 3 Histological comparison of the spikelet glumes between ZH11 and the *gs3/gw8/g9#1* triple mutant. (a, b) Scanning electron microscopy analyses of the glume of ZH11 and *gs3/gw8/g9#1*. (b) is magnified views (enlarged by 200-fold) of the red boxes areas in (a). (c) The cell length in longitude indicated with red boxes in (a). Bars indicate SEM (*n* = 5). (d) The cell number in the areas indicated with red boxes in (a). Bars indicate SEM (*n* = 5). (e) Spikelet morphology of ZH11 and *gs3/gw8/g9#1* before anthesis. The yellow dashed line indicates the position of the cross-sections shown in (f). Bar = 1 cm. (f) Transverse sections of spikelet. The right-hand images show magnified views of the red boxed region. The red arrow indicates lower epidermal cells. Bar = 100 μm. (g, h) Quantification analyses of cell number (g) and spikelet perimeter (h) of palea and lemma in ZH11 and *gs3/gw8/g9#1*. Bars indicate SEM (*n* = 3). Asterisks indicate significant differences (***P* < 0.01) between ZH11 and *gs3/gw8/g9#1* by two-tailed Student's *t*-test. Data are shown as means ± SEM.

that there are about 1.7-fold, 3.7-fold and 3.8-fold increases of SER in *gs3*, *gw8*, *gs9* single mutant separately in comparison to ZH11, suggesting that *GW8* and *GS9* play more predominant roles than *GS3* in regulating SER. SER of the double mutants (16.1–25.1%) is obviously higher than that of the single mutants (7.3–16.1%). Notably, SER of the *gs3/gw8/g9* triple mutant (54.1–64.2%) is significantly higher than that of the *gw8/g9* double mutant (16.1–25.1%) (Figure 2y; Figure S3u), suggesting that *GS3*, *GW8* and *GS9* may function in a synergistic fashion to regulate SER. Further studies are required to clarify their genetic interaction in SER regulation. In addition, it is worth noting that stigma viability is also an important factor for the success of outcrossing seed setting (Qi and Wu, 2022). However, whether *GS3*, *GW8* and *GS9* affect stigma vitality also awaits detailed evaluation in future studies. Regardless, our findings hold great potential in targeted improvement of SER for the available male sterile lines as well as facilitating the breeding of new male sterile lines with the superior combining ability and hybrid vigour, thus promoting the utilization and commercialization of hybrid rice.

In addition, as most of the currently planted hybrid rice varieties were intra-subspecific hybrids of the *indica* subspecies, and their yields have reached a plateau due to the narrow genetic diversity of the parental lines. The *indica-japonica* inter-subspecific hybrid rice has stronger heterosis than intra-subspecific hybrids of the *indica* subspecies, and has the potential to boost the yield by an additional 20–30% (Peng *et al.*, 1999; Yuan and Virmani, 1988). However, utilization of the strong *indica-japonica* inter-subspecific hybrid vigour is currently restrained by several bottlenecks, including low fertility of the *F*₁ plants due to reproduction barriers between the *indica* and *japonica* subspecies, tall plant height/lodging, prolonged life cycle, poor grain quality and low production of hybrid seeds. In particular, the extremely low level of SER (about 5%) in *japonica* varieties is a major constraint for *indica-japonica* inter-subspecific hybrid seed production. Our findings that both SER and outcrossing rate could be significantly improved in ZH11 (a *japonica* variety) and Zhu6S (an *indica* male sterile line) illustrate an effective approach to overcome this barrier, and thus contributing to the

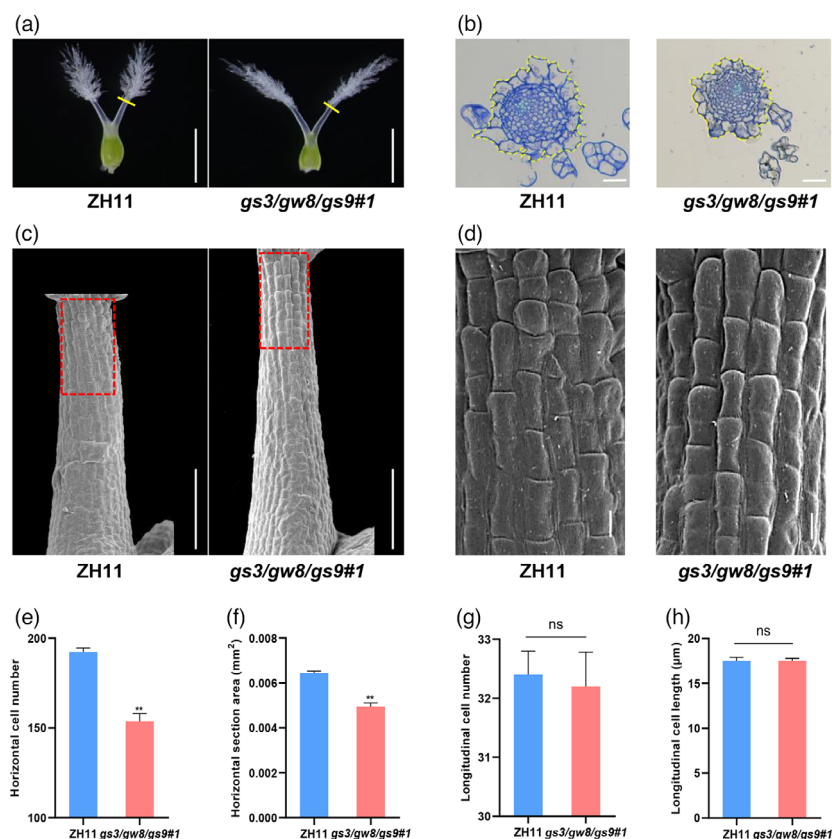


Figure 4 Histological comparison of the styles between ZH11 and *gs3/gw8/gw9#1*. (a) Pistil morphology of ZH11 and *gs3/gw8/gw9#1*. The yellow lines indicate the position of the cross-sections shown in (b). Bar = 1 mm. (b) Transverse sections of ZH11 and *gs3/gw8/gw9#1* styles. Bar = 20 μm. (c) Scanning electron microscopy analyses of ZH11 and *gs3/gw8/gw9#1* styles. Bar = 100 μm. The dashed boxes highlight the region for comparison of the cell number and cell length in the style between ZH11 and *gs3/gw8/gw9#1*. (d) The magnified views of the boxed regions in (c). Bar = 10 μm. (e, f) The horizontal cell number (e) and area (f) indicated with dashed lines in (b). Bars indicate SEM ($n = 4$). (g, h) Quantification analyses of average parenchymal cell number (g) and cell length (h) shown in (d). Bars in (g) indicate SEM ($n = 5$) and Bars in (h) indicate SEM ($n = 120$). Asterisks indicate significant differences ($**P < 0.01$) between ZH11 and *gs3/gw8/gw9#1* by two-tailed Student's t -test. Data are shown as means \pm SEM.

development and commercialization of *indica-japonica* intersubspecific hybrids in the future.

Besides being an important agronomic trait for hybrid seed production in rice, stigma exertion is also a key trait of rice domestication. The wild rice ancestor *O. rufipogon* is known to have high SER (80%) and superior outcrossing habit (allogamous), whereas the Asian cultivated rice has greatly reduced SER (on average below 15% in *indica* rice and ~5% in *japonica* rice), rendering the cultivated rice become a strictly selfing (autogamous) species (Xu and Sun, 2021). However, the biological significance and regulatory mechanisms underlying such a transition remain largely mysterious. A recent study demonstrated that *GS3* and *GW5* likely contributed to this change. Based on population genetic analyses, it was inferred that wild rice should have the wild combination of *GW5/GS3* and that in the process of rice domestication, gain of *GS3* function and loss of *GW5* function may have contributed greatly to the change of outcrossing habit of rice to selfing (Zhou et al., 2017). In this study, we showed that knocking out *GW8* and *GS9* could significantly increase both SER and outcrossing rate of cultivated rice. Thus, it will be of great interest to explore the genetic diversity of these genes (*GS3*, *GW5*, *GW8* and *GS9*) in wild rice and examine how their haplotype combinations have been artificially selected during rice domestication and modern

breeding process. Such analyses may lead to the identification of superior haplotype combinations that confer male sterile lines with desired grain shape/grain quality and high SER for hybrid seed production, with minimal detrimental effects on other agronomic traits, thus contributing to improved breeding efficiency and yield of hybrid rice.

Methods

Plant materials and growth conditions

The *GS3*, *GW8* and *GS9* gene were knocked out in the *Oryza sativa* cv. *Japonica* cultivar Zhonghua 11 (ZH11) and the *indica* thermo-sensitive genic male sterile line Zhu6S through the CRISPR/cas9 technology. The orange-red-grained astaxanthin rice was kindly provided by Zhu et al. (2018). All rice plants were cultivated in the experimental field at the South China Agricultural University in Guangzhou (23°7'N, 113°15'E) from March to November in 2021 and 2022, and in Lingshui, Hainan (18°22'N, 109°45'E) from November to April in 2021 and 2022.

Investigation of spikelet shape, pistil-related traits and agronomic traits

Spikelets of ZH11 and *gs3/gw8/gw9* at different developmental stages were captured and photographed under a light

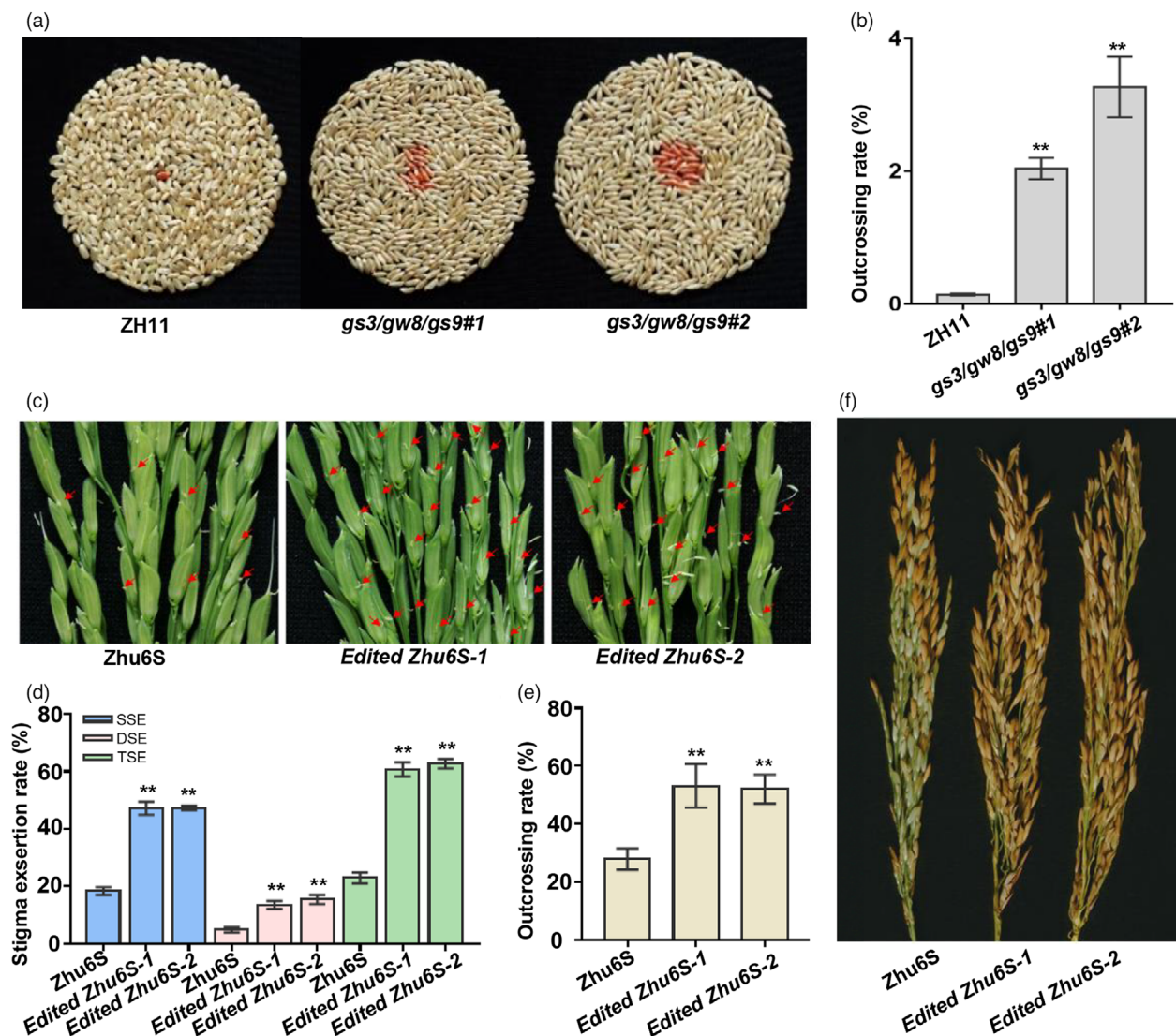


Figure 5 Knocking out *GS3*, *GW8* and *GS9* significantly increase outcrossing rates of ZH11 and Zhu6S. (a) The F₁ seeds from the crossings of ZH11 or *gs3/gw8/gw9* and the orange-red-grained astaxanthin rice. The orange-red grains represent outcrossing seeds. (b) Measurement of the outcrossing rate of ZH11 and *gs3/gw8/gw9*. Bars indicate SEM ($n = 4$). (c) The stigma exertion phenotype of Zhu6S and two edited lines (with *GW8* and *GS9* knockout). The red arrows indicate the exerted stigmas. (d) Statistical analysis of stigma exertion rate shown in (c). Bars indicate SEM ($n = 10$). (e) Measurement of the outcrossing rate of Zhu6S and two edited lines after natural cross-pollination with Tianfeng B. Bars indicate SEM ($n = 3$). (f) Panicle morphologies of Zhu6S and two edited lines after natural cross-pollination with Tianfeng B. Asterisks indicate significant differences (** $P < 0.01$) from ZH11 or Zhu6S, as determined by two-tailed Student's *t*-test. Data are shown as means \pm SEM.

microscope (Zeiss Stemi 508). For investigating the pistil-related traits, the pistils were carefully separated from the spikelets and photographed under a light microscope (Zeiss Stemi 508). The length and width of the spikelet and the length of stigma and style were measured using the ImageJ software.

To analyse the agronomic traits, the wild type ZH11 and two *gs3/gw8/gw9* lines were grown at the experimental field in Guangzhou from March to July 2021, and eight plants of ZH11 and each mutant line were randomly selected for measurement of grain length, grain width, 1000-grain weight, panicle length, number of primary branches, number of second branches, plant height, tiller number and grain number.

To calculate the stigma exertion rate (SER), SER could be gauged by three categories: the single stigma exertion rate (SSE), the dual stigma exertion rate and the total stigma exertion rate (TSE). After anthesis, 10 main panicles from 10 individuals of

ZH11, Zhu6S and each mutant line were used to calculate the number of spikelets with single exerted stigma (SES), dual exerted stigma (DES), and no exerted stigma (NES). SER is calculated using the following formulas:

$$\text{SSE (\%)} = [\text{SES}/(\text{SES} + \text{DES} + \text{NES})] \times 100\%.$$

$$\text{DSE (\%)} = [\text{DES}/(\text{SES} + \text{DES} + \text{NES})] \times 100\%.$$

$$\text{TSE (\%)} = [(\text{DES} + \text{SES})/(\text{SES} + \text{DES} + \text{NES})] \times 100\%.$$

Histological analysis

Fresh young spikelet hulls and pistils were firstly fixed in FAA and dehydrated through a graded series of ethanol, then were embedded in epoxy resin (Pon812 Epoxy Embedding Kit; Sigma-Aldrich, Saint Louis, MO, USA) and polymerized. 3- μm -thick

sections for pistils and 8- μ m-thick sections for spikelet hulls were stained with filtered 1% toluidine blue and examined under a light microscope (Nikon, Y-TV55). The cell number and cell area were measured using ImageJ. To analyse the surface cells of pistils, scanning electron microscopy (SEM) examination was performed as described by Juarez *et al.* (2004) with some modifications. Fresh pistils were fixed in a glutaraldehyde fixative solution (2.5% glutaraldehyde in 0.08 M phosphoric acid buffer) for 24 h at 4°C and then dehydrated through a graded ethanol series (30%, 50%, 70%, 95% and 100%). Dehydrated samples were then dried by a critical point dryer with liquid CO₂. Finally, the samples were coated with gold palladium using a Desk II sputter coater (Denton Vacuum, Moorestown, NJ) for 45 s before observation under a Hitachi S-3400N SEM (Hitachi, Kyoto, Japan). To analyse the surface cells of the glumes, mature spikelet glumes were dried and coated with gold palladium, then were observed with a Hitachi S-3400N SEM with an accelerating voltage of 5 kV.

Total RNA extraction, RT-qPCR analyses and RNA-seq

Total RNA was extracted from the S11b stage pistil using the TRIzol reagent (Thermo Fisher). For RT-qPCR analysis, approximate 1 μ g total RNA of each sample was converted to cDNA using a Hifair® III 1st Strand cDNA Synthesis SuperMix Kit (Yeasen Biotechnology, Shanghai, China) according to the manufacturer's instructions. RT-qPCR was performed using the Hieff UNICON® qPCR SYBR Green Master Mix (Yeasen Biotechnology) with a LightCycler® 96 System. The *Actin1* gene (*LOC_Os03g50885*) was used as a reference gene. All primer sequences are listed in Table S2.

For RNA-seq, total RNA of fresh pistils was extracted using Trizol according to the manufacturer's protocol. Two biological replicates were used for each sample. A total of 2.0 μ g RNA per sample was used to construct cDNA libraries using the mRNA-seq V3 Library Prep Kit (Vazyme, Nanjing, China) according to the manufacturer's instruction. The Bioanalyzer 2100 (Agilent, Palo Alto, CA, USA) was used to quantify and assess the quality of the RNA samples and cDNA libraries. The paired-end 2 × 150-base sequencing was performed on Illumina HiSeq X sequencing platform.

The connectors and low-quality reads were filtered using Cutadapt (V1.9.1) (Martin, 2011). The processed reads were mapped to the rice Nipponbare reference genome and genes (downloaded from <ftp://ftp.ensemblgenomes.org/pub/>) using Hisat2 (V2.0.1) (Kim *et al.*, 2015). HTSeq (V0.6.1) (Putr *et al.*, 2022) was used to count the numbers of reads mapped to each gene. EdgeR Bioconductor package was used to screen differential expression genes (DEGs) at the thresholds of false discovery rate (FDR) \leq 0.05 and log₂ Fold-Change \geq 1. Gene Ontology (GO) and Kyoto Encyclopedia of Genes and Genomes (KEGG) pathway analyses were analysed using an online tool DAVID (<https://david.ncifcrf.gov/>). Significantly enriched GO terms and KEGG pathway were selected with an empirical *P* value \leq 0.05, and the enrichment results were plotted using the ggplot2 package. All DEGs are listed in Dataset S1. Enriched GO terms and KEGG pathway are listed in Dataset S1 and S3, respectively.

Evaluation of outcrossing rate

To compare the outcrossing rate between ZH11 and the *gs3/gw8/gs9* mutants, ZH11 and two *gs3/gw8/gs9* lines were selected as the female parent, while orange-red-grained astaxanthin rice as the male parent. The female and male lines were planted in a 2:4

row ratio, and two rows of female parents were planted in the middle encompassed by four rows of each male line. During the flowering stage, artificial supplementary pollination was performed twice per day. After approximately 30 days, the seeds of the ZH11 and two *gs3/gw8/gs9* mutants were harvested. The outcrossing rate was evaluated by calculating the percentage of orange-red grain in the F₁ seeds (including white self-pollinated seeds and orange-red hybrid seeds). Four replicates were conducted for each combination.

For the natural outcrossing test, the unedited-Zhu6S and two edited-Zhu6S were planted as the female parents together with Tianfeng B (an *indica* variety with a similar heading day as Zhu6S) as the male parent. The female and male lines were planted in a 1:4 row ratio, and one row of female parents was planted in the middle encompassed by four rows of each male line. The crosses between the male and female naturally occurred without being aided by artificial pollination. After approximately 30 days, the seeds of the unedited- and edited-Zhu6S were harvested. The natural outcrossing rate was evaluated by calculating the seed setting rate of the female lines. Six replicates were conducted for each combination.

Accession numbers

The gene sequence data from this article can be found in the Rice MSU Genome Annotation Release 7 under the following accession numbers: *GW8* (LOC_Os08g41940), *GS3* (LOC_Os04g56400.1), *GS9* (LOC_Os09g27590), *CYCL4Zm* (LOC_Os01g59120), *CSLD4* (LOC_Os12g36890), *CYCB2;2* (LOC_Os06g51110), *CDKB2* (LOC_Os08g40170), *CYCA2;1* (LOC_Os12g31810), *PME1* (LOC_Os03g19610), *PME2* (LOC_Os01g20980), *PME31* (LOC_Os11g08750) and *KIN7J* (LOC_Os09g35890).

Acknowledgements

This work was supported by the National Natural Science Foundation of China (31921004, 32172056) and the Natural Science Foundation of Guangdong Province (2019B1515120061).

Conflict of interest

The authors declare they have no conflict of interest.

Author contributions

R.S. and H.W. conceived and designed the project. X.Z., and Y.G. performed the research. W.D., Y.L., D.Z., X.L., C.L. and C.W. participated in some experiments. X.Z., Y.G., and Y.H. analysed the data. R.S. and Y.H. wrote the article. H.W. revised the article.

References

- Bakti, C. and Tanaka, J. (2019) Detection of dominant QTLs for stigma exertion ratio in rice derived from *Oryza rufipogon* accession 'W0120'. *Breeding Science*, **69**, 143–150.
- Dang, X., Yang, Y., Zhang, Y., Chen, X., Fan, Z., Liu, Q., Ji, J. *et al.* (2020) *OsSYL2^{AA}*, an allele identified by gene-based association, increases style length in rice (*Oryza sativa* L.). *Plant J.* **104**, 1491–1503.
- Fan, C., Xing, Y., Mao, H., Lu, T., Han, B., Xu, C., Li, X. *et al.* (2006) *GS3*, a major QTL for grain length and weight and minor QTL for grain width and thickness in rice, encodes a putative transmembrane protein. *Theor. Appl. Genet.* **112**, 1164–1171.

- Food and Agriculture Organization of the United Nations Agriculture Databases (2021) FAO. <https://www.fao.org/worldfoodsituation/csdb/en/>
- Huang, X., Kurata, N., Wei, X., Wang, Z., Wang, A., Zhao, Q., Zhao, Y. et al. (2012) A map of rice genome variation reveals the origin of cultivated rice. *Nature* **490**, 497–501.
- Juarez, M., Twigg, R. and Timmermans, M. (2004) Specification of adaxial cell fate during maize leaf development. *Development* **131**, 4533–4544.
- Kato, H. and Namai, H. (1987) Floral characteristics and environmental factors for increasing natural outcrossing rate for F₁ hybrid seed production of rice (*Oryza sativa* L.). *Japanese Journal of Breeding* **37**, 318–330.
- Kim, D., Langmead, B. and Salzberg, S.L. (2015) HISAT: a fast spliced aligner with low memory requirements. *Nat. Methods* **12**, 357–360.
- Li, C., Sun, C., Mu, P., Chen, L. and Wang, X. (2001) QTL analysis of anther length and ratio of stigma exertion, two key traits of classification for cultivated rice (*Oryza sativa* L.) and common wild rice (*Oryza rufipogon* Griff.). *Acta Genetica Sinica* **28**, 746–751.
- Li, P., Zhang, Q. and He, Y. (2014) Genetic mapping and validation of quantitative trait loci for stigma exertion rate in rice. *Mol. Breeding* **34**, 2131–2138.
- Li, N., Xu, R. and Li, Y. (2019) Molecular networks of seed size control in plants. *Annu. Rev. Plant Biol.* **70**, 435–463.
- Ling, Z. and Xu, B. (1988) Study on stigma exertion after anthesis in rice I. variation of stigma exertion. *Acta Agriculturae Universitatis Pekinensis* **14**, 388–392.
- Liu, Q., Qin, J., Li, T., Liu, E., Fan, D., Edzesi, W., Liu, J. et al. (2015) Fine mapping and candidate gene analysis of *qSTL3*, a stigma length-conditioning locus in rice (*Oryza sativa* L.). *PLoS One* **10**, e127938.
- Liu, J., Chen, J., Zheng, X., Wu, F., Lin, Q., Heng, Y., Tian, P. et al. (2017) *GW5* acts in the brassinosteroid signalling pathway to regulate grain width and weight in rice. *Nat. Plants* **3**, 17043.
- Liu, Y., Zhang, A., Wang, F., Kong, D. and Luo, L. (2019) Fine mapping a quantitative trait locus, *qSER-7*, that controls stigma exertion rate in rice (*Oryza sativa* L.). *Rice* **12**, 46.
- Lou, J., Yue, G., Yang, W., Mei, H. and Lu, H. (2014) Mapping QTLs influencing stigma exertion in rice. *Bulgarian J. Agr. Sci.* **20**, 1450–1456.
- Mao, H., Sun, S., Yao, J., Wang, C., Yu, S., Xu, C., Li, X. et al. (2010) Linking differential domain functions of the GS3 protein to natural variation of grain size in rice. *Proc. Natl. Acad. Sci.* **107**, 19579–19584.
- Marathi, B. and Jena, K. (2015) Floral traits to enhance outcrossing for higher hybrid seed production in rice: present status and future prospects. *Euphytica* **201**, 1–14.
- Martin, M. (2011) Cutadapt removes adapter sequences from high-throughput sequencing reads. *Embnet J.* **17**, 10–12.
- Peng, S., Cassman, K., Virmani, S., Sheehy, J. and Khush, G. (1999) Yield potential trends of tropical rice since the release of IR8 and the challenge of increasing rice yield potential. *Crop. Sci.* **39**, 1552–1559.
- Putr, G., Anders, S., Py, P., Pimanda, J. and Zanini, F. (2022) Analysing high-throughput sequencing data in Python with HTSeq 2.0. *Bioinformatics* **38**, 2938–2945.
- Qi, B. and Wu, C. (2022) Potential roles of stigma exertion on spikelet fertility in rice (*Oryza sativa* L.) under heat stress. *Front. Plant Sci.* **13**, 983070.
- Rahman, M., Zhang, Y., Zhang, K., Rahman, M., Barman, H., Riaz, A., Chen, Y. et al. (2017a) Genetic dissection of the major quantitative trait locus (*qSE11*), and its validation as the major influence on the rate of stigma exertion in rice (*Oryza sativa* L.). *Front Plant Sci.* **8**, 1818.
- Rahman, M., Zhang, Y., Sun, L., Zhang, K., Rahman, M., Wu, W., Zhan, X. et al. (2017b) Genetic mapping of quantitative trait loci for the stigma exertion rate in rice (*Oryza sativa* L.). *J. Integr. Agric.* **16**, 1423–1431.
- Song, X., Huang, W., Shi, M., Zhu, M. and Lin, H. (2007) A QTL for rice grain width and weight encodes a previously unknown RING-type E3 ubiquitin ligase. *Nat. Genet.* **39**, 623–630.
- Takano-Kai, N., Jiang, H., Kubo, T., Sweeney, M., Matsumoto, T., Kanamori, H., Padhukasahasram, B. et al. (2009) Evolutionary history of *gs3*, a gene conferring grain length in rice. *Genetics* **182**, 1323–1334.
- Tan, Q., Zou, T., Zheng, M., Ni, Y., Luan, X., Li, X., Yang, W. et al. (2020) Substitution mapping of the major quantitative trait loci controlling stigma exertion rate from *Oryza glumaepatula*. *Rice* **13**, 37.
- Tian, D. (1993) Studies on mechanism of outcrossing rate in hybrid rice seed production. *Hybrid Rice* **8**, 12–14.
- Uga, Y., Fukuta, Y., Cai, H.W., Iwata, H., Ohsawa, R., Morishima, H. and Fujimura, T. (2003) Mapping QTLs influencing rice floral morphology using recombinant inbred lines derived from a cross between *Oryza sativa* L. and *Oryza rufipogon* Griff. *Theor. Appl. Genet.* **107**, 218–226.
- Uga, Y., Siangliw, M., Nagamine, T., Ohsawa, R., Fujimura, T. and Fukuta, Y. (2010) Comparative mapping of QTLs determining glume, pistil and stamen sizes in cultivated rice (*Oryza sativa* L.). *Plant Breed.* **129**, 657–669.
- Virmani, S., Aquino, R. and Khush, G. (1982) Heterosis breeding in rice (*Oryza sativa* L.). *Theor. Appl. Genet.* **63**, 373–380.
- Wang, S., Wu, K., Yuan, Q., Liu, X., Liu, Z., Lin, X., Zeng, R. et al. (2012) Control of grain size, shape and quality by *OsSPL16* in rice. *Nat. Genet.* **44**, 950–954.
- Wen, G., Yong, L., Agrama, H., Luo, D., Gao, F., Lu, X. and Ren, G. (2009) Association mapping of stigma and spikelet characteristics in rice (*Oryza sativa* L.). *Mol. Breed.* **24**, 277–292.
- Xu, R., and Sun, C. (2021) What happened during domestication of wild to cultivated rice. *Crop J.* **9**, 564–576.
- Yan, A. (1999) *Manual for hybrid rice seed production and MS line multiplication*. Beijing, China: China Agriculture Press.
- Yan, W.G., Li, Y., Agrama, H.A., Luo, D., Gao, F., Lu, X., and Ren, G. (2009) Association mapping of stigma and spikelet characteristics in rice (*Oryza sativa* L.). *Mol. Breed.* **24**, 277–292.
- Ying, C. and Zhang, S. (1989) Studies on the character of stigma exertion among some of *Oryza* species. *Chin. J. Rice Sci.* **3**, 62–66.
- Yuan, L. (2002) *Hybrid Rice*. Beijing, China: China Agriculture Press.
- Yuan, L. and Virmani, S.S. (1988) *Status of Hybrid Rice Research and Development. Hybrid Rice. Proceedings of the International Symposium on Hybrid Rice*. Manila, Philippines: International Rice Research Institute.
- Zhang, Z., Lu, Y., Liu, X., Feng, J. and Zhang, G. (2006) Cytological mechanism of pollen abortion resulting from allelic interaction of F₁ pollen sterility locus in rice (*Oryza sativa* L.). *Genetica* **127**, 295–302.
- Zhang, D., Xue, L. and Zhu, L. (2011) Cytological analysis and genetic control of rice anther development. *J. Genet. Genomics* **38**, 379–390.
- Zhang, K., Zhang, Y., Wu, W., Zhan, X., Anis, G., Rahman, M., Hong, Y. et al. (2018) *qSE7* is a major quantitative trait locus (QTL) influencing stigma exertion rate in rice (*Oryza sativa* L.). *Sci. Rep.* **8**, 14523.
- Zhao, D., Li, Q., Zhang, C., Zhang, C., Yang, Q., Pan, L., Ren, X. et al. (2018) *GS9* acts as a transcriptional activator to regulate rice grain shape and appearance quality. *Nat. Commun.* **9**, 1240.
- Zhou, H., Li, P., Xie, W., Hussain, S., Li, Y., Xia, D., Zhao, H. et al. (2017) Genome-wide association analyses reveal the genetic basis of stigma exertion in rice. *Mol. Plant* **10**, 634–644.
- Zhu, Y. (2016) Fifty years of hybrid rice research in China. *Chin. Sci. Bull.* **61**, 3740–3747.
- Zhu, Q., Zeng, D., Yu, S., Cui, C., Li, J., Li, H., Chen, J. et al. (2018) From golden rice to aSTARice: bioengineering astaxanthin biosynthesis in rice endosperm. *Mol. Plant* **11**, 1440–1448.

Supporting information

Additional supporting information may be found online in the Supporting Information section at the end of the article.

Dataset S1 Gene list and FPKM of DEGs in RNA-Seq.

Dataset S2 Gene Ontology (GO) term enrichment analyses of differentially expressed genes (DEGs).

Dataset S3 Kyoto Encyclopedia of Genes and Genomes (KEGG) pathway terms of differentially expressed genes (DEGs).

Figure S1 Correlation relationship between stigma and style length and spikelet traits.

Figure S2 *GS3*, *GW8* and *GS9* mutation sites in various knockout lines generated by the CRISPR/Cas9 technology.

Figure S3 *GS3*, *GW8* and *GS9* synchronously regulate glume, pistil growth and stigma exertion in rice.

Figure S4 Correlation relationship between stigma exertion rate and spikelet traits.

Figure S5 The effect of *GS3*, *GW8* and *GS9* on several agronomic traits in rice.

Figure S6 The dynamic change of spikelet and pistil for the ZH11 and *gs3/gw8/gs9#1* during the stages of spikelet development.

Figure S7 Transcriptome analysis of the pistil of ZH11 and the *gs3/gw8/gs9* mutant at stage 11.

Figure S8 *GW8* and *GS9* mutation in Zhu6S generated by the CRISPR/Cas9 technology.

Table S1 List of genes involved in rice grain shape controls.

Table S2 List of primers used in this study.



Cover image: Pictured is a gentoo and a chinstrap penguin along the Antarctic Peninsula. Kelton W. McMahon et al. examined the diets of chinstrap and gentoo penguins in the Antarctic Peninsula by analyzing amino acid isotopes in feathers from the 1930s, 1960s, 1980s, and 2010s. The authors found that both species consumed krill during times of whaling-induced krill surpluses, but that over the past 40 years gentoo penguins expanded their diets to include fish and squid and their populations increased. Chinstrap penguins, however, experienced population declines and continued to feed only on krill, even during times of climate change-induced krill shortages, suggesting that species with specialized diets may be vulnerable to anthropogenic environmental changes. See the article by McMahon et al. on pages 25721–25727. Image courtesy of Jim Wilson (Irishwildlife.net).

From the Cover

- 25721 Penguin populations and climate change
- 25468 Greenland Ice Sheet lake drainage
- 25677 Germ cells and gonadal colonization
- 25707 Green wave and migrating bison
- 25800 Multiple sclerosis and myelin-specific lymphocytes

Contents

THIS WEEK IN PNAS

- 25365 In This Issue

EDITORIAL

- 25368 Joint statement on EPA proposed rule and public availability of data (2019)
H. Holden Thorp, Magdalena Skipper, Veronique Kiermer, May Berenbaum, Deborah Sweet, and Richard Horton

CORE CONCEPTS—A brief introduction to emerging topics in science

- 25369 Albedo is a simple concept that plays complicated roles in climate and astronomy
Sid Perkins

COMMENTARIES

- 25372 *Mycobacterium tuberculosis* enters macrophages with aid from a bacterial lipid
Klaus Gawrisch
→ See companion article on page 25649
- 25374 Quelling germ cell pluripotency on the genital ridge
Dustin L. Updike
→ See companion article on page 25677
- 25376 Unraveling the T-B tangle in anti-CD20 multiple sclerosis therapy
Ari Waisman and Anna Ebering
→ See companion article on page 25800

LETTERS

- 25378 Divergent contributions of autistic traits to social psychological knowledge
Emily C. Taylor, Lucy A. Livingston, Mitchell J. Callan, and Punit Shah
- 25380 Reply to Taylor et al.: Acknowledging the multidimensionality of autism when predicting social psychological skill
Anton Gollwitzer, Cameron Martel, James C. McPartland, and John A. Bargh
- 25382 Behavior is the ultimate arbiter: An alternative explanation for the inhibitory effect of fluoxetine on the ovulatory homolog model of orgasm in rabbits
Gonzalo R. Quintana, Conall E. Mac Cionnaith, and James G. Pfaus

- 25384** Reply to Quintana et al.: Behavior is an unlikely mediator of fluoxetine effects on ovulation in rabbits

Günter P. Wagner and Mihaela Pavlicev

BRIEF REPORTS

- 25386** Heritability of education rises with intergenerational mobility
Per Engzell and Felix C. Tropsf
- 25389** Repurposing dichloroacetate for the treatment of women with endometriosis
Andrew W. Horne, S. Furquan Ahmad, Roderick Carter, Ioannis Simitsidellis, Erin Greaves, Chloe Hogg, Nicholas M. Morton, and Philippa T. K. Saunders
- 25392** Epstein–Barr virus EBER1 and murine gammaherpesvirus TMER4 share conserved in vivo function to promote B cell egress and dissemination
Brett A. Hoffman, Yiping Wang, Emily R. Feldman, and Scott A. Tibbetts
- 25395** Metabolite-mediated TOR signaling regulates the circadian clock in *Arabidopsis*
Nan Zhang, Yanyan Meng, Xu Li, Yu Zhou, Liuyin Ma, Liwen Fu, Markus Schwarzländer, Hongtao Liu, and Yan Xiong

PHYSICAL SCIENCES

APPLIED MATHEMATICS

- 25398** Evolutionary dynamics with game transitions
Qi Su, Alex McAvoy, Long Wang, and Martin A. Nowak
- 25405** Learning stable and predictive structures in kinetic systems
Niklas Pfister, Stefan Bauer, and Jonas Peters

APPLIED PHYSICAL SCIENCES

- 25412** Bubble pinch-off in turbulence
Daniel J. Ruth, Wouter Mostert, Stéphane Perrard, and Luc Deike
- 25418** Solidification and superlubricity with molecular alkane films
Alexander M. Smith, James E. Hallett, and Susan Perkin
- 25424** Confinement of surface spinners in liquid metamaterials
Jean-Baptiste Gorce, Hua Xia, Nicolas Francois, Horst Punzmann, Gregory Falkovich, and Michael Shats

BIOPHYSICS AND COMPUTATIONAL BIOLOGY

- 25430** Shaping the zebrafish myotome by intertissue friction and active stress
S. Tlili, J. Yin, J.-F. Rupprecht, M. A. Mendieta-Serrano, G. Weissbart, N. Verma, X. Teng, Y. Toyama, J. Prost, and T. E. Saunders
- 25440** Universal phase behaviors of intracellular lipid droplets
Shunsuke F. Shimobayashi and Yuki Ohsaki
- 25446** Probing transient excited states of the bacterial cell division regulator MinE by relaxation dispersion NMR spectroscopy
Mengli Cai, Ying Huang, Yang Shen, Min Li, Michiyo Mizuuchi, Rodolfo Ghirlando, Kiyoshi Mizuuchi, and G. Marius Clore
- 25456** Method to extract multiple states in F_1 -ATPase rotation experiments from jump distributions
Sándor Volkán-Kacsó, Luan Q. Le, Kaicheng Zhu, Haibin Su, and Rudolph A. Marcus

- 25462** Mechanical stress compromises multicomponent efflux complexes in bacteria

Lauren A. Genova, Melanie F. Roberts, Yu-Chern Wong, Christine E. Harper, Ace George Santiago, Bing Fu, Abhishek Srivastava, Won Jung, Lucy M. Wang, Łukasz Krzemiński, Xianwen Mao, Xuanhao Sun, Chung-Yuen Hui, Peng Chen, and Christopher J. Hernandez

EARTH, ATMOSPHERIC, AND PLANETARY SCIENCES

- 25468** Supraglacial lake drainage at a fast-flowing Greenlandic outlet glacier
Thomas R. Chudley, Poul Christoffersen, Samuel H. Doyle, Marion Bougamont, Charlotte M. Schoonman, Bryn Hubbard, and Mike R. James
- 25478** Subglacial meltwater supported aerobic marine habitats during Snowball Earth
Maxwell A. Lechte, Malcolm W. Wallace, Ashleigh van Smeerdijk Hood, Weiqiang Li, Ganqing Jiang, Galen P. Halverson, Dan Asael, Stephanie L. McColl, and Noah J. Planavsky

ENGINEERING

- 25484** Linking energy loss in soft adhesion to surface roughness
Siddhesh Dalvi, Abhijeet Gujrati, Subarna R. Khanal, Lars Pastewka, Ali Dhinojwala, and Tevis D. B. Jacobs
- 25555** A bioinspired approach to engineer seed microenvironment to boost germination and mitigate soil salinity
Augustine T. Zvinavashe, Eugene Lim, Hui Sun, and Benedetto Marelli
- 25562** Development of an autonomous and bifunctional quorum-sensing circuit for metabolic flux control in engineered *Escherichia coli*
Christina V. Dinh and Kristala L. J. Prather
- 25756** Optimizing photoswitchable MEK
Aleena L. Patel, Eyan Yeung, Sarah E. McGuire, Andrew Y. Wu, Jared E. Toettcher, Rebecca D. Burdine, and Stanislav Y. Shvartsman
- 25784** Treg-inducing microparticles promote donor-specific tolerance in experimental vascularized composite allotransplantation
James D. Fisher, Stephen C. Balmert, Wensheng Zhang, Riccardo Schweizer, Jonas T. Schnider, Chiaki Komatsu, Liwei Dong, Vasil E. Erbas, Jignesh V. Unadkat, Ali Mübin Aral, Abhinav P. Acharya, Yalcin Kulahci, Heth R. Turnquist, Angus W. Thomson, Mario G. Solari, Vijay S. Gorantla, and Steven R. Little
- 25932** Engineering geometrical 3-dimensional untethered in vitro neural tissue mimic
Gelson J. Pagan-Diaz, Karla P. Ramos-Cruz, Richard Sam, Mikhail E. Kandel, Onur Aydin, M. Taher A. Saif, Gabriel Popescu, and Rashid Bashir

ENVIRONMENTAL SCIENCES

- 25491** Inland water bodies in China: Features discovered in the long-term satellite data
Shuailong Feng, Shuguang Liu, Zhihong Huang, Lei Jing, Meifang Zhao, Xi Peng, Wende Yan, Yiping Wu, Yihe Lv, Andrew R. Smith, Morag A. McDonald, Sopan D. Patil, Arbi J. Sarkissian, Zhihua Shi, Jun Xia, and U. S. Ogbodo
- 25497** Tracking emissions in the US electricity system
Jacques A. de Chalendar, John Taggart, and Sally M. Benson

PHYSICS

- 25503** Optical waveguiding by atomic entanglement in multilevel atom arrays
Ana Asenjo-Garcia, H. J. Kimble, and Darrick E. Chang

- 25512 Intermolecular coupling and fluxional behavior of hydrogen in phase IV**
Alexander F. Goncharov, Irina Chuvashova, Cheng Ji, and Ho-kwang Mao
- 25516 Determination and evaluation of the nonadditivity in wetting of molecularly heterogeneous surfaces**
Zhi Luo, Anna Murello, David M. Wilkins, Filip Kovacik, Joachim Kohlbrecher, Aurel Radulescu, Halil I. Okur, Quy K. Ong, Sylvie Roke, Michele Ceriotti, and Francesco Stellacci
- 25524 Magnetoelastoresistance in WTe₂: Exploring electronic structure and extremely large magnetoresistance under strain**
Na Hyun Jo, Lin-Lin Wang, Peter P. Orth, Sergey L. Bud'ko, and Paul C. Canfield
- 25530 Pressure-induced topological phase transition in noncentrosymmetric elemental tellurium**
Toshiya Ideue, Motoaki Hirayama, Hiroaki Taiko, Takanari Takahashi, Masayuki Murase, Takashi Miyake, Shuichi Murakami, Takao Sasagawa, and Yoshihiro Iwasa
- 25569 Burrowing dynamics of aquatic worms in soft sediments**
Arshad Kudrolli and Bernny Ramirez

SOCIAL SCIENCES

PSYCHOLOGICAL AND COGNITIVE SCIENCES

- 25535 Replicator degrees of freedom allow publication of misleading failures to replicate**
Christopher J. Bryan, David S. Yeager, and Joseph M. O'Brien
- 25941 The association between serotonin transporter availability and the neural correlates of fear bradycardia**
Pieter Schipper, Marlies Hiemstra, Kari Bosch, Desiree Nieuwenhuis, Annalisa Adinolfi, Sabine Glotzbach, Bart Borghans, Dora Lopresto, Guillén Fernández, Floris Klumpers, Erno J. Hermans, Karin Roelofs, Marloes J. A. G. Henckens, and Judith R. Homberg

SOCIAL SCIENCES

- 25546 The Justinianic Plague: An inconsequential pandemic?**
Lee Mordechai, Merle Eisenberg, Timothy P. Newfield, Adam Izdebski, Janet E. Kay, and Hendrik Poinar

BIOLOGICAL SCIENCES

AGRICULTURAL SCIENCES

- 25555 A bioinspired approach to engineer seed microenvironment to boost germination and mitigate soil salinity**
Augustine T. Zvinavashe, Eugene Lim, Hui Sun, and Benedetto Marelli

APPLIED BIOLOGICAL SCIENCES

- 25562 Development of an autonomous and bifunctional quorum-sensing circuit for metabolic flux control in engineered *Escherichia coli***
Christina V. Dinh and Kristala L. J. Prather
- 25569 Burrowing dynamics of aquatic worms in soft sediments**
Arshad Kudrolli and Bernny Ramirez

BIOCHEMISTRY

- 25575 Molecular basis for allosteric regulation of the type 2 ryanodine receptor channel gating by key modulators**
Ximin Chi, Deshun Gong, Kang Ren, Gewei Zhou, Gaoxingyu Huang, Jianlin Lei, Qiang Zhou, and Nieng Yan

- 25583 Methylofuran is a prosthetic group of the formyltransferase/hydrolase complex and shuttles one-carbon units between two active sites**
Jethro L. Hemmann, Tristan Wagner, Seigo Shima, and Julia A. Vorholt
- 25591 A gatekeeping function of the replicative polymerase controls pathway choice in the resolution of lesion-stalled replisomes**
Seungwoo Chang, Karel Naiman, Elizabeth S. Thrall, James E. Kath, Slobodan Jergic, Nicholas E. Dixon, Robert P. Fuchs, and Joseph J. Loparo
- 25602 Molecular determinants of chaperone interactions on MHC-I for folding and antigen repertoire selection**
Andrew C. McShan, Christine A. Devlin, Sarah A. Overall, Jihye Park, Jugmohit S. Toor, Danai Moschidi, David Flores-Solis, Hannah Choi, Sarvind Tripathi, Erik Procko, and Nikolaos G. Sgourakis
- 25614 Efficient nonenzymatic cyclization and domain shuffling drive pyrrolopyrazine diversity from truncated variants of a fungal NRPS**
Daniel Berry, Wade Mace, Katrin Grage, Frank Wesche, Sagar Gore, Christopher L. Schardl, Carolyn A. Young, Paul P. Dijkwel, Adrian Leuchtmann, Helge B. Bode, and Barry Scott
- 25624 Cellular redox sensor HSCARG negatively regulates the translesion synthesis pathway and exacerbates mammary tumorigenesis**
Weicheng Zang, Chuazhen Yang, Tingting Li, Liming Liao, and Xiaofeng Zheng
- 25634 Mix-and-inject XFEL crystallography reveals gated conformational dynamics during enzyme catalysis**
Medhanjali Dasgupta, Dominik Budday, Saulo H. P. de Oliveira, Peter Madzelan, Darya Marchany-Rivera, Javier Seravalli, Brandon Hayes, Raymond G. Sierra, Sébastien Boutet, Mark S. Hunter, Roberto Alonso-Mori, Alexander Batyuk, Jennifer Wierman, Artem Lyubimov, Aaron S. Brewster, Nicholas K. Sauter, Gregory A. Applegate, Virendra K. Tiwari, David B. Berkowitz, Michael C. Thompson, Aina E. Cohen, James S. Fraser, Michael E. Wall, Henry van den Bedem, and Mark A. Wilson

BIOPHYSICS AND COMPUTATIONAL BIOLOGY

- 25446 Probing transient excited states of the bacterial cell division regulator MinE by relaxation dispersion NMR spectroscopy**
Mengli Cai, Ying Huang, Yang Shen, Min Li, Michiyo Mizuuchi, Rodolfo Ghirlando, Kiyoshi Mizuuchi, and G. Marius Clore
- 25641 Energetic dependencies dictate folding mechanism in a complex protein**
Kaixian Liu, Xiuqi Chen, and Christian M. Kaiser
- 25649 The conical shape of DIM lipids promotes *Mycobacterium tuberculosis* infection of macrophages**
Jacques Augenstreich, Evert Haanappel, Guillaume Ferré, Georges Czaplicki, Franck Jolibois, Nicolas Destainville, Christophe Guilhot, Alain Milon, Catherine Astarie-Dequeker, and Matthieu Chavent
→ See Commentary on page 25372
- 25659 Mechanisms of noncanonical binding dynamics in multivalent protein-protein interactions**
Wesley J. Errington, Bence Bruncsics, and Casim A. Sarkar
- 25668 QTY code designed thermostable and water-soluble chimeric chemokine receptors with tunable ligand affinity**
Rui Qing, Qiuyi Han, Michael Skuhersky, Haeyoon Chung, Myriam Badr, Thomas Schubert, and Shuguang Zhang

DEVELOPMENTAL BIOLOGY

- 25430** **Shaping the zebrafish myotome by intertissue friction and active stress**
S. Tili, J. Yin, J.-F. Rupprecht, M. A. Mendieta-Serrano, G. Weissbart, N. Verma, X. Teng, Y. Toyama, J. Prost, and T. E. Saunders
- 25677** **Mammalian germ cells are determined after PGC colonization of the nascent gonad**
Peter K. Nicholls, Hubert Schorle, Sahin Naqvi, Yueh-Chiang Hu, Yuting Fan, Michelle A. Carmell, Ina Dobrinski, Adrienne L. Watson, Daniel F. Carlson, Scott C. Fahrenkrug, and David C. Page
→ See Commentary on page 25374
- 25688** **Palmitoylation of BMPR1a regulates neural stem cell fate**
Thomas Wegleiter, Kilian Buthey, Daniel Gonzalez-Bohorquez, Martina Hruzova, Muhammad Khadeesh bin Imtiaz, Andrin Abegg, Iliana Mebert, Adriano Molteni, Dominik Kollegger, Pawel Pelczar, and Sebastian Jessberger
- 25697** **WNT/RYK signaling restricts goblet cell differentiation during lung development and repair**
Hyun-Taek Kim, Wenguang Yin, Yuko Nakamichi, Paolo Panza, Beate Grohmann, Carmen Buettner, Stefan Guenther, Clemens Ruppert, Yasuhiro Kobayashi, Andreas Guenther, and Didier Y. R. Stainier

ECOLOGY

- 25491** **Inland water bodies in China: Features discovered in the long-term satellite data**
Shuailong Feng, Shuguang Liu, Zhihong Huang, Lei Jing, Meifang Zhao, Xi Peng, Wende Yan, Yiping Wu, Yihe Lv, Andrew R. Smith, Morag A. McDonald, Sopan D. Patil, Arbi J. Sarkissian, Zhihua Shi, Jun Xia, and U. S. Ogbodo
- 25707** **Migrating bison engineer the green wave**
Chris Geremia, Jerod A. Merkle, Daniel R. Eacker, Rick L. Wallen, P. J. White, Mark Hebblewhite, and Matthew J. Kauffman
- 25714** **Unveiling dimensions of stability in complex ecological networks**
Virginia Domínguez-García, Vasilis Dakos, and Sonia Kéfi
- 25721** **Divergent trophic responses of sympatric penguin species to historic anthropogenic exploitation and recent climate change**
Kelton W. McMahon, Chantel I. Michelson, Tom Hart, Matthew D. McCarthy, William P. Patterson, and Michael J. Polito
- 25728** **Fungal aerobiota are not affected by time nor environment over a 13-y time series at the Mauna Loa Observatory**
Laura Tipton, Geoffrey Zahn, Erin Datlof, Stephanie N. Kivlin, Patrick Sheridan, Anthony S. Amend, and Nicole A. Hynson

ENVIRONMENTAL SCIENCES

- 25734** **The impact of rising CO₂ and acclimation on the response of US forests to global warming**
John S. Sperry, Martin D. Venturas, Henry N. Todd, Anna T. Trugman, William R. L. Anderegg, Yujie Wang, and Xiaonan Tai

EVOLUTION

- 25398** **Evolutionary dynamics with game transitions**
Qi Su, Alex McAvoy, Long Wang, and Martin A. Nowak

- 25745** **Solenodon genome reveals convergent evolution of venom in eulipotyphlan mammals**

Nicholas R. Casewell, Daniel Petras, Daren C. Card, Vivek Suranase, Alexis M. Mychajliw, David Richards, Ivan Koludarov, Laura-Oana Albulescu, Julien Slagboom, Benjamin-Florian Hempel, Neville M. Ngum, Rosalind J. Kennerley, Jorge L. Brocca, Gareth Whiteley, Robert A. Harrison, Fiona M. S. Bolton, Jordan Debono, Freek J. Vonk, Jessica Alföldi, Jeremy Johnson, Elinor K. Karlsson, Kerstin Lindblad-Toh, Ian R. Mellor, Roderich D. Süßmuth, Bryan G. Fry, Sanjaya Kuruppu, Wayne C. Hodgson, Jeroen Kool, Todd A. Castoe, Ian Barnes, Kartik Sunagar, Eivind A. B. Undheim, and Samuel T. Turvey

GENETICS

- 25756** **Optimizing photoswitchable MEK**
Aleena L. Patel, Eyan Yeung, Sarah E. McGuire, Andrew Y. Wu, Jared E. Toettcher, Rebecca D. Burdine, and Stanislav Y. Shvartsman
- 25764** **Functional genetic validation of key genes conferring insecticide resistance in the major African malaria vector, *Anopheles gambiae***
Adriana Adolfi, Beth Poulton, Amalia Anthousi, Stephanie Macilwee, Hilary Ranson, and Gareth J. Lycett
- 25773** **Sleep–wake-driven and circadian contributions to daily rhythms in gene expression and chromatin accessibility in the murine cortex**
Charlotte N. Hor, Jake Yeung, Maxime Jan, Yann Emmenegger, Jeffrey Hubbard, Ioannis Xenarios, Felix Naef, and Paul Franken

IMMUNOLOGY AND INFLAMMATION

- 25784** **Treg-inducing microparticles promote donor-specific tolerance in experimental vascularized composite allotransplantation**
James D. Fisher, Stephen C. Balmert, Wensheng Zhang, Riccardo Schweizer, Jonas T. Schnider, Chiaki Komatsu, Liwei Dong, Vasil E. Erbas, Jignesh V. Unadkat, Ali Mübin Aral, Abhinav P. Acharya, Yalcin Kulahci, Heth R. Turnquist, Angus W. Thomson, Mario G. Solari, Vijay S. Gorantla, and Steven R. Little
- 25790** **Homeobox protein Hhex negatively regulates Treg cells by inhibiting Foxp3 expression and function**
Sung Woong Jang, Soo Seok Hwang, Hyeong Su Kim, Min Kyung Kim, Woo Ho Lee, Soh Un Hwang, Jinu Gwak, Si Kyoung Yew, Richard A. Flavell, and Gap Ryol Lee
- 25800** **Anti-CD20 therapy depletes activated myelin-specific CD8⁺ T cells in multiple sclerosis**
Joseph J. Sabatino Jr, Michael R. Wilson, Peter A. Calabresi, Stephen L. Hauser, Jonathan P. Schneck, and Scott S. Zamvil
→ See Commentary on page 25376
- 25808** **Alcohol shifts gut microbial networks and ameliorates a murine model of neuroinflammation in a sex-specific pattern**
Blaine Caslin, Cole Maguire, Aditi Karmakar, Kailey Mohler, Dennis Wylie, and Esther Melamed
- 25816** **Cross-talk between iNKT cells and CD8 T cells in the spleen requires the IL-4/CCL17 axis for the generation of short-lived effector cells**
M. Valente, Y. Dölen, E. van Dinther, L. Vimeux, M. Fallet, V. Feuillet, and C. G. Figdor
- 25828** **The IκB-protein BCL-3 controls Toll-like receptor-induced MAPK activity by promoting TPL-2 degradation in the nucleus**
Patricia E. Collins, Domenico Somma, David Kerrigan, Felicity Herrington, Karen Keeshan, Robert J. B. Nibbs, and Ruaidhrí J. Carmody

25839 **Critical role for TRIM28 and HP1 β/γ in the epigenetic control of T cell metabolic reprogramming and effector differentiation**
 Ulf Gehrmann, Marianne Burbage, Elina Zueva, Christel Goudot, Cyril Esnault, Mengliang Ye, Jean-Marie Carpiere, Nina Burgdorf, Thomas Hoyler, Guadalupe Suarez, Leonel Joannas, Sandrine Heurtebise-Chrétien, Sylvère Durand, Rébecca Panes, Angélique Bellemare-Pelletier, Pablo J. Sáez, Fanny Aprahamian, Deborah Lefevre, Veronique Adoue, Amal Zine El Aabidine, Maqbool Muhammad Ahmad, Claire Hivroz, Olivier Joffre, Florence Cammas, Guido Kroemer, Etienne Gagnon, Jean-Christophe Andrau, and Sebastian Amigorena

25850 **B cell receptor ligation induces display of V-region peptides on MHC class II molecules to T cells**
 Peter Csaba Huszthy, Ramakrishna Prabhu Gopalakrishnan, Johanne Tracey Jacobsen, Ole Audun Werner Haabeth, Geir Åge Løset, Ranveig Braathen, Karl Schenck, Anders Aune Tveita, Ludvig Andre Munthe, and Bjarne Bogen

25860 **Smad7 in intestinal CD4⁺ T cells determines autoimmunity in a spontaneous model of multiple sclerosis**
 Steffen Hauptelshofer, Teresa Leichsenring, Sarah Berg, Xiomara Pedreiturria, Stephanie C. Joachim, Iris Tischoff, Jan-Michel Otte, Tobias Bopp, Massimo C. Fantini, Charlotte Esser, Dieter Willbold, Ralf Gold, Simon Faissner, and Ingo Kleiter

MEDICAL SCIENCES

25870 **An absence of lamin B1 in migrating neurons causes nuclear membrane ruptures and cell death**
 Natalie Y. Chen, Ye Yang, Thomas A. Weston, Jason N. Belling, Patrick Heizer, Yiping Tu, Paul Kim, Lovelyn Edillo, Steven J. Jonas, Paul S. Weiss, Loren G. Fong, and Stephen G. Young

25880 **Fbxw7 is a driver of uterine carcinosarcoma by promoting epithelial-mesenchymal transition**
 Ileana C. Cuevas, Subhransu S. Sahoo, Ashwani Kumar, He Zhang, Jill Westcott, Mitzi Aguilar, Jeremy D. Cortez, Stephanie A. Sullivan, Chao Xing, D. Neil Hayes, Rolf A. Brekken, Victoria L. Bae-Jump, and Diego H. Castrillon

MICROBIOLOGY

25891 **Combined HIV-1 sequence and integration site analysis informs viral dynamics and allows reconstruction of replicating viral ancestors**
 Sean C. Patro, Leah D. Brandt, Michael J. Bale, Elias K. Halvas, Kevin W. Joseph, Wei Shao, Xiaolin Wu, Shuang Guo, Ben Murrell, Ann Wiegand, Jonathan Spindler, Castle Raley, Christopher Hautman, Michele Sobolewski, Christine M. Fennessey, Wei-Shau Hu, Brian Luke, Jenna M. Hasson, Aurelie Niyongabo, Adam A. Capoferri, Brandon F. Keele, Jeff Milush, Rebecca Hoh, Steven G. Deeks, Frank Maldarelli, Stephen H. Hughes, John M. Coffin, Jason W. Rausch, John W. Mellors, and Mary F. Kearney

25900 **Metatranscriptomic reconstruction reveals RNA viruses with the potential to shape carbon cycling in soil**
 Evan P. Starr, Erin E. Nuccio, Jennifer Pett-Ridge, Jillian F. Banfield, and Mary K. Firestone

25909 **Division of labor in honey bee gut microbiota for plant polysaccharide digestion**
 Hao Zheng (郑浩), Julie Perreau, J. Elijah Powell, Benfeng Han (韩本凤), Zijing Zhang (张紫晶), Waldan K. Kwong, Susannah G. Tringe, and Nancy A. Moran

25917 **Structure and function of an unusual flavodoxin from the domain Archaea**
 Divya Prakash, Prashanti R. Iyer, Suharti Suharti, Karim A. Walters, Michel Geovanni Santiago-Martinez, John H. Golbeck, Katsuhiko S. Murakami, and James G. Ferry

25923 **MAIT Cells Are Major Contributors to the Cytokine Response in Group A Streptococcal Toxic Shock Syndrome**
 Johanna Emgård, Helena Bergsten, John K. McCormick, Israel Barrantes, Steinar Skrede, Johan K. Sandberg, and Anna Norrby-Teglund

NEUROSCIENCE

25932 **Engineering geometrical 3-dimensional untethered in vitro neural tissue mimic**
 Gelson J. Pagan-Diaz, Karla P. Ramos-Cruz, Richard Sam, Mikhail E. Kandel, Onur Aydin, M. Taher A. Saif, Gabriel Popescu, and Rashid Bashir

25941 **The association between serotonin transporter availability and the neural correlates of fear bradycardia**
 Pieter Schipper, Marlies Hiemstra, Kari Bosch, Desiree Nieuwenhuis, Annalisa Adinolfi, Sabine Glotzbach, Bart Borghans, Dora Lopresto, Guillén Fernández, Floris Klumpers, Erno J. Hermans, Karin Roelofs, Marloes J. A. G. Henckens, and Judith R. Homberg

25948 **Otogelin, otogelin-like, and stereocilin form links connecting outer hair cell stereocilia to each other and the tectorial membrane**
 Paul Avan, Sébastien Le Gal, Vincent Michel, Typhaine Dupont, Jean-Pierre Hardelin, Christine Petit, and Elisabeth Verpy

25958 **Brain-wide genetic mapping identifies the indusium griseum as a prenatal target of pharmacologically unrelated psychostimulants**
 Janos Fuzik, Sabah Rehman, Fatima Girach, Andras G. Miklosi, Solomiia Korchynska, Gloria Arque, Roman A. Romanov, János Hanics, Ludwig Wagner, Konstantinos Meletis, Yuchio Yanagawa, Gabor G. Kovacs, Alán Alpár, Tomas G. M. Hökfelt, and Tibor Harkany

25968 **$\beta 2^*$ nAChRs on VTA dopamine and GABA neurons separately mediate nicotine aversion and reward**
 Taryn E. Grieder, Morgane Besson, Geith Maal-Bared, Stéphanie Pons, Uwe Maskos, and Derek van der Kooy

25974 **Targeting liver aldehyde dehydrogenase-2 prevents heavy but not moderate alcohol drinking**
 Adrien Guillot, Tianyi Ren, Tony Jourdan, Robert J. Pawlosky, Elaine Han, Seung-Jin Kim, Li Zhang, George F. Koob, and Bin Gao

25982 **Endogenous retroviruses are associated with hippocampus-based memory impairment**
 Roman Sankowski, Joshua J. Strohl, Tomás S. Huerta, Elham Nasiri, Andrea N. Mazzarello, Cristina D'Abramo, Kai Fan Cheng, Ori Staszewski, Marco Prinz, Patricio T. Huerta, and Yousef Al-Abed

25991 **Characterization of the activity, aggregation, and toxicity of heterodimers of WT and ALS-associated mutant Sod1**
 Aline de Araújo Brasil, Mariana Dias Castela de Carvalho, Ellen Gerhardt, Daniela Dias Queiroz, Marcos Dias Pereira, Tiago Fleming Outeiro, and Elis Cristina Araujo Eleutherio

PHARMACOLOGY

26001 **Crystal structure of the M₅ muscarinic acetylcholine receptor**
 Ziva Vuckovic, Patrick R. Gentry, Alice E. Berizzi, Kunio Hirata, Swapna Varghese, Geoff Thompson, Emma T. van der Westhuizen, Wessel A. C. Burger, Raphaël Rahmani, Celine Valant, Christopher J. Langmead, Craig W. Lindsley, Jonathan B. Baell, Andrew B. Tobin, Patrick M. Sexton, Arthur Christopoulos, and David M. Thal

- 26008** **TRPA1 modulation by piperidine carboxamides suggests an evolutionarily conserved binding site and gating mechanism**
 Tania Chernov-Rogan, Eleonora Gianti, Chang Liu, Elisia Villemure, Andrew P. Cridland, Xiaoyu Hu, Elisa Ballini, Wienke Lange, Heike Deisemann, Tianbo Li, Stuart I. Ward, David H. Hackos, Steven Magnuson, Brian Safina, Michael L. Klein, Matthew Volgraf, Vincenzo Carnevale, and Jun Chen

PHYSIOLOGY

- 26020** **Polarized PtdIns(4,5)P₂ distribution mediated by a voltage-sensing phosphatase (VSP) regulates sperm motility**
 Takafumi Kawai, Haruhiko Miyata, Hiroki Nakanishi, Souhei Sakata, Shin Morioka, Junko Sasaki, Masahiko Watanabe, Kenji Sakimura, Toyoshi Fujimoto, Takehiko Sasaki, Masahito Ikawa, and Yasushi Okamura

- 26029** **A critical role for microglia in maintaining vascular integrity in the hypoxic spinal cord**
 Sebok K. Halder and Richard Milner

- 26038** **Corpora amylacea act as containers that remove waste products from the brain**
 Marta Riba, Elisabet Augé, Joan Campo-Sabariz, David Moral-Anter, Laura Molina-Porcel, Teresa Ximelis, Ruth Ferrer, Raquel Martín-Venegas, Carme Pelegrí, and Jordi Vilaplana

PLANT BIOLOGY

- 26049** **BBX4, a phyB-interacting and modulated regulator, directly interacts with PIF3 to fine tune red light-mediated photomorphogenesis**
 Yueqin Heng, Yan Jiang, Xianhai Zhao, Hua Zhou, Xuncheng Wang, Xing Wang Deng, and Dongqing Xu

- 26057** **Glutathionylation primes soluble glyceraldehyde-3-phosphate dehydrogenase for late collapse into insoluble aggregates**
 Mirko Zaffagnini, Christophe H. Marchand, Marco Malferrari, Samuel Murail, Sara Bonacchi, Damiano Genovese, Marco Montalti, Giovanni Venturoli, Giuseppe Falini, Marc Baaden, Stéphane D. Lemaire, Simona Fermani, and Paolo Trost

- 26066** **Insect-damaged *Arabidopsis* moves like wounded *Mimosa pudica***
 Andrzej Kurenda, Chi Tam Nguyen, Aurore Chételat, Stéphanie Stolz, and Edward E. Farmer

PSYCHOLOGICAL AND COGNITIVE SCIENCES

- 26072** **Young children spontaneously recreate core properties of language in a new modality**
 Manuel Bohn, Gregor Kachel, and Michael Tomasello

SUSTAINABILITY SCIENCE

- 26078** **The influence of the global electric power system on terrestrial biodiversity**
 Robert A. Holland, Kate Scott, Paolo Agnolucci, Chrysanthi Rapti, Felix Eigenbrod, and Gail Taylor

SYSTEMS BIOLOGY

- 25405** **Learning stable and predictive structures in kinetic systems**
 Niklas Pfister, Stefan Bauer, and Jonas Peters
- 25440** **Universal phase behaviors of intracellular lipid droplets**
 Shunsuke F. Shimobayashi and Yuki Ohsaki

CORRECTIONS

ENVIRONMENTAL SCIENCES, SUSTAINABILITY SCIENCE

- 26085** **Linking global drivers of agricultural trade to on-the-ground impacts on biodiversity**
 Jonathan M. H. Green, Simon A. Croft, América P. Durán, Andrew P. Balmford, Neil D. Burgess, Steve Fick, Toby A. Gardner, Javier Godar, Clément Suavet, Malika Virah-Sawmy, Lucy E. Young, and Christopher D. West

MEDICAL SCIENCES

- 26087** **An open challenge to advance probabilistic forecasting for dengue epidemics**
 Michael A. Johansson, Karyn M. Apfeldorf, Scott Dobson, Jason Devita, Anna L. Buczak, Benjamin Baugher, Linda J. Moniz, Thomas Bagley, Steven M. Babin, Erhan Guven, Teresa K. Yamana, Jeffrey Shaman, Terry Moschou, Nick Lothian, Aaron Lane, Grant Osborne, Gao Jiang, Logan C. Brooks, David C. Farrow, Sangwon Hyun, Ryan J. Tibshirani, Roni Rosenfeld, Justin Lessler, Nicholas G. Reich, Derek A. T. Cummings, Stephen A. Lauer, Sean M. Moore, Hannah E. Clapham, Rachel Lowe, Trevor C. Bailey, Markel García-Díez, Marilia Sá Carvalho, Xavier Rodó, Tridip Sardar, Richard Paul, Evan L. Ray, Krzysztof Sakrejda, Alexandria C. Brown, Xi Meng, Osonde Osoba, Raffaele Vardavas, David Manheim, Melinda Moore, Dhananjai M. Rao, Travis C. Porco, Sarah Ackley, Fengchen Liu, Lee Worden, Matteo Convertino, Yang Liu, Abraham Reddy, Eloy Ortiz, Jorge Rivero, Humberto Brito, Alicia Juarrero, Leah R. Johnson, Robert B. Gramacy, Jeremy M. Cohen, Erin A. Mordecai, Courtney C. Murdock, Jason R. Rohr, Sadie J. Ryan, Anna M. Stewart-Ibarra, Daniel P. Weikel, Antarpreet Jutla, Rakibul Khan, Marissa Poultney, Rita R. Colwell, Brenda Rivera-García, Christopher M. Barker, Jesse E. Bell, Matthew Biggerstaff, David Swardlow, Luis Mier-y-Teran-Romero, Brett M. Forshey, Juli Trtanj, Jason Asher, Matt Clay, Harold S. Margolis, Andrew M. Hebbeler, Dylan George, and Jean-Paul Chretien

MICROBIOLOGY

- 26089** **Global selective sweep of a highly inbred genome of the cattle parasite *Neospora caninum***
 Asis Khan, Ayako Wendy Fujita, Nadine Randle, Javier Regidor-Cerrillo, Jahangheer S. Shaik, Kui Shen, Andrew J. Oler, Mariam Quinones, Sarah M. Latham, Bartholomew D. Akanmori, Sarah Cleaveland, Elizabeth A. Innes, Una Ryan, Jan Šlapeta, Gereon Schares, Luis M. Ortega-Mora, Jitender P. Dubey, Johnathan M. Wastling, and Michael E. Grigg

NEUROSCIENCE

- 26090** **Spatiotemporal activation of the C/EBPβ/δ-secretase axis regulates the pathogenesis of Alzheimer's disease**
 Hualong Wang, Xia Liu, Shengdi Chen, and Keqiang Ye

BBX4, a phyB-interacting and modulated regulator, directly interacts with PIF3 to fine tune red light-mediated photomorphogenesis

Yueqin Heng^{a,b,1}, Yan Jiang^{a,1}, Xianhai Zhao^c, Hua Zhou^c, Xuncheng Wang^d, Xing Wang Deng^{b,d,2}, and Dongqing Xu^{a,2}

^aState Key Laboratory of Crop Genetics and Germplasm Enhancement, College of Agriculture, Nanjing Agricultural University, 210095 Nanjing, China; ^bPeking University–Southern University of Science and Technology Joint Institute of Plant and Food Sciences, Department of Biology, Southern University of Science and Technology, 518055 Shenzhen, China; ^cState Key Laboratory of Hybrid Rice, College of Life Sciences, Wuhan University, 430072 Hubei, China; and ^dState Key Laboratory of Protein and Plant Gene Research, Peking–Tsinghua Center for Life Sciences, School of Advanced Agriculture Sciences and School of Life Sciences, Peking University, 100871 Beijing, China

Contributed by Xing Wang Deng, October 23, 2019 (sent for review September 3, 2019; reviewed by Sourav Datta and Min Ni)

Phytochrome B (phyB) absorbs red light signals and subsequently initiates a set of molecular events in plant cells to promote photomorphogenesis. Here we show that phyB directly interacts with B-BOX CONTAINING PROTEIN 4 (BBX4), a positive regulator of red light signaling, and positively controls its abundance in red light. BBX4 associates with PHYTOCHROME INTERACTING FACTOR 3 (PIF3) and represses PIF3 transcriptional activation activity and PIF3-controlled gene expression. The degradation of BBX4 in darkness is dependent on CONSTITUTIVELY PHOTOMORPHOGENIC 1 (COP1) and the 26S proteasome system. Collectively, BBX4 acts as a key component of the phyB-PIF3-mediated signaling module and fine tunes the red light action. phyB promotes the accumulation of BBX4, which in turn serves to repress PIF3 action through direct physical interaction to promote photomorphogenic development in red light.

phyB | COP1 | BBX4 | photomorphogenesis | light signaling

Light signals are perceived by a variety of wavelength-specific photoreceptors, including phytochromes (phys), cryptochromes, phototropins, and UV-B resistance locus 8 (1–5). Of these, phys sense red (R) and far-red (FR) light signals to mediate various developmental processes in plants, including seed germination, photomorphogenesis, shade avoidance, flowering, and senescence (6, 7). The phys can be photoconverted between 2 states, an inactive Pr form absorbing R light and a biologically active Pfr form sensing FR light. phyA-phyE have both unique and overlapping functions, among which phyB is the primary R light photoreceptor in *Arabidopsis* (8, 9).

Photoactivated phyB translocates from the cytoplasm to the nucleus, where it interacts directly with a subset of basic helix-loop-helix (bHLH) transcription factors, termed phytochrome-interacting factors (PIFs) including PIF1, PIF3, PIF4, and PIF5. Subsequently, this molecular event leads to the promotion of their degradation and their sequestration from their target promoters (10). PIF3, the founding member of the PIFs, is identified by a yeast two-hybrid screen using phyB as the bait (11). phyB interacts with and recruits PIF3 into nuclear bodies during the dark-to-light transition before its degradation (12). PIF3 is a key repressor of phyB-mediated signaling, which regulates hypocotyl elongation, cotyledon expansion of seedlings, and chloroplast development (13, 14). In the dark, 2 E3 ubiquitin ligases defined by CONSTITUTIVELY PHOTOMORPHOGENIC 1 (COP1) and DE-ETIOLATED 1, stabilize the abundance of PIF3 (15, 16). Thus, PIF3 is enriched in the nucleus and mediates the expression levels of a large group of target genes to maintain the state of skotomorphogenesis in plants. On light illumination, photoactivated phyA and phyB interact directly with PIF3 and rapidly trigger its phosphorylation on multiple residues and subsequent degradation through the 26S proteasome system (17, 18). The phosphorylation of PIF3 is directly mediated by phy and

photoregulatory protein kinases (19, 20). The SCF^{EBF1/2} E3 ligase complex targets phosphorylated PIF3 for ubiquitination and degradation under a wide range of light intensity conditions (21), while under high light conditions, the CUL3^{LRBs} E3 ligase complex simultaneously targets both phyB and phosphorylated PIF3 for ubiquitination and concurrent degradation to reduce the sensitivity of plant cells to red light (22). In addition, it has been shown that PIF3 promotes the degradation of phyB to attenuate plant light responses (18, 23, 24).

Recent work has revealed that a subset of B box-containing proteins (BBXs) play critical roles in light-dependent development in plants. Multiple BBXs, acting downstream of various photoreceptors, function in COP1- and HY5-mediated light signaling pathways in promoting or repressing seedling development (25–29). BBX4 (also known as CONSTANS-LIKE 3 [COL3]) contains 2 tandem B-box domains in its N-terminal half and a conserved CCT (CO, COL, TOC1) domain in its C-terminal region (30). BBX4 directly associates with *FLOWERING LOCUS T* (*FT*) promoter through its CCT domain in the presence of BBX32 to repress *FT* expression and flowering (31). In addition to repressing flowering, BBX4 is also involved in various physiological and

Significance

Phytochrome B (phyB) is the predominant red light photoreceptor that transduces red light signals to downstream signaling. On red light exposure, photoactivated phyB interacts with a transcription factor termed PHYTOCHROME INTERACTING FACTOR 3 (PIF3), a repressor of red light signaling, triggering its rapid phosphorylation and subsequent degradation. Thus, phyB-PIF3 defines a critical regulatory hub for red light-mediated seedling development. In this study, we show that B-BOX CONTAINING PROTEIN 4 (BBX4) is a key component involved in the phyB-PIF3 regulatory module. phyB directly interacts with BBX4 and positively controls the abundance of BBX4 in red light. Accumulated BBX4 directly interacts with PIF3 to inhibit its transcriptional activation activity toward target genes, thereby promoting photomorphogenesis.

Author contributions: X.W.D. and D.X. designed research; Y.H., Y.J., X.Z., H.Z., X.W., and D.X. performed research; X.W.D. and D.X. analyzed data; and X.W.D. and D.X. wrote the paper.

Reviewers: S.D., Indian Institute of Science Education and Research; and M.N., University of Minnesota Twin Cities.

The authors declare no competing interest.

Published under the [PNAS license](#).

¹Y.H. and Y.J. contributed equally to this work.

²To whom correspondence may be addressed. Email: dongqingxu@njau.edu.cn or deng@pku.edu.cn.

This article contains supporting information online at <https://www.pnas.org/lookup/suppl/doi:10.1073/pnas.1915149116/-DCSupplemental>.

First published November 27, 2019.

developmental processes, including photomorphogenesis, formation of lateral root and shoot branching, shoot elongation, and accumulation of anthocyanin (32). A loss-of-function *bbx4* mutant specifically displays elongated hypocotyls in R light, but not in blue (B) and FR light (32). This indicates that BBX4 acts as a positive regulator of phyB-mediated signaling. However, the molecular mechanism underlying BBX4 in the regulation of R light-mediated inhibition of hypocotyl elongation has remained largely unknown.

In this study, we demonstrated that 2 key regulators of R light signaling, phyB and PIF3, both physically interact with BBX4 in response to R light. BBX4 protein level accumulated to high abundance in R light in a phyB-dependent manner. BBX4 genetically acts upstream of PIF3 and represses its transcriptional activation activity. In short, on R light illumination, photo-activated phyB directly associates with BBX4 and promotes its accumulation. Thus, accumulated BBX4 interacts with PIF3 to inhibit its transcriptional activation activity, thereby promoting photomorphogenic development.

Results

BBX4 Is a Positive Regulator of Red Light Signaling. BBX4 acts as a positive regulator of the phyB-mediated inhibition of hypocotyl elongation (32). Consistently, 2 independent *bbx4* single mutants, *bbx4-1* and *bbx4-2*, which were generated by the clustered regulatory interspaced short palindromic repeats (CRISPR)/Cas9 technique (ref. 33 and *SI Appendix, Fig. S1A*), showed similar hypocotyl phenotypes with Col (wild-type [WT]) when grown in the dark (D), B, and FR light conditions (*SI Appendix, Fig. S1*). However, they displayed significantly elongated hypocotyls compared with Col grown in white (W) and R light conditions (*SI*

Appendix, Fig. S1 D–G). These data further confirm BBX4 as a positive regulator of R light signaling.

To verify these genetic results, we generated 2 independent YFP-tagged *BBX4* (*YFP-BBX4*) transgenic lines, in which the expression of *BBX4* was overexpressed and YFP-BBX4 protein was clearly detectable (*SI Appendix, Fig. S2 A and B*). They showed a similar etiolated phenotype as Col (WT) when grown in darkness (*SI Appendix, Fig. S2 C and D*); however, these 2 transgenic lines overexpressing *BBX4* displayed markedly shortened hypocotyls in the W, B, R, and FR light conditions tested (*SI Appendix, Fig. S2 E–L*), indicating that overexpression of *BBX4* confers hypersensitivity to inhibition of hypocotyl elongation in response to various wavelength-specific light signals in *Arabidopsis*.

phyB Genetically and Physically Interacts with BBX4. Considering that phyB is the predominant R light photoreceptor and BBX4 functions in R light signaling (9, 32), we investigated the genetic interplay between *phyB* and *BBX4*. Both *bbx4-1* and *phyB-9* showed longer hypocotyls than Col, and hypocotyl length was obviously longer in *phyB-9* mutant seedlings compared with *bbx4-1* seedlings in R light (Fig. 1 *A* and *B*). The double-mutant *phyB-9 bbx4-1* was indistinguishable from *phyB-9* grown in R light (Fig. 1 *A* and *B*). *YFP-BBX4* showed shortened hypocotyls compared with Col and *phyB-9*. The hypocotyl length of *YFP-BBX4 phyB-9* was shorter than that of *phyB-9*, but longer than that of Col and *YFP-BBX4* (Fig. 1 *C* and *D*). In addition, the PBC (*phyB-CFP phyB-9*) transgenic line showed shorter hypocotyls than Col and *bbx4-1*, and *PBC bbx4-1* exhibited similar hypocotyl phenotypes as PBC grown in R light (*SI Appendix, Fig. S3 A and B*). These genetic results

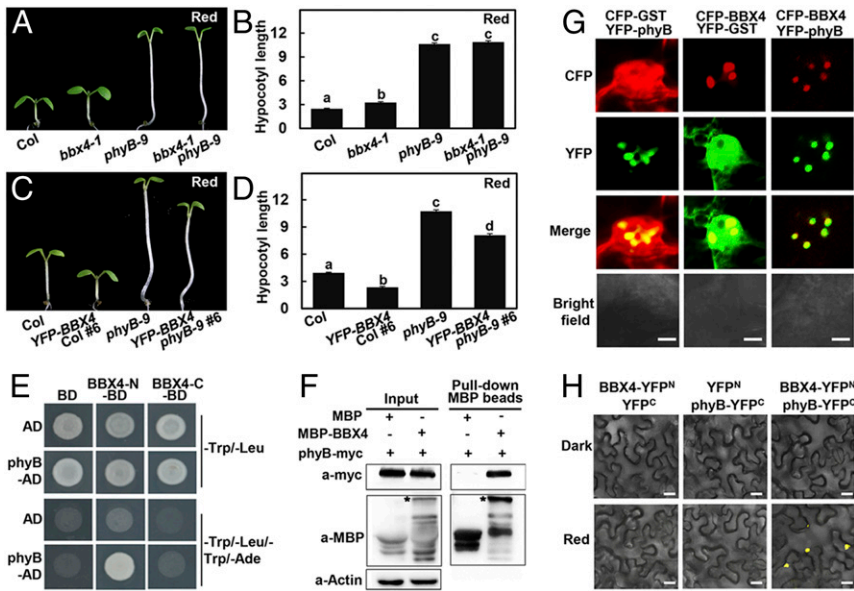


Fig. 1. *phyB* genetically and physically interacts with BBX4. (*A* and *B*) Hypocotyl phenotype (*A*) and length (*B*) of 4-d-old Col, *bbx4-1*, *phyB-9*, and *bbx4-1 phyB-9* seedlings grown in R (115.8 $\mu\text{mol}/\text{m}^2/\text{s}$) light. The unit of hypocotyl length is millimeters. The experiments were performed 3 times with similar results. The graphs depict one of these experiments. Error bars represent SE ($n \geq 20$). Letters above the bars indicate significant differences ($P < 0.05$), as determined by 1-way ANOVA with Tukey's post hoc analysis. (*C* and *D*) Hypocotyl phenotype (*C*) and length (*D*) of 4-d-old Col, *YFP-BBX4* #6, *phyB-9*, and *YFP-BBX4 phyB-9* #6 seedlings grown in R light (115.8 $\mu\text{mol}/\text{m}^2/\text{s}$). The unit of hypocotyl length is millimeters. The experiments were performed 3 times, with similar results. The graphs depict 1 of these experiments. Error bars represent SE ($n \geq 20$). Letters above the bars indicate significant differences ($P < 0.05$), as determined by 1-way ANOVA with Tukey's post hoc analysis. (*E*) Yeast two-hybrid interactions between the BBX4 and *phyB*. (*F*) Semi-in vivo pull-down assay of BBX4 with *phyB*. Total plant protein was extracted from 4-d-old *phyB-myc* transgenic seedlings grown in R light (115.8 $\mu\text{mol}/\text{m}^2/\text{s}$). Equal amounts of MBP and MBP-BBX4 proteins were added to total plant protein extracts. The asterisk indicates MBP-BBX4. Actin served as a negative control. (*G*) BBX4 and *phyB* colocalize to the nuclear bodies in tobacco cells. CFP-BBX4 and YFP-*phyB* were transiently coexpressed in tobacco leaves. CFP-GST and YFP-GST served as negative controls. (Scale bars: 5 μm .) (*H*) BiFC assay showing the interaction of BBX4 with *phyB* in R light. BBX4 and *phyB* were fused to the N- and C-terminal fragments of YFP (YFP^N and YFP^C, respectively). Unfused YFP^N and YFP^C fragments served as negative controls. (Scale bars: 20 μm .)

suggest that BBX4 likely acts downstream of phyB in mediating part of R light signaling.

We next examined whether BBX4 interacts with phyB at the protein level. As full-length and middle portion of BBX4 (103 to 201) showed self-activation activity in yeast cells (SI Appendix, Fig. S4), we fused binding domain (BD) with the BBX4 N-terminal half (BBX4-N, 1 to 102) containing 2 conserved B-box domains or the C-terminal region (BBX4-C, 202 to 294) carrying an intact CCT domain for yeast two-hybrid assays. Both of these BBX4 truncation proteins were expressed at comparable levels in yeast cells when coexpressed with phyB (SI Appendix, Fig. S5). BBX4-N, but not BBX4-C, was able to interact with phyB in yeast cells (Fig. 1E).

Next, purified MBP-fused BBX4 (MBP-BBX4) recombinant protein and cell extracts from the transgenic seedlings expressing myc-phyB grown in R light were used for pull-down assays. MBP-BBX4, but not the MBP (negative control) could pull down the myc-phyB protein as detected on immunoblot assays (Fig. 1F). In addition, phyB-YFP and CFP-BBX4 colocalized in the nuclear bodies when transiently coexpressed in *Arabidopsis* protoplasts. The negative controls GST-CFP and phyB-YFP, or CFP-BBX4 and GST-YFP, did not exhibit any colocalization in the same experiments (Fig. 1G).

We next used a bimolecular fluorescence complementation (BiFC) assay and fused BBX4 with a split N-terminal of YFP

(YFP^N) and phyB with a split C-terminal of YFP (YFP^C). YFP signals could not be observed when transiently coexpressed BBX4-YFP^N and phyB-YFP^C in *Nicotiana benthamiana* leaves were incubated in darkness; however, strong YFP signals were clearly detected on transference to R light (Fig. 1H). These data suggest that phyB physically interacts with BBX4 likely in an R light-dependent manner.

phyB Stabilizes the Abundance of BBX4 in Red Light. Photoactivated phyB interacts with PIF3 and subsequently promotes its phosphorylation and degradation (11, 17, 34). Therefore, to examine the functional consequence of phyB-BBX4 interaction, we introduced a *phyB-9* mutation into the *YFP-BBX4* transgenic line by genetic crossing and examined whether phyB affects the abundance of BBX4 in R light. YFP-BBX4 was abundant in *YFP-BBX4* seedlings but obviously decreased in *YFP-BBX4 phyB-9* seedlings grown in constant R light (Fig. 2A). In addition, *YFP-BBX4* accumulated markedly more YFP-BBX4 protein compared with *YFP-BBX4 phyB-9* on transference to R light for 1 h and 3 h (Fig. 2B). Consistently, the YFP signals in *YFP-BBX4 phyB* seedlings were clearly reduced compared with those in *YFP-BBX4* grown in constant R light or on 1 h of R light irradiation (Fig. 2C and D). The transcript levels of *BBX4* in *YFP-BBX4* were only slightly reduced compared with those in *YFP-BBX4 phyB-9* when grown in darkness for 4 d on transference to red light for 3 h or

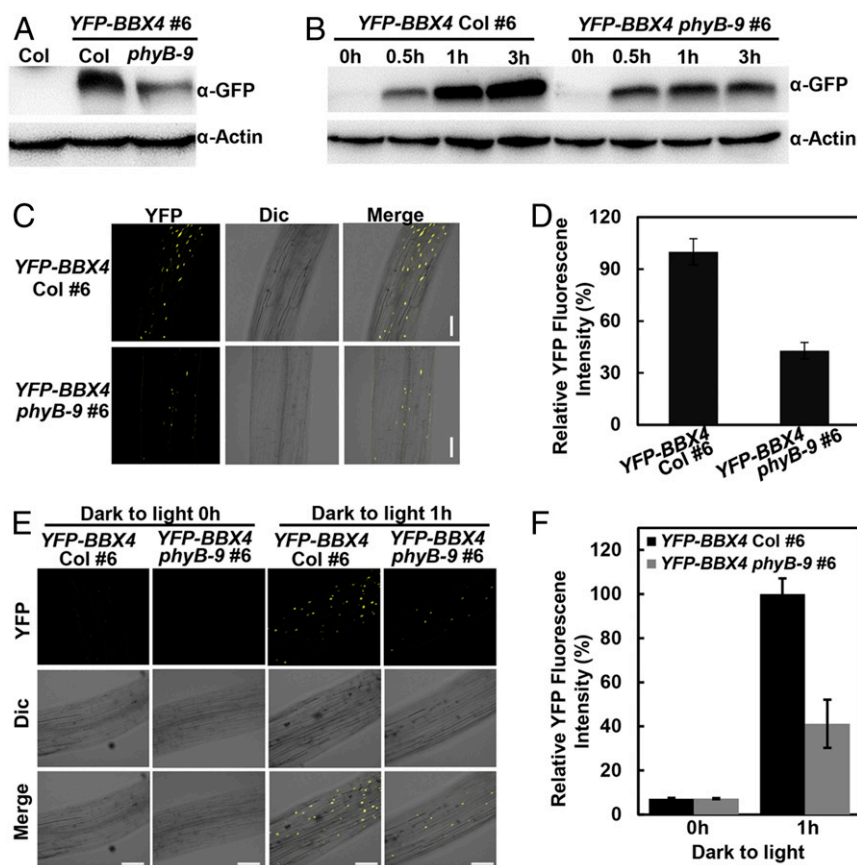


Fig. 2. phyB stabilizes BBX4 in R light. (A) YFP-BBX4 protein levels in *YFP-BBX4* Col #6 and *YFP-BBX4 phyB-9* #6 grown in R light ($115.8 \mu\text{mol}/\text{m}^2/\text{s}$) for 4 d. Col served as a negative control. (B) Immunoblot analysis of YFP-BBX4 protein levels in *YFP-BBX4* Col #6 and *YFP-BBX4 phyB-9* #6 grown in the dark for 4 d and then transferred to R light ($115.8 \mu\text{mol}/\text{m}^2/\text{s}$) for 0, 0.5, 1, and 3 h, as indicated. Actin served as a loading control. (C and D) Analysis of YFP fluorescence signals in hypocotyls of *YFP-BBX4* Col #6 and *YFP-BBX4 phyB-9* #6 seedlings grown in R light ($115.8 \mu\text{mol}/\text{m}^2/\text{s}$) for 4 d. The corresponding fluorescence intensity was measured using ImageJ and was compared between the overall signals from the images, as shown in D. Data are mean \pm SE ($n \geq 10$). (Scale bars: 100 μm .) (E and F) Analysis of YFP fluorescence signals in hypocotyls of *YFP-BBX4* Col #6 and *YFP-BBX4 phyB-9* #6 seedlings grown in the dark for 4 d, then transferred to R light ($115.8 \mu\text{mol}/\text{m}^2/\text{s}$) for 0 and 1 h. The corresponding fluorescence intensity was measured using ImageJ software and compared between the overall signals from the images, as shown in F. Data are mean \pm SE ($n \geq 10$). (Scale bars: 100 μm .)

grown in red light, respectively (SI Appendix, Fig. S6). These results suggest that phyB positively modulates BBX4 abundance in R light.

Because phyB rapidly forms nuclear bodies on R light exposure (35), we examined whether BBX4 has any effect on the formation of phyB nuclear bodies. Nuclear bodies were clearly detectable in *PBC*, consistent with previous studies (35). Nuclear bodies observed in the nucleus of *PBC bbx4-1* were similar to those in *PBC* (SI Appendix, Fig. S7), implying that BBX4 might not affect the formation of phyB nuclear bodies.

BBX4 Undergoes COP1-Mediated Degradation in Darkness. A previous study showed that COP1 physically interacts with BBX4 (32), and thus we examined whether COP1 mediates the degradation of BBX4. We first examined whether BBX4 is degraded via the 26S proteasome system. For this, 4-d-old dark-grown *YFP-BBX4* transgenic seedlings were applied with DMSO or various concentrations of MG132 (a proteasome inhibitor) for 3 h. *YFP-BBX4* protein levels were clearly increased when the transgenic seedlings were treated with 200 μ M MG132 (SI Appendix, Fig. S8A).

Next, we introduced *cop1-4* and *cop1-6* mutations into *YFP-BBX4* transgenic lines by genetic crossing. Etiolated *YFP-BBX4 cop1-4* and *YFP-BBX4 cop1-6* transgenic lines displayed clearly stronger YFP signals compared with *YFP-BBX4* transgenic seedlings (SI Appendix, Fig. S8B). These observations indicate that COP1 promotes the degradation of BBX4 via the 26S proteasome system in etiolated seedlings.

BBX4 Genetically and Physically Interacts with PIF3. PIF3, acting directly downstream of phyB, represses R light-mediated seedling

development (11). We thus investigated the genetic interaction between *BBX4* and *PIF3*. As reported, *bbx4-1* displayed longer hypocotyls but *pif3-1* had shorter hypocotyls compared with Col when grown in R light. The hypocotyl length of *bbx4-1 pif3-1* was indistinguishable from that of *pif3-1*, indicating that BBX4 and PIF3 function in the same pathway in the regulation of R light-mediated hypocotyl growth (Fig. 3 A and B).

We next tested whether BBX4 interacts with PIF3. Both BBX4-N and BBX4-C proteins were expressed at similar levels in yeast cells when coexpressed with PIF3 (SI Appendix, Fig. S5). BBX4-N, but not BBX4-C, could interact with PIF3 in yeast cells, indicating that B-box domain of BBX4 might mediate its interaction with PIF3 (Fig. 3C). We carried out fluorescence resonance energy transfer (FRET) experiments to verify these results. CFP-PIF3 with YFP-BBX4 were coexpressed in onion epidermal cells. After excitation with 405- and 514-nm wavelength light sources, emission of YFP-BBX4 was reduced dramatically, whereas emission from CFP-PIF3 increased (Fig. 3 D and E), indicating that FRET had occurred between CFP-PIF3 and YFP-BBX4 proteins before the bleach in living plant cells. Furthermore, we performed BiFC analysis and transiently coexpressed BBX4-YFP^N and PIF3-YFP^C in *N. benthamiana* leaves. We did not observe any YFP signals when *N. benthamiana* leaves incubated in darkness; however, YFP signals were clearly detectable on R light exposure. The negative controls BBX4-YFP^N and YFP^C, or YFP^N and PIF3-YFP^C could not produce any detectable YFP signals (Fig. 3F). Taken together, these data support a conclusion that BBX4 physically interacts with PIF3 likely in an R light-dependent manner.

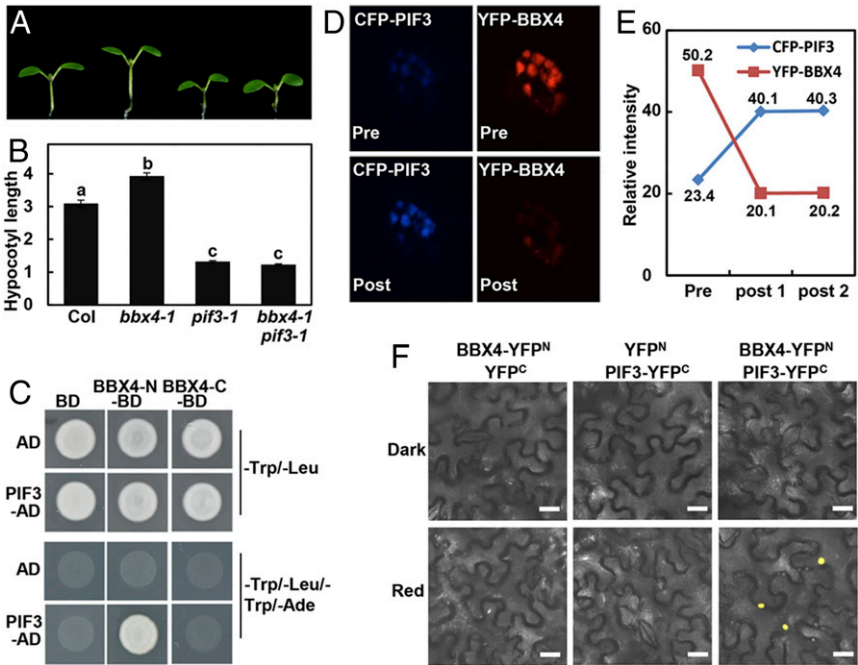
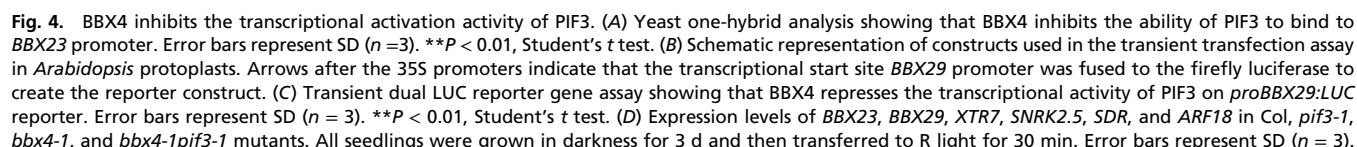


Fig. 3. BBX4 genetically and physically interacts with PIF3. (A and B) Hypocotyl phenotype (A) and length (B) of 4-d-old Col, *bbx4-1*, *pif3-1* and *bbx4-1 pif3-1* seedlings grown in R light (115.8 μ mol/m²/s). The unit of hypocotyl length is millimeters. The experiments were performed 3 times, with similar results. The graphs depict 1 of these experiments. Error bars represent SE ($n \geq 20$). Letters above the bars indicate significant differences ($P < 0.05$), as determined by 1-way ANOVA with Tukey's post hoc analysis. (C) Yeast two-hybrid interactions between the BBX4 and PIF3. (D) FRET between CFP-PIF3 and YFP-BBX4 analyzed by acceptor bleaching in nuclei. (Top) Representative prebleach nuclei coexpressing YFP-BBX4 and CFP-PIF3 excited with a 514-nm or 405-nm laser, resulting in emission from YFP or CFP, respectively. (Bottom) The same nuclei after bleaching excited with a 514-nm or 405-nm laser. (E) The relative intensities of both YFP and CFP inside the nuclei were measured once before and twice after the bleaching, as indicated in D. (F) BiFC assay showing the interaction of BBX4 with PIF3 in red light. BBX4 and PIF3 were fused to the N- and C-terminal fragments of YFP (YFP^N and YFP^C, respectively). Unfused YFP^N and YFP^C fragments served as negative controls. (Scale bars: 40 μ m.)

regulates gene expression, at least in part, in a PIF3-dependent manner.

R light is predominantly perceived by phyB, which mediates a variety of light-dependent physiological and developmental processes in plants (38). phyB maintains a biologically inactive form in the cytoplasm of plant cells in darkness. On R light irradiation, phyB is converted to a biologically active state and translocates into the nucleus, in which it interacts with multiple families of transcription factors, such as PIF3 and EIN3, to induce their degradation (11, 17, 34, 39). Here we show that BBX4 is a phyB-interacting protein, but phyB mediates a high level of BBX4 accumulation in R light. Accumulated BBX4 associates with PIF3 to repress its transcriptional activation activity and PIF3-controlled gene expression, consequently promoting phyB-mediated photomorphogenic development.

Photoactivated phyB promptly shifts into the nucleus and interacts with the COP1-SPA1 E3 ubiquitin ligase complex to interfere with its biochemical activity (40). COP1 interacts and colocalizes with BBX4 in yeast and living plant cells, respectively.



Mutation in *BBX4* partially suppresses the constitutively photomorphogenic phenotype of *cop1* in darkness (32). The degradation of BBX4 in dark-grown seedlings was dependent on COP1 as well as on the 26S proteasome system (*SI Appendix, Fig. S8*). These facts imply that phyB-mediated inhibition of COP1 activity might lead to the accumulation of BBX4 in response to R light (Fig. 2). phyB was seen to directly interact with BBX4 (Fig. 1), and this molecular event might also contribute to the stabilization of BBX4 in R light. The robust increase of BBX4 is a necessary step for phyB-mediated seedling development. Although phyB rapidly induces the phosphorylation and degradation of the majority of PIF3 on R light exposure, the abnormal hypocotyl phenotypes of *pi3* mutant and transgenic seedlings overexpressing *PIF3* grown in R light support the conclusion that the remaining pool of PIF3 also has a negative role on photomorphogenesis in R light (41). BBX4 physically associates with PIF3 (Fig. 3), thereby inhibiting PIF3 transcriptional activation activity to affect PIF3-regulated gene expression (Fig. 4). Consequently, these molecular events result in the promotion of photomorphogenic development in R light. BBX4 could directly bind to the *FT* promoter and repress its expression in the presence of BBX32 (31), suggesting that BBX4 functions as a transcription factor in regulating physiological and developmental processes. Therefore, light induced-BBX4 could also directly associate with a number of target gene promoters to control their transcription and mediate photomorphogenesis.

phyB was found to stabilize BBX4 (Fig. 2) but to promote the degradation of PIF3 (17, 18), demonstrating that phyB has opposite effects on the stability of these 2 types of transcription factors. BBX4 and PIF3 antagonistically regulate phyB-mediated signaling, and BBX4 acts as a positive regulator of R light signaling (ref. 32 and *SI Appendix, Figs. S1 and S2*), while PIF3 represses R light-dependent seedling development (11). Taken together, this evidence supports the conclusion that phyB promotes photomorphogenesis in R light not only by promoting degradation of negative regulators like PIF3, but also by facilitating the accumulation of positive regulators like BBX4.

Global transcriptomic analysis has revealed that phyB is able to associate with a large number of gene promoter regions and affect massive gene expression on R light irradiation (42, 43). phyB lacks any recognizable DNA-binding domain (9), indicating that binding of phyB to DNA requires additional transcription factors. Consistently, an increasing number of studies have shown that phyB regulates downstream gene expression by interacting with multiple transcription factors. phyB interacts with PHOTOPERIODIC CONTROL OF HYPOCOTYL 1 (PCH1) to repress *LONG HYPOCOTYL IN FAR-RED (HFR1)*, *ARABIDOPSIS THALIANA HOMEODOMAIN PROTEIN 2 (ATHB2)*, and *PIF4* transcription (44). phyB can form a tripartite complex with PHYTOCHROME-DEPENDENT LATEFLOWERING (PHL) and CONSTANS (CO) to activate the expression of *FT* (45). Previous studies (12) and the present study have revealed that phyB, BBX4, and PIF3 can physically interact with one another (Figs. 1 and 3), implying that they might coexist in a protein complex in some circumstances, most likely early after R light exposure. Formation of a phyB-BBX4-PIF3 tripartite complex also might be required for R light- and phyB-mediated transcriptional reprogramming. phyB inhibits PIF3 action not only by triggering its degradation, but also by sequestering it from its target sites (46, 47). phyB promoted the accumulation of BBX4 that could inhibit PIF3 biochemical activity (Figs. 2 and 4), indicating that phyB might also repress PIF3 action by increasing the abundance of BBX4.

In conclusion, we demonstrate that BBX4 is a previously unidentified phyB-interacting protein whose abundance positively modulated by phyB in R light. It appears that phyB, BBX4, and PIF3 function coordinately in R light signaling. On one hand, photoactivated phyB promotes the degradation of PIF3. On the

other hand, phyB interferes with the biochemical activity of COP1-SPA1 complex, thus leading to the accumulation of BBX4 on R light irradiation. Accumulated BBX4 physically interacts with the remaining pool of PIF3 and inhibit its transcriptional activity, strengthening the phyB-mediated R light inactivation of PIF3 activity. Consequently, phyB-BBX4-PIF3 might be a critical regulatory module that fine tunes photomorphogenic development in responsiveness of R light (Fig. 5).

Materials and Methods

Plant Materials and Growth Conditions. The *Arabidopsis thaliana* *phyB-9* (48) and *pi3-1* (40) mutants, *PHYB-CFP (PBC; ref. 35)* and *myc-phyB* (49) transgenic lines were of the Col-0 ecotype. Double-mutant/transgenic plants were generated by genetic crossing, and homozygous lines were verified by PCR genotyping or antibiotic screen. Seeds were surface-sterilized with 30% commercial Clorox bleach and sown on 1× Murashige and Skoog (MS) medium containing 1% sucrose and 0.8% agar. The seeds were stratified in darkness for 3 d at 4 °C, then transferred to light chambers maintained at 22 °C. The fluence rates of the light growth chambers were 13.24 μmol/m²/s for W light, 3.88 μmol/m²/s for B light, 115.8 μmol/m²/s for R light, and 4.3 μmol/m²/s for FR light.

Plasmid Construction. The full-length *BBX4*, *phyB*, or *PIF3* coding sequence (CDS) were cloned into the *pDONR223* vector using Gateway BP Clonase enzyme mix (Invitrogen) and introduced into the plant binary vector *pEarlyGate 102*, *pEarlyGate 104*, *pSPYNE*, or *pSPYCE* (50) using Gateway LR Clonase enzyme mix (Invitrogen). To produce constructs for yeast two-hybrid assays, full-length *BBX4*, *BBX4-N* (1–102) and *BBX4-C* (202–294) fragments were cloned into the *EcoRI/BamHI* sites of *pGBKT7* vector (Clontech). Full-length *phyB* and *PIF3* were cloned into the *EcoRI/BamHI* sites of *pGADT7* vector (Clontech). To produce constructs for purification of MBP-BBX4 recombinant protein, full-length *BBX4* was cloned into *EcoRI/SalI* site of *pMAL-c2x* vector. The primers used for plasmids construction were listed in *SI Appendix, Table S1*.

Generation of *bbx4* Mutants Using CRISPR/Cas9 Technique. The *bbx4* mutants were generated by *CRISPR/Cas9* technique as described previously (51), and 23-bp target sites (5′-N₂₀NGG-3′) were searched on the web site of CRISPR-GE (<http://skl.scau.edu.cn/>) (33). The *sgRNA* target sites of *BBX4* were subcloned into a *pHEE401E* vector. After transformation into *Agrobacterium tumefaciens* GV3101 by the freeze-thaw method, the binary constructs were introduced into Col via the floral dip method. The T₀ plants were sowed on the MS plates containing 50 mg/L hygromycin. The resistant seedlings (T₁) were transferred to soil. The mutations in *BBX4* were identified by PCR amplification and sequencing.

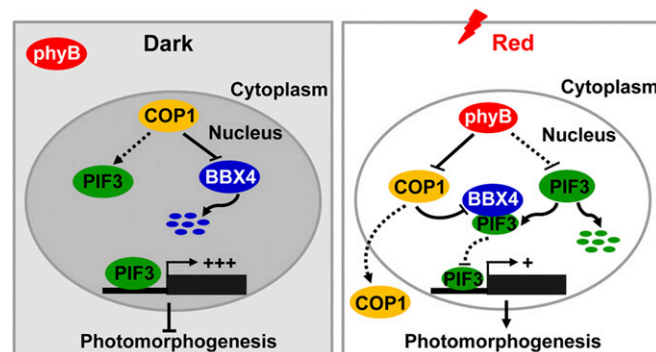


Fig. 5. A proposed working model depicting the mechanism of BBX4 in phyB-PIF3-mediated light signaling. In darkness, phyB is in inactive form in the cytoplasm. COP1 stabilizes PIF3 and interacts with BBX4 to promote its degradation via the 26S proteasome system. Highly accumulated PIF3 induces the expression of its direct-target genes to repress photomorphogenesis. On R light illumination, phyB is converted to a biologically active form and translocated into the nucleus. Photoactivated phyB promotes PIF3 protein degradation and induces the accumulation of BBX4 protein, likely by inhibiting the COP1-BBX4 association. In addition, accumulated BBX4 interacts with the remaining PIF3 to inhibit the transcription of PIF3 direct-target genes and promote photomorphogenesis.

Homozygous mutants were crossed with Col to remove the T-DNA insertion including *CRISPER/Cas9*.

Transgenic Plants. The *pEarlyGate104-BBX4* construct was transformed into *A. tumefaciens* GV3101 by the freeze-thaw method. The floral dip method was used to generate transgenic plants (52). Transgenic plants were selected on MS medium containing 20 mg/L Basta. Homozygous lines were used for genetic and biochemical studies.

Measurement of Hypocotyl Length. To measure the hypocotyl length of seedlings, seeds were surface-sterilized and sown on MS plates. After stratification at 4 °C in darkness for 3 d, the seeds were placed in continuous white light for 8 h to induce uniform germination. The seeds were then transferred to dark or different light conditions and incubated at 22 °C for 4 d. The hypocotyl length of seedlings was measured using ImageJ software.

Immunoblot Analysis. For immunoblot analysis, *Arabidopsis* seedlings were homogenized in protein extraction buffer containing 100 mM NaH₂PO₄, 10 mM Tris-HCl pH 8.0, 200 mM NaCl, 8 M urea, 1 mM PMSF, and 1× complete protease inhibitor mixture (Roche). The primary antibodies used in this study were anti-GFP (Abmart; catalog no. M20004M), anti-myc (Sigma-Aldrich; catalog no. M4439), and anti-actin (Sigma-Aldrich; catalog no. A0480).

Yeast Two-Hybrid Assays. For the GAL4 two-hybrid assays, the respective combinations of *pGAD-T7* and *pGBK-T7* fusion plasmids were cotransformed into yeast strain Y2HGold via the lithium acetate transformation procedure, as described in the *Yeast Protocols Handbook* (Clontech). The empty *pGAD-T7* and *pGBK-T7* vectors were cotransformed in parallel as negative controls. The interactions were examined on SD/-Trp/-Leu/-His/-Ade medium (Clontech).

BiFC Assay. The YFP^N and YFP^C fused plasmids were transformed into *Agrobacterium* strain GV3101, and the indicated transformants pairs were infiltrated into *N. benthamiana* leaves. After incubation in darkness or exposure to the red light for 36 h, the YFP fluorescence signals were observed and imaged under a Carl Zeiss LSM510 Meta confocal laser scanning microscope. YFP fluorescence was excited by a 514-nm laser and detected between 517 and 589 nm.

FRET Assay. The FRET experiments were carried out as described previously (32, 53). In brief, the *35S::CFP-PIF3* and *35S::YFP-BBX4* constructs were introduced into onion (*Allium cepa*) epidermal cells by particle bombardment and incubated, and live cell images were acquired using a Zeiss Axiovert 200 microscope equipped with a laser scanning confocal imaging LSM 510 Meta system. Cells were visualized at 24 h after particle bombardment using the confocal microscope through a Plan-Neofluor 403/1.3 oil (differential interference

contrast) objective. The multitracking mode was used to eliminate spillover between fluorescence channels. The CFP was excited by a 405-nm laser diode and the YFP was excited by an argon-ion laser, both at low intensities. Regions of interest were selected and bleached over 100 iterations using the argon-ion laser at 100%.

Semi-in Vivo Pull-Down Assay. The total protein of 4-d-old red light-grown *phyB-myc* seedlings was extracted with extraction buffer containing 150 mM NaCl, 10 mM Tris-HCl pH 7.5, 2 mM EDTA, 0.5% Nonidet P-40, and 1× protease inhibitor mixture (Roche). MBP-BBX4 or MBP purified recombinant proteins were mixed with total proteins and then incubated with anti-MBP beads (Sigma-Aldrich) for 4 h at 4 °C. The anti-MBP (New England BioLabs; catalog no. E8032S), anti-myc (Sigma-Aldrich; catalog no. M4439), and anti-actin (Sigma-Aldrich; catalog no. A0480) antibodies were used for immunoblotting detection.

Total RNA Isolation and qRT-PCR. Four-d-old *Arabidopsis* seedlings grown in R light (115.8 μmol/m²/s) were used to isolate total RNA with the Qiagen RNeasy Plant Mini Kit. cDNA synthesis reactions were performed with 5× All-In-One RT MasterMix (Applied Biological Materials) according to the manufacturer's instructions. cDNA templates and primer sets were mixed with Hieff qPCR SYBR Green Master Mix (Yeasen), and real-time PCR was performed on a StepOnePlus Real-Time PCR system (Applied Biosystems). Each experiment was performed at least 3 times with similar results, and 3 technical replicates were performed for each sample. The expression levels were normalized to that of housekeeping gene *PP2A*. The primers used in the qRT-PCR analyses are listed in *SI Appendix, Table S1*.

Statistical Analysis. Statistical analyses were performed using Microsoft Excel, GraphPad Prism version 5.0, and an online program (https://astatsa.com/OneWay_Anova_with_TukeyHSD/).

Data Availability. Sequence data from this article are available in the *Arabidopsis* Genome Initiative database libraries (<https://www.arabidopsis.org/>) under the following accession nos.: AT2G18790 for *phyB*, AT1G09530 for *PIF3*, AT2G24790 for *BBX4*, and AT2G32950 for *COP1*.

ACKNOWLEDGMENTS. We thank Dr. Magnus Holm (deceased) for help with the FRET experiments and in initiating this study, and Dr. Meng Chen for the *phyB-CFP phyB-9* seeds. This work was supported by grants from National Key R&D Program of China (2017YFA0503800), National Natural Science Foundation of China (31621001, 31900210, and 31970258), Peking-Tsinghua Center for Life Sciences, Southern University of Science and Technology, and Nanjing Agricultural University.

1. R. A. Sharrock, P. H. Quail, Novel phytochrome sequences in *Arabidopsis thaliana*: Structure, evolution, and differential expression of a plant regulatory photoreceptor family. *Genes Dev.* **3**, 1745–1757 (1989).
2. S. Gallagher, T. W. Short, P. M. Ray, L. H. Pratt, W. R. Briggs, Light-mediated changes in two proteins found associated with plasma membrane fractions from pea stem sections. *Proc. Natl. Acad. Sci. U.S.A.* **85**, 8003–8007 (1988).
3. C. Lin *et al.*, Association of flavin adenine dinucleotide with the *Arabidopsis* blue light receptor CRY1. *Science* **269**, 968–970 (1995).
4. H. Guo, H. Yang, T. C. Mockler, C. Lin, Regulation of flowering time by *Arabidopsis* photoreceptors. *Science* **279**, 1360–1363 (1998).
5. L. Rizzini *et al.*, Perception of UV-B by the *Arabidopsis* UVR8 protein. *Science* **332**, 103–106 (2011).
6. C. Kami, S. Lorrain, P. Hornitschek, C. Fankhauser, Light-regulated plant growth and development. *Curr. Top. Dev. Biol.* **91**, 29–66 (2010).
7. K. A. Franklin, P. H. Quail, Phytochrome functions in *Arabidopsis* development. *J. Exp. Bot.* **61**, 11–24 (2010).
8. G. Bae, G. Choi, Decoding of light signals by plant phytochromes and their interacting proteins. *Annu. Rev. Plant Biol.* **59**, 281–311 (2008).
9. M. Chen, J. Chory, Phytochrome signaling mechanisms and the control of plant development. *Trends Cell Biol.* **21**, 664–671 (2011).
10. V. N. Pham, P. K. Kathare, E. Huq, Phytochromes and phytochrome interacting factors. *Plant Physiol.* **176**, 1025–1038 (2018).
11. M. Ni, J. M. Tepperman, P. H. Quail, PIF3, a phytochrome-interacting factor necessary for normal photoinduced signal transduction, is a novel basic helix-loop-helix protein. *Cell* **95**, 657–667 (1998).
12. M. Ni, J. M. Tepperman, P. H. Quail, Binding of phytochrome B to its nuclear signalling partner PIF3 is reversibly induced by light. *Nature* **400**, 781–784 (1999).
13. E. Park *et al.*, Degradation of phytochrome interacting factor 3 in phytochrome-mediated light signaling. *Plant Cell Physiol.* **45**, 968–975 (2004).
14. P. G. Stephenson, C. Fankhauser, M. J. Terry, PIF3 is a repressor of chloroplast development. *Proc. Natl. Acad. Sci. U.S.A.* **106**, 7654–7659 (2009).
15. D. Bauer *et al.*, Constitutive photomorphogenesis 1 and multiple photoreceptors control degradation of phytochrome interacting factor 3, a transcription factor required for light signaling in *Arabidopsis*. *Plant Cell* **16**, 1433–1445 (2004).
16. J. Dong *et al.*, *Arabidopsis* DE-ETIOLATED1 represses photomorphogenesis by positively regulating phytochrome-interacting factors in the dark. *Plant Cell* **26**, 3630–3645 (2014).
17. B. Al-Sady, W. Ni, S. Kircher, E. Schäfer, P. H. Quail, Photoactivated phytochrome induces rapid PIF3 phosphorylation prior to proteasome-mediated degradation. *Mol. Cell* **23**, 439–446 (2006).
18. W. Ni *et al.*, Multisite light-induced phosphorylation of the transcription factor PIF3 is necessary for both its rapid degradation and concomitant negative feedback modulation of photoreceptor phyB levels in *Arabidopsis*. *Plant Cell* **25**, 2679–2698 (2013).
19. A. Y. Shin *et al.*, Evidence that phytochrome functions as a protein kinase in plant light signalling. *Nat. Commun.* **7**, 11545 (2016).
20. W. Ni *et al.*, PPKs mediate direct signal transfer from phytochrome photoreceptors to transcription factor PIF3. *Nat. Commun.* **8**, 15236 (2017).
21. J. Dong *et al.*, Light-dependent degradation of PIF3 by SCF^{EBF1/2} promotes a photomorphogenic response in *Arabidopsis*. *Curr. Biol.* **27**, 2420–2430.e6 (2017).
22. W. Ni *et al.*, A mutually assured destruction mechanism attenuates light signaling in *Arabidopsis*. *Science* **344**, 1160–1164 (2014).
23. B. Al-Sady, E. A. Kikis, E. Monte, P. H. Quail, Mechanistic duality of transcription factor function in phytochrome signaling. *Proc. Natl. Acad. Sci. U.S.A.* **105**, 2232–2237 (2008).
24. I. C. Jang, R. Henriques, H. S. Seo, A. Nagatani, N. H. Chua, *Arabidopsis* PHYTOCHROME INTERACTING FACTOR proteins promote phytochrome B polyubiquitination by COP1 E3 ligase in the nucleus. *Plant Cell* **22**, 2370–2383 (2010).
25. D. Xu *et al.*, BBX21, an *Arabidopsis* B-box protein, directly activates HY5 and is targeted by COP1 for 26S proteasome-mediated degradation. *Proc. Natl. Acad. Sci. U.S.A.* **113**, 7655–7660 (2016).
26. D. Xu, Y. Jiang, J. Li, M. Holm, X. W. Deng, The B-box domain protein BBX21 promotes photomorphogenesis. *Plant Physiol.* **176**, 2365–2375 (2018).

27. F. Lin *et al.*, B-BOX DOMAIN PROTEIN28 negatively regulates photomorphogenesis by repressing the activity of transcription factor HY5 and undergoes COP1-mediated degradation. *Plant Cell* **30**, 2006–2019 (2018).
28. Y. Heng *et al.*, B-Box containing proteins BBX30 and BBX31, acting downstream of HY5, negatively regulate photomorphogenesis in Arabidopsis. *Plant Physiol.* **180**, 497–508 (2019).
29. A. Yadav *et al.*, The B-Box-Containing microProtein miP1a/BBX31 regulates photomorphogenesis and UV-B protection. *Plant Physiol.* **179**, 1876–1892 (2019).
30. R. Khanna *et al.*, The Arabidopsis B-box zinc finger family. *Plant Cell* **21**, 3416–3420 (2009).
31. P. Tripathi, M. Carvallo, E. E. Hamilton, S. Preuss, S. A. Kay, Arabidopsis B-BOX32 interacts with CONSTANS-LIKE3 to regulate flowering. *Proc. Natl. Acad. Sci. U.S.A.* **114**, 172–177 (2017).
32. S. Datta, G. H. Hettiarachchi, X. W. Deng, M. Holm, Arabidopsis CONSTANS-LIKE3 is a positive regulator of red light signaling and root growth. *Plant Cell* **18**, 70–84 (2006).
33. Z. P. Wang *et al.*, Egg cell-specific promoter-controlled CRISPR/Cas9 efficiently generates homozygous mutants for multiple target genes in Arabidopsis in a single generation. *Genome Biol.* **16**, 144 (2015).
34. R. Khanna *et al.*, A novel molecular recognition motif necessary for targeting photoactivated phytochrome signaling to specific basic helix-loop-helix transcription factors. *Plant Cell* **16**, 3033–3044 (2004).
35. M. Chen, Y. Tao, J. Lim, A. Shaw, J. Chory, Regulation of phytochrome B nuclear localization through light-dependent unmasking of nuclear-localization signals. *Curr. Biol.* **15**, 637–642 (2005).
36. X. Zhang *et al.*, A PIF1/PIF3-HY5-BBX23 transcription factor cascade affects photomorphogenesis. *Plant Physiol.* **174**, 2487–2500 (2017).
37. Y. Zhang *et al.*, A quartet of PIF bHLH factors provides a transcriptionally centered signaling hub that regulates seedling morphogenesis through differential expression-patterning of shared target genes in Arabidopsis. *PLoS Genet.* **9**, e1003244 (2013).
38. N. C. Rockwell, Y. S. Su, J. C. Lagarias, Phytochrome structure and signaling mechanisms. *Annu. Rev. Plant Biol.* **57**, 837–858 (2006).
39. H. Shi *et al.*, The red light receptor phytochrome B directly enhances substrate-E3 ligase interactions to attenuate ethylene responses. *Dev. Cell* **39**, 597–610 (2016).
40. X. D. Lu *et al.*, Red-light-dependent interaction of phyB with SPA1 promotes COP1-SPA1 dissociation and photomorphogenic development in Arabidopsis. *Mol. Plant* **8**, 467–478 (2015).
41. J. Kim *et al.*, Functional characterization of phytochrome interacting factor 3 in phytochrome-mediated light signal transduction. *Plant Cell* **15**, 2399–2407 (2003).
42. J. M. Tepperman *et al.*, Expression profiling of phyB mutant demonstrates substantial contribution of other phytochromes to red-light-regulated gene expression during seedling de-etiolation. *Plant J.* **38**, 725–739 (2004).
43. J. H. Jung *et al.*, Phytochromes function as thermosensors in Arabidopsis. *Science* **354**, 886–889 (2016).
44. H. Huang *et al.*, PCH1 integrates circadian and light-signaling pathways to control photoperiod-responsive growth in Arabidopsis. *eLife* **5**, e13292 (2016).
45. M. Endo, Y. Tanigawa, T. Murakami, T. Araki, A. Nagatani, PHYTOCHROME-DEPENDENT LATE-FLOWERING accelerates flowering through physical interactions with phytochrome B and CONSTANS. *Proc. Natl. Acad. Sci. U.S.A.* **110**, 18017–18022 (2013).
46. E. Park *et al.*, Phytochrome B inhibits binding of phytochrome-interacting factors to their target promoters. *Plant J.* **72**, 537–546 (2012).
47. E. Park, Y. Kim, G. Choi, Phytochrome B requires PIF degradation and sequestration to induce light responses across a wide range of light conditions. *Plant Cell* **30**, 1277–1292 (2018).
48. M. M. Neff, J. Chory, Genetic interactions between phytochrome A, phytochrome B, and cryptochrome 1 during Arabidopsis development. *Plant Physiol.* **118**, 27–35 (1998).
49. P. Xu *et al.*, Phytochrome B and AGB1 coordinately regulate photomorphogenesis by antagonistically modulating PIF3 stability in Arabidopsis. *Mol. Plant* **12**, 229–247 (2019).
50. K. W. Earley *et al.*, Gateway-compatible vectors for plant functional genomics and proteomics. *Plant J.* **45**, 616–629 (2006).
51. X. Xie *et al.*, CRISPR-GE: A convenient software toolkit for CRISPR-based genome editing. *Mol. Plant* **10**, 1246–1249 (2017).
52. S. J. Clough, A. F. Bent, Floral dip: A simplified method for Agrobacterium-mediated transformation of Arabidopsis thaliana. *Plant J.* **16**, 735–743 (1998).
53. S. Datta, C. Hettiarachchi, H. Johansson, M. Holm, SALT TOLERANCE HOMOLOG2, a B-box protein in Arabidopsis that activates transcription and positively regulates light-mediated development. *Plant Cell* **19**, 3242–3255 (2007).

On the Cover: Photosynthetic activity of *pp7l* mutants during seedling development is most strongly affected in young seedlings and recovers gradually over 10 days during subsequent seedling development. These seedling and the PAM images shown represent the cotyledon phenotypes and various photosynthetic parameters of 4-to-10-day-old Col-0, *pp7l-1* and *sig2* and *sig6* mutants. Credit: Duorong Xu and Tatjana Kleine.

ON THE INSIDE

Peter V. Minorsky 1

NEWS AND VIEWS

Salicylic Acid, Senescence, and Heterosis. Lisa M. Smith 3

Diverse Strategies Coping with Winter in Barley and its Relatives. Yunqing Yu 5

Epigenetic Regulation of mRNA Polyadenylation Site Selection. Lisa M. Smith 7

A Bridge between Kingdoms: Introduction of a Golden Gate-Based Tool Kit for Cyanobacteria. Raimund Nagel 10

Plastid Sulfate Transporters Open Doors to Abiotic Stress Resistance. Charlotte M.M. Gommers 12

Cutting the Mustard: Evolving Endoplasmic Reticulum Structures into Endoplasmic Reticulum Bodies for Plant Defense. Kim L. Johnson 14

Two Is Better than One: Dual SEC11 Binding Sites Regulate SYP121-Mediated Vesicle Trafficking. Lynn G.L. Richardson 16

BRacing for Water Stress: Brassinosteroid Signaling Promotes Drought Survival in Wheat. Scott Hayes 18

Balance under Stress: A Case of Mixed Signals. Bethany Huot 20

LETTERS

^[OPEN]Nitrate Modulates the Differentiation of Root Distal Stem Cells. Yalu Wang, Zhizhong Gong, Jiri Friml, and Jing Zhang 22

Nitrate regulation of root stem cell activity is auxin-dependent. 22

UPDATE

^[OPEN]Genetic Engineering for Disease Resistance in Plants: Recent Progress and Future Perspectives. Oliver Xiaou Dong and Pamela C. Ronald 26

A review of the recent progress in plant genetic engineering for disease resistance highlights future challenges and opportunities in the field. 26

BREAKTHROUGH TECHNOLOGIES

^[OPEN]CyanoGate: A Modular Cloning Suite for Engineering Cyanobacteria Based on the Plant MoClo Syntax. Ravendran Vasudevan, Grant A.R. Gale, Alejandra A. Schiavon, Anton Puzorjov, John Malin, Michael D. Gillespie, Konstantinos Vavitsas, Valentin Zulkower, Baojun Wang, Christopher J. Howe, David J. Lea-Smith, and Alistair J. McCormick 39

A Golden Gate-based assembly standard developed for cloning and transformation in cyanobacteria is compatible with, and builds on, the broadly established plant modular cloning syntax. 39

An Efficient System for Ds Transposon Tagging in *Brachypodium distachyon*. Hongyu Wu, Xiaodong Xue, Caihua Qin, Yi Xu, Yuyu Guo, Xiang Li, Wei Lv, Qinxia Li, Chuangxue Mao, Luzhao Li, Suzhen Zhao, Xiaoquan Qi, and Hailong An 56

Ds transposon tagging is an efficient system in *Brachypodium distachyon* for large-scale insertional mutagenesis. 56

Continued on next page

RESEARCH REPORT

[OPEN] Synergistic Pectin Degradation and Guard Cell Pressurization Underlie Stomatal Pore Formation. Yue Rui, Yintong Chen, Hojae Yi, Taylor Purzycki, Virendra M. Puri, and Charles T. Anderson

Degradation of pectic homogalacturonan, but not other cell wall components, promotes stomatal pore initiation, and homogalacturonan degradation and turgor increase both contribute to pore enlargement. 66

[OPEN] Regeneration of *Solanum tuberosum* Plants from Protoplasts Induces Widespread Genome Instability. Michelle Fossi, Kirk Amundson, Sundaram Kuppu, Anne Britt, and Luca Comai

Genome sequencing in potato plants regenerated from protoplasts reveals widespread changes in chromosome number and structure. 78

RESEARCH ARTICLES

BIOCHEMISTRY AND METABOLISM

[OPEN] A MYB Triad Controls Primary and Phenylpropanoid Metabolites for Pollen Coat Patterning. Maor Battat, Asa Eitan, Ilana Rogachev, Kati Hanhineva, Alisdair Fernie, Takayuki Tohge, Jules Beekwilder, and Asaph Aharoni

A triad of Arabidopsis MYB transcription factors controls the production of flavonols and additional phenylpropanoids that are embedded as pollen coat material. 87

[OPEN] Extensive Variations in Diurnal Growth Patterns and Metabolism Among *Ulva* spp. Strains. Antoine Fort, Morgane Lebrault, Margot Allaire, Alberto A. Esteves-Ferreira, Marcus McHale, Francesca Lopez, Jose M. Fariñas-Franco, Saleh Alseikh, Alisdair R. Fernie, and Ronan Sulpice

*Sea lettuce (*Ulva* spp.) strains show extensive variation in growth and metabolism, demonstrating a large potential for strain selection in boosting biomass and metabolite yields in aquaculture.* 109

[OPEN] Isoprene Acts as a Signaling Molecule in Gene Networks Important for Stress Responses and Plant Growth. Zhaojiang Zuo, Sarathi M. Weraduwage, Alexandra T. Lantz, Lydia M. Sanchez, Sean E. Weise, Jie Wang, Kevin L. Childs, and Thomas D. Sharkey

Arabidopsis, which does not normally emit isoprene, was engineered to emit isoprene, and growth and development as well as gene expression were analyzed to determine how isoprene affects plants. 124

Deficiency in the Phosphorylated Pathway of Serine Biosynthesis Perturbs Sulfur Assimilation. Armand D. Anoman, María Flores-Tornero, Ruben M. Benstein, Samira Blau, Sara Rosa-Téllez, Andrea Bräutigam, Alisdair R. Fernie, Jesús Muñoz-Bertomeu, Sören Schilasky, Andreas J. Meyer, Stanislav Kopriva, Juan Segura, Stephan Krueger, and Roc Ros

The Phosphorylated Pathway of L-Ser Biosynthesis in Arabidopsis thaliana provides Ser for thiol assimilation in heterotrophic tissues such as roots. 153

CYP79D73 Participates in Biosynthesis of Floral Scent Compound 2-Phenylethanol in *Plumeria rubra*. Savitha Dhandapani, Jingjing Jin, Vishweshwaran Sridhar, Nam-Hai Chua, and In-Cheol Jang

A cytochrome P450 enzyme contributes to the production of 2-phenylethanol and nitrogen-containing volatiles in Plumeria. 171

[OPEN] Appropriate Thiamin Pyrophosphate Levels Are Required for Acclimation to Changes in Photoperiod. Laise Rosado-Souza, Sebastian Proost, Michael Moulin, Susan Bergmann, Samuel E. Bocobza, Asaph Aharoni, Teresa B. Fitzpatrick, Marek Mutwil, Alisdair R. Fernie, and Toshihiro Obata

Plants over-accumulating vitamin B₁ lose metabolic network flexibility and therefore cannot acclimate to an altered photoperiod. 185

CELL BIOLOGY

[OPEN] Mitochondrial Pyruvate Carriers Prevent Cadmium Toxicity by Sustaining the TCA Cycle and Glutathione Synthesis. Lilong He, Ying Jing, Jianlin Shen, Xining Li, Huiping Liu, Zilong Geng, Mei Wang, Yongqing Li, Donghua Chen, Jianwei Gao, and Wei Zhang

Response to heavy metals requires glutamate and mitochondrial pyruvate carriers. 198

Continued on next page

[OPEN] A Family of NAI2-Interacting Proteins in the Biogenesis of the ER Body and Related Structures. *Zhe Wang, Xifeng Li, Nana Liu, Qi Peng, Yuexia Wang, Baofang Fan, Cheng Zhu, and Zhixiang Chen*

Three related NAI2-interacting proteins from Arabidopsis are critical components in the biogenesis of ER bodies found only in the Brassicales and related structures likely also present in other plants.

212

[CC-BY] Dual Sites for SEC11 on the SNARE SYP121 Implicate a Binding Exchange during Secretory Traffic. *Ben Zhang, Rucha Karnik, Jonas Alvim, Naomi Donald, and Michael R. Blatt*

The regulatory protein SEC11 binds differentially via two motifs on the Qa-SNARE SYP121 N-terminus, only one of which overlaps with the K⁺ channel-binding motif, to facilitate a binding exchange during SNARE complex assembly.

228

GENES, DEVELOPMENT AND EVOLUTION

[OPEN] Senescence and Defense Pathways Contribute to Heterosis. *Rebeca Gonzalez-Bayon, Yifei Shen, Michael Groszmann, Anyu Zhu, Aihua Wang, Annapurna D. Allu, Elizabeth S. Dennis, W. James Peacock, and Ian K. Greaves*

Reduction of levels of salicylic acid in Arabidopsis C24/Ler hybrids results in a decrease in the expression of defense response genes and a delay in senescence.

240

ABC Transporter-Mediated Transport of Glutathione Conjugates Enhances Seed Yield and Quality in Chickpea. *Udita Basu, Hari D. Upadhyaya, Rishi Srivastava, Anurag Daware, Naveen Malik, Akash Sharma, Deepak Bajaj, Laxmi Narnoliya, Virevol Thakro, Alice Kujur, Shailesh Tripathi, Chellapilla Bharadwaj, V.S. Hegde, Ajay K. Pandey, Ashok K. Singh, Akhilesh K. Tyagi, and Swarup K. Parida*

An integrated genomic strategy delineated superior alleles of an ABC transporter gene, whose marker-assisted introgression enhanced the yield of chickpea by modulating glutathione-conjugate transport.

253

[OPEN] Histone Deacetylase HDA19 Affects Root Cortical Cell Fate by Interacting with SCARECROW. *Wen-Qian Chen, Colleen Drapek, Dong-Xu Li, Zhi-Hong Xu, Philip N. Benfey, and Shu-Nong Bai*

Histone deacetylase HDA19 acts through SCARECROW to regulate Arabidopsis root cortical cell fate and epidermal cell patterning.

276

The AAA-ATPase MIDASIN 1 Functions in Ribosome Biogenesis and Is Essential for Embryo and Root Development. *Peng-Cheng Li, Ke Li, Juan Wang, Chuan-Zhi Zhao, Shu-Zhen Zhao, Lei Hou, Han Xia, Chang-Le Ma, and Xing-Jun Wang*

AtMDN1 plays roles in embryogenesis and root meristem maintenance, and its mutation leads to defects in nuclear export of the pre-60S ribosome and in pre-rRNA processing.

289

[OPEN] Control of Cognate Sense mRNA Translation by cis-Natural Antisense RNAs. *Jules Deforges, Rodrigo S. Reis, Philippe Jacquet, Shaoline Sheppard, Veerendra P. Gadekar, Gene Hart-Smith, Andrea Tanzer, Ivo L. Hofacker, Christian Iseli, Ioannis Xenarios, and Yves Poirier*

A robust pipeline identifies and experimentally validates cis-natural antisense transcripts controlling cognate sense mRNA translation.

305

[OPEN] Extrachloroplastic PP7L Functions in Chloroplast Development and Abiotic Stress Tolerance. *Duorong Xu, Giada Marino, Andreas Klingl, Beatrix Enderle, Elena Monte, Joachim Kurth, Andreas Hiltbrunner, Dario Leister, and Tatjana Kleine*

Arabidopsis protein phosphatase PP7-like (PP7L) is a predominantly nuclear-localized protein that promotes chloroplast translation and development, thus contributing to abiotic stress tolerance.

323

[OPEN] HDA9-PWR-HOS15 Is a Core Histone Deacetylase Complex Regulating Transcription and Development. *Kevin S. Mayer, Xiangsong Chen, Dean Sanders, Jiani Chen, Jianjun Jiang, Phu Nguyen, Mark Scalf, Lloyd M. Smith, and Xuehua Zhong*

Arabidopsis HISTONE DEACETYLASE9 requires both PWR and HOS15 to regulate histone modifications, gene expression, and plant development.

342

ESA1 Is Involved in Embryo Sac Abortion in Interspecific Hybrid Progeny of Rice. Jingjing Hou, Caihong Cao, Yini Ruan, Yanyan Deng, Yaxin Liu, Kun Zhang, Lubin Tan, Zuofeng Zhu, Hongwei Cai, Fengxia Liu, Hongying Sun, Ping Gu, Chuanqing Sun, and Yongcai Fu

ESA1 is involved in embryo sac abortion in hybrid backcross progeny derived from common wild rice and cultivated rice. 356

[OPEN] *FT Modulates Genome-Wide DNA-Binding of the bZIP Transcription Factor FD.* Silvio Collani, Manuela Neumann, Levi Yant, and Markus Schmid

Genomic and biochemical analyses identify targets of the flowering time regulator FD at the genome-wide scale and shed light on the requirement for interaction with the florigen FLOWERING LOCUS T. 367

[OPEN] *Ubiquitin Specific Protease 15 Has an Important Role in Regulating Grain Width and Size in Rice.* Cuilan Shi, Yulong Ren, Linglong Liu, Fan Wang, Huan Zhang, Peng Tian, Tian Pan, Yongfei Wang, Ruonan Jing, Tianzhen Liu, Fuqing Wu, Qibing Lin, Cailin Lei, Xin Zhang, Shanshan Zhu, Xiuping Guo, Jiulin Wang, Zhichao Zhao, Jie Wang, Huqu Zhai, Zhijun Cheng, and Jianmin Wan

OsUBP15, encoding a ubiquitin-specific protease15, regulates grain width and size in rice. 381

Antagonistic Actions of FPA and IBM2 Regulate Transcript Processing from Genes Containing Heterochromatin. Aurélie Deremetz, Clémentine Le Roux, Yassir Idir, Cécile Brousse, Astrid Agorio, Isabelle Gy, Jane E. Parker, and Nicolas Bouché

Intronic heterochromatic marks, associated with alternative polyadenylation sites, are decoded by RNA-binding proteins like FPA and IBM2, to tune the expression of key regulator genes such as IBM1 or RPP7. 392

[OPEN] *Evolution of Cold Acclimation and Its Role in Niche Transition in the Temperate Grass Subfamily Pooideae.* Marian Schubert, Lars Grønvold, Simen R. Sandve, Torgeir R. Hvidsten, and Siri Fjellheim

Comparative analysis of cold response in Pooideae species shows that cold acclimation is common in Pooideae but that this adaptation has largely evolved independently in different tribes. 404

Genetics of Variable Disease Expression Conferred by Inverse Gene-For-Gene Interactions in the Wheat-Parastagonospora nodorum Pathosystem. Amanda R. Peters Haugrud, Zengcui Zhang, Jonathan K. Richards, Timothy L. Friesen, and Justin D. Faris

Host gene-effector interactions in the wheat-P. nodorum pathosystem display additivity, epistasis, differential effector gene expression, and complex interplay of genetic regulation. 420

[OPEN] *Comparative Transcriptomic Analysis Provides Insight into the Domestication and Improvement of Pear (P. pyrifolia) Fruit.* Xiaolong Li, Lun Liu, Meiling Ming, Hongju Hu, Mingyue Zhang, Jing Fan, Bobo Song, Shaoling Zhang, and Jun Wu

Genes associated with stone cell formation, fruit size, and sugar content underwent directional selection during pear domestication and improvement, which contributed to drastic changes of cultivated pears. 435

[OPEN] *An Essential Role for miRNA167 in Maternal Control of Embryonic and Seed Development.* Xiaozhen Yao, Jilin Chen, Jie Zhou, Hanchuanzhi Yu, Chennan Ge, Min Zhang, Xiuhua Gao, Xinhua Dai, Zhong-Nan Yang, and Yunde Zhao

Complete deletion of the four MIR167 genes in Arabidopsis using CRISPR/Cas9 leads to late flowering and defects in flower and seed development. 453

MEMBRANES, TRANSPORT AND BIOENERGETICS

[OPEN] *The Potassium Transporter SIHAK10 Is Involved in Mycorrhizal Potassium Uptake.* Jianjian Liu, Junli Liu, Jinhui Liu, Miaomiao Cui, Yujuan Huang, Yuan Tian, Aiqun Chen, and Guohua Xu

The gene SIHAK10 encodes a mycorrhiza-specific potassium transporter of the KT/KUP/HAK family that mediates K⁺ uptake at the intraradical symbiotic interface in tomato. 465

SIGNALING AND RESPONSE

[OPEN] Identification of Novel Inhibitors of Auxin-Induced Ca^{2+} Signaling via a Plant-Based Chemical Screen. Kjell De Vriese, Ellie Himschoot, Kai Dünser, Long Nguyen, Andrzej Drozdzecki, Alex Costa, Moritz K. Nowack, Jürgen Kleine-Vehn, Dominique Audenaert, Tom Beeckman, and Steffen Vanneste

Screening of an annotated library of biologically active molecules for inhibitory effects on auxin-induced Ca^{2+} entry in BY-2 cells yielded several new inhibitors for investigating Ca^{2+} signaling. 480

B-Box Containing Proteins BBX30 and BBX31, Acting Downstream of HY5, Negatively Regulate Photomorphogenesis in Arabidopsis. Yueqin Heng, Fang Lin, Yan Jiang, Mingquan Ding, Tingting Yan, Hongxia Lan, Hua Zhou, Xianhai Zhao, Dongqing Xu, and Xing Wang Deng

Two repressors of light signaling, BBX30 and BBX31, are transcriptionally and negatively regulated by the transcription factor HY5 through direct binding to the G-box cis-element present in their promoters. 497

Mesorhizobium huakuii HtpG Interaction with nsLTP AsE246 Is Required for Symbiotic Nitrogen Fixation. Donglai Zhou, Yanan Li, Xuting Wang, Fuli Xie, Dasong Chen, Binguang Ma, and Youguo Li

The Mesorhizobium huakuii molecular chaperone HtpG interacts with the lipid transfer protein AsE246, which plays an essential role in effective root nodule development and symbiotic nitrogen fixation. 509

The R2R3-MYB Transcription Factor MYB49 Regulates Cadmium Accumulation. Ping Zhang, Ruling Wang, Qiong Ju, Weiqiang Li, Lam-Son Phan Tran, and Jin Xu

ABI5 interacts with MYB49 and represses its function by preventing its binding to the downstream genes bHLH38, bHLH101, HIP22, and HIP44, resulting in inactivation of IRT1 and reduced Cd uptake. 529

Proteolytic Processing of SERK3/BAK1 Regulates Plant Immunity, Development, and Cell Death. Jinggeng Zhou, Ping Wang, Lucas A.N. Claus, Daniel V. Savatin, Guangyuan Xu, Shujing Wu, Xiangzong Meng, Eugenia Russinova, Ping He, and Libo Shan

Arabidopsis BAK1, a co-receptor of multiple receptor-like kinases, undergoes a proteolytic cleavage process that is essential for its functions in plant immunity, growth, and cell death control. 543

Independent Regulation of Symbiotic Nodulation by the SUNN Negative and CRA2 Positive Systemic Pathways. Carole Laffont, Emeline Huault, Pierre Gautrat, Gabriella Endre, Peter Kalo, Virginie Bourion, Gérard Duc, and Florian Frugier

SUNN and CRA2 negative and positive systemic pathways independently regulate symbiotic nodulation in Medicago truncatula. 559

[CC-BY] AVR2 Targets BSL Family Members, Which Act as Susceptibility Factors to Suppress Host Immunity. Dionne Turnbull, Haixia Wang, Susan Breen, Marek Malec, Shaista Naqvi, Lina Yang, Lydia Welsh, Piers Hemsley, Tian Zhendong, Frederic Brunner, Eleanor M. Gilroy, and Paul R.J. Birch

Late blight pathogen Phytophthora infestans uses effector Avr2 to target BSL phosphatases to suppress plant immunity. 571

The Chromatin Factor HNI9 and ELONGATED HYPOCOTYL5 Maintain ROS Homeostasis under High Nitrogen Provision. Fanny Bellegarde, Amel Maghiaoui, Jossia Boucherez, Gabriel Krouk, Laurence Lejay, Liên Bach, Alain Gojon, and Antoine Martin

Excessive nitrogen supply leads to reactive oxygen species accumulation and requires the function of major transcriptional regulators to maintain physiological balance. 582

SULTR3s Function in Chloroplast Sulfate Uptake and Affect ABA Biosynthesis and the Stress Response. Zhen Chen, Ping-Xia Zhao, Zi-Qing Miao, Guo-Feng Qi, Zhen Wang, Yang Yuan, Nisar Ahmad, Min-Jie Cao, Ruediger Hell, Markus Wirtz, and Cheng-Bin Xiang

The sultr3 quintuple mutant unequivocally demonstrates that sulfate transporter subfamily 3 is responsible for more than half of the chloroplast sulfate uptake and influences downstream sulfate assimilation and ABA biosynthesis as well as sulfate-induced stomatal closure. 593

[OPEN] BES/BZR Transcription Factor TaBZR2 Positively Regulates Drought Responses by Activation of *TaGST1*.
Xiao-Yu Cui, Yuan Gao, Jun Guo, Tai-Fei Yu, Wei-Jun Zheng, Yong-Wei Liu, Jun Chen, Zhao-Shi Xu, and You-Zhi Ma

A BES/BZR-type transcription factor, TaBZR2, activates TaGST1 to scavenge reactive oxygen species and mediates crosstalk between brassinosteroids and drought signaling pathways.

605

High-CO₂/Hypoxia-Responsive Transcription Factors DkERF24 and DkWRKY1 Interact and Activate *DkPDC2* Promoter. Qing-gang Zhu, Zi-yuan Gong, Jingwen Huang, Donald Grierson, Kun-song Chen, and Xue-ren Yin

Two high-CO₂/hypoxia responsive transcription factors from persimmon fruit, DkERF24 and DkWRKY1, form a complex and synergistically transactivate the promoter of the hypoxia-responsive gene DkPDC2.

621

[OPEN] ANAC017 Coordinates Organellar Functions and Stress Responses by Reprogramming Retrograde Signaling. Xiangxiang Meng, Lu Li, Inge De Clercq, Reena Narsai, Yue Xu, Andreas Hartmann, Diego Lozano Claros, Eddie Custovic, Mathew G. Lewsey, James Whelan, and Oliver Berkowitz

Overexpression of ANAC017 in Arabidopsis leads to restricted growth, cell death, and early senescence due to impaired organellar retrograde signaling and transcriptomic reprogramming.

634

SYSTEMS AND SYNTHETIC BIOLOGY

[OPEN] Highly Resolved Systems Biology to Dissect the Etioplast-to-Chloroplast Transition in Tobacco Leaves. Tegan Armarego-Marriott, Łucja Kowalewska, Asdrubal Burgos, Axel Fischer, Wolfram Thiele, Alexander Erban, Deserah Strand, Sabine Kahlau, Alexander Hertle, Joachim Kopka, Dirk Walther, Ziv Reich, Mark Aurel Schöttler, and Ralph Bock

A comprehensive, high-resolution overview is presented of the molecular, ultrastructural, and physiological events involved in chloroplast differentiation and thylakoid biogenesis.

654

[CC-BY] Article free via Creative Commons CC-BY 4.0 license.

[OPEN] Articles can be viewed online without a subscription.

B-Box Containing Proteins BBX30 and BBX31, Acting Downstream of HY5, Negatively Regulate Photomorphogenesis in *Arabidopsis*¹

Yueqin Heng,^{a,b,2} Fang Lin,^{a,2} Yan Jiang,^b Mingquan Ding,^c Tingting Yan,^a Hongxia Lan,^a Hua Zhou,^a Xianhai Zhao,^a Dongqing Xu,^{b,3} and Xing Wang Deng^{a,d,3,4}

^aInstitute of Plant and Food Sciences, Department of Biology, Southern University of Science and Technology, Shenzhen 518055, China

^bState Key Laboratory of Crop Genetics and Germplasm Enhancement, College of Agriculture, Nanjing Agricultural University, Nanjing 210095, China

^cKey Laboratory for Quality Improvement of Agricultural Products of Zhejiang Province, College of Agriculture and Food Science, Zhejiang A&F University, Lin'an 311300, China

^dState Key Laboratory of Protein and Plant Gene Research, Peking-Tsinghua Center for Life Sciences, School of Advanced Agriculture Sciences and School of Life Sciences, Peking University, Beijing 100871, China

ORCID IDs: 0000-0002-2478-5231 (F.L.); 0000-0003-4659-3115 (Y.J.); 0000-0002-6541-0444 (D.X.); 0000-0003-0590-8993 (X.W.D.).

Light-mediated seedling development is coordinately controlled by a variety of key regulators. Here, we identified two B-box (BBX)-containing proteins, BBX30 and BBX31, as repressors of photomorphogenesis. ELONGATED HYPOCOTYL5, a central regulator of light signaling, directly binds to the *G-box cis*-element present in the promoters of BBX30 and BBX31 and negatively controls their transcription levels in the light. Seedlings with mutations in BBX30 or BBX31 are hypersensitive to light, whereas the overexpression of BBX30 or BBX31 leads to hypo-photomorphogenic growth in the light. Furthermore, transgenic and phenotypic analysis revealed that the B-box domain of BBX30 or BBX31 is essential for their respective functioning in the regulation of photomorphogenic development in plants. In conclusion, BBX30 and BBX31 act as key negative regulators of light signaling, and their transcription is repressed by ELONGATED HYPOCOTYL5 through directly associating with their promoters.

As sessile organisms, plants respond dynamically to changes in light conditions throughout their life cycle. To optimize their growth and development, plants have evolved the ability to continuously monitor the quality, quantity, duration, and direction of light (Jiao et al., 2007). Plants undergo two distinct developmental processes depending on the absence or presence of light at the seedling stage. In the absence of light, germinated

seeds develop elongated hypocotyls, closed cotyledons, and apical hooks, which is termed skotomorphogenesis. In the presence of light, seedlings display short hypocotyls and expanded cotyledons, which is known as photomorphogenesis (Sullivan and Deng, 2003). These two light-controlled developmental processes enable a seedling to emerge from a buried seed and penetrate through the soil.

At least four classes of photoreceptors are responsible for perceiving various wavelength spectra of light, which in turn initiate and control transcriptional reprogramming during the transition between skotomorphogenic and photomorphogenic development (Huang et al., 2014; Podolec and Ulm, 2018). Up to one-third of the genes in the *Arabidopsis* (*Arabidopsis thaliana*) genome are significantly altered during dark-to-light transition, indicating that these light-activated photoreceptors mediate the massive transcriptional reprogramming of molecular events to promote photomorphogenesis (Ma et al., 2001; Tepperman et al., 2004; Lau and Deng, 2012; Huang et al., 2014; Podolec and Ulm, 2018). ELONGATED HYPOCOTYL5 (HY5) acts downstream of all photoreceptors and is a central regulator of the light signal transduction pathway. Mutants impaired in HY5 exhibit dramatically elongated hypocotyls in white, blue, red, and far-red light (Oyama et al., 1997; Ang et al., 1998).

¹This work was supported by grants from National Key R&D Program of China (2017YFA0503800), National Natural Science Foundation of China (31330048, 31621001), Peking-Tsinghua Center for Life Sciences (to X.W.D.), US NIH grant (GM-47850), and by Nanjing Agricultural University and Southern University of Science and Technology (to D.X.).

²These authors contributed equally to the article.

³Senior authors.

⁴Author for contact: deng@sustc.edu.cn.

The author responsible for distribution of materials integral to the findings presented in this article in accordance with the policy described in the Instructions for Authors (www.plantphysiol.org) is: Xing Wang Deng (deng@sustc.edu.cn).

D.X. and X.W.D. designed the project; Y.H., F.L., T.Y., H.L., Y.J., H.Z., and X.Z. performed the research; M.D. performed bioinformatics analysis; D.X. and X.W.D. analyzed the data; D.X. and X.W.D. wrote the article.

www.plantphysiol.org/cgi/doi/10.1104/pp.18.01244

The abundance of HY5 is tightly controlled by CONSTITUTIVELY PHOTOMORPHOGENIC/DE-ETIOLATED/FUSCA (COP/DET/FUS) proteins, the biochemical activities of which are inhibited by photoreceptors upon light irradiation (Osterlund et al., 2000; Podolec and Ulm, 2018). As a b-ZIP-type transcription factor, HY5 preferentially binds to the ACGT-containing (ACE) *cis*-elements present in the promoters of approximately one-third of Arabidopsis genes and controls their transcription, which in turn ultimately promotes photomorphogenic development in the light (Lee et al., 2007; Zhang et al., 2011).

There are 32 B-box (BBX)-containing proteins in *Arabidopsis*, multiple members of which have been documented to play critical roles in the regulation of photomorphogenesis. BBX4, BBX19, BBX20, BBX21, BBX22, and BBX23 are positive regulators of light signaling (Datta et al., 2006, 2007, 2008; Fan et al., 2012; Wang et al., 2015a; Xu et al., 2016, 2018; Zhang et al., 2017), while BBX24, BBX25, BBX28, and BBX32 repress photomorphogenic development (Indorf et al., 2007; Holtan et al., 2011; Gangappa et al., 2013; Lin et al., 2018). Extensive genetic and biochemical studies have revealed that all of these BBX proteins converge on HY5 at transcriptional and/or protein levels through distinct regulatory mechanisms that mediate photomorphogenesis, suggesting that these BBX proteins together with HY5 constitute a complex but delicate signaling network in light-mediated seedling development that acts downstream of photoreceptors and the COP/DET/FUS system (Holm et al., 2001, 2002; Datta et al., 2006, 2007, 2008; Indorf et al., 2007; Chang et al., 2011; Holtan et al., 2011; Fan et al., 2012; Wang et al., 2015a; Xu et al., 2016, 2018; Zhang et al., 2017; Lin et al., 2018). BBX21 promotes photomorphogenesis by directly binding to the *T/G-box cis*-element present in the HY5 promoter to activate its expression (Xu et al., 2016, 2018). HY5 interacts with the promoter of BBX22 and up-regulates its gene expression (Chang et al., 2008). Each of BBX21, BBX22, BBX23, BBX24, BBX25, and BBX28 can form heterodimers with HY5, which serve to modulate the biochemical activity of HY5. Interestingly, BBX21, BBX22, and BBX23 may enhance the activity of HY5 (Datta et al., 2007, 2008; Zhang et al., 2017), whereas BBX24, BBX25, and BBX28 repress the transcriptional activity of HY5 (Gangappa et al., 2013; Lin et al., 2018). Specifically, BBX24 and BBX25 repress HY5 transcriptional activity toward BBX22 (Gangappa et al., 2013). In addition, BBX32 forms a potentially inactive heterodimer with BBX21 that interferes with the biochemical activity of the BBX21-HY5 complex (Holtan et al., 2011). Thus, the BBXs-HY5 module appears to act as a central regulatory hub in the light signal transduction pathway.

In this study, we report that BBX30 and BBX31, two B-box-containing proteins, constitute two previously uncharacterized negative regulators of light signaling that act directly downstream of the transcription factor HY5. HY5 directly binds to the *G-box* DNA *cis*-element within the *BBX30* and *BBX31* promoters and represses

their transcription. *bbx30* and *bbx31* mutant seedlings displayed shortened hypocotyls, while transgenic seedlings overexpressing *BBX30* or *BBX31* showed elongated hypocotyls. In addition, the destruction of the B-box domain in BBX30 and BBX31 results in the full impairment of their biochemical activity in plants. Collectively, we have identified BBX30 and BBX31 as two repressors of photomorphogenesis that are negatively regulated by HY5 at the transcriptional level.

RESULTS

HY5 Represses the Expression of *BBX30* and *BBX31*

As a previous genome-wide expression study indicated that *BBX31* might be a negative target of HY5 (Lee et al., 2007), we thus tested if HY5 represses the transcript levels of *BBX30* (a close homolog of *BBX31*; Khanna et al., 2009) and *BBX31* using real-time quantitative PCR (RT-qPCR). As expected, the expression of both *BBX30* and *BBX31* dramatically increased in two independent *hy5* (*hy5-215* and *hy5-51*) mutants but decreased in *HA-HY5 hy5-215* transgenic seedlings compared to the wild type (Fig. 1, A and B), demonstrating that HY5 indeed negatively controls the transcript levels of *BBX30* and *BBX31* in plants.

Next, we examined whether *BBX30* and *BBX31* are regulated by light signals. The expression of both *BBX30* and *BBX31* in wild-type seedlings grown under various light conditions (white [W], blue [B], red [R], and far-red [FR]) was significantly increased when compared to that in etiolated seedlings (Fig. 1C). Moreover, the transcript levels of both *BBX30* and *BBX31* were markedly elevated when the dark-grown wild-type seedlings were transferred to W light for the various indicated times (1, 3, 6, 12, and 24 h; Fig. 1D). As distinct wavelength-specific light is perceived by various photoreceptors in plants, we thus investigated whether photoreceptors, including phyA (FR light photoreceptor), phyB (R light photoreceptor), CRY1-TOCHROME 1 (CRY1), and CRY2 (B light photoreceptors), affect the expression levels of *BBX30* and *BBX31*. The transcripts of both *BBX30* and *BBX31* were obviously decreased in *phyA-211* grown in FR, in *phyB-9* grown in R, as well as in *cry1* and *cry2* grown in B light compared to those in the wild type grown in the corresponding wavelength-specific light conditions (Fig. 1, E–G). Together, these data suggest that light induces the expression of both *BBX30* and *BBX31* at the transcriptional level, and photoreceptors play positive roles in the light-induced transcription of *BBX30* and *BBX31*.

To examine whether light affects the stability of BBX30 and BBX31, we generated yellow fluorescent protein (YFP)-tagged *BBX30* or *BBX31* transgenic lines in the Col background, in which *BBX30* or *BBX31* was overexpressed and their respective gene products were detectable (Supplemental Fig. S1, A and B). Either *YFP-BBX30* Col #3 or *YFP-BBX31* Col #5 transgenic

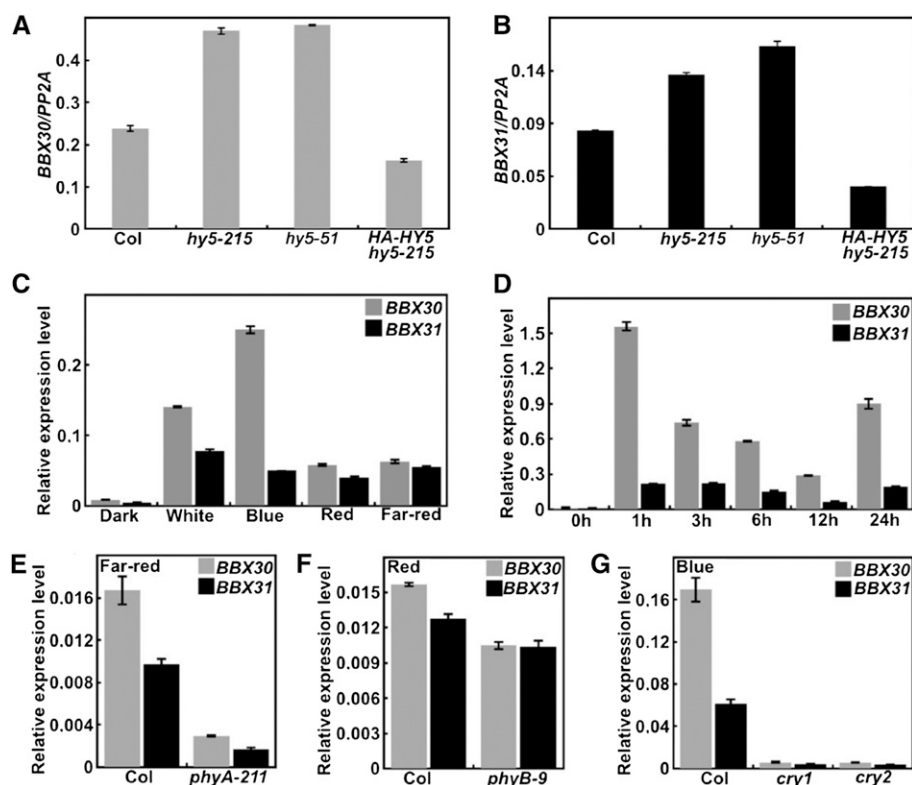


Figure 1. The transcript levels of *BBX30* and *BBX31* are repressed by HY5 but induced by light. A and B, The expression levels of *BBX30* (A) and *BBX31* (B) in 4-d-old Col, *hy5-215*, *hy5-51*, and *HA-HY5 hy5-215* seedlings grown in white light. C, The expression levels of *BBX30* and *BBX31* in 4-d-old Col grown in dark, white, blue (B), red (R), and far-red (FR) light conditions. D, The expression levels of *BBX30* and *BBX31* in 4-d-old dark-grown Col upon being transferred to white light at indicated time points. E to G, The expression levels of *BBX30* and *BBX31* in 4-d-old Col, *phyA-211*, *phyB-9*, *cry1*, and *cry2* under different light (FR, R, and B) conditions as indicated. Data are means \pm se; $n = 3$. PCR was performed in triplicate for each sample, and the expression levels were normalized to that of a *PP2A* gene. The experiments were performed three times with similar results. The graphs depict the results of one of three experiments.

seedlings grown under various light conditions (dark [D], W, B, R, and FR) accumulated comparable YFP-BBX30 or YFP-BBX31 protein levels, respectively (Supplemental Fig. S2, A and B). When these two dark-grown transgenic lines were transferred to W light for different time periods (1, 3, 6, 12, and 24 h), they also accumulated similar abundances of YFP-BBX30 or YFP-BBX31 (Supplemental Fig. S2, C and D). These data suggest that light may have little effect on BBX30 and BBX31 accumulation in plants.

HY5 Directly Binds to the Promoters of *BBX30* and *BBX31*

Being a b-ZIP-type transcription factor, HY5 can directly bind to the *ACE cis*-element within the promoters of its downstream target genes (Lee et al., 2007; Zhang et al., 2011). We therefore analyzed the 1789-bp *BBX30* promoter and 1869-bp *BBX31* promoter upstream of the start codon (ATG). This indicated five *ACE cis*-elements and one typical *G-box* in either the *BBX30* or *BBX31* promoter (Fig. 2A). We thus performed yeast-one hybrid assays, and the results showed that HY5 could activate both the *BBX30pro::LacZ* and *BBX31pro::LacZ* reporters (Fig. 2B). Next, we divided the *BBX30* or *BBX31* promoter into two portions (A and B; Fig. 2A). Furthermore, yeast-one hybrid assays revealed that HY5 was able to activate *BBX30proA::LacZ* and *BBX31proA::LacZ*, but not *BBX30proB::LacZ* and *BBX31proB::LacZ* (Fig. 2B), suggesting that HY5 binding sites may reside within the *BBX30proA* and *BBX31proA*

portions. *BBX30proA* contains one *ACE* and one *G-box*, and *BBX31proA* possesses two *ACE* and one *G-box* (Fig. 2C). The activation of HY5 on the reporters was completely abolished when *G-box* was mutated, but not *ACE* (Fig. 2, C and D), in the yeast cells, suggesting that the *G-box* sites in *BBX30* and *BBX31* promoters are necessary and required for HY5 binding. To substantiate these results, we further performed an in vitro electrophoretic mobility shift (EMSA) assay. Recombinant HY5-His indeed was able to bind to the *BBX30* or *BBX31* promoter DNA subfragments containing an intact *G-box* motif (Fig. 3, A and B). As the amount of non-biotin-labeled *BBX30* or *BBX31* promoter DNA probes (competitor) increased, the HY5 binding affinity to biotin-labeled probes was clearly decreased (Fig. 3, A and B). Moreover, HY5 binding of these DNA subfragments was completely abolished when the *G-box cis*-elements were mutated (cacgtg was mutated to cggggg; Fig. 3, C and D). Next, chromatin immunoprecipitation (ChIP) experiments assays using *HA-HY5 hy5-215* transgenic plants and an anti-HA antibody were employed to confirm the binding of HY5 to the *BBX30* and *BBX31* promoters in vivo. The *HA-HY5* protein could immunoprecipitate the *BBX30* and *BBX31* promoter region containing an intact *G-box* (Fig. 3E), suggesting that HY5 associates with the *BBX30* and *BBX31* promoters in vivo. Together, these data suggest that HY5 can directly bind to the promoters of *BBX30* and *BBX31* and the *G-box cis*-elements present in the *BBX30* and *BBX31* promoters are the binding sites for HY5.

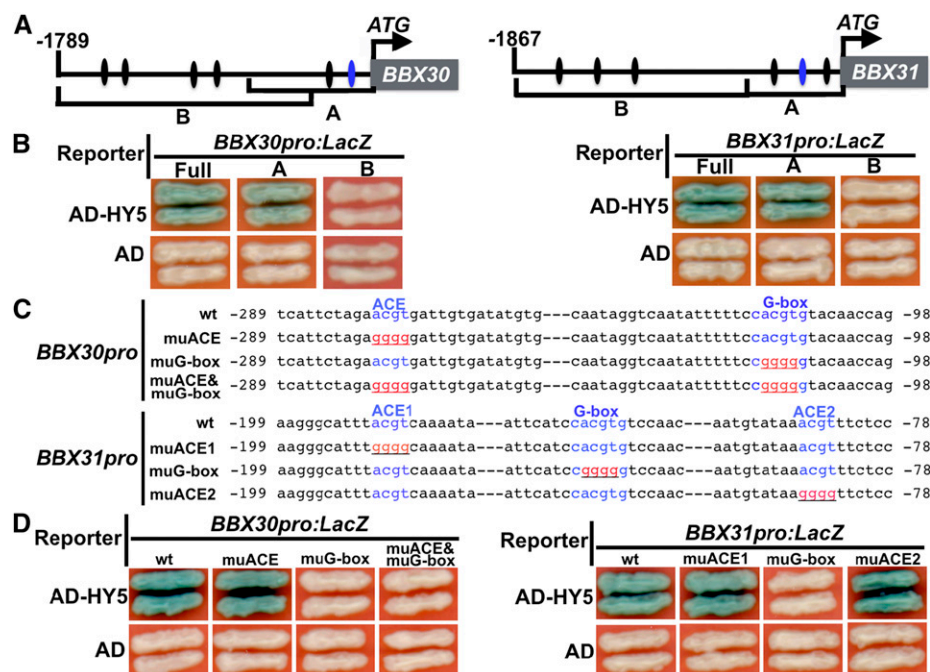


Figure 2. HY5 binds to the G-box present in the promoters of *BBX30* and *BBX31* in yeast cells. A, Diagram of the promoter fragments of the *BBX30* and *BBX31*. The adenine residue of the translational start codon (ATG) was assigned position +1, and the numbers flanking the sequences of the subfragment were counted based on this number. A and B indicate the corresponding promoter subfragments used in yeast one-hybrid assays shown in B. The ovals in black indicate ACE motifs, and the ovals in blue represent G-box motifs. B, Yeast one-hybrid assays showing that HY5 binds to the A fragments of *BBX30* and *BBX31* promoters. Empty vector expressing AD domain alone was used as negative control. C, Diagram of the wild type (wt) and mutant (mu) *BBX30* and *BBX31* subfragments used to drive *LacZ* reporter gene expression in yeast one-hybrid assays. Wild-type G-box elements are shown in blue, and nucleotide substitutions in the mutant subfragments are shown in red and underlined. D, Yeast one-hybrid assays showing that G-box motifs mediate HY5 binding to *BBX30* and *BBX31* promoters. The subfragments of the *BBX30* and *BBX31* promoters were mutated to abolish ACE and G-box alone or both ACE and G-box used to drive *LacZ* reporter gene expression.

bbx30 and *bbx31* Mutants Are Hypersensitive to Light

To examine the function of *BBX30* and *BBX31* in light signaling, we generated two *bbx30* (*bbx30-1* and *bbx30-2*) and two *bbx31* (*bbx31-1* and *bbx31-2*) mutants using the clustered regulatory interspaced short palindromic repeats (CRISPR)/Cas9 technique (Wang et al., 2015b; Supplemental Fig. S3). Each of two independent *bbx30* and *bbx31* mutant lines were grown in darkness for 4 d, and they displayed indistinguishable hypocotyl phenotypes compared to wild type (Supplemental Fig. S4). However, all the *bbx30* and *bbx31* single-mutant seedlings developed shortened hypocotyls in the various constant light conditions tested (W, B, R, and FR; Fig. 4). In addition, the hypocotyl length of the *bbx30-2 bbx31-2* double mutant was significantly shorter than the wild type, *bbx30-2*, or *bbx31-2* single mutant in the various light conditions tested (W, B, R, and FR; Fig. 4). These genetic results suggest that both *BBX30* and *BBX31* act as negative regulators of light signaling, and these two factors may function additively in the promotion of hypocotyl elongation in the light.

Transgenic Seedlings Overexpressing *BBX30* or *BBX31* Are Hypersensitive to Light

To verify the negative roles of *BBX30* and *BBX31* in controlling photomorphogenesis, we analyzed the hypocotyl phenotypes of YFP-tagged *BBX30* or *BBX31* transgenic lines (Supplemental Fig. S1, A and B). Each of the *BBX30* or *BBX31* overexpressors showed similar hypocotyl lengths compared with wild type when grown in the dark (Supplemental Fig. S1, C and D) but exhibited significantly elongated hypocotyls compared to wild type when grown in the various light conditions tested (W, B, R, and FR; Fig. 5). These genetic results are consistent with the notion that both *BBX30* and *BBX31* negatively regulate photomorphogenic development.

Global Analysis of Genes Targeted by *BBX30* and *BBX31*

To identify the genes regulated by *BBX30* and *BBX31* at the genome-wide scale, we performed a paired-end RNA sequencing (RNA-Seq) assay and compared the gene expression profile between the Col (wild type) and *bbx30-2 bbx31-2* double mutant. Our RNA-Seq data

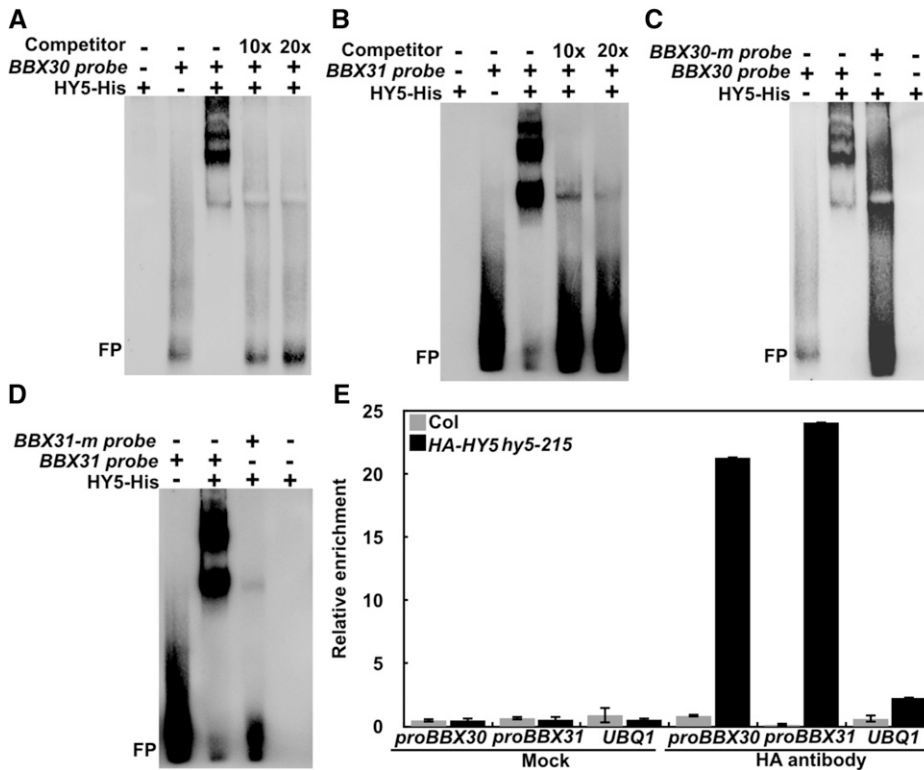


Figure 3. Binding of HY5 to *BBX30* and *BBX31* promoters both in vitro and in vivo. A and B, EMSA showing that the HY5 binds to the *BBX30* and *BBX31* promoter subfragments in vitro. “–” indicates the absence of corresponding probes or proteins. For HY5-His, “+” indicates that 5.4 pmol is present; for *BBX30* and *BBX31* probes, “+” indicate that 2.1 pmol are present. Competitor indicates non-biotin-labeled *BBX30* or *BBX31* probes. FP, Free probe. C and D, EMSA showing that HY5 does not bind to *BBX30* or *BBX31* promoter subfragments carrying mutated *G*-box motifs in vitro. E, ChIP-qPCR showing binding of HY5 to *BBX30* and *BBX31* promoters in vivo. Col and *UBQ1* were used as negative controls.

showed that the expression of 861 genes was significantly changed in *bbx30-2 bbx31-2* compared with that in Col (Fig. 6A; Supplemental Table S1). Of these genes, 627 (72.8%) were up-regulated in *bbx30-2 bbx31-2*, while

234 (27.2%) were down-regulated in *bbx30-2 bbx31-2* when compared to Col. To validate the RNA-Seq data, we conducted RT-qPCR analyses and validated selected differential genes (Supplemental Fig. S5). Gene

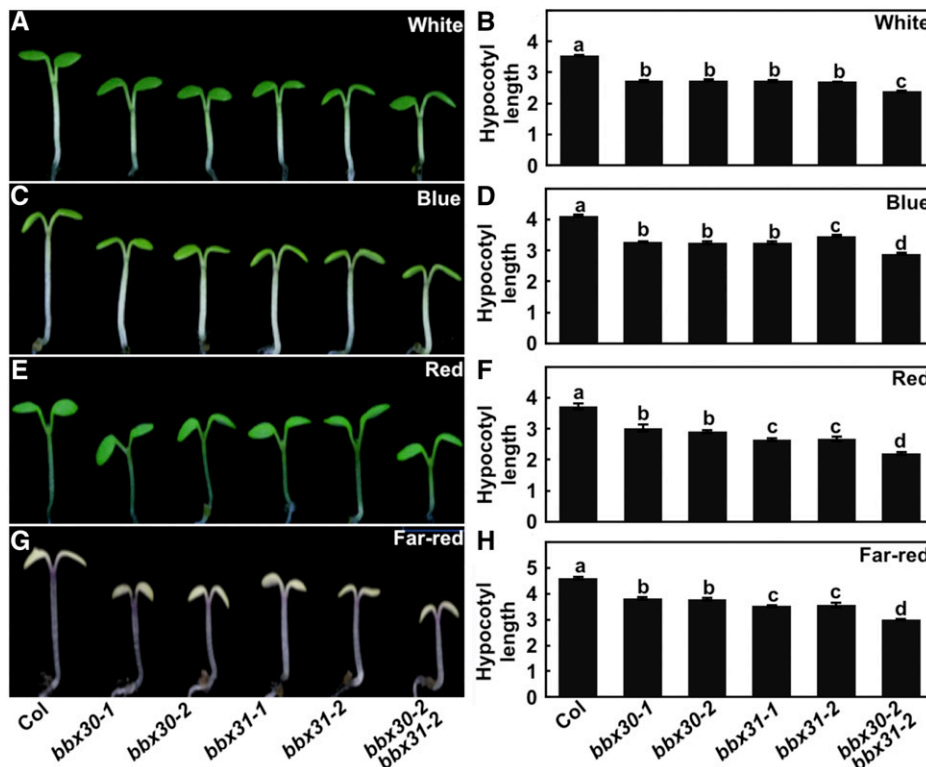
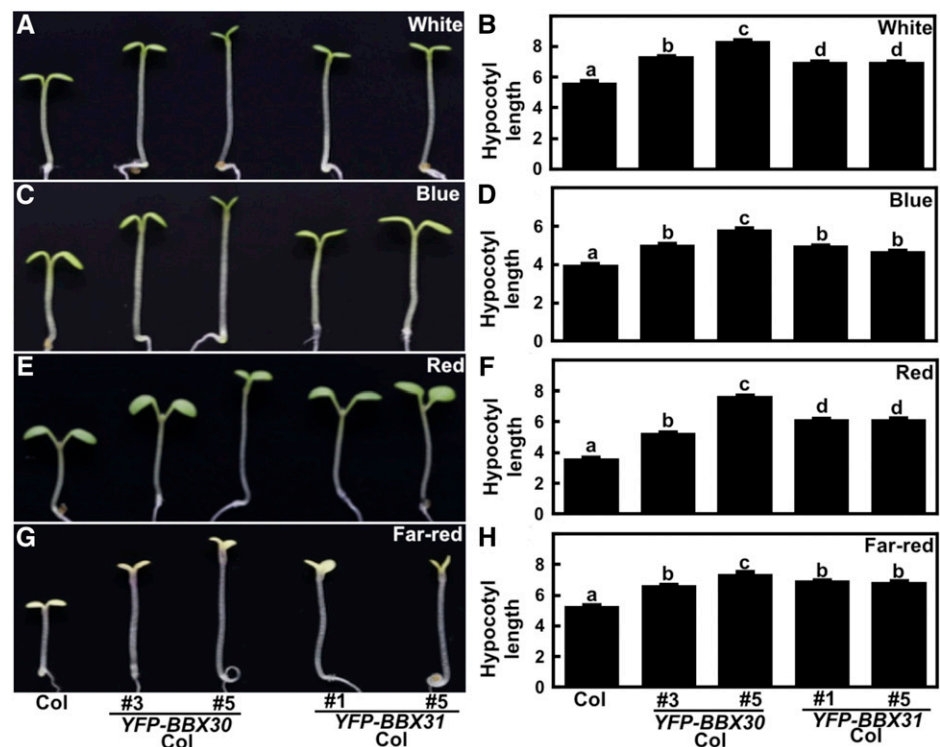


Figure 4. *bbx30* and *bbx31* are hypersensitive to light. Hypocotyl length and phenotype of 4-d-old Col, *bbx30*, *bbx31*, and *bbx30 bbx31* mutant seedlings W ($17.5 \mu\text{mol}/\text{m}^2/\text{s}$; A and B), B ($3.88 \mu\text{mol}/\text{m}^2/\text{s}$; C and D), R ($75.1 \mu\text{mol}/\text{m}^2/\text{s}$; E and F), and FR ($2.05 \mu\text{mol}/\text{m}^2/\text{s}$; G and H) light conditions. Hypocotyl length is expressed in mm. Data are means \pm se; $n \geq 20$. Letters above the bars indicate significant differences ($P < 0.05$), as determined by one-way ANOVA with Tukey's post-hoc analysis. The experiments were performed three times with similar results. The graphs depict the results of one of three experiments.

Figure 5. *BBX30* and *BBX31* transgenic seedlings are hyposensitive to light. Hypocotyl length and phenotype of 4-d-old Col and each of two independent *BBX30* and *BBX31* transgenic lines grown in W (33.3 $\mu\text{mol}/\text{m}^2/\text{s}$; A and B), B (3.28 $\mu\text{mol}/\text{m}^2/\text{s}$; C and D), R (75.1 $\mu\text{mol}/\text{m}^2/\text{s}$; E and F), and FR (2.05 $\mu\text{mol}/\text{m}^2/\text{s}$; G and H) conditions. Hypocotyl length is expressed in mm. Data are means \pm se; $n \geq 20$. Letters above the bars indicate significant differences ($P < 0.05$) as determined by one-way ANOVA with Tukey's post-hoc analysis. The experiments were performed three times with similar results. The graphs depict one of three experiments.



Ontology (GO) and Kyoto Encyclopedia of Genes and Genomes (KEGG) enrichment analysis revealed that *BBX30*- and *BBX31*-regulated genes are involved in the response to multiple stimuli, particularly light and auxin (Fig. 6, B and C; Supplemental Tables S2 and S3), suggesting that *BBX30* and *BBX31* promote hypocotyl elongation, at least in part, by controlling the expression of a set of light- and auxin-regulated genes.

The Short Hypocotyl Phenotype of *bbx30 bbx31* Is Dependent on a Functional *HY5*

HY5 directly bound to the *G-box* present in the promoters of *BBX30* and *BBX31* and repressed their transcription (Figs. 1–3). We therefore generated *hy5-215 bbx30-2*, *hy5-215 bbx31-1*, and *hy5-215 bbx30-2 bbx31-2* double or triple mutants to examine the genetic interactions among *BBX30*, *BBX31*, and *HY5*. All of the mutants we tested showed similar hypocotyl phenotypes in darkness (Supplemental Fig. S6). Consistent with previous studies and our data (Fig. 7; Oyama et al., 1997), *bbx30-2*, *bbx31-2*, and *bbx30-2 bbx31-2* displayed shortened hypocotyls, while *hy5-215* exhibited dramatically elongated hypocotyls when grown under various light conditions (W, B, R, and FR). The hypocotyl length of *hy5-215 bbx30-2*, *hy5-215 bbx31-2*, and *hy5-215 bbx30-2 bbx31-2* was obviously longer than that of Col, *bbx30-2*, *bbx31-2*, and *bbx30-2 bbx31-2*. The double mutant *hy5-215 bbx30-2* or *hy5-215 bbx31-2* showed intermediate hypocotyl length compared with *hy5-215* and *hy5-215 bbx30-2 bbx31-2* (Fig. 7). These genetic data suggest that *BBX30* and *BBX31* may

function downstream or independently of *HY5* in the regulation of light-inhibited hypocotyl elongation.

BBX30 and *BBX31* Repress Flowering

The ectopic overexpression of either *BBX30* or *BBX31* (also known as *miP1a* or *miP1b*) cause delayed flowering under inductive long-day conditions (16 h light/8 h dark; Graeff et al., 2016). We thus verified the function of *BBX30* and *BBX31* in the regulation of flowering using *bbx30-2 bbx31-2* and transgenic plants overexpressing *BBX30* or *BBX31*. The *bbx30-2 bbx31-2* double mutant consistently flowered earlier compared with wild type (Col), while the overexpression of *BBX30* or *BBX31* led to a significantly delayed flowering phenotype under long-day conditions (Supplemental Fig. S7). These data are consistent with a previous study showing that *BBX30* and *BBX31* play negative and essential roles in controlling flowering under inductive long-day conditions (Graeff et al., 2016).

The B-Box Domain in *BBX30* or *BBX31* Is Essential for Repressing Photomorphogenesis in Plants

Either *BBX30* or *BBX31* possesses one B-box domain in the N-terminal region (Khanna et al., 2009), and the B-box domain plays critical roles in developmental processes in plants (Wang et al., 2015a; Xu et al., 2018). We thus investigated whether the B-box domain in *BBX30* or *BBX31* is essential for their functioning in plants. We substituted a conserved Asp residue (D46)

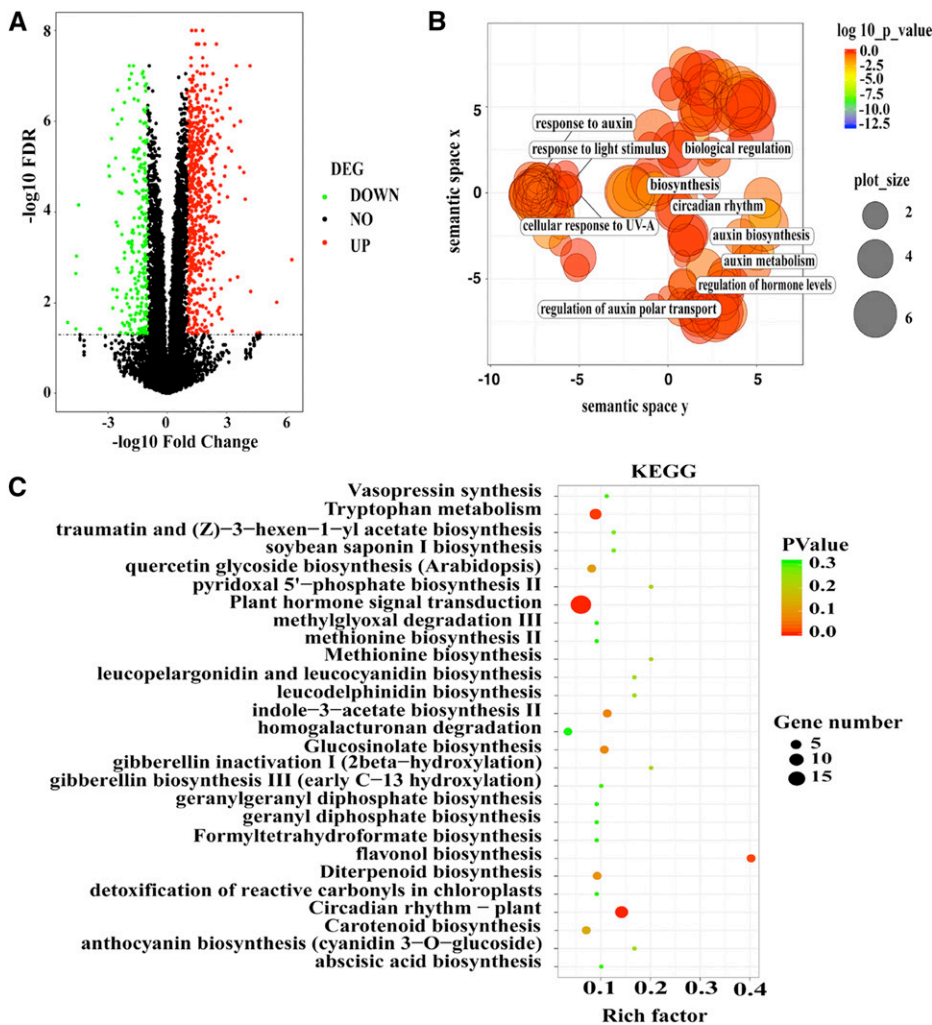


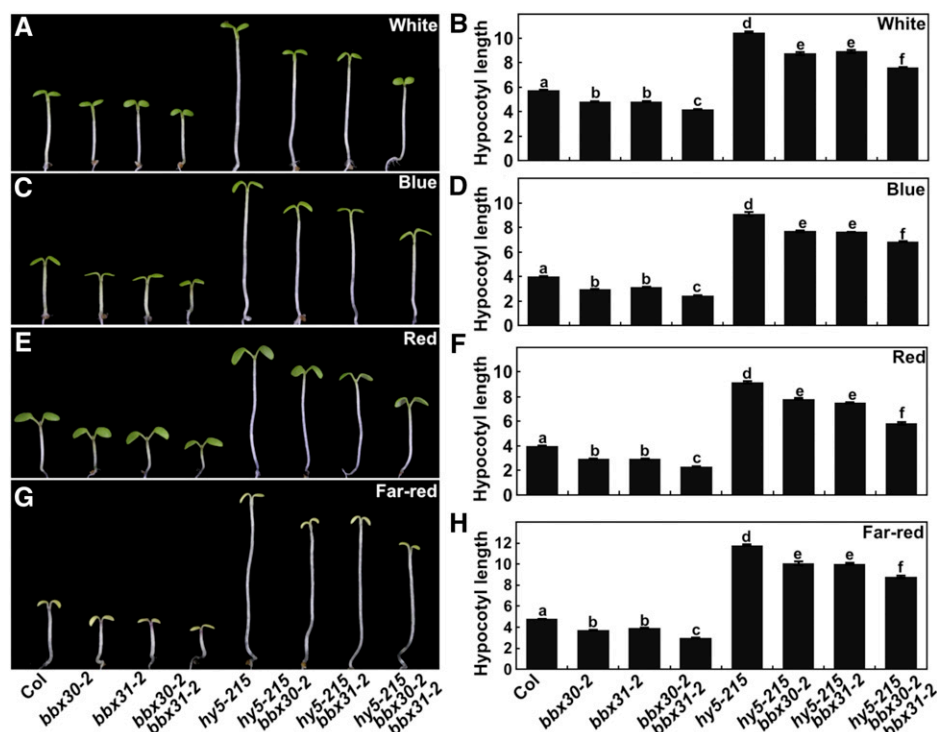
Figure 6. Globe analysis of target genes regulated by BBX30 and BBX31. A, Volcano plot shows the differentially expressed genes in the *bbx30-2 bbx31-2* double mutant. Green spot indicates significant down-regulated genes in the mutant; red spot indicates significantly up-regulated genes; black spot indicates no-change genes. Genes with ratios above 2 or below 0.5. Corrected *P* value (FDR) ≤ 0.05 was considered as the significant differentially expressed genes (DEG). B, The scatterplot shows the cluster representatives in a two-dimensional space derived by applying multidimensional scaling to a matrix of the enriched GO terms' semantic similarities (down-regulated genes in the *bbx30-2 bbx31-2* double mutant). Bubble color indicates enriched GO term's *P* value; size indicates the frequency of the GO term in the GO database (bubbles of more general terms are larger). C, The scatterplot shows the significantly enriched KEGG pathways in the *bbx30-2 bbx31-2* double mutant. Bubble color indicates the enriched KEGG pathway's *P* value. Significant enriched pathways are marked as red color. Bubble size indicates the gene number in the specific KEGG pathway. Rich factor defines the ratio of input gene number (differentially expressed genes detected in this pathway/background genes of this pathway).

in BBX30 or D45 in BBX31. Each of them is the fourth zinc ion-ligating residue in the B-box domain of BBX30 or BBX31 (Supplemental Fig. S8, A and B). Both YFP-tagged BBX30^{D46A} carrying a D46A substitution (YFP-BBX30^{D46A}) and YFP-tagged BBX31^{D45A} carrying a D45A substitution (YFP-BBX31^{D45A}) driven by the 35S promoter were transformed into wild type (Col). As shown in Supplemental Fig. S8, C to F, a mutated BBX30 or BBX31 gene and protein was obviously overexpressed and detectable in each of two independent YFP-BBX30^{D46A} or YFP-BBX31^{D45A} transgenic lines, respectively. However, unlike the YFP-BBX30 or YFP-BBX31 overexpressors, these independent transgenic plants exhibited indistinguishable hypocotyl phenotypes from wild type grown under various light conditions (D, W, B, R, and FR; Supplemental Fig. S9; Fig. 8). These results indicate that neither BBX30^{D46A} nor BBX31^{D45A} could confer light hyposensitive responsiveness in plants, and the intact structure of the B-box domain of BBX30 or BBX31 is indispensable for their biological function in plants.

DISCUSSION

BBX proteins play critical roles in a variety of cellular and developmental processes, including photomorphogenesis, thermomorphogenesis, flowering, and the responsiveness of various phytohormones (Datta et al., 2006; Gangappa and Botto, 2014; Xu et al., 2014, 2016, 2018; Zhang et al., 2017; Ding et al., 2018). A previous study indicated that BBX30 and BBX31 could interact with CONSTANSE and TOPLESS, thereby likely forming a CO-BBX30/31-TOPLESS complex. This leads to a severe delay in flowering due to the inhibition of CO transcriptional activity toward *FT* under long-day conditions (Graeff et al., 2016). Here, we not only verified that BBX30 and BBX31 indeed repress flowering but also provided evidence showing that they negatively regulate photomorphogenesis downstream of HY5. HY5 directly binds to the *G-box cis*-element present in the promoters of BBX30 and BBX31 to repress their transcription. An HY5-BBX30/BBX31-mediated regulatory module may play a critical role in the regulation of seedling development.

Figure 7. Genetic interaction between *BBX30*, *BBX31*, and *HY5*. Hypocotyl length and phenotype of 4-d-old Col, *bbx30-2*, *bbx31-2*, *bbx30-2 bbx31-2*, *hy5-215*, *hy5-215 bbx30-2*, *hy5-215 bbx31-2*, and *hy5-215 bbx30-2 bbx31-2* seedlings grown in W (33.3 $\mu\text{mol}/\text{m}^2/\text{s}$; A and B), B (3.28 $\mu\text{mol}/\text{m}^2/\text{s}$; C and D), R (75.1 $\mu\text{mol}/\text{m}^2/\text{s}$; E and F), and FR (2.05 $\mu\text{mol}/\text{m}^2/\text{s}$; G and H) conditions. Hypocotyl length is expressed in mm. Data are means \pm SE; $n \geq 20$. Letters above the bars indicate significant differences ($P < 0.05$) as determined by one-way ANOVA with Tukey's post-hoc analysis. The experiments were performed three times with similar results. The graphs depict one of three experiments.



A group of BBX proteins mediates photomorphogenetic development, either positively or negatively (Datta et al., 2007; Gangappa and Botto, 2014; Xu et al., 2016; Zhang et al., 2017; Lin et al., 2018). *BBX30* or *BBX31* loss-of-function mutants showed shortened hypocotyls, while *BBX30* or *BBX31* gain-of-function transgenic seedlings exhibited elongated hypocotyls in the light (Figs. 4 and 5). These phenotypic and genetic observations firmly demonstrated that both *BBX30* and *BBX31* promote hypocotyl growth and act as negative regulators of light signaling. A set of 32 BBX proteins is divided into five groups according to the domain structure in Arabidopsis (Khanna et al., 2009). Either *BBX30* or *BBX31* only contain one conserved B-box domain in the N terminus and belong to subfamily V, which consists of seven members (*BBX26*–*BBX32*; Khanna et al., 2009). Of these, *BBX28* and *BBX32* have been shown to repress photomorphogenesis. *bbx28* mutant seedlings, but not *bbx32*, show a shortened hypocotyl phenotype, while both *BBX28* and *BBX32* overexpressors display elongated hypocotyl phenotypes (Holtan et al., 2011; Lin et al., 2018). Thus, at least four members in subfamily V are involved in light signaling, and all of them play negative roles. Whether the other three members (*BBX26*, *BBX27*, and *BBX29*) function in the regulation of seedling photomorphogenesis requires further detailed genetic and biochemical evaluation. It has been documented that the disruption of the B-box domain structure in BBXs led to the impairment of their biological function in regulating developmental processes such as hypocotyl growth and flowering (Wang et al., 2014; Xu et al., 2018). Similarly, neither *BBX30*^{D46A} nor *BBX31*^{D45A} with a

disrupted B-box structure could regulate hypocotyl elongation (Fig. 8). All of this evidence suggests that the intact B-box domain structure in BBX proteins is essential for their proper functioning in plants.

Extensive genetic and biochemical studies have revealed a very tight link between BBX proteins and the *HY5*-mediated transduction pathway in the regulation of photomorphogenesis (Gangappa and Botto, 2014). *BBX21* directly binds to the *T/G-box* present in the *HY5* promoter through its second B-box domain, and its C-terminal half likely activates *HY5* transcription (Xu et al., 2016, 2017, 2018). *BBX32* forms heterodimers with *BBX21*, which in turn serves to inhibit *HY5* activity (Holtan et al., 2011). In addition, *BBX21*, *BBX22*, *BBX24*, *BBX25*, and *BBX28* directly interact with *HY5* to enhance or repress *HY5* biochemical activity (Datta et al., 2007, 2008; Gangappa et al., 2013; Lin et al., 2018). Therefore, BBX proteins regulate *HY5* at least at two distinct layers, both at the transcriptional and protein levels. *BBX30* and *BBX31* function directly downstream of *HY5*, and they are transcriptionally and negatively modulated by *HY5* (Figs. 1–3). Upon light exposure, both *HY5* transcript and protein levels increase in plants predominantly due to the light-mediated inactivation of the COP/DET/FUS system (Osterlund et al., 2000; Hoecker, 2017; Podolec and Ulm, 2018). However, *BBX30* and *BBX31* transcript levels are up-regulated by light signals but down-regulated by *HY5* (Fig. 1). These facts imply that light-induced *BBX30* and *BBX31* expression is possibly independent of *HY5* and/or additional yet unidentified factor(s) are likely responsible for the induction of *BBX30* and *BBX31* in response to light.

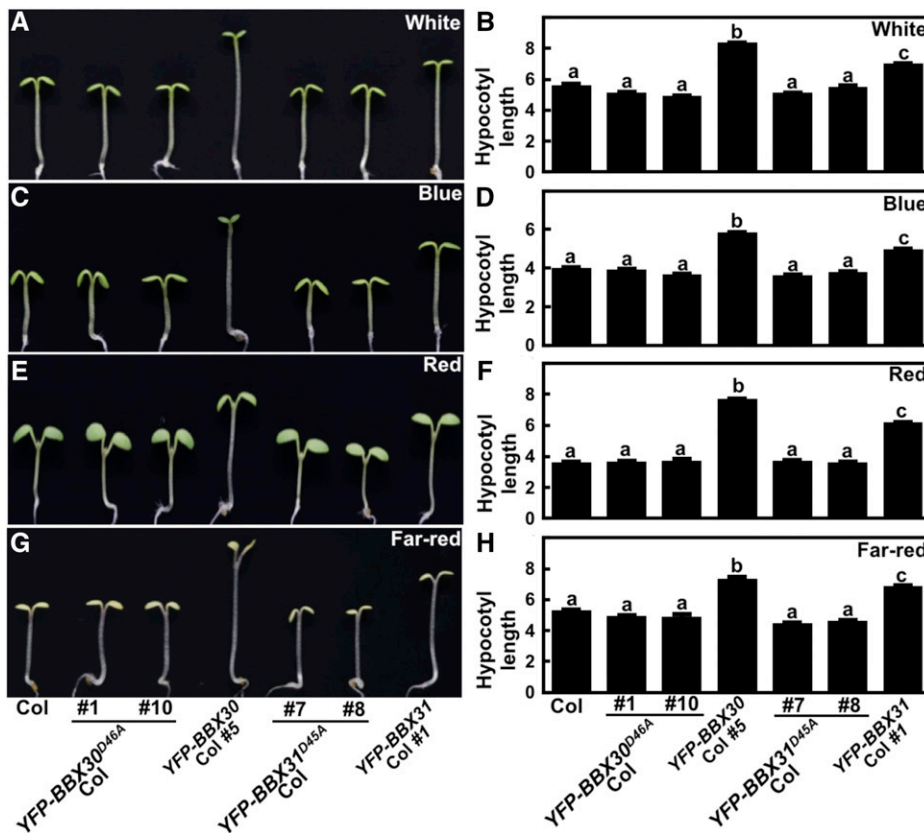


Figure 8. *BBX30^{D46A}* and *BBX31^{D45A}* transgenic seedlings show similar hypocotyl phenotypes with wild type. Hypocotyl length and phenotype of 4-d-old Col, *BBX30^{D46A}*, *BBX30*, *BBX31^{D45A}*, and *BBX31* transgenic seedlings grown in W (33.3 $\mu\text{mol}/\text{m}^2/\text{s}$; A and B), B (0.62 $\mu\text{mol}/\text{m}^2/\text{s}$; C and D), R (6.78 $\mu\text{mol}/\text{m}^2/\text{s}$; E and F), and FR (1.46 $\mu\text{mol}/\text{m}^2/\text{s}$; G and H) conditions. Hypocotyl length is expressed in mm. Data are means \pm SE; $n \geq 20$. Letters above the bars indicate significant differences ($P < 0.05$) as determined by one-way ANOVA with Tukey's post-hoc analysis. The experiments were performed three times with similar results. The graphs depict one of three experiments.

HY5, acting downstream of photoreceptors and COP/DET/FUS in the light signal transduction pathway, directly or indirectly controls the expression of over 3000 genes in Arabidopsis (Lee et al., 2007; Zhang et al., 2011). *BBX30* and *BBX31* are two direct and negative targets of HY5. HY5 promotes photomorphogenesis, whereas *BBX30* and *BBX31* function as negative regulators of light-mediated seedling development, suggesting that HY5 positively influences photomorphogenic development not only by controlling numerous positive regulators but also by regulating a portion of negative regulators of light signaling, including *BBX30* and *BBX31*. In summary, HY5 directly binds to the *G-box* present in the *BBX30* and *BBX31* promoters, thereby repressing their transcription. *BBX30* and *BBX31* negatively regulate photomorphogenic development in the light (Fig. 9).

MATERIALS AND METHODS

Plant Materials and Growth Conditions

The *hy5-215* (Ang et al., 1998) and *hy5-51* (Salk_096651; Ruckle et al., 2007, 2012) are in the Columbia-0 (Col-0) ecotype. Seeds were surface sterilized with 30% (v/v) commercial Clorox bleach and 0.02% (v/v) Triton X-100 for 5 min, washed three times with sterile water, and sown on 1 \times Murashige and Skoog (MS) medium supplemented with 0.8% (v/w) Agar (Difco) and 1% (w/v) Suc. The seeds were stratified in darkness for 3 d at 4°C and then transferred to light chambers maintained at 22°C.

Generation of *bbx30* and *bbx31* Mutant Using CRISPR/Cas9 Technique

Gene editing using CRISPR/Cas9 technique was performed as previously described (Wang et al., 2015b). Twenty-three-base-pair target sites (5'-N20NGG-3') within exons of genomic DNA sequences of *BBX30* or *BBX31* were manually searched and identified, and then each of these sites was evaluated target specificities on the website of potential off-target finder (<http://www.rgenome.net/cas-offinder/>). Two independent sgRNA target sites of *BBX30* or *BBX31* were subcloned into pHEE401E vector. These vectors were transformed into *Agrobacterium tumefaciens* GV3101 by the freeze-thaw method, respectively, and then introduced into Col plants via the floral-dip method.

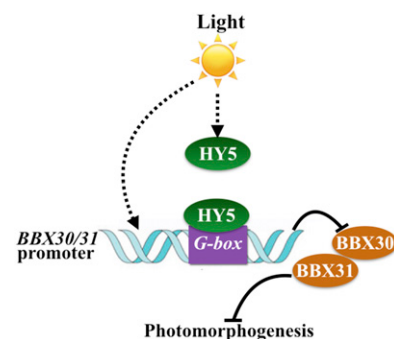


Figure 9. A working model depicting *BBX30* and *BBX31* in the regulation of photomorphogenesis. Light induces the accumulation of transcription factor HY5 and expression of *BBX30* and *BBX31*. Accumulated HY5 directly binds to the *G-boxes* present in the promoters of *BBX30* and *BBX31*, thereby inhibiting their expression. Both *BBX30* and *BBX31* negatively regulate photomorphogenic development.

(Clough and Bent, 1998). T1 transgenic plants were selected on MS medium containing 25 mg/L hygromycin. The specific mutations in *BBX30* or *BBX31* were analyzed using gene-specific primers by PCR amplification and sequencing. The *pHEE401* transfer-DNA insertion region including *CRISPER/Cas9* in *bbx30* or *bbx31* single mutant at T1 generation was removed by genetic crossing with Col.

Construction of Plasmids

The full-length *BBX30*, *BBX30*^{D46A}, *BBX31*, or *BBX31*^{D45A} open reading frame were cloned into the *pDONR-223* vector (Invitrogen) and introduced into the plant binary vector *pEarley Gateway 104* (Earley et al., 2006) under the 35S promoter using Gateway LR Clonase enzyme mix (Invitrogen). *pEarley Gateway-YFP-BBX30*, *pEarley Gateway-YFP-BBX30*^{D46A}, *pEarley Gateway-YFP-BBX31*, and *pEarley Gateway-YFP-BBX31*^{D45A} constructs were generated.

One-thousand-seven-hundred-eighty-nine-base-pair *BBX30* and 1869-bp *BBX31* promoters upstream of ATG were amplified by PCR with the respective pairs of primers and then cloned into the *KpnI/XhoI* sites of the *pLacZ-2u* vector (Lin et al., 2007). *pET28a-HY5-His* (Xu et al., 2016) and *pB42AD-HY5* (Lin et al., 2018) constructs were described previously. The primers used for plasmids construction were listed in Supplemental Table S1.

Transgenic Plants

The *pEarley Gateway-YFP-BBX30*, *pEarley Gateway-YFP-BBX30*^{D46A}, *pEarley Gateway-YFP-BBX31*, and *pEarley Gateway-YFP-BBX31*^{D45A} constructs were transformed into *Agrobacterium tumefaciens* GV3101 by the freeze-thaw method and then introduced into Col plants via the floral-dip method (Clough and Bent, 1998). Transgenic plants were selected on MS medium containing 20 mg/L Basta.

Measurement of Hypocotyl Length

To measure the hypocotyl length of seedlings, seeds were sown on plates and stratified at 4°C in darkness for 3 d and then kept in continuous white light for 8 h in order to induce uniform germination. The seeds were then transferred to D, W, B, R, and FR light conditions and incubated at 22°C for 4 d (Xu et al., 2016). The hypocotyl length of seedlings was measured using ImageJ software.

Immunoblot Analysis

For immunoblots, Arabidopsis (*Arabidopsis thaliana*) wild-type or transgenic seedlings were homogenized in a protein extraction buffer containing 100 mM NaH₂PO₄, 10 mM Tris-HCl, 200 mM NaCl, 8 M Urea, pH 8.0, 1 mM phenylmethylsulfonyl fluoride, and 1× complete protease inhibitor cocktail (Roche). Primary antibodies used in this study were anti-GFP (Abmart) and anti-Actin (Sigma-Aldrich).

EMSA Assays

EMSA assays were performed using biotin-labeled probes and the Light Shift Chemiluminescent EMSA kit (Thermo Scientific) as described previously (Xu et al., 2014). The promoter subfragment of *BBX30* (32 bp, −94 to −125 bp) and *BBX31* (32 bp, −143 to −174 bp) upstream of ATG were PCR amplified and then mixed with biotin and kept in UV light for 30 min for biotin labeling. Next, purified HY5-His protein as indicated were incubated together with 40 fmol biotin-labeled probes in a 20-μL reaction mixture containing 10 mM Tris-HCl, pH 7.5, 0.05% NP40, 10 mM MgCl₂, 5% (v/v) glycerol, and 0.1 μg/mL poly (dI•dC). Reactions were incubated at 25°C for 20 min and separated on 6% native polyacrylamide gels in 0.5× Tris-borate/EDTA buffer. Then, gels were electrophoretically transferred to Hybond N+ (Milipore) nylon membranes in 0.5× Tris-borate/EDTA for 40 min, and the labeled probes were detected according to the manufacturer's protocols provided with the EMSA kit. The probes used in this study were listed in Supplemental Table S1.

Yeast One-Hybrid Assays

For the yeast one-hybrid assay, the respective combinations of activation domain-fusion effectors and LacZ reporters were cotransformed into yeast strain EGY48, and transformants were selected and grown on SD/-Trp-Ura

dropout media. Yeast transformation and liquid assay were conducted as described in the Yeast Protocols Handbook (BD Clontech).

ChIP

The ChIP assays were performed as described by Xu et al. (2016). Chromatin isolation was performed using Col and *HA-HY5 hy5-215* transgenic seedlings grown under constant white light for 4 d. The resuspended chromatin was sonicated at 4°C to 250- to 500-bp fragments. The sheared chromatin was immunoprecipitated, washed, reverse cross linked, and finally amplified. About 10% of sonicated but nonimmunoprecipitated chromatin was reverse cross linked and used as an input DNA control. Both immunoprecipitated DNA and input DNA were analyzed by RT-PCR (Applied Biosystems). Monoclonal anti-HA antibody (Sigma-Aldrich) was used for the assays. All primers used for this assay are listed in Supplemental Table S1.

RNA-Seq Analysis

Total RNA was extracted from the 4-d-old Col and *bbx30-2 bbx31-2* seedlings grown in constant W light (17.5 μmol/m²/s) conditions. Then, mRNA sequencing libraries were constructed, and sequencing was performed using the Illumina HiSeq 2500 platform according to the manufacturer's instruction (HiSeq 2500 user guide) by Shanghai Hanyu-Bio. Three independent biological replicates were performed. RNA-Seq reads were mapped to Arabidopsis TAIR 10 using Hisat2 (version 2.05; Kim et al., 2015) software using default parameters. Then, raw reads for each gene were calculated by HTseq (Anders et al., 2015) before calculating differential gene expression. Then, differentially expressed genes among two conditions were identified using the general linear models method in the edgeR package (version 3.12.0; Robinson et al., 2010) with false positive rate of 0.05 and fold-change of 2. GO analysis was performed by topGO (Bioconductor) software (<http://www.bioconductor.org/packages/2.11/bioc/HTML/topGO.html>), and the result was plotted using REVIGO with R (Supek et al., 2011). KEGG enrichment analysis was conducted by KOBAS 3.0 (Xie et al., 2011) and the enriched pathways were plotted by R software.

RT-qPCR

Total RNA was extracted from 4-d-old Arabidopsis seedlings grown under white light using the RNeasy plant mini kit (QIAGEN). Complementary DNAs (cDNA) were synthesized from 2 μg of total RNA using the 5× All-In-One RT Master Mix cDNA synthesis system (Applied Biological Materials) according to the manufacturer's instructions. Then, cDNA were subjected to RT-qPCR assays. RT-qPCR was performed using the Step One Plus RT-PCR detection system (Applied Biosystems) and SYBR Green PCR Master Mix (Takara). PCR was performed in triplicate for each sample, and the expression levels were normalized to that of a *PP2A* gene. The primers used in this study were listed in Supplemental Table S1.

Accession Numbers

Sequence data from this article can be found in the Genome Initiative or GenBank/EMBL data libraries under the following accession numbers: *BBX30* (At4g15248), *BBX31* (At3g21890), and *HY5* (At5g11260).

Supplemental Data

The following supplemental materials are available:

Supplemental Figure S1. Hypocotyl phenotype and length in various *BBX30* and *BBX31* transgenic seedlings grown in darkness.

Supplemental Figure S2. Light does not affect the accumulation of YFP-*BBX30* or YFP-*BBX31*.

Supplemental Figure S3. Mutations in each of the two independent *bbx30* and *bbx31* alleles created by the CRISPER/Cas9 method.

Supplemental Figure S4. Hypocotyl phenotype and length in *bbx30*, *bbx31*, and *bbx30 bbx31* seedlings grown in darkness.

Supplemental Figure S5. Validation of 18 target genes of *BBX30* and *BBX31* identified by RNA-Seq using RT-qPCR.

Supplemental Figure S6. Hypocotyl phenotype and length in *hy5-215 bbx30-2*, *hy5-215 bbx31-2*, and *hy5-215 bbx30-2 bbx31-2* grown in darkness.

Supplemental Figure S7. *bbx30-2 bbx31-2* display earlier flowering phenotype, but *BBX30* and *BBX31* transgenic plants show delayed flowering phenotype under long-day conditions.

Supplemental Figure S8. *BBX30^{D46A}* and *BBX31^{D45A}* gene and protein expression levels in each of two independent transgenic lines.

Supplemental Figure S9. Hypocotyl phenotype and length in *BBX30^{D46A}* and *BBX31^{D45A}* transgenic seedlings grown in darkness.

Supplemental Table S1. List of up- and down-regulated gene in the *bbx30-2 bbx31-2* double mutant compared with the wild type.

Supplemental Table S2. Enriched GO terms (biological process) and genes of the down-regulated genes in the *bbx30-2 bbx31-2* double mutant.

Supplemental Table S3. Enriched KEGG pathways and genes of the down-regulated genes in the *bbx30-2 bbx31-2* double mutant.

Supplemental Table S4. List of primers used in this study.

ACKNOWLEDGMENTS

The authors thank all the lab members at SUSTech for their discussion on the project.

Received October 9, 2018; accepted February 4, 2019; published February 14, 2019.

LITERATURE CITED

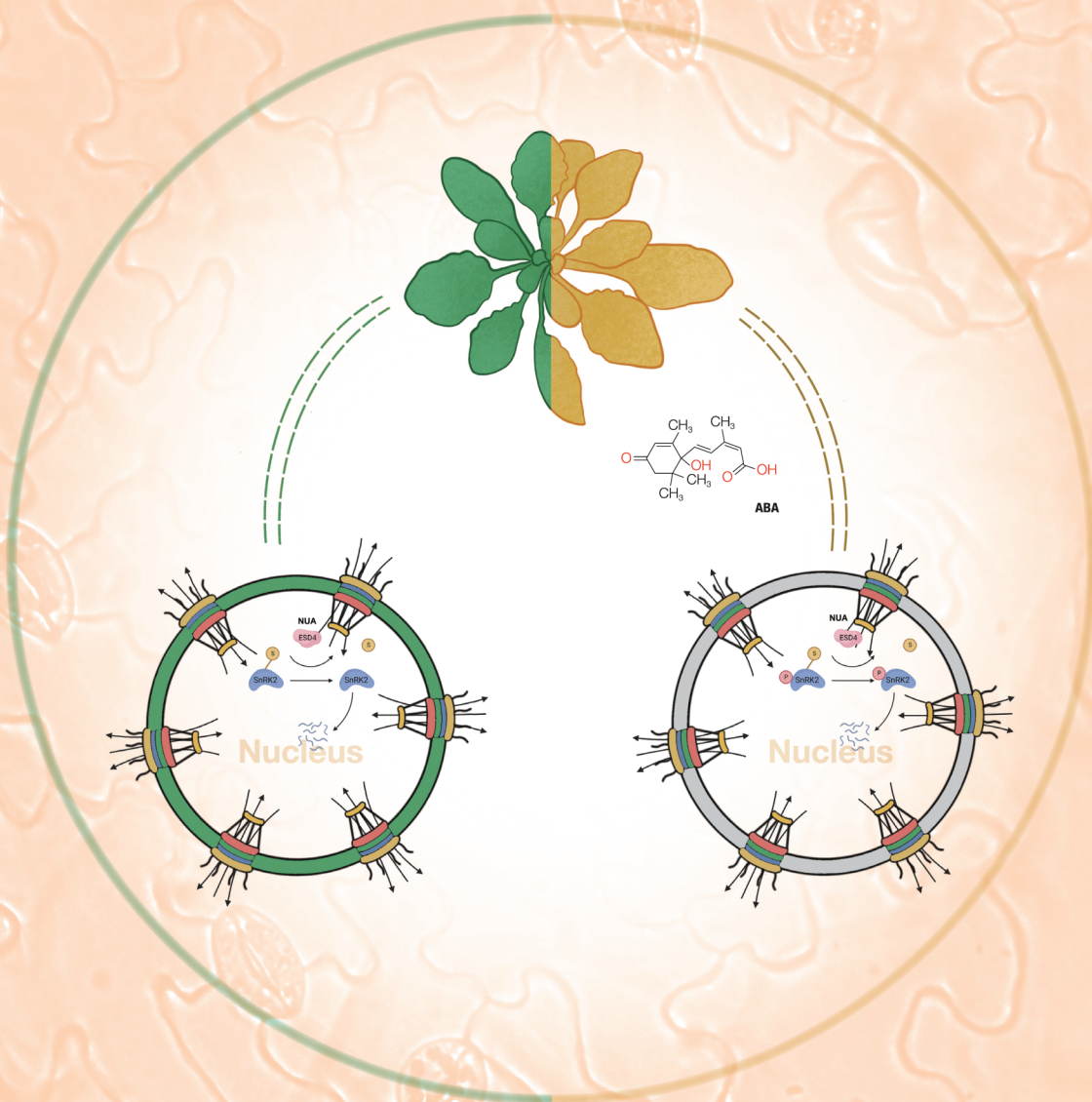
- Anders S, Pyl PT, Huber W (2015) HTSeq—a Python framework to work with high-throughput sequencing data. *Bioinformatics* **31**: 166–169
- Ang LH, Chattopadhyay S, Wei N, Oyama T, Okada K, Batschauer A, Deng XW (1998) Molecular interaction between COP1 and HY5 defines a regulatory switch for light control of *Arabidopsis* development. *Mol Cell* **1**: 213–222
- Chang CS, Li YH, Chen LT, Chen WC, Hsieh WP, Shin J, Jane WN, Chou SJ, Choi G, Hu JM, et al (2008) LZFI, a HY5-regulated transcriptional factor, functions in *Arabidopsis* de-etiolation. *Plant J* **54**: 205–219
- Chang CS, Maloof JN, Wu SH (2011) COP1-mediated degradation of BBX22/LZFI optimizes seedling development in *Arabidopsis*. *Plant Physiol* **156**: 228–239
- Clough SJ, Bent AF (1998) Floral dip: a simplified method for *Agrobacterium*-mediated transformation of *Arabidopsis thaliana*. *Plant J* **16**: 735–743
- Datta S, Hettiarachchi GH, Deng XW, Holm M (2006) *Arabidopsis* CONSTANS-LIKE3 is a positive regulator of red light signaling and root growth. *Plant Cell* **18**: 70–84
- Datta S, Hettiarachchi C, Johansson H, Holm M (2007) SALT TOLERANCE HOMOLOG2, a B-box protein in *Arabidopsis* that activates transcription and positively regulates light-mediated development. *Plant Cell* **19**: 3242–3255
- Datta S, Johansson H, Hettiarachchi C, Irigoyen ML, Desai M, Rubio V, Holm M (2008) LZFI/SALT TOLERANCE HOMOLOG3, an *Arabidopsis* B-box protein involved in light-dependent development and gene expression, undergoes COP1-mediated ubiquitination. *Plant Cell* **20**: 2324–2338
- Ding L, Wang S, Song ZT, Jiang Y, Han JJ, Lu SJ, Li L, Liu JX (2018) Two B-box domain proteins, BBX18 and BBX23, interact with ELF3 and regulate thermomorphogenesis in *Arabidopsis*. *Cell Reports* **25**: 1718–1728.e4
- Earley KW, Haag JR, Pontes O, Opper K, Juehne T, Song K, Pikaard CS (2006) Gateway-compatible vectors for plant functional genomics and proteomics. *Plant J* **45**: 616–629
- Fan XY, Sun Y, Cao DM, Bai MY, Luo XM, Yang HJ, Wei CQ, Zhu SW, Sun Y, Chong K, et al (2012) BZS1, a B-box protein, promotes photomorphogenesis downstream of both brassinosteroid and light signaling pathways. *Mol Plant* **5**: 591–600
- Gangappa SN, Botto JF (2014) The BBX family of plant transcription factors. *Trends Plant Sci* **19**: 460–470
- Gangappa SN, Crocco CD, Johansson H, Datta S, Hettiarachchi C, Holm M, Botto JF (2013) The *Arabidopsis* B-BOX protein BBX25 interacts with HY5, negatively regulating BBX22 expression to suppress seedling photomorphogenesis. *Plant Cell* **25**: 1243–1257
- Graeff M, Straub D, Eguen T, Dolde U, Rodrigues V, Brandt R, Wenkel S (2016) MicroProtein-mediated recruitment of CONSTANS into a TOPLESS trimeric complex represses flowering in *Arabidopsis*. *PLoS Genet* **12**: e1005959
- Hoecker U (2017) The activities of the E3 ubiquitin ligase COP1/SPA, a key repressor in light signaling. *Curr Opin Plant Biol* **37**: 63–69
- Holm M, Hardtke CS, Gaudet R, Deng XW (2001) Identification of a structural motif that confers specific interaction with the WD40 repeat domain of *Arabidopsis* COP1. *EMBO J* **20**: 118–127
- Holm M, Ma LG, Qu LJ, Deng XW (2002) Two interacting bZIP proteins are direct targets of COP1-mediated control of light-dependent gene expression in *Arabidopsis*. *Genes Dev* **16**: 1247–1259
- Holtan HE, Bandong S, Marion CM, Adam L, Tiwari S, Shen Y, Maloof JN, Maszle DR, Ohto MA, Preuss S, et al (2011) BBX32, an *Arabidopsis* B-box protein, functions in light signaling by suppressing HY5-regulated gene expression and interacting with STH2/BBX21. *Plant Physiol* **156**: 2109–2123
- Huang X, Ouyang X, Deng XW (2014) Beyond repression of photomorphogenesis: Role switching of COP/DET/FUS in light signaling. *Curr Opin Plant Biol* **21**: 96–103
- Indorf M, Cordero J, Neuhaus G, Rodríguez-Franco M (2007) Salt tolerance (STO), a stress-related protein, has a major role in light signalling. *Plant J* **51**: 563–574
- Jiao Y, Lau OS, Deng XW (2007) Light-regulated transcriptional networks in higher plants. *Nat Rev Genet* **8**: 217–230
- Khanna R, Kronmiller B, Maszle DR, Coupland G, Holm M, Mizuno T, Wu SH (2009) The *Arabidopsis* B-box zinc finger family. *Plant Cell* **21**: 3416–3420
- Kim D, Langmead B, Salzberg SL (2015) HISAT: A fast spliced aligner with low memory requirements. *Nat Methods* **12**: 357–360
- Lau OS, Deng XW (2012) The photomorphogenic repressors COP1 and DET1: 20 years later. *Trends Plant Sci* **17**: 584–593
- Lee J, He K, Stolz V, Lee H, Figueroa P, Gao Y, Tongprasit W, Zhao H, Lee I, Deng XW (2007) Analysis of transcription factor HY5 genomic binding sites revealed its hierarchical role in light regulation of development. *Plant Cell* **19**: 731–749
- Lin F, Jiang Y, Li J, Yan T, Fan L, Liang J, Chen ZJ, Xu D, Deng XW (2018) B-BOX DOMAIN PROTEIN28 negatively regulates photomorphogenesis by repressing the activity of transcription factor HY5 and undergoes COP1-mediated degradation. *Plant Cell* **30**: 2006–2019
- Lin R, Ding L, Casola C, Ripoll DR, Feschotte C, Wang H (2007) Transposase-derived transcription factors regulate light signaling in *Arabidopsis*. *Science* **318**: 1302–1305
- Ma L, Li J, Qu L, Hager J, Chen Z, Zhao H, Deng XW (2001) Light control of *Arabidopsis* development entails coordinated regulation of genome expression and cellular pathways. *Plant Cell* **13**: 2589–2607
- Osterlund MT, Hardtke CS, Wei N, Deng XW (2000) Targeted destabilization of HY5 during light-regulated development of *Arabidopsis*. *Nature* **405**: 462–466
- Oyama T, Shimura Y, Okada K (1997) The *Arabidopsis* HY5 gene encodes a bZIP protein that regulates stimulus-induced development of root and hypocotyl. *Genes Dev* **11**: 2983–2995
- Podolec R, Ulm R (2018) Photoreceptor-mediated regulation of the COP1/SPA E3 ubiquitin ligase. *Curr Opin Plant Biol* **45**(Pt A): 18–25
- Robinson MD, McCarthy DJ, Smyth GK (2010) edgeR: A Bioconductor package for differential expression analysis of digital gene expression data. *Bioinformatics* **26**: 139–140
- Ruckle ME, DeMarco SM, Larkin RM (2007) Plastid signals remodel light signaling networks and are essential for efficient chloroplast biogenesis in *Arabidopsis*. *Plant Cell* **19**: 3944–3960
- Ruckle ME, Burgoon LD, Lawrence LA, Sinkler CA, Larkin RM (2012) Plastids are major regulators of light signaling in *Arabidopsis*. *Plant Physiol* **159**: 366–390
- Sullivan JA, Deng XW (2003) From seed to seed: the role of photoreceptors in *Arabidopsis* development. *Dev Biol* **260**: 289–297
- Supek F, Bošnjak M, Škunca N, Šmuc T (2011) REVIGO summarizes and visualizes long lists of gene ontology terms. *PLoS One* **6**: e21800

- Tepperman JM, Hudson ME, Khanna R, Zhu T, Chang SH, Wang X, Quail PH (2004) Expression profiling of phyB mutant demonstrates substantial contribution of other phytochromes to red-light-regulated gene expression during seedling de-etiolation. *Plant J* **38**: 725–739
- Wang CQ, Guthrie C, Sarmast MK, Dehesh K (2014) BBX19 interacts with CONSTANS to repress *FLOWERING LOCUS T* transcription, defining a flowering time checkpoint in *Arabidopsis*. *Plant Cell* **26**: 3589–3602
- Wang CQ, Sarmast MK, Jiang J, Dehesh K (2015a) The transcriptional regulator BBX19 promotes hypocotyl growth by facilitating COP1-mediated EARLY FLOWERING3 degradation in *Arabidopsis*. *Plant Cell* **27**: 1128–1139
- Wang ZP, Xing HL, Dong L, Zhang HY, Han CY, Wang XC, Chen QJ (2015b) Egg cell-specific promoter-controlled CRISPR/Cas9 efficiently generates homozygous mutants for multiple target genes in *Arabidopsis* in a single generation. *Genome Biol* **16**: 144
- Xie C, Mao X, Huang J, Ding Y, Wu J, Dong S, Kong L, Gao G, Li CY, Wei L (2011) KOBAS 2.0: A web server for annotation and identification of enriched pathways and diseases. *Nucleic Acids Res* **39**(suppl_2): W316–22
- Xu D, Li J, Gangappa SN, Hettiarachchi C, Lin F, Andersson MX, Jiang Y, Deng XW, Holm M (2014) Convergence of Light and ABA signaling on the *ABI5* promoter. *PLoS Genet* **10**: e1004197
- Xu D, Jiang Y, Li J, Lin F, Holm M, Deng XW (2016) BBX21, an *Arabidopsis* B-box protein, directly activates *HY5* and is targeted by COP1 for 26S proteasome-mediated degradation. *Proc Natl Acad Sci USA* **113**: 7655–7660
- Xu DB, Gao SQ, Ma YN, Wang XT, Feng L, Li LC, Xu ZS, Chen YF, Chen M, Ma YZ (2017) The G-protein β subunit AGB1 promotes hypocotyl elongation through inhibiting transcription activation function of BBX21 in *Arabidopsis*. *Mol Plant* **10**: 1206–1223
- Xu D, Jiang Y, Li J, Holm M, Deng XW (2018) The B-box domain protein BBX21 promotes photomorphogenesis. *Plant Physiol* **176**: 2365–2375
- Zhang H, He H, Wang X, Wang X, Yang X, Li L, Deng XW (2011) Genome-wide mapping of the HY5-mediated gene networks in *Arabidopsis* that involve both transcriptional and post-transcriptional regulation. *Plant J* **65**: 346–358
- Zhang X, Huai J, Shang F, Xu G, Tang W, Jing Y, Lin R (2017) A PIF1/PIF3-HY5-BBX23 transcription factor cascade affects photomorphogenesis. *Plant Physiol* **174**: 2487–2500

JIPB Journal of Integrative Plant Biology

www.jipb.net 植物学报(英)
VOLUME 64, ISSUE 11
NOVEMBER 2022

10 µm
I



WILEY



第143页

COP1 SUPPRESSOR 6 represses the PIF4 and PIF5 action to promote light-inhibited hypocotyl growth

Hongxia Lan^{1†}, Yueqin Heng^{1†}, Jian Li^{1†}, Mengdi Zhang¹, Yeting Bian², Li Chu², Yan Jiang¹, Xuncheng Wang³, Dongqing Xu^{2*} and Xing Wang Deng^{1,4*}

1. Key Laboratory of Molecular Design for Plant Cell Factory of Guangdong Higher Education Institutes, Department of Biology, Institute of Plant and Food Sciences, School of Life Sciences, Southern University of Science and Technology, Shenzhen 518055, China

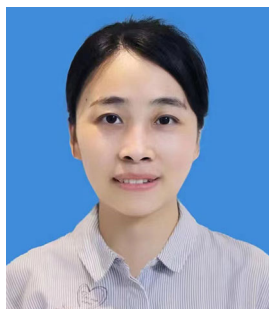
2. State Key Laboratory of Crop Genetics and Germplasm Enhancement, National Center for Soybean Improvement, College of Agriculture, Nanjing Agricultural University, Nanjing 210095, China

3. Beijing Key Laboratory of Environment Friendly Management on Fruit Diseases and Pests in North China, Institute of Plant and Environment Protection, Beijing Academy of Agriculture and Forestry Sciences, Beijing 100097, China

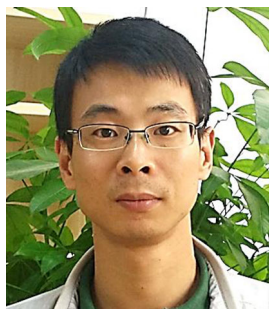
4. State Key Laboratory of Protein and Plant Gene Research, Peking-Tsinghua Center for Life Sciences, School of Advanced Agriculture Sciences and School of Life Sciences, Peking University, Beijing 100871, China

[†]These authors contributed equally to this work.

*Correspondences: Dongqing Xu (dongqingxu@njau.edu.cn, Dr. Xu is fully responsible for the distributions of all materials associated with this article); Xing Wang Deng (deng@pku.edu.cn)



Yueqin Heng



Dongqing Xu

ABSTRACT

Light signaling precisely controls photomorphogenic development in plants. PHYTOCHROME INTERACTING FACTOR 4 and 5 (PIF4 and PIF5) play critical roles in the regulation of this developmental process. In this study, we report CONSTITUTIVELY PHOTOMORPHOGENIC 1 SUPPRESSOR 6 (CSU6) functions as a key regulator of light signaling. Loss of CSU6 function

largely rescues the *cop1-6* constitutively photomorphogenic phenotype. CSU6 promotes hypocotyl growth in the dark, but inhibits hypocotyl elongation in the light. CSU6 not only associates with the promoter regions of *PIF4* and *PIF5* to inhibit their expression in the morning, but also directly interacts with both PIF4 and PIF5 to repress their transcriptional activation activity. CSU6 negatively controls a group of PIF4- and PIF5-regulated gene expressions. Mutations in *PIF4* and/or *PIF5* are epistatic to the loss of CSU6, suggesting that CSU6 acts upstream of *PIF4* and *PIF5*. Taken together, CSU6 promotes light-inhibited hypocotyl elongation by negatively regulating PIF4 and PIF5 transcription and biochemical activity.

Keywords: COP1, CSU6, light signaling, photomorphogenesis, PIF4, PIF5

Lan, H., Heng, Y., Li, J., Zhang, M., Bian, Y., Chu, L., Jiang, Y., Wang, X., Xu, D., and Deng, X.W. (2022). COP1 SUPPRESSOR 6 represses the PIF4 and PIF5 action to promote light-inhibited hypocotyl growth. *J. Integr. Plant Biol.* **64**: 2097–2110.

INTRODUCTION

In nature, a germinating seedling undergoes skotomorphogenic development (etiolation) to emerge from the covered soil to reach light. Upon light exposure, etiolated seedling promptly initiates photomorphogenesis (de-etiolation). These two distinct developmental processes are tightly controlled by the absence or presence of light signals. Dark-grown seedlings display dramatically elongated hypocotyls, curved apical hooks and closed cotyledons with etioplasts termed

skotomorphogenesis, while they switch to photomorphogenesis showing inhibition of hypocotyl growth, expanded cotyledons with developed chloroplasts in the light (Sullivan and Deng, 2003; Jiao et al., 2007). The transition from skotomorphogenic to photomorphogenic development appropriately enables a buried seed to penetrate the covered soil and to become a normal seedling.

CONSTITUTIVELY PHOTOMORPHOGENIC 1 (COP1) acts as a central repressor of light signaling (Lau and Deng, 2012; Han et al., 2020). Loss of COP1 function leads to a

constitutively photomorphogenic phenotype even in the dark (Deng et al., 1991, 1992). COP1 and SUPPRESSOR OF PHYTOCHROME A (SPA) form stable complexes that directly target a group of photomorphogenesis-promoting factors including ELONGATED HYPOCOTYL 5 (HY5), HY5 HOMOLOG (HYH), B-BOX PROTEINS (BBXs) for ubiquitination and thus accelerate their degradation (Han et al., 2020; Song et al., 2020; Xu, 2020). Additionally, COP1 facilitates the stabilization of photomorphogenesis-inhibiting factors PHYTOCHROME INTERACTING FACTORS (PIFs: PIF1, PIF3, PIF4, and PIF5) in darkness (Paik et al., 2017; Pham et al., 2018a). The photoreceptors perceive the various wave-length spectra of light signals to initiate the photomorphogenesis in plants. Upon light irradiation, the light-activated photoreceptors phytochrome A (phyA), phyB, CRYPTOCHROME 1 (CRY1), and CRY2 inhibit the COP1 activity and promote the degradation of PIFs through distinct modes of action (Lian et al., 2011; Liu et al., 2011; Zuo et al., 2011; Zheng et al., 2013; Yadav et al., 2020; Cheng et al., 2021). Prolonged light exposure triggers the translocation of COP1 from the nucleus to the cytoplasm (von Arnim and Deng, 1994). Thus, these molecular events consequently lead to the accumulation of photomorphogenesis-promoting factors like HY5 and HYH as well as low abundance of PIFs, ultimately promoting photomorphogenesis in the light.

The basic helix-loop-helix (bHLH) type transcription factors PIF4 and PIF5, acting directly downstream of photoreceptors phyA and CRYs, regulate photomorphogenesis, shade avoidance, and thermomorphogenesis predominantly by controlling the expression of auxin biosynthesis and signaling-related genes (Huq and Quail, 2002; Khanna et al., 2007; Hornitschek et al., 2009; Nusinow et al., 2011; Sun et al., 2012, 2013; Jung et al., 2016; Legris et al., 2016; Paik et al., 2017; Pham et al., 2018a; Qi et al., 2022). PIF4 and PIF5 proteins are abundant in the nucleus in the plant cells where they regulate a number of target genes to promote skotomorphogenesis. Photo-excited phyB directly interacts with PIF4 and PIF5, and triggers their phosphorylation, ubiquitination and subsequent degradation (Paik et al., 2017; Pham et al., 2018a; Cheng et al., 2021). Upon prolonged red light irradiation, PIF4 and PIF5 proteins re-accumulate in the plant cells to promote the hypocotyl growth (Park et al., 2018; Yan et al., 2020). The R2R3-MYB transcription factor MYB30 promotes the accumulation of PIF4 and PIF5 (Yan et al., 2020), whereas BBX11 negatively controls the PIF4 abundance under prolonged red light irradiation (Song et al., 2021). Shade and warm temperature stimuli trigger a portion of Pfr phyB to convert into the inactive Pr form, which in turn releases the repression of PIF4 and PIF5 as well as PIF4- and PIF5-controlled genes (Hornitschek et al., 2009; Jung et al., 2016; Legris et al., 2016; Cheng et al., 2021). PIF4 and PIF5 are diurnally regulated both at transcriptional and protein levels by the circadian clock. The morning expressed circadian clock proteins CIRCADIAN CLOCK-ASSOCIATED 1 (CCA1) and LATE ELONGATED HYPOCOTYL (LHY) activate the expression of PIF4 (Niwa et al., 2009). CSU4 inhibits

CCA1 transcription in the early morning and PIF4 expression in the early evening (Zhao et al., 2018), while the COLD-REGULATED 27 (COR27) up-regulates the PIF4 transcription at noon (Zhu et al., 2020). PSEUDO RESPONSE REGULATORS (PRRs) and the evening complex ELF3-ELF4-LUX repress transcription of PIF4 and PIF5 (Nusinow et al., 2011; Li et al., 2020). Both the ELF3 and TOC1 inhibit the PIF4 activity by directly interacting with PIF4 (Nieto et al., 2015; Zhu et al., 2016). In a consequence, these molecular events synergistically and coordinately contribute to the circadian clock-mediated hypocotyl growth.

In this study, we report a previously unknown regulator of photomorphogenesis, CSU6. Mutations in CSU6 largely suppressed the constitutively photomorphogenic phenotype of *cop1-6*. Loss of CSU6 function mutant seedlings exhibited shortened hypocotyls in the dark, but elongated hypocotyls in the light. On one hand, CSU6 associated with the promoter regions of PIF4 and PIF5 to inhibit their transcription in the morning. On the other hand, CSU6 directly interacted with both PIF4 and PIF5, and repressed their transcriptional activity toward downstream target genes. CSU6 acted upstream of PIF4 and PIF5, and negatively regulated the expression of numerous PIF4- and PIF5-mediated genes. Collectively, CSU6 functions as a transcriptional repressor in repressing PIF4 and PIF5 transcription and biochemical activity to inhibit hypocotyl growth in the light.

RESULTS

Mutation in CSU6 suppresses *cop1-6* phenotype in darkness

COP1 is a central repressor of light signaling (Han et al., 2020). Null *cop1* (e.g., *cop1-5*) mutant is lethal at the seedling stage, and weak *cop1* (e.g., *cop1-4* and *cop1-6*) mutants display constitutively photomorphogenic phenotype in darkness (McNelli et al., 1994). To explore the unidentified and uncharacterized key components of COP1 signaling, we have performed a forward genetic screen to isolate mutants that suppress the constitutively photomorphogenic phenotype of *cop1-6* in darkness as previously described (Xu et al., 2014, 2015; Lin et al., 2017). *csu6-1*, which is an extragenic and recessive suppressor, was recovered in the same screen. *csu6-1 cop1-6* were slightly shorter than Columbia-0 (Col-0) (wild-type), but they were dramatically longer than *cop1-6* when grown in darkness. Although the cotyledons of *csu6-1 cop1-6* were obviously expanded, their cotyledon angles were significantly smaller than *cop1-6* (Figure 1A–D). Together, these genetic results suggest that *csu6-1* largely suppresses *cop1-6* short hypocotyl phenotype and partially suppresses *cop1-6* opened cotyledon phenotype in darkness. Moreover, *csu6* partially suppressed the dwarf phenotypes, but not early flowering phenotypes of *cop1-6* when grown in long-d conditions (16 h light/8 h dark) (Figure S1).

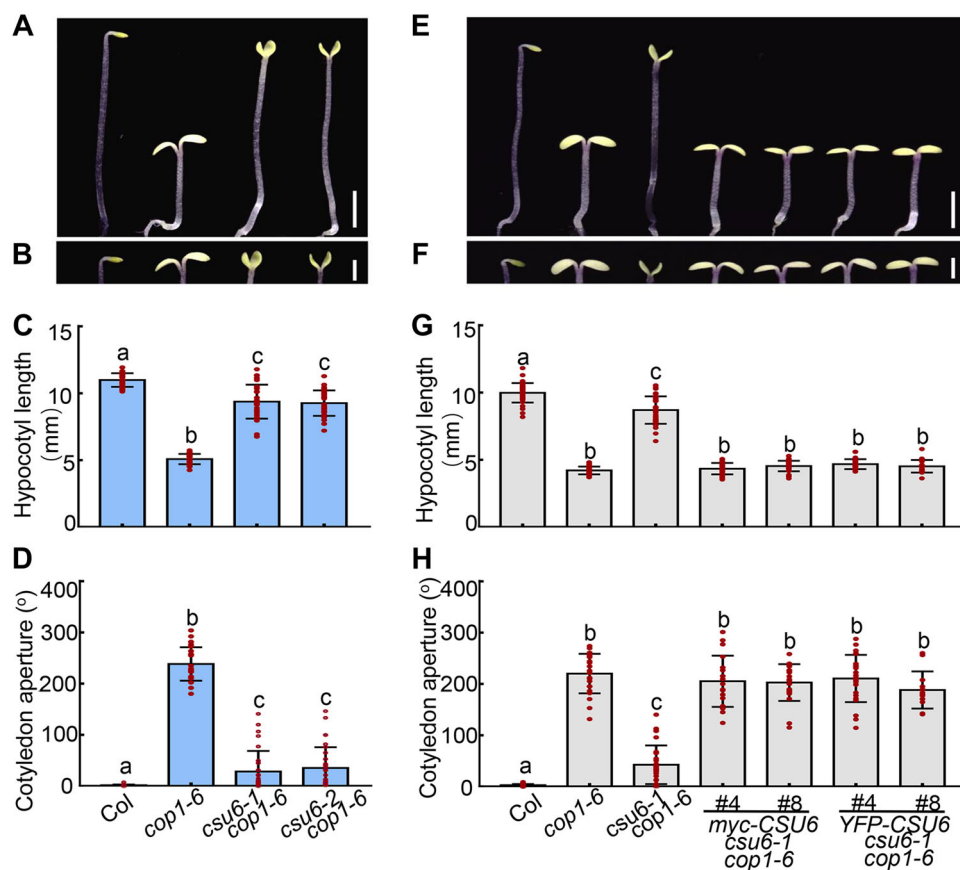


Figure 1. Mutation in *CSU6* suppresses *cop1-6* in darkness

(A, B) Hypocotyl (A) and cotyledon (B) phenotypes of Columbia (Col), *cop1-6*, and *csu6 cop1-6* seedlings grown in the dark for 4 d. Bars, 2 mm (A), 1 mm (B). (C, D) Hypocotyl length (C) and cotyledon angle (D) of Col, *cop1-6*, and *csu6 cop1-6* seedlings grown in the dark for 4 d. Error bars represent SD ($n \geq 20$). Letters above the bars indicate significant differences ($P < 0.05$) as determined by one-way analysis of variance (ANOVA) with Tukey's post-hoc analysis. (E, F) Hypocotyl (E) and cotyledon (F) phenotypes of Col-0, *cop1-6*, *csu6-1 cop1-6*, and four independent transgenic lines *myc-CSU6 csu6-1 cop1-6*, *YFP-CSU6 csu6-1 cop1-6* grown in darkness for 4 d. Bars, 2 mm (E), 1 mm (F). (G, H) Hypocotyl length (G) and cotyledon separation angle (H) of Col-0, *cop1-6*, *csu6-1 cop1-6*, and four independent transgenic lines *myc-CSU6 csu6-1 cop1-6*, *YFP-CSU6 csu6-1 cop1-6* grown in darkness for 4 d. Error bars represent SD ($n \geq 20$). Letters above the bars indicate significant differences ($P < 0.05$) as determined by one-way ANOVA with Tukey's post-hoc analysis.

Map-based cloning of *CSU6*

To identify the genetic location of *CSU6*, we first mapped *CSU6* to an approximately 953 kb region between markers 3-AC009325-0089 and 3-AC022287-0495 on the top arm of chromosome 3 using a map-based cloning method (Figure 2A). We next re-sequenced the whole genome of *csu6-1 cop1-6* and analyzed the specific sequence alterations of the mapped region on chromosome 3. This analysis identified a “g” to “a” substitution at the site of 1672 from the start code in At3g02860, leading to the splicing junction “ag” at the 3' end of intron six to “aa.” As a consequence, this point mutation most likely disrupted the splicing principles of At3g02860 (Figure 2A, B). At3g02860 encodes a C2H2-type zinc-finger domain containing protein consisting of 313 amino acids (Figure 2C). To verify the mutation in *CSU6* indeed suppressed *cop1-6*, we obtained a T-DNA insertion mutant (SALK_030445; named *csu6-2*), in which *CSU6* transcripts were significantly decreased (Figure S2), and generated *csu6-2 cop1-6* double mutants by genetic crossing.

csu6-2 cop1-6 displayed similar phenotypes with *csu6-1 cop1-6* in darkness (Figure 1A–D). Moreover, we transformed *CSU6* coding sequences fused with myc or yellow fluorescent protein (YFP) at the N-terminus driven by the cauliflower mosaic virus 35S promoter (35S:*myc-CSU6* or 35S:*YFP-CSU6*) into *csu6-1 cop1-6* double mutant plants. Each of two independent *myc-CSU6 csu6-1 cop1-6* and *YFP-CSU6 csu6-1 cop1-6* transgenic lines resembled *cop1-6* phenotypes showing shortened hypocotyls and opened cotyledons in darkness (Figure 1E–H). Together, these results demonstrate that mutation in *CSU6* indeed largely suppresses the *cop1-6* phenotype and a functional *CSU6* complements the phenotype conferred by *csu6-1 cop1-6* in the dark.

CSU6 promotes hypocotyl elongation in the dark, but represses hypocotyl growth in the light

To investigate the roles of *CSU6* in light signaling, we isolated the *csu6-1* single mutant from the F_2 progeny of *csu6-1 cop1-6* crossed with Col-0 and analyzed the

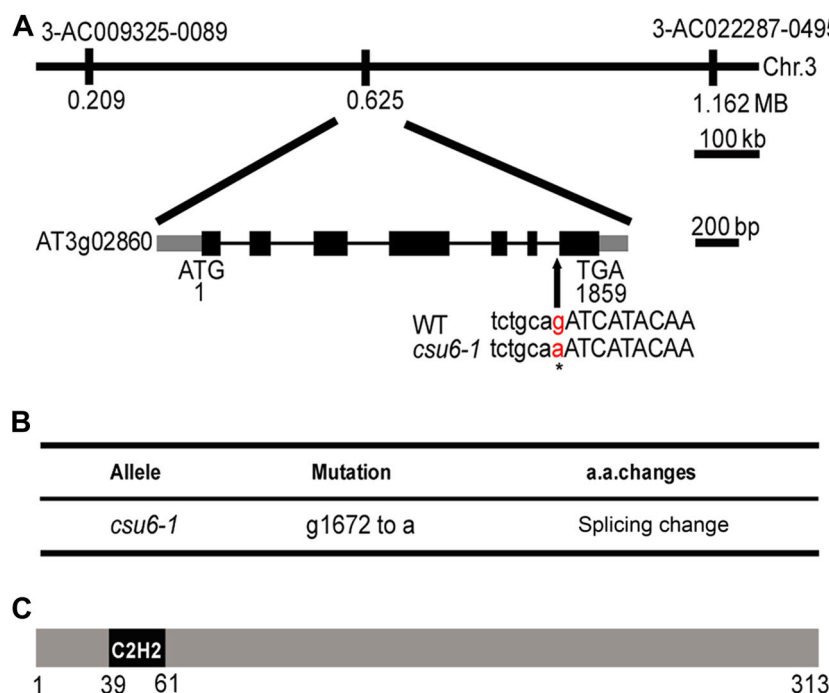


Figure 2. Map-based cloning of CSU6

(A) Map of the *CSU6* locus and *CSU6* gene structure. The exons are indicated with black boxes, and the introns are indicated with black lines. The point mutation in *csu6-1* is marked in red with an asterisk. **(B)** Mutation identified in the *csu6-1*. The mutation results in splicing change of the *CSU6*. **(C)** Protein structure of CONSTITUTIVELY PHOTOMORPHOGENIC 1 SUPPRESSOR 6 (*CSU6*). C2H2 indicates C2H2 type zinc-finger domain.

hypocotyl phenotypes of *csu6-1* and *csu6-2* mutants grown in various light conditions. The hypocotyl length of both *csu6-1* and *csu6-2* was shorter than that of Col-0 when grown in the dark (Figure 3A, B). Both *csu6-1* and *csu6-2* displayed significantly elongated hypocotyls compared to Col-0 when grown in the white (W), blue (B), red (R), and far-red (FR) light conditions tested (Figure 3C–J). These genetic data suggest that CSU6 promotes hypocotyl elongation in the dark, but inhibits hypocotyl growth in the light. To verify the roles of CSU6 in the regulation of hypocotyl growth, we transformed *CSU6* fused with green fluorescent protein (GFP) driven by its own promoter at the C-terminus (*CSU6pro:CSU6-GFP*) into *csu6-1* and *csu6-2* respectively. CSU6-GFP proteins were detectable using immunoblot assays in each of two independent *proCSU6:CSU6-GFP csu6-1* and *proCSU6:CSU6-GFP csu6-2* transgenic lines (Figure S3). All four independent transgenic lines were indistinguishable from Col-0 when grown in the dark or various light conditions tested (W, B, R, and FR) (Figure S4). In comparison with *csu6-1* or *csu6-2*, they were significantly longer in the dark, but clearly shorter in all light conditions tested (W, B, R, and FR) (Figure S4). These results suggest that *CSU6-GFP* transgene complements the abnormal hypocotyl phenotypes of *csu6* both in the dark and light, and further demonstrate that CSU6 promotes hypocotyl growth in the dark, but represses hypocotyl elongation in the light.

Transcriptomic analysis of CSU6-regulated genes

To explore the molecular roles for CSU6 in promoting photomorphogenesis, we performed RNA sequencing analysis using Col-0 and *csu6-2* seedlings grown in W light for 5 d. There were 97% sequenced reads that uniquely mapped to the TAIR10 reference genome for each sample (Table S1). Pearson correlation analysis showed high gene expression correlation in biological replicates for each condition (Table S2). The results showed that CSU6 may regulate 1 144 gene expressions, among which 406 were negatively, and 738 were positively controlled by CSU6 (Figure 4A; Tables S3, S4). Functional enrichment analysis of these differentially expressed genes in biological processes showed them enriched in photosynthesis, protein–chromophore linkage, response to light stimulus, response to light radiation and response to low light intensity stimulus (Figure 4B). Among these differentially expressed genes, the transcription of two growth-promoting factors *PIF4* and *PIF5* were significantly increased in *csu6-2*, indicating that CSU6 inhibits the expression of *PIF4* and *PIF5* (Figure 4C, D).

CSU6 represses the transcription of *PIF4* and *PIF5* in the morning

PIF4 and *PIF5* are two critical growth-promoting factors and their transcript levels were diurnally regulated (Nusinow et al., 2011; Pham et al., 2018a). We next employed real-time quantitative polymerase chain reaction (qPCR) assays to investigate the expression patterns of *PIF4* and *PIF5* in Col-0,

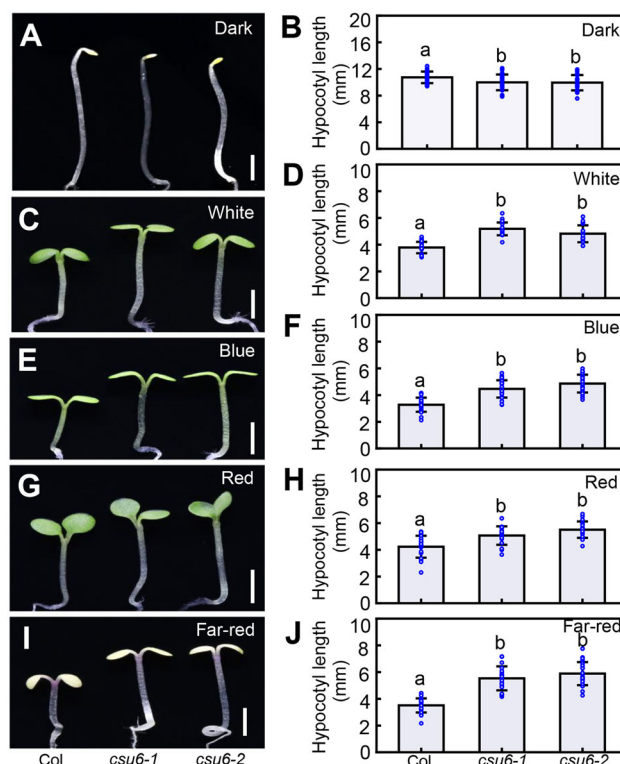


Figure 3. The *csu6* seedlings are hyposensitive to light

(A–J) Hypocotyl phenotypes and length of Columbia (Col), *csu6-1*, and *csu6-2* seedlings grown in darkness (A, B), white ($10.89 \mu\text{mol}/\text{m}^2/\text{s}$) (C, D), blue ($1.80 \mu\text{mol}/\text{m}^2/\text{s}$) (E, F), red ($41.75 \mu\text{mol}/\text{m}^2/\text{s}$) (G, H) and far-red light ($4.31 \mu\text{mol}/\text{m}^2/\text{s}$) (I, J) light conditions for 4 d. Bars, 2 mm. Error bars represent SD ($n \geq 18$). Letters above the bars indicate significant differences ($P < 0.05$) as determined by one-way analysis of variance with Tukey's post-hoc analysis.

csu6-1 and *csu6-2* grown in long-d (16 h light/8 h dark) conditions. The expression of *PIF4* was significantly increased in *csu6-1* and *csu6-2* at zeitgeber time (ZT) 8 and ZT12 (predominantly at ZT8) (Figure 5A). The *PIF5* transcript level was elevated in *csu6-1* and *csu6-2* specifically at ZT8 (Figure 5B). These data indicate that CSU6 negatively regulates *PIF4* and *PIF5* expression specifically in the morning. When we transiently co-expressed 35S:CSU6 with *PIF4pro::LUC* or *PIF5pro::LUC* reporters in *Nicotiana benthamiana* leaves, the relative luciferase (LUC) activity was significantly decreased compared with the internal control (Figure 5C, D), supporting the notion that CSU6 represses the transcription of *PIF4* and *PIF5*. We next performed chromatin immunoprecipitation (ChIP)-qPCR experiments using Col-0 and *CSU6pro::CSU6-GFP csu6-1* transgenic plants. As shown in Figure 5F and 5G, CSU6 associated with the promoter regions of *PIF4* and *PIF5*. Together, these data suggest that CSU6 binds to the *PIF4* and *PIF5* promoters to repress their transcription in the morning.

CSU6 interacts with PIF4 and PIF5

Next, we performed bimolecular fluorescence complementation (BiFC) assays to explore whether CSU6 interacts with PIF4 or PIF5. Strong YFP signals were observed when transiently co-expressed PIF4-YFPⁿ with CSU6-YFP^c or PIF5-YFPⁿ with CSU6-YFP^c in *Arabidopsis* protoplasts.

However, YFP signals were not detectable when transiently co-expressed with negative controls as indicated (Figure 6A). In agreement, strong LUC signals were produced when we transiently co-expressed cLUC-CSU6 with PIF4-nLUC or cLUC-CSU6 with PIF5-nLUC in *Nicotiana benthamiana* leaves. The various negative controls as indicated when transiently co-expressed in *Nicotiana benthamiana* leaves were not able to produce any detectable LUC activity (Figure 6B, C). We further carried out a pull-down assay using recombinant His-CSU6 and PIF4-myc or PIF5-myc transgenic plants. His-CSU6 could pull down the PIF4-myc or PIF5-myc proteins when incubated with cell extracts from PIF4-myc or PIF5-myc seedlings as detected by immunoblot analysis (Figure 6D, E). Together, these data demonstrate that CSU6 physically interacts with PIF4 and PIF5 *in planta*.

CSU6 represses PIF4 and PIF5 activity and the transcription of their target genes

To investigate the biological significance of CSU6-PIF4 or CSU6-PIF5 interactions, we sought to examine whether CSU6 has any effects on PIF4 and PIF5 activity. *IAA19* and *SAUR19* are directly activated by PIF4 and PIF5 (Sun et al., 2012, 2013). Consistent with previous studies, PIF4 and PIF5 could activate the *IAA19pro::LUC* or *SAUR19pro::LUC* reporters. CSU6 did not have any effects on these two reporters. The activation of PIF4 and PIF5 on these reporters

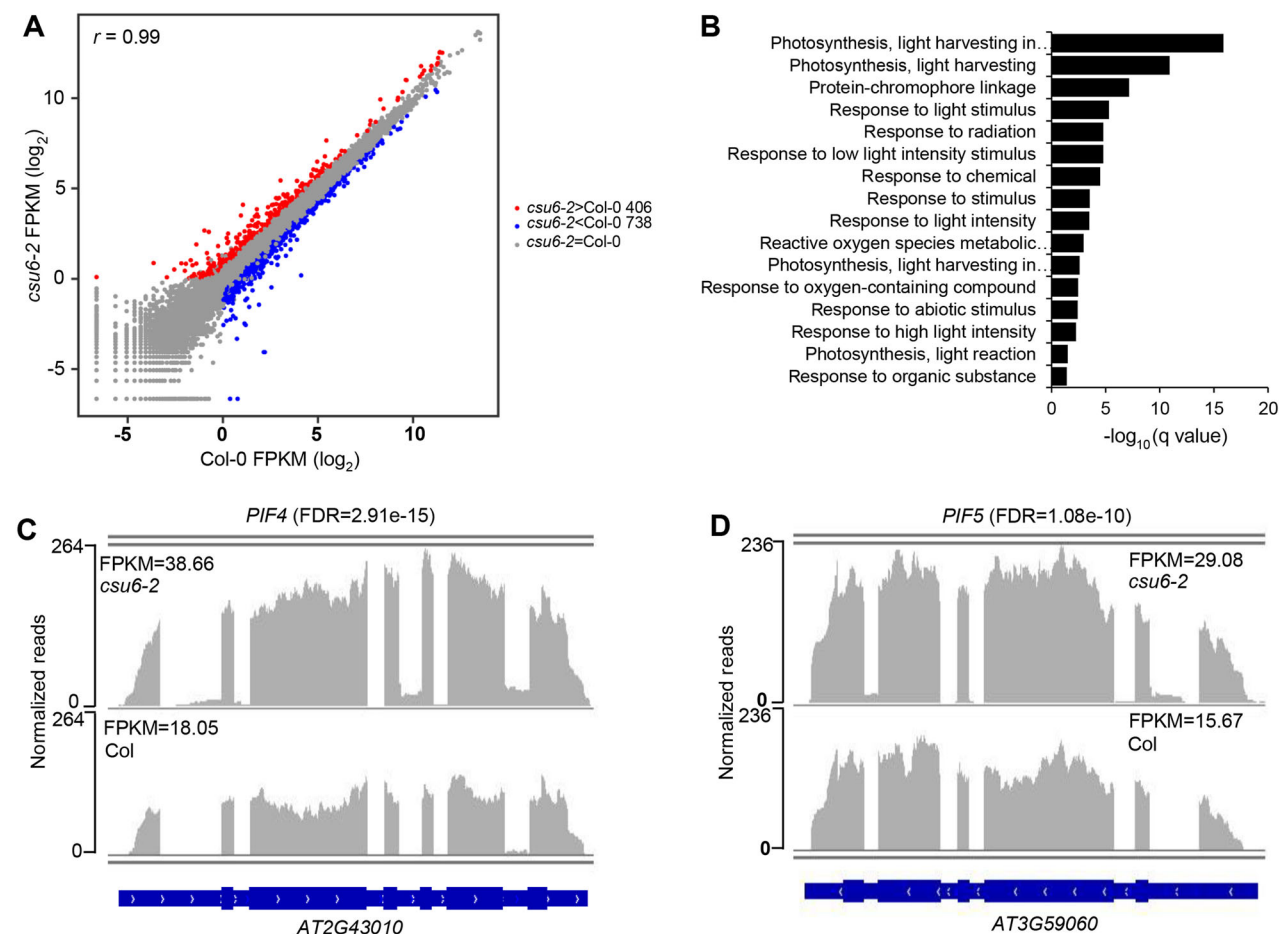


Figure 4. Global analysis of genes regulated by CONSTITUTIVELY PHOTOMORPHOGENIC 1 SUPPRESSOR 6 (CSU6) in *Arabidopsis* (A) Correlation between the transcriptomes of Columbia-0 (Col-0) and *csu6-2*. Pearson's correlation coefficient r is shown in each scatterplot. FPKM, fragments per kilobase million. (B) Top 16 Gene Ontology (GO) term enrichments (biological process aspect) for significantly changed genes in *csu6-2*. (C, D) Gene expression analysis of *PIF4* (C) and *PIF5* (D) in Col and *csu6-2* mutant seedlings.

were significantly reduced in the presence of CSU6 in the same experimental setting (Figure 7A–C), suggesting that CSU6 represses the PIF4 and PIF5 transcriptional activation activity toward their target genes. To further validate these results, we examined the transcription of *IAA19* and *SAUR19* as well as the other nine PIF4- and PIF5-controlled genes in Col-0, *csu6-1* and *csu6-2*. The transcript levels of all these genes tested were significantly increased in *csu6-1* and *csu6-2* (Figures 7D, S5), suggesting that CSU6 represses the transcription of these PIF4 and PIF5 target genes.

CSU6 acts upstream of PIF4 and PIF5

We next examined the genetic interactions between CSU6 and PIF4 or PIF5. Consistent with previous studies, the *pif4-2*, *pif5-3* and *pif4-2 pif5-3* mutant exhibited shorter hypocotyls as compared with wild-type (WT) in W and R light conditions (Figure 8A–D). The hypocotyl length of *csu6-2 pif4-2* were similar with that of *pif4-2*. *csu6-2 pif5-3* displayed intermediate hypocotyls, longer than *pif5-3*, but shorter than *csu6-2*. The *csu6-2 pif4-2 pif5-3* triple mutant seedlings were slightly longer than *pif4-2 pif5-3* in the W and R light

(Figure 8A–D). All these data suggest that PIF4 and PIF5 act genetically downstream of CSU6 with respect to hypocotyl growth in the light.

DISCUSSION

Skotomorphogenesis is an essential and indispensable developmental process that ensures a buried seed penetrates soil to reach light and then initiate photomorphogenesis. COP1, PIF4, and PIF5 are key repressors of light signaling, acting downstream of various photoreceptors. All of them promote skotomorphogenesis and inhibit photomorphogenesis. COP1 is an E3 ubiquitin ligase that targets a group of photomorphogenesis-promoting factors for ubiquitination and degradation, but stabilizes PIF4 and PIF5 (Han et al., 2020). PIF4 and PIF5 are enriched in the nucleus where they regulate a burst of target gene expressions in darkness (Paik et al., 2017; Pham et al., 2018a). Light inactivates the action of COP1, PIF4, and PIF5 through distinct regulatory mechanisms to promote

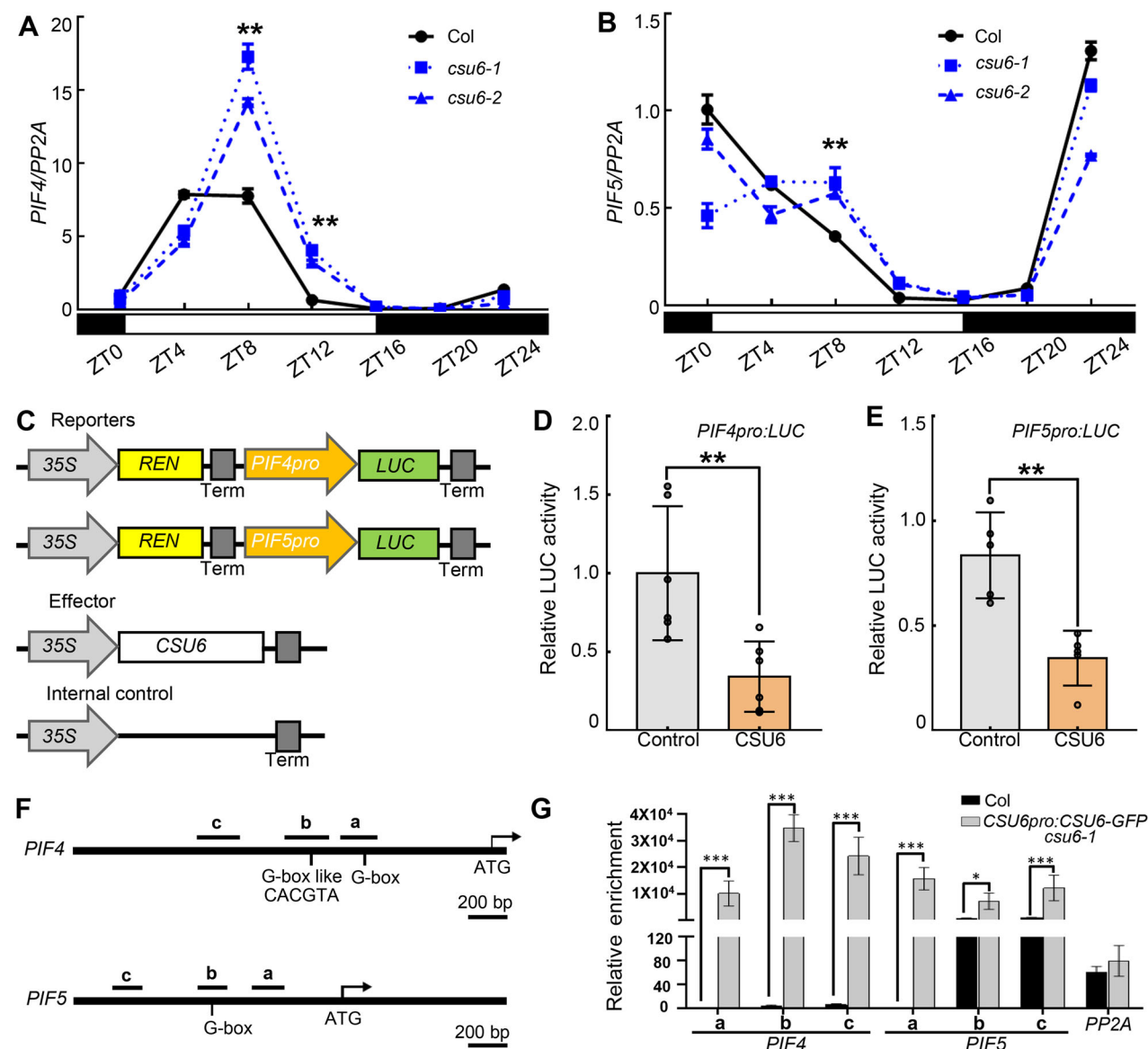


Figure 5. CONSTITUTIVELY PHOTOMORPHOGENIC 1 SUPPRESSOR 6 (CSU6) binds to *PIF4* and *PIF5* promoters and represses their transcription in the morning

(A, B) Real-time quantitative polymerase chain reaction (qPCR) analysis of *PIF4* and *PIF5* transcript levels in Columbia (Col), *csu6-1* and *csu6-2* seedlings grown under long-d conditions (16 h light/8 h dark) for 5 d. Error bars represent SD ($n = 3$). Asterisks indicate significant differences (** $P < 0.01$), as determined by two-tailed Student's *t*-test. (C) Schematic representation of constructs used for the transient transfection assay in *Nicotiana benthamiana* leaves. The *PIF4* and *PIF5* promoters were separately fused to the firefly luciferase (LUC) gene to create the reporter constructs. (D, E) Transient dual-LUC assay showing that *CSU6* represses the transcription of *PIF4pro::LUC* and *PIF5pro::LUC* reporters in *Nicotiana benthamiana* leaves. Error bars represent SD ($n \geq 5$). Asterisks indicate significant differences (** $P < 0.01$), as determined by two-tailed Student's *t*-test. (F) Diagram of the promoter structure of *PIF4* and *PIF5* with the fragments used for chromatin immunoprecipitation (ChIP)-qPCR. The positions of the fragments are shown. (G) ChIP-qPCR assays showing that *CSU6* associates with the *PIF4* and *PIF5* promoters *in vivo*. The 7-d-old Col and *CSU6pro::CSU6-GFP csu6-2* seedlings were used for ChIP assays. Chromatin fragments were immunoprecipitated using green fluorescent protein (GFP)-Trap and analyzed by qPCR. The *PP2A* gene was used as the negative control. Error bars represent SD ($n = 3$). Asterisks indicate significant differences (* $P < 0.05$, *** $P < 0.001$), as determined by two-tailed Student's *t*-test.

photomorphogenesis (Paik et al., 2017; Pham et al., 2018a; Han et al., 2020; Cheng et al., 2021). In this study, we report that *CSU6* promotes hypocotyl elongation in the dark, but inhibits hypocotyl growth in the light. *CSU6* associated with the promoter regions of *PIF4* and *PIF5* and inhibited their transcription. On the other hand, *CSU6* interacted with *PIF4* and *PIF5* to repress their transcriptional

activation activity toward target genes. *CSU6* thus negatively controlled the expression of the *PIF4*- and *PIF5*-regulated genes and promoted light-inhibition of hypocotyl growth. *PIF4* itself can associate with its own promoter and activate its own expression (Zhai et al., 2020). Hence *CSU6* might impair the *PIF4* transcriptional activation activity toward its own promoter in the light.

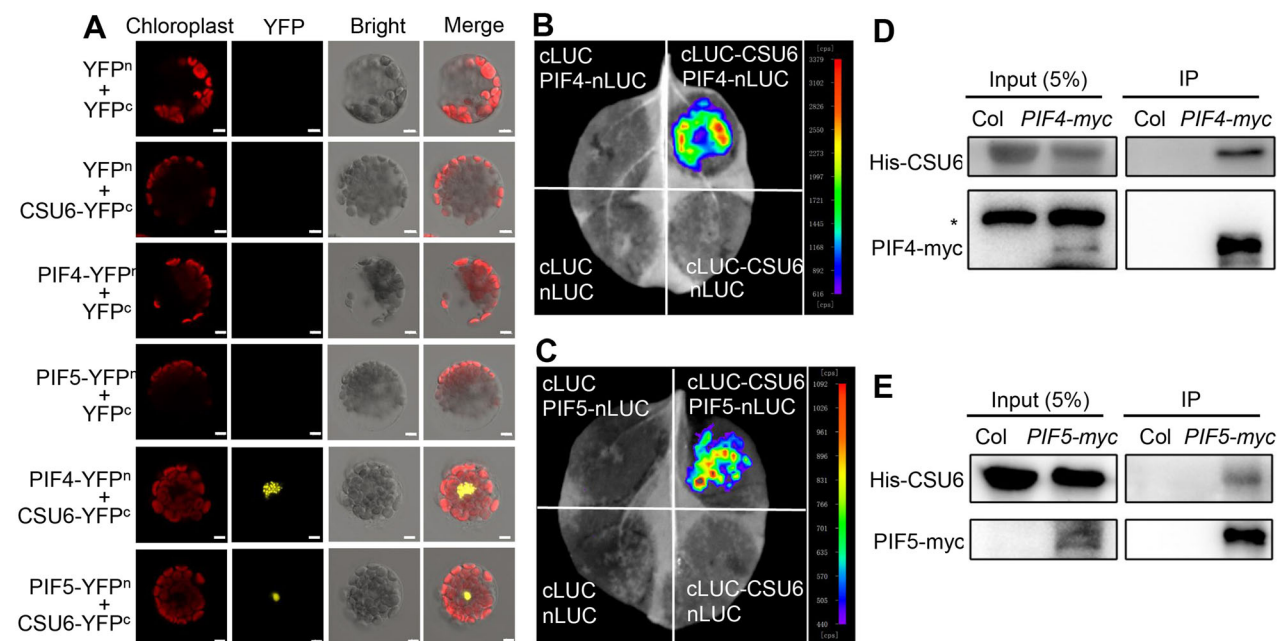


Figure 6. CONSTITUTIVELY PHOTOMORPHOGENIC 1 SUPPRESSOR 6 (CSU6) physically interacts with PHYTOCHROME INTERACTING FACTOR 4 (PIF4) and PIF5

(A) Bimolecular fluorescence complementation (BiFC) assays showing that CSU6 interacts with PIF4 and PIF5 in *Arabidopsis* protoplast. Full-length of PIF4 or PIF5 was fused to N-terminal fragment of yellow fluorescent protein (YFPⁿ), and CSU6 was fused to C-terminal fragment of YFP (YFP^c). Unfused YFPⁿ and YFP^c fragments served as negative controls. Scale bars, 5 μ m. **(B, C)** Luciferase (LUC) complementation imaging assays showing that CSU6 interacts with PIF4 and PIF5 in *Nicotiana benthamiana* leaves. The C-terminal half of firefly LUC (cLUC) was fused to CSU6 and PIF4 or PIF5 was fused to the N-terminal half of firefly LUC (nLUC). **(D, E)** Semi-*in vivo* pull-down assays of PIF4 and PIF5 with CSU6. Total plant proteins were extracted from 4-d-old Columbia (Col), *PIF4-myc* and *PIF5-myc* transgenic seedlings grown in darkness. The immunoprecipitates were detected using anti-His and anti-myc antibodies, respectively. The asterisk indicates a non-specific band.

COP1 is a central repressor of light signaling. Loss of COP1 function displays constitutively photomorphogenic development in darkness. A forward genetic screen has been performed to uncover the mutants that rescue *cop1-6* phenotype. Six recessive *cop1-6* suppressors (CSU1–CSU6) have been successfully recovered from this genetic screen (Xu et al., 2014, 2015; Lin et al., 2017; Zhao et al., 2018; Zhou et al., 2022; this study). Among these, CSU4 and CSU6 promote the photomorphogenesis by modulating PIF4 and/or PIF5 action. CSU4 inhibits the *PIF4* transcript level in the early evening (Zhao et al., 2018), and CSU6 repressed *PIF4* and *PIF5* in the morning (Figure 4A, B). In addition, CSU6 negatively affected the PIF4 and PIF5 biochemical activity (Figure 7A–C). Therefore, CSU4 and CSU6 may work in concert to modulate PIF4 and/or PIF5 signaling and gate the hypocotyl growth under diurnal conditions. However, the exact molecular interconnections between CSU4 and CSU6 await further detailed investigation. Overexpression of *PIF4* or *PIF5* in *cop1* mutant background partially suppressed the short hypocotyl phenotypes (Zhao et al., 2018; Pham et al., 2018b). Considering that CSU6 negatively controls the PIF4 and PIF5 action (Figures 4A, B, 7A–C), the suppression of *cop1-6* in the *csu6* mutants likely, at least partially, resulted from the increased PIF4 and PIF5 action.

PIF4 and PIF5 are growth-promoting factors that directly bind to the promoter regions of multiple auxin

biosynthetic and signaling-related genes to activate their transcription, thus leading to cell elongation and hypocotyl growth (Sun et al., 2012, 2013; Paik et al., 2017; Pham et al., 2018a). The external signals such as light, shade and warm temperature and internal cues like the circadian clock tightly control PIF4 and PIF5 at the transcriptional and protein levels (Paik et al., 2017; Pham et al., 2018a). Light triggers the degradation of PIF4 and PIF5, while shade and warm temperature promote their accumulation in the plant cells (Casal, 2013; Cheng et al., 2021). In addition, multiple components of the circadian clock modulate the *PIF4* and/or *PIF5* transcript levels at different time points under diurnal conditions (Zhang et al., 2021). The morning complex CCA1-LHY up-regulates the transcription of *PIF4* to promote hypocotyl growth during the day (Niwa et al., 2009; Lu et al., 2012). The evening complex ELF3-ELF4-LUX represses *PIF4* and *PIF5* expression to inhibit hypocotyl growth in the evening (Nusinow et al., 2011). ELF3 and TOC1 repress PIF4 activity through direct protein-protein interactions (Nieto et al., 2015; Zhu et al., 2016). CSU6 not only negatively regulated *PIF4* and *PIF5* transcription specifically in the morning (Figure 5A, B), but also interacted with PIF4 and PIF5 to repress their biochemical activity (Figures 6, 7A–C), suggesting that CSU6 plays a critical role in gating diurnal regulation of hypocotyl growth probably through suppression of PIF4 and PIF5

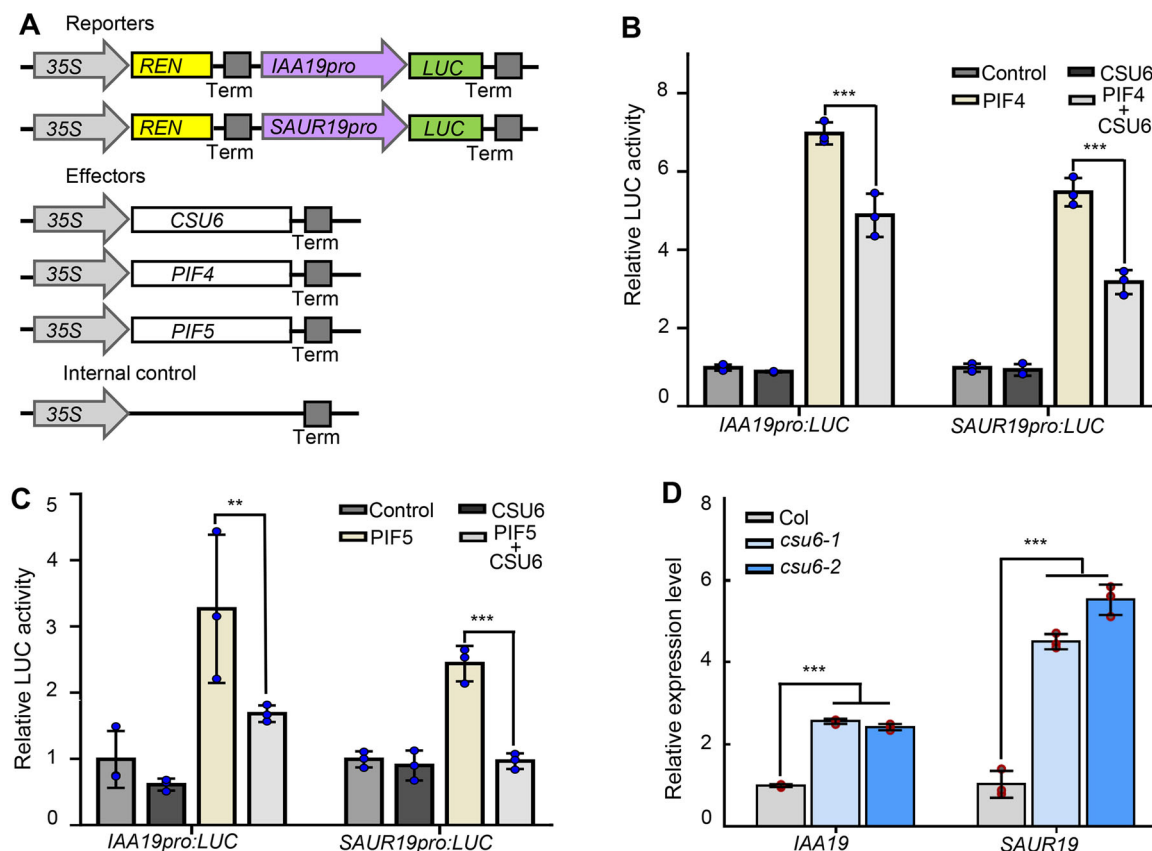


Figure 7. CONSTITUTIVELY PHOTOMORPHOGENIC 1 SUPPRESSOR 6 (CSU6) represses the transcriptional activity of PHYTOCHROME INTERACTING FACTOR 4 (PIF4) and PIF5 toward target genes

(A) Schematic representation of constructs used for the transient transfection assay in *Arabidopsis* protoplasts. The *IAA19* and *SAUR19* promoters were separately fused to the firefly luciferase (LUC) gene to create the reporter constructs. For the effector constructs, *CSU6*, *PIF4* and *PIF5* were driven by 35S promoter. (B, C) Transient dual-LUC assay showing that *CSU6* represses the transcriptional activation activity of *PIF4* or *PIF5* on *IAA19pro::LUC* and *SAUR19pro::LUC* reporters. Error bars represent SD ($n = 3$). Asterisks indicate significant differences (** $P < 0.01$, *** $P < 0.001$), as determined by two-tailed Student's *t*-test.

action in the morning. It has been documented that *PIF4* and *PIF5* promote shade avoidance or thermomorphogenesis under shade or warm temperature conditions (Hornitschek et al., 2009; Sun et al., 2012; Jung et al., 2016; Legris et al., 2016). However, whether *CSU6* is also involved in these two physiological and developmental processes needs additional detailed analysis. Nevertheless, *CSU6*-*PIF4* and *PIF5* regulatory modules may represent a key signaling hub linking light and circadian rhythm to the control of seedling development. *CSU6* exerted opposite roles in the regulation of hypocotyl growth in the dark and light. *CSU6* promoted hypocotyl elongation in the dark, whereas it represses hypocotyl growth in various light conditions tested (Figure 3). Our studies revealed that *CSU6* negatively controlled the transcription and biochemical activity of *PIF4* and *PIF5* to inhibit hypocotyl elongation in the light (Figures 4–6). However, the exact molecular basis for *CSU6* promoting hypocotyl growth in the dark still remains obscure and requires further biochemical and genetic studies.

Collectively, *CSU6* promotes light-inhibited hypocotyl growth through *PIF4*- and *PIF5*-mediated signaling. *CSU6* associates with the *PIF4* and *PIF5* promoters to inhibit their expression in the morning. On the other hand, *CSU6* interacts with *PIF4* and *PIF5* to repress their transcriptional activation activity toward target genes. Consequently, these molecular regulatory events result in the repression of numerous *PIF4*- and *PIF5*-controlled genes and hence inhibition of hypocotyl growth in the light (Figure 8E). *CSU6* may ensure a precise and delicate control of *PIF4* and *PIF5* action to enable plants to respond rapidly and properly to their surrounding changing light conditions.

MATERIALS AND METHODS

Plant materials and growth conditions

The *Arabidopsis thaliana* *cop1-6* (McNelli et al., 1994), *csu6-1* *cop1-6*, *csu6-1*, *csu6-2*, *pi4-2* (Leivar et al., 2008), *pi5-3* (Khanna et al., 2007), *pi4-2 pi5-3* (Nozue et al., 2007) mutants, *proCSU6*: *CSU6*-GFP *csu6-1* and *proCSU6*: *CSU6*-GFP *csu6-2* transgenic lines were all in the Col-0 ecotype. The *csu6-1* *cop1-6* double

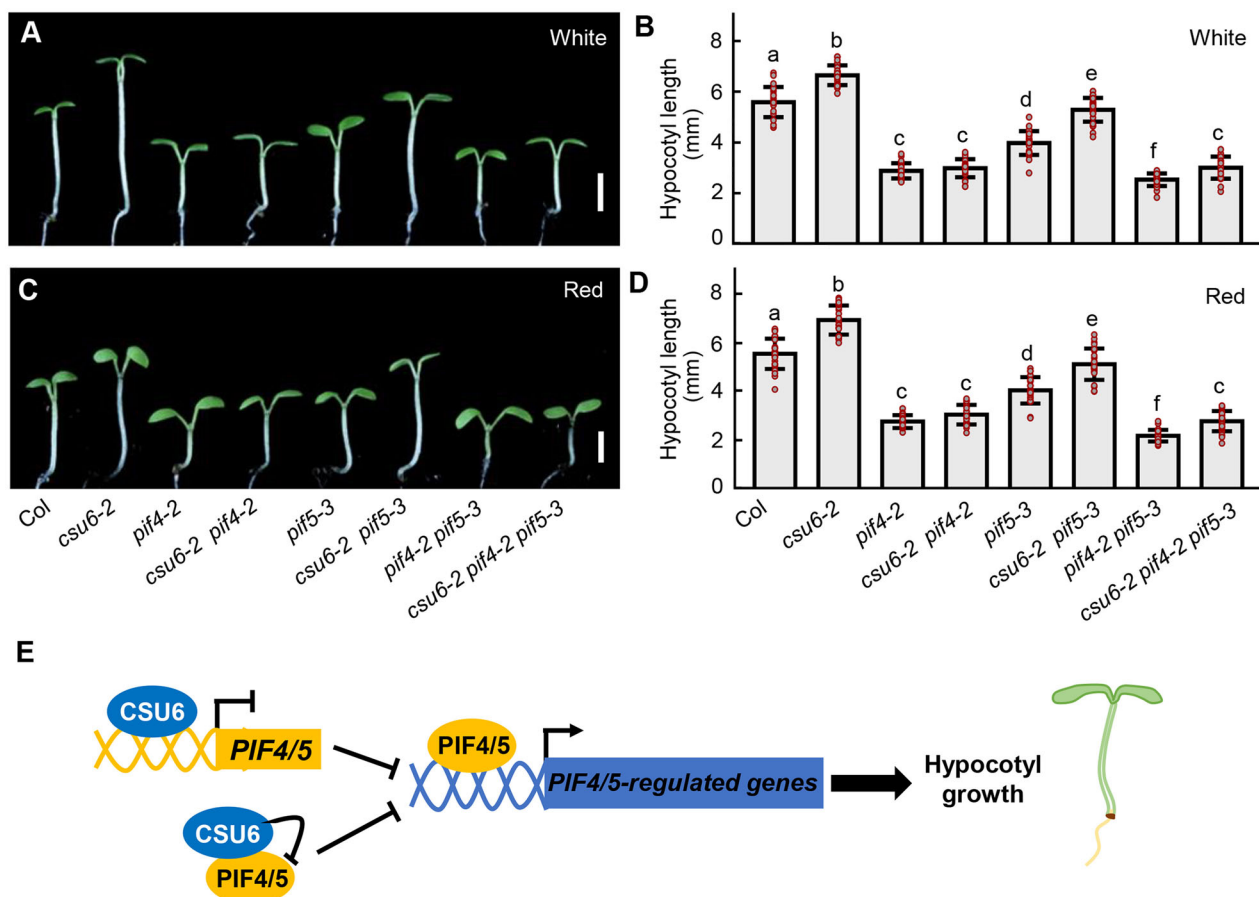


Figure 8. CONSTITUTIVELY PHOTOMORPHOGENIC 1 SUPPRESSOR 6 (CSU6) genetically acts upstream of PHYTOCHROME INTERACTING FACTOR 4 (PIF4) and PIF5

(A–D) Hypocotyl phenotypes and lengths of Columbia (Col), *csu6-2*, *pif4-2*, *csu6-2 pif4-2*, *pif5-3*, *csu6-2 pif5-3*, *pif4-2 pif5-3* and *csu6-2 pif4-2 pif5-3* seedlings grown in white ($10.89 \mu\text{mol}/\text{m}^2/\text{s}$) (A, B) and red ($113.30 \mu\text{mol}/\text{m}^2/\text{s}$) (C, D) light conditions for 4 d. Bars, 2 mm. Error bars represent SD ($n \geq 20$). Letters above the bars indicate significant differences ($P < 0.05$) as determined by one-way analysis of variance with Tukey's post-hoc analysis. (E) A working model depicting how CSU6 promotes photomorphogenesis in *Arabidopsis*. On one hand, CSU6 associates with the promoter regions of *PIF4* and *PIF5* to repress their transcription. On the other hand, CSU6 interacts with PIF4 and PIF5 to repress their transcriptional activation activity toward target genes, consequently inhibiting hypocotyl elongation.

mutant was obtained from the suppressors screening of *cop1-6* seeds mutagenized with ethyl methanesulfonate (EMS). The *csu6-1* mutant was isolated from the F_2 population of *csu6-1 cop1-6* crossed with Col-0. The *csu6-2* mutant (SALK_030445) was obtained from the *Arabidopsis* Biological Resource Center (ABRC) and homozygous plants were identified by PCR-based genotyping. The *csu6-2 cop1-6*, *csu6-2 pif4-2*, *csu6-2 pif5-3* and *csu6-2 pif4-2 pif5-3* mutants were generated by genetic crossing. *Arabidopsis* seeds were grown on 1× Murashige and Skoog (MS) medium supplemented with 1% sucrose and 0.8% agar. After stratification in darkness at 4°C for 3 d, seeds were transferred to light chambers (PERCIVAL) maintained at 22°C.

Map-based cloning of CSU6

The *csu6-1* mutation was identified as previously described (Zhao et al., 2018; Zhou et al., 2022). Briefly, the F_2 mapping population was constructed from a cross between *csu6-1 cop1-6* mutant (Col-0 background) and Landsberg with a *cop1-6*

mutation. Suppressor seedlings with longer hypocotyls from F_2 population were selected for mapping. The markers used for mapping were designed based on the *Arabidopsis* Mapping Platform (<http://amp.genomics.org.cn>) and the standards previously described (Jander et al., 2002). The *csu6-1* mutation was mapped to an interval between the markers 3-AC009325-0089 and 3-AC022287-0495 on chromosome 3. The candidate gene was further identified by SOLiD sequencing as previously described (Zhao et al., 2018; Zhou et al., 2022).

Measurement of hypocotyl length

For hypocotyl measurement, surface-sterilized seeds were sown on 1×MS plates and stratified in darkness at 4°C for 3 d. After exposition to continuous white light for 8 h at 22°C to induce uniform germination, the seeds were then transferred to dark or different light conditions and incubated at 22°C for 4 d. The hypocotyl length of seedlings was measured using ImageJ software.

Plasmid construction

To generate constructs for genomic complementation test, the full-length of *CSU6* coding sequence was cloned into the *pDONR-223* vector (Invitrogen) and introduced into the *pEarley Gateway 203* and *pEarley Gateway 104* binary vectors (Earley et al., 2006) to produce *35S::myc-CSU6* and *35S::YFP-CSU6* constructs, using Gateway LR Clonase enzyme mix (Invitrogen). For BiFC assay, the coding sequences of *PIF4* and *PIF5* were cloned into the *XbaI/BamHI* sites of *pUC-SPYNE* vector to generate *pUC-SPYNE-PIF4* and *pUC-SPYNE-PIF5* constructs. The *CSU6* coding sequence was cloned into the *XbaI/BamHI* sites of *pUC-SPYCE* vector to generate *pUC-SPYCE-CSU6* construct. For LUC complementation imaging assay, the coding sequences of *PIF4* and *PIF5* were cloned into the *KpnI/SalI* sites of *pCAMBIA1300-nLUC* vector and the coding sequence of *CSU6* were cloned into the *KpnI/SalI* sites of *pCAMBIA1300-cLUC* vector to generate the corresponding constructs. For the transient expression assay, the promoters of *PIF4*, *PIF5*, *IAA19* and *SAUR19* were amplified and cloned into the *KpnI/NcoI* sites of *pGreen0800II-LUC* vector to generate the *pGreen0800II-proPIF4:LUC*, *pGreen0800II-proPIF5:LUC*, *pGreen0800II-proIAA19:LUC* and *pGreen0800II-proSAUR19:LUC* constructs. The coding sequences of *CSU6*, *PIF4* and *PIF5* were cloned into the *XbaI/KpnI* sites of *pGreenII 62-SK* vector to generate *pGreenII 62-SK-CSU6*, *pGreenII 62-SK-PIF4* and *pGreenII 62-SK-PIF5* effector constructs. To generate *proCSU6::CSU6-GFP* construct, the *CSU6* promoter, *CSU6* coding sequence, *GFP* gene sequence and *CSU6* terminator were ligated into the *pCAMBIA1300* vector at the *EcoRI/PstI* sites.

Plant transformation

The *35S::myc-CSU6*, *35S::YFP-CSU6* and *proCSU6::CSU6-GFP* constructs were transformed into *Agrobacterium tumefaciens* strain GV3101 by the freeze-thaw method. All the transgenic plants were generated by floral dip method (Clough and Bent, 1998). The *35S::myc-CSU6* and *35S::YFP-CSU6* were transformed into *csu6-1 cop1-6* background to obtain *35S::myc-CSU6 csu6-1 cop1-6* and *35S::YFP-CSU6 csu6-1 cop1-6* plants. The *proCSU6::CSU6-GFP* was transformed into *csu6-1* background to obtain *proCSU6::CSU6-GFP csu6-1* plants. Homozygous lines were used for genetic and biochemical studies. The primers used for plasmids construction are listed in Table S5.

Real-time qPCR

Total RNA was extracted from 5-d-old *Arabidopsis* seedlings grown on 1× MS plates using Plant RNA Kit (Omega). For the circadian experiments, seedlings were collected every 4 h under the 16 h light (10.89 μmol/m²/s)/8 h dark photoperiod conditions. The complementary DNA (cDNA) synthesis reactions were performed with 5× All-In-One RT Master Mix (Applied Biological Materials) according to the manufacturer's instructions. Real-time qPCR was performed using a Step One Plus Real-Time PCR detection system (Applied

Biosystems) and SYBR Green Master Mix (Yeasen), following the manufacturer's instructions. Each experiment was performed with three biological replicates, and each sample was analyzed in triplicate. The gene expression levels were normalized to the internal control *PP2A* gene. The primers used in the qRT-PCR analyses are listed in Table S5.

RNA sequencing

Total RNA was extracted and processed following standard protocols of the Novogene Company for preparing Illumina RNA-Seq libraries. Paired-end sequencing was then performed to generate 150 bp paired-end reads on three independent biological replicates. RNA-seq reads were then cleaned and mapped to the TAIR10 genome using Hisat2 with default parameter (Kim et al., 2015). Differential expression was subsequently assessed using the R/Bioconductor package limma (v.3.0.8) (Ritchie et al., 2015). Genes with a false discovery rate <0.05 and a fold change >1.5 were considered differentially expressed. The functional enrichment analysis of differentially expressed genes were conducted by g:Profiler (Raudvere et al., 2019), with adjusted *P*-values <0.05 considered statistically significant.

Bimolecular fluorescence complementation assay

The *pUC-SPYNE-PIF4*, *pUC-SPYNE-PIF5* and *pUC-SPYCE-CSU6* plasmids were co-transformed into *Arabidopsis* protoplasts as desired combinations according to the detailed method previously described (Yoo et al., 2007). After incubation in darkness at 22°C for 16 h, the YFP fluorescence signals were observed under a confocal laser scanning microscope (LSM510 Meta; Carl Zeiss, Germany). YFP fluorescence was excited by a 514-nm laser and detected between 517 and 589 nm.

Firefly LUC complementation assay

The firefly LUC complementation assay in *Nicotiana benthamiana* leaves was performed as previously described (Chen et al., 2008). Briefly, *Agrobacterium tumefaciens* strain GV3101 cells harboring *pCAMBIA1300-cLUC-CSU6* or *pCAMBIA1300-PIF4/5-nLUC* constructs were co-infiltrated into *Nicotiana benthamiana* leaves as indicated pairs. The corresponding empty vector *pCAMBIA1300-cLUC* or *pCAMBIA1300-nLUC* was infiltrated as a negative control. After infiltration, plants were incubated under long-d conditions (16 h light/8 h dark) for 3 d, the leaves were sprayed with 1 mmol/L D-luciferin (Sigma) and the LUC luminescence was examined using Night SHADE LB985 imaging system (Berthod, Germany).

Transient LUC expression assay

Arabidopsis mesophyll cell protoplasts were prepared and transfected according to the detailed method previously described (Yoo et al., 2007). For the transient transcriptional activity assay, the promoter-reporters used were *pGreen0800II-proPIF4:LUC*, *pGreen0800II-proPIF5:LUC*, *pGreen0800II-proIAA19:LUC* and *pGreen0800II-proSAUR19:LUC*. *pGreenII 62-SK-CSU6*, *pGreenII 62-SK-PIF4* and

pGreenII 62-SK-PIF5 were used as effectors. The reporters and effectors were transformed into *Arabidopsis* protoplasts in different combinations and incubated in darkness at 22°C for 16 h. Firefly LUC and Renilla LUC (Ren) were detected using the Dual-LUC Reporter Assay System (Promega), according to the manufacturer's instructions. Ren driven by a cauliflower mosaic virus 35S promoter was used as an internal control. The relative activity was expressed as the LUC/Ren ratios.

Immunoblot analysis

Total proteins were extracted from 5-d-old *Arabidopsis* seedlings with protein extraction buffer (100 mmol/L NaH₂PO₄, 10 mmol/L Tris-HCl, pH 8.0, 200 mmol/L NaCl, 8 M urea, 1 mmol/L phenylmethylsulfonyl fluoride and 1× complete protease inhibitor cocktail). The protein samples were added with 5× sodium dodecyl sulfate (SDS) loading buffer, and boiled at 100°C for 3 min. After separation by 10% (w/v) SDS-polyacrylamide gel electrophoresis, the protein abundance of CSU6-GFP was detected using anti-GFP antibody (Abmart). Anti-Actin (Sigma-Aldrich) was used as an internal control.

Semi-in vivo pull-down assays

Total proteins of Col-0, *PIF4-myc* or *PIF5-myc* seedlings were extracted using the lysis buffer (25 mmol/L Tris-HCl (pH 7.5), 150 mmol/L NaCl, 1 mmol/L ethylenediaminetetraacetic acid (EDTA), 10% glycerol, 0.1% Tween-20); 8 µg freshly purified His-CSU6 was mixed with 200 µg total proteins of Col, *PIF4-myc* and *PIF5-myc* respectively, for 4 h; 10 µL Myc-trap beads were added in and incubated with the mixture for an additional 2 h at 4°C. Beads were then washed three times with 25 column volumes of washing buffer (25 mmol/L Tris-Cl (pH 7.5), 300 mmol/L NaCl, 1 mM EDTA, 10% glycerol). Finally, the beads were heated in 1× SDS loading buffer at 100°C for 5 min. The eluted proteins were then analyzed by immuno-blotting using anti-GFP, anti-myc and anti-Actin antibodies.

Chromatin immunoprecipitation

The ChIP assay was performed as previously described (Zhu et al., 2020). Briefly, protein–chromatin complexes were isolated from 2 g seedlings grown in the light. The chromatin solution was sonicated and then pre-cleared by incubation of binding control agarose beads (ChromoTek). After that, the protein–chromatin complexes were immunoprecipitated with GFP-trap agarose beads (ChromoTek). DNA fragments were recovered by reversal of cross-linking and used to perform RT-qPCR. Values of ChIP were normalized to those of input DNA. Primers used in this study are listed in Table S5.

Accession numbers

Sequence data from this article can be found in the *Arabidopsis* Genome Initiative database or the GenBank/European Molecular Biology Laboratory libraries under the following accession numbers: *COP1* (At2g32950); *CSU6* (At3g02860); *PIF4* (At2g43010); *PIF5* (At3g59060). RNA-seq data have

been deposited into the Gene Expression Omnibus with the following accession number GSE201389.

ACKNOWLEDGEMENTS

This work was supported by the National Natural Science Foundation of China (Grant Nos 32100199, 31900210, and 31970258), the Peking-Tsinghua Center for Life Sciences (to X.W.D), the Southern University of Science and Technology (to X.W.D); the Jiangsu Natural Science Foundation for Distinguished Young Scholars (Grant No. BK20211525); the Jiangsu “Innovative and Entrepreneurial Talent” program (to D.X.), the Nanjing Agricultural University (start-up funding to D.X.), and the Jiangsu Collaborative Innovation Center for Modern Crop Production (to D.X.).

CONFLICTS OF INTEREST

The authors declare they have no competing interests.

AUTHOR CONTRIBUTIONS

H.L., Y.H., J.L., M.Z., Y.B., L.C., and Y.J. conducted the experiments. X.W. performed bioinformatic analysis. X.W.D and D.X. designed the experiments. X.W.D. and D.X. analyzed the data. X.W.D and D.X. wrote the article. All authors read and approved of this manuscript.

Edited by: Hongtao Liu, Center for Excellence in Molecular Plant Sciences, Institute of Plant Physiology and Ecology, CAS, China

Received May 29, 2022; **Accepted** Aug. 26, 2022; **Published** Aug. 27, 2022

REFERENCES

- Casal, J.J. (2013). Photoreceptor signaling networks in plant responses to shade. *Annu. Rev. Plant Biol.* **64**: 403–427.
- Chen, H., Zou, Y., Shang, Y., Lin, H., Wang, Y., Cai, R., Tang, X., and Zhou, J. (2008). Firefly luciferase complementation imaging assay for protein-protein interactions in plants. *Plant Physiol.* **146**: 323–324.
- Cheng, M.-C., Kathare, P.K., Paik, I., and Huq, E. (2021). Phytochrome signaling networks. *Annu. Rev. Plant Biol.* **72**: 217–244.
- Clough, S.J., and Bent, A.F. (1998). Floral dip: A simplified method for *Agrobacterium*-mediated transformation of *Arabidopsis thaliana*. *Plant J.* **16**: 735–743.
- Deng, X.W., Caspar, T., and Quail, P.H. (1991). cop1: A regulatory locus involved in light-controlled development and gene expression in *Arabidopsis*. *Genes Dev.* **5**: 1172–1182.
- Deng, X.W., Matsui, M., Wei, N., Wagner, D., Chu, A.M., Feldmann, K. A., and Quail, P.H. (1992). COP1, an *Arabidopsis* regulatory gene, encodes a protein with both a zinc-binding motif and a G beta homologous domain. *Cell* **71**: 791–801.
- Earley, K.W., Haag, J.R., Pontes, O., Opper, K., Juehne, T., Song, K., and Pikaard, C.S. (2006). Gateway-compatible vectors for plant functional genomics and proteomics. *Plant J.* **45**: 616–629.

- Han, X., Huang, X., and Deng, X.W. (2020). The photomorphogenic central repressor COP1: Conservation and functional diversification during evolution. *Plant Commun.* **1**: 100044.
- Hornitschek, P., Lorrain, S., Zoete, V., Michielin, O., and Fankhauser, C. (2009). Inhibition of the shade avoidance response by formation of non-DNA binding bHLH heterodimers. *EMBO J.* **28**: 3893–3902.
- Huq, E., and Quail, P.H. (2002). PIF4, a phytochrome-interacting bHLH factor, functions as a negative regulator of phytochrome B signaling in *Arabidopsis*. *EMBO J.* **21**: 2441–2450.
- Jander, G., Norris, S.R., Rounsley, S.D., Bush, D.F., Levin, I.M., and Last, R.L. (2002). *Arabidopsis* map-based cloning in the post-genome era. *Plant Physiol.* **129**: 440–450.
- Jiao, Y., Lau, O.S., and Deng, X.W. (2007). Light-regulated transcriptional networks in higher plants. *Nat. Rev. Genet.* **8**: 217–230.
- Jung, J.H., Domijan, M., Klose, C., Biswas, S., Ezer, D., Gao, M., Khattak, A.K., Box, M.S., Charoensawan, V., Cortijo, S., Kumar, M., Grant, A., Locke, J.C., Schäfer, E., Jaeger, K.E., and Wigge, P.A. (2016). Phytochromes function as thermosensors in *Arabidopsis*. *Science* **354**: 886–889.
- Khanna, R., Shen, Y., Marion, C.M., Tsuchisaka, A., Theologis, A., Schäfer, E., and Quail, P.H. (2007). The basic helix-loop-helix transcription factor PIF5 acts on ethylene biosynthesis and phytochrome signaling by distinct mechanisms. *Plant Cell* **19**: 3915–3929.
- Kim, D., Langmead, B., and Salzberg, S.L. (2015). HISAT: A fast spliced aligner with low memory requirements. *Nat. Methods* **12**: 357–360.
- Lau, O.S., and Deng, X.W. (2012). The photomorphogenic repressors COP1 and DET1: 20 years later. *Trends Plant Sci.* **17**: 584–593.
- Legris, M., Klose, C., Burgie, E.S., Rojas, C.C., Neme, M., Hiltbrunner, A., Wigge, P.A., Schäfer, E., Vierstra, R.D., and Casal, J.J. (2016). Phytochrome B integrates light and temperature signals in *Arabidopsis*. *Science* **354**: 897–900.
- Leivar, P., Monte, E., Al-Sady, B., Carle, C., Storer, A., Alonso, J.M., Ecker, J.R., and Quail, P.H. (2008a). The *Arabidopsis* phytochrome-interacting factor PIF7, together with PIF3 and PIF4, regulates responses to prolonged red light by modulating phyB levels. *Plant Cell* **20**: 337–352.
- Li, N., Zhang, Y., He, Y., Wang, Y., and Wang, L. (2020). Pseudo response regulators regulate photoperiodic hypocotyl growth by repressing PIF4/5 transcription. *Plant Physiol.* **183**: 686–699.
- Lian, H.L., He, S.B., Zhang, Y.C., Zhu, D.M., Zhang, J.Y., Jia, K.P., Sun, S.X., Li, L., and Yang, H.Q. (2011). Blue-light-dependent interaction of cryptochrome 1 with SPA1 defines a dynamic signaling mechanism. *Genes Dev.* **25**: 1023–1028.
- Lin, F., Xu, D., Jiang, Y., Chen, H., Holm, M., Fan, L., and Deng, X.W. (2017). Phosphorylation and negative regulation of CONSTITUTIVELY PHOTOMORPHOGENICALLY 1 by PINOID in *Arabidopsis*. *Proc. Natl. Acad. Sci. U.S.A.* **114**: 6617–6622.
- Liu, B., Zuo, Z., Liu, H., Liu, X., and Lin, C. (2011). *Arabidopsis* cryptochrome 1 interacts with SPA1 to suppress COP1 activity in response to blue light. *Genes Dev.* **25**: 1029–1034.
- Lu, S.X., Webb, C.J., Knowles, S.M., Kim, S.H., Wang, Z., and Tobin, E. M. (2012). CCA1 and ELF3 interact in the control of hypocotyl length and flowering time in *Arabidopsis*. *Plant Physiol.* **158**: 1079–1088.
- McNelli, T.W., von Arnim, A.G., Araki, T., Komeda, Y., Misera, S., and Deng, X.W. (1994). Genetic and molecular analysis of an allelic series of *cop1* mutants suggests functional roles for the multiple protein domains. *Plant Cell* **6**: 487–500.
- Nieto, C., López-Salmerón, V., Davière, J.M., and Prat, S. (2015). ELF3-PIF4 interaction regulates plant growth independently of the evening complex. *Curr. Biol.* **25**: 187–193.
- Niwa, Y., Yamashino, T., and Mizuno, T. (2009). The circadian clock regulates the photoperiodic response of hypocotyl elongation through a coincidence mechanism in *Arabidopsis thaliana*. *Plant Cell Physiol.* **50**: 838–854.
- Nozue, K., Covington, M., Duek, P., Lorrain, S., Fankhauser, C., Harmer, S., and Maloof, J. (2007). Rhythmic growth explained by coincidence between internal and external cues. *Nature* **448**: 358–361.
- Nusinow, D.A., Helfer, A., Hamilton, E.E., King, J.J., Imaizumi, T., Schultz, T.F., Farré, E.M., and Kay, S.A. (2011). The ELF4-ELF3-LUX complex links the circadian clock to diurnal control of hypocotyl growth. *Nature* **475**: 398–402.
- Paik, I., Kathare, P.K., Kim, J.-I., and Huq, E. (2017). Expanding roles of PIFs in signal integration from multiple processes. *Mol. Plant* **10**: 1035–1046.
- Park, E., Kim, Y., and Choi, G. (2018). Phytochrome B requires PIF degradation and sequestration to induce light responses across a wide range of light conditions. *Plant Cell* **30**: 1277–1292.
- Pham, V.N., Kathare, P.K., and Huq, E. (2018a). Phytochromes and phytochrome interacting factors. *Plant Physiol.* **176**: 1025–1038.
- Pham, V.N., Xu, X., and Huq, E. (2018b). Molecular bases for the constitutive photomorphogenic phenotypes in *Arabidopsis*. *Development* **145**: dev169870.
- Qi, L., Shi, Y., Terzaghi, W., Yang, S., and Li, J. (2022). Integration of light and temperature signaling pathways in plants. *J. Integr. Plant Biol.* **64**: 393–411.
- Ritchie, M.E., Phipson, B., Wu, D., Hu, Y., Law, C.W., Shi, W., and Smyth, G.K. (2015). Limma powers differential expression analyses for RNA-sequencing and microarray studies. *Nucleic Acids Res.* **43**: e47.
- Raudvere, U., Kolberg, L., Kuzmin, I., Arak, T., Adler, P., Peterson, H., and Vilo, J. (2019). g:Profiler: A web server for functional enrichment analysis and conversions of gene lists (2019 update). *Nucleic Acids Res.* **47**: W191–W198.
- Song, Z., Bian, Y., Liu, J., Sun, Y., and Xu, D. (2020). B-box Proteins: Pivotal players in light-mediated development in plants. *J. Integr. Plant Biol.* **62**: 1293–1309.
- Song, Z., Heng, Y., Bian, Y., Deng, X.W., and Xu, D. (2021). BBX11 promotes red light-mediated photomorphogenic development by modulating phyB-PIF4 signaling. *ABIOTECH* **2**: 117–130.
- Sun, J., Qi, L., Li, Y., Chu, J., and Li, C. (2012). PIF4-mediated activation of YUCCA8 expression integrates temperature into the auxin pathway in regulating *Arabidopsis* hypocotyl growth. *PLoS Genet.* **8**: e1002594.
- Sun, J., Qi, L., Li, Y., Zhai, Q., and Li, C. (2013). PIF4 and PIF5 transcription factors link blue light and auxin to regulate the phototropic response in *Arabidopsis*. *Plant Cell* **25**: 2102–2114.
- Sullivan, J.A., and Deng, X.W. (2003). From seed to seed: The role of photoreceptors in *Arabidopsis* development. *Dev. Biol.* **260**: 289–297.
- von Arnim, A.G., and Deng, X.W. (1994). Light inactivation of *Arabidopsis* photomorphogenic repressor COP1 involves a cell-specific regulation of its nucleocytoplasmic partitioning. *Cell* **79**: 1035–1045.
- Xu, D. (2020). COP1 and BBXs-HY5-mediated light signal transduction in plants. *New Phytol.* **228**: 1748–1753.
- Xu, D., Lin, F., Jiang, Y., Huang, X., Li, J., Ling, J., Hettiarachchi, C., Tellgren-Roth, C., Holm, M., and Deng, X.W. (2014). The RING-Finger E3 ubiquitin ligase COP1 SUPPRESSOR1 negatively regulates COP1 abundance in maintaining COP1 homeostasis in dark-grown *Arabidopsis* seedlings. *Plant Cell* **26**: 1981–1991.
- Xu, D., Lin, F., Jiang, Y., Ling, J., Hettiarachchi, C., Tellgren-Roth, C., Holm, M., Wei, N., and Deng, X.W. (2015). *Arabidopsis* COP1 SUPPRESSOR 2 represses COP1 E3 ubiquitin ligase activity through their coiled-coil domains association. *PLoS Genet.* **11**: e1005747.

- Yadav, A., Singh, D., Lingwan, M., Yadukrishnan, P., Masakapalli, S.K., and Datta, S. (2020). Light signaling and UV-B-mediated plant growth regulation. *J. Integr. Plant. Biol.* **62**: 1270–1292.
- Yan, Y., Li, C., Dong, X., Li, H., Zhang, D., Zhou, Y., Jiang, B., Peng, J., Qin, X., Cheng, J., Wang, X., Song, P., Qi, L., Zheng, Y., Li, B., Terzaghi, W., Yang, S., Guo, Y., and Li, J. (2020). MYB30 is a key negative regulator of *Arabidopsis* photomorphogenic development that promotes PIF4 and PIF5 protein accumulation in the light. *Plant Cell* **32**: 2196–2215.
- Yoo, S.D., Cho, Y.H., and Sheen, J. (2007). *Arabidopsis* mesophyll protoplasts: A versatile cell system for transient gene expression analysis. *Nat. Protoc.* **2**: 1565–1572.
- Zhai, H., Xiong, L., Li, H., Lyu, X., Yang, G., Zhao, T., Liu, J., and Liu, B. (2020). Cryptochrome 1 inhibits shoot branching by repressing the self-activated transcription loop of PIF4 in *Arabidopsis*. *Plant Commun.* **1**: 100042.
- Zhang, L.L., Luo, A., Davis, S.J., and Liu, J.X. (2021). Timing to grow: Roles of clock in thermomorphogenesis. *Trends Plant Sci.* **26**: 1248–1257.
- Zhao, X., Jiang, Y., Li, J., Huq, E., Chen, Z.J., Xu, D., and Deng, X.W. (2018). COP1 SUPPRESSOR 4 promotes seedling photomorphogenesis by repressing CCA1 and PIF4 expression in *Arabidopsis*. *Proc. Natl. Acad. Sci. U.S.A.* **115**: 11631–11636.
- Zuo, Z., Liu, H., Liu, B., Liu, X., and Lin, C. (2011). Blue light-dependent interaction of CRY2 with SPA1 regulates COP1 activity and floral initiation in *Arabidopsis*. *Curr. Biol.* **21**: 841–847.
- Zheng, X., Wu, S., Zhai, H., Zhou, P., Song, M., Su, L., Xi, Y., Li, Z., Cai, Y., Meng, F., Yang, L., Wang, H., and Yang, J. (2013). *Arabidopsis* phytochrome B promotes SPA1 nuclear accumulation to repress photomorphogenesis under far-red light. *Plant Cell* **25**: 115–133.
- Zhou, H., Zhu, W., Wang, X., Bian, Y., Jiang, Y., Wang, L., Yin, P., Deng, X.W., and Xu, D. (2022). A missense mutation in WRKY32 converts its function from a positive regulator to a repressor of photomorphogenesis. *New Phytol.* **235**: 111–125.

- Zhu, J.Y., Oh, E., Wang, T., and Wang, Z.Y. (2016). TOC1-PIF4 interaction mediates the circadian gating of thermoresponsive growth in *Arabidopsis*. *Nat. Commun.* **7**: 13692.
- Zhu, W., Zhou, H., Lin, F., Zhao, X., Jiang, Y., Xu, D., and Deng, X.W. (2020). COLD-REGULATED GENE27 integrates signals from light and the circadian clock to promote hypocotyl growth in *Arabidopsis*. *Plant Cell* **32**: 3155–3169.

SUPPORTING INFORMATION

Additional Supporting Information may be found online in the supporting information tab for this article: <http://onlinelibrary.wiley.com/doi/10.1111/jipb.13350/supinfo>

Figure S1. Mutations in *CSU6* partially suppress the dwarf phenotypes of *cop1-6* in long-d conditions

Figure S2. Identification of *csu6-2* T-DNA insertion mutant

Figure S3. The CONSTITUTIVELY PHOTOMORPHOGENIC 1 SUPPRESSOR 6 (*CSU6*) protein levels in each of two independent *CSU6pro:CSU6-GFP csu6* transgenic lines

Figure S4. *CSU6pro-CSU6-GFP* transgene complements the *csu6* mutant phenotypes both in the dark and light

Figure S5. CONSTITUTIVELY PHOTOMORPHOGENIC 1 SUPPRESSOR 6 (*CSU6*) negatively regulates the expression of *PIF4*- and *PIF5*-controlled genes

Table S1. Mapping of RNA sequencing reads to TAIR10 reference genome

Table S2. Analysis of gene expression correlation in biological replicates

Table S3. Differential gene expression analysis in *csu6-2* than Columbia-0 (Col-0) (*csu6-2* > Col)

Table S4. Differential gene expression analysis in *csu6-2* than Columbia-0 (Col-0) (*csu6-2* < Col)

Table S5. List of primers used in this study



Scan using WeChat with your smartphone to view JIPB online



Scan with iPhone or iPad to view JIPB online

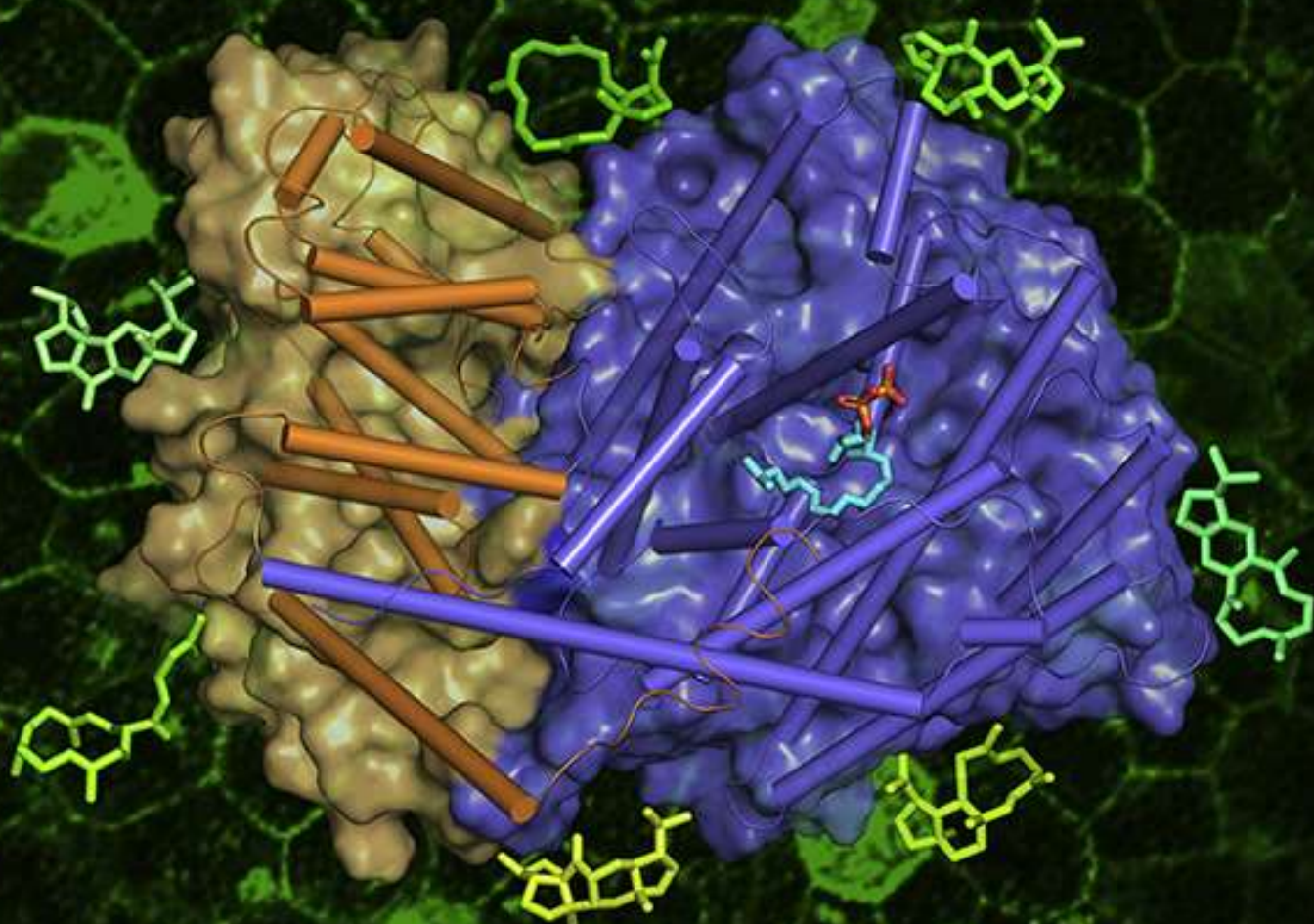
ISSN (ONLINE) 2590-3462

植物通讯

Volume 1 Number 5 September 14, 2020

www.cell.com/plant-communications

Plant Communications



CSPB
IPPE, CAS

CellPress
Partner Journal

A Positive Feedback Loop of BBX11–BBX21–HY5 Promotes Photomorphogenic Development in *Arabidopsis*

Xianhai Zhao^{1,4,5}, Yueqin Heng^{1,5}, Xuncheng Wang², Xing Wang Deng^{1,2,*} and Dongqing Xu^{3,*}

¹Institute of Plant and Food Sciences, Department of Biology, Southern University of Science and Technology, Shenzhen 518055, China

²State Key Laboratory of Protein and Plant Gene Research, Peking-Tsinghua Center for Life Sciences, School of Advanced Agriculture Sciences and School of Life Sciences, Peking University, Beijing 100871, China

³State Key Laboratory of Crop Genetics and Germplasm Enhancement, College of Agriculture, Nanjing Agricultural University, Nanjing 210095, China

⁴Present address: Biology Department, Brookhaven National Laboratory, Upton, NY 11973, USA

⁵These authors contributed equally to this article.

*Correspondence: Xing Wang Deng (deng@pku.edu.cn), Dongqing Xu (dongqingxu@njau.edu.cn)

<https://doi.org/10.1016/j.xplc.2020.100045>

ABSTRACT

Light is the most important environmental factor affecting many aspects of plant development. In this study, we report that B-box protein 11 (BBX11) acts as a positive regulator of red light signaling. BBX11 loss-of-function mutant seedlings display significantly elongated hypocotyls under conditions of both red light and long day, whereas BBX11 overexpression causes markedly shortened hypocotyls under various light states. BBX11 binds to the HY5 promoter to activate its transcription, while both BBX21 and HY5 associate with the promoter of BBX11 to positively regulate its expression. Taken together, our results reveal positive feedback regulation of photomorphogenesis consisting of BBX11, BBX21, and HY5, thus substantiating a transcriptional regulatory mechanism in the response of plants to light during normal development.

Keywords: BBX, HY5, COP1, photomorphogenesis, light signaling

Zhao X., Heng Y., Wang X., Deng X.W., and Xu D. (2020). A Positive Feedback Loop of BBX11–BBX21–HY5 Promotes Photomorphogenic Development in *Arabidopsis*. Plant Comm. 1, 100045.

INTRODUCTION

Plants have evolved a fine-tuned molecular mechanism in their responsiveness to dynamically changing light conditions throughout their life span. Different wavelength-specific light signals are perceived by a variety of photoreceptors in plants. Phytochromes (phyA to phyE) perceive far-red (FR) and red (R) light (Sharrock and Quail, 1989); cryptochromes (CRY1 and CRY2) and phototropins (PHOT1 and PHOT2) sense UV-A and/or blue (B) light (Gallagher et al., 1988; Lin et al., 1995; Guo et al., 1998); and UV-B resistance locus 8 (UVR8) absorbs UV-B light (Rizzini et al., 2011). Proper light exposure converts these photoreceptors into biologically active isoforms that work synergistically with downstream components to initiate diverse molecular events and promote photomorphogenesis (Chen et al., 2014; Ma et al., 2016; Pedmale et al., 2016; Wei et al., 2020; Yadav et al., 2020; Yang and Liu, 2020; Zhai et al., 2020).

Two key regulators of light signaling, constitutively photomorphogenic 1 (COP1) and elongated hypocotyl 5 (HY5), function downstream of a variety of photoreceptors and control approximately one-third of genes in the *Arabidopsis* genome that modulate skoto-

morphogenic or photomorphogenic development (Ma et al., 2003; Lee et al., 2007; Zhang et al., 2011). The E3 ubiquitin ligase COP1 precisely controls the abundance of HY5, a bZIP-type transcription factor (Oyama et al., 1997; Osterlund et al., 2000). In etiolated seedlings, COP1 is enriched in the nucleus, where it directs the polyubiquitination of HY5 and promotes its degradation via the 26S proteasome. Upon light irradiation, the nuclear activity of COP1 is largely inhibited, thus promoting the accumulation of HY5 in de-etiolated seedlings. This eventually leads to changes in HY5-regulated gene expression, and thus, physiological processes in response to light in plants (Oyama et al., 1997; Ang et al., 1998; Osterlund et al., 2000). Thus, the light-regulated COP1–HY5 complex represents a key node in the transition from skotomorphogenesis to photomorphogenesis.

Light can rapidly alter the transcriptome of plants, ultimately promoting seedling development (Ma et al., 2001). A group

Published by the Plant Communications Shanghai Editorial Office in association with Cell Press, an imprint of Elsevier Inc., on behalf of CSPB and IPPE, CAS.

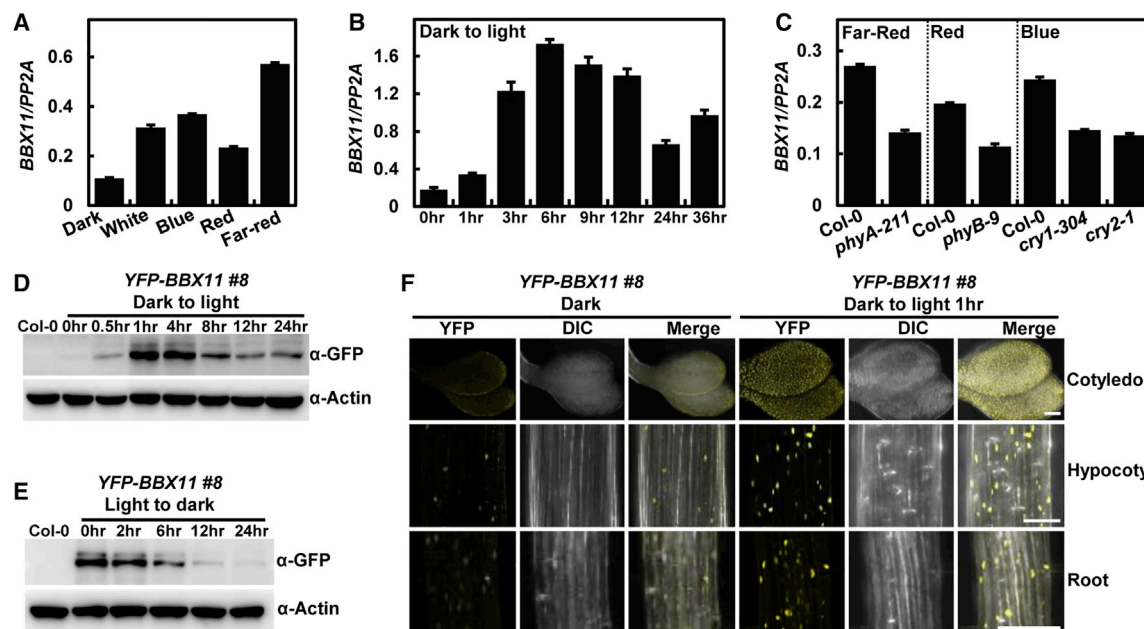


Figure 1. Transcript and Protein Levels of BBX11 Are Positively Regulated by Light.

(A) qRT-PCR analysis of the *BBX11* transcript level in 4-day-old Col-0 seedlings grown in various conditions (darkness; white, blue, red, and far-red light). (B) qRT-PCR analysis of the *BBX11* transcript level during the dark-to-light transition. Four-day-old Col-0 seedlings grown in darkness were transferred to white light for 1–36 h as indicated.

(C) qRT-PCR analysis of the *BBX11* transcript level in different photoreceptor mutants. Col-0 and *phyA-211*, *phyB-9*, *cry1-304*, and *cry2-1* mutants were grown in far-red, red, and blue light for 4 days.

(D and E) YFP-BBX11 protein level in YFP-BBX11 #8 transgenic seedlings during the dark-to-light (D) or light-to-dark (E) transition. Four-day-old dark-grown seedlings were transferred to white light for 0.5–24 h as indicated (D). Five-day-old white-light-grown seedlings were transferred to darkness for 2–24 h as indicated (E). Five-day-old white-light-grown Col-0 seedlings served as the negative control.

(F) Relative YFP fluorescence in 4-day-old YFP-BBX11 #8 transgenic seedlings grown in darkness before and after 1 h of white light exposure. YFP, yellow fluorescent protein channel; DIC, differential interference contrast in the light microscope mode; Merge, merged images of YFP and DIC. Scale bars, 100 μ m.

In (A) to (C), the *BBX11* expression level was normalized to that of *PP2A*. Data are presented as means \pm SD ($n = 3$).

of transcription factors mediates the light-controlled reprogramming of a variety of transcripts. Of these, HY5 is a key component that directly binds to the promoters of light-regulated genes to control their expression (Lee et al., 2007; Zhang et al., 2011; Burko et al., 2020). HY5 and B-box proteins (BBXs) are components of a delicate regulatory network, in which light optimally controls the timely expression of a variety of genes (Gangappa and Botto, 2014; Xu, 2019; Song et al., 2020). BBX21 and BBX22 promote HY5 activity by forming heterodimers (Datta et al., 2007, 2008), whereas BBX24, BBX25, and BBX28 inhibit its transcriptional activity through a similar molecular mechanism (Gangappa et al., 2013; Lin et al., 2018). In addition, BBX21 directly binds to the *T/G-box cis*-element present in the *HY5* promoter through its second B-box domain to activate its expression (Xu et al., 2016, 2018), whereas HY5 positively controls *BBX22* and represses *BBX30* and *BBX31* at the transcriptional level (Chang et al., 2008; Heng et al., 2019a; Yadav et al., 2019). BBX23 and HY5 associate with each other to regulate the expression of downstream targets that promote photomorphogenesis (Zhang et al., 2017). Thus, HY5 and specific BBXs constitute a critical regulatory network, whose function is to gain absolute control over the expression of thousands of genes to ensure normal plant growth and development (Xu, 2019; Song et al., 2020).

In this study, we characterized a previously unidentified positive regulator of R light signaling, BBX11, which contains two tandem conserved B-box domains in the N-terminal region. *BBX11* loss-of-function mutants show elongated hypocotyls under conditions of both R light and long day (LD; 16 h light/8 h dark), whereas *BBX11* overexpression results in shortened hypocotyls under white (W), B, R, and FR light. BBX11 associates with HY5 chromatin regions and promotes its expression, whereas both BBX21 and HY5 bind to the *BBX11* promoter and activate its transcription, suggesting that BBX11, BBX21, and HY5 form a positive feedback loop at the transcriptional level. These results demonstrate that BBX11, BBX21, and HY5 promote photomorphogenesis, and this positive feedback regulation is critical for light-mediated seedling development.

RESULTS

Light Induces BBX11 at Both Transcriptional and Protein Levels

It has been shown that multiple BBX proteins are involved in light-regulated seedling development (Gangappa and Botto, 2014; Xu, 2019; Song et al., 2020). In an effort to identify the previously uncharacterized BBX member(s) acting in light signaling, we examined the transcript levels of a group of BBXs in wild-type *Arabidopsis* (Columbia-0 [Col-0] ecotype) grown under various

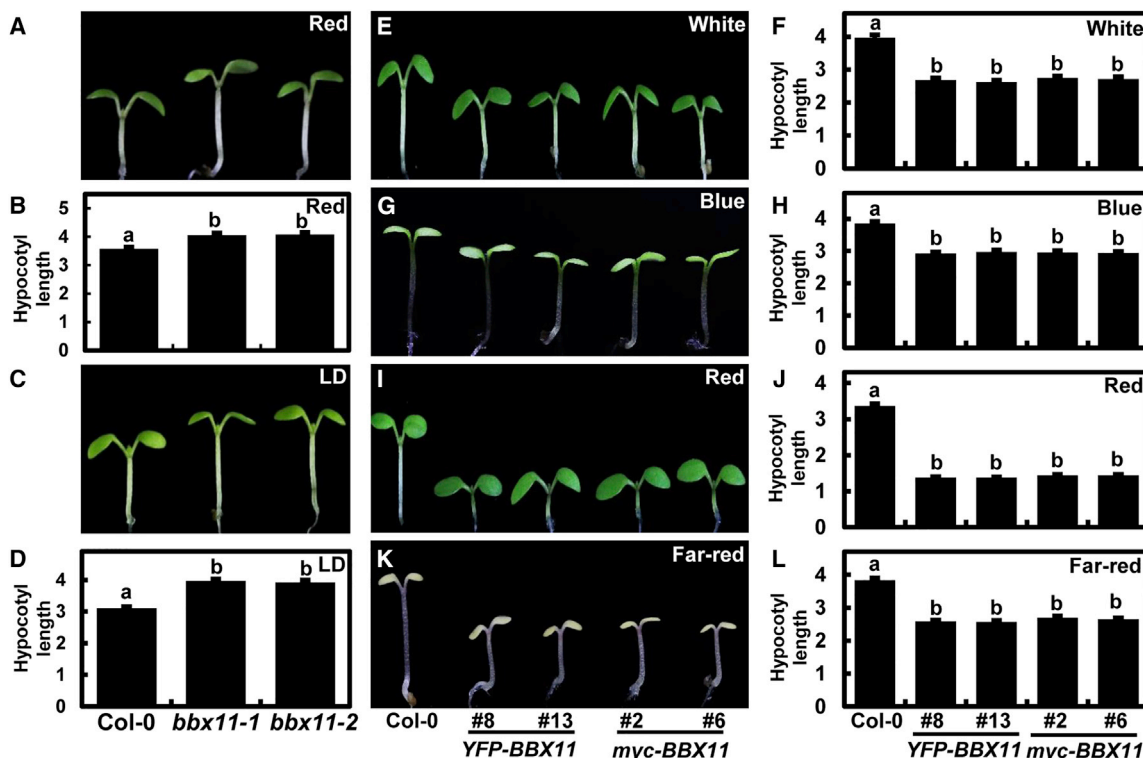


Figure 2. *Bbx11* Mutant Seedlings Grown in Red Light Show Elongated Hypocotyls.

Hypocotyl phenotype and length of 5-day-old Col-0 and two independent *bbx11* single-mutant seedlings grown in red light ($129 \mu\text{mol}/\text{m}^2/\text{s}$) (A and B) and LD conditions (16 h light/8 h dark) (C and D). Hypocotyl phenotype and length of 5-day-old Col-0 and *BBX11* transgenic seedlings grown in white ($14.74 \mu\text{mol}/\text{m}^2/\text{s}$) (E and F), blue ($10.5 \mu\text{mol}/\text{m}^2/\text{s}$) (G and H), red ($129 \mu\text{mol}/\text{m}^2/\text{s}$) (I and J), and far-red ($4.5 \mu\text{mol}/\text{m}^2/\text{s}$) (K and L) light. The unit of hypocotyl length is millimeters. Data are presented as the means \pm SE ($n \geq 60$) of three biological replicates. Letters above the bars indicate significant differences ($P < 0.05$), as determined by one-way ANOVA with Tukey's post hoc analysis.

light conditions (darkness; W, B, R, and FR light). The transcript level of *BBX11* in light-grown Col-0 seedlings was much higher than that in dark-grown seedlings (Figure 1A), indicating that *BBX11* is induced by light, and thus, a candidate for functioning in light signaling. We also found that the expression level of *BBX11* significantly increased when dark-grown seedlings were transferred to W light for various time points as indicated in Figure 1B. These results indicate that light can induce the expression of *BBX11*. As different light signals are perceived by different photoreceptors, we investigated whether phyA, phyB, CRY1, and CRY2 could affect *BBX11* at the transcriptional level. The expression of *BBX11* in FR light-grown *phyA-211*, R light-grown *phyB-9*, and B light-grown *cry1-304* and *cry2-1* mutant seedlings was significantly decreased compared with that in Col-0 seedlings grown in the corresponding wavelength-specific light conditions (Figure 1C), suggesting that photoreceptors phyA, phyB, CRY1, and CRY2 positively regulate *BBX11* expression in response to light, respectively.

To examine whether light can regulate the abundance of *BBX11*, we generated YFP-tagged *BBX11* (YFP-*BBX11*) transgenic plants overexpressing *BBX11* (Supplemental Figure 1) and characterized the amount of YFP-*BBX11* during the transition from dark to light. YFP-*BBX11* accumulated and peaked at 1–4 h after light illumination and then gradually decreased (Figure 1D). In addition, YFP-*BBX11* gradually decreased when light-grown YFP-*BBX11* overexpressing plants were transferred

to dark conditions for various time points (Figure 1E). Consistent with these observations, YFP signals were only slightly detectable in the cotyledons and hypocotyls of dark-grown YFP-*BBX11* seedlings; however, they became significantly evident at 4 h after light illumination (Figure 1F). Taken collectively, these data indicate that *BBX11* degrades in the dark but accumulates in the light.

BBX11 Acts as a Positive Regulator of Red Light Signaling

To characterize the role of *BBX11* in light signaling, we generated two independent *bbx11* loss-of-function mutants, namely *bbx11-1* and *bbx11-2*, using the clustered regulatory interspaced short palindromic repeats (CRISPR)/Cas9 technique (Wang et al., 2015) (Supplemental Figure 2). The *bbx11* mutants showed a phenotype similar to that of Col-0 when grown in the dark and W, B, and FR light (Supplemental Figures 3 and 4), whereas the two independent *bbx11* mutants displayed significantly elongated hypocotyls when grown in R light (Figure 2A and 2B), suggesting that *BBX11* promotes photomorphogenic development in R light. Next, we investigated the expression pattern of *BBX11* under LD conditions. The transcript level of *BBX11* was under diurnal control with peak expression in the morning (zeitgeber time 8) (Supplemental Figure 5), indicating that the *BBX11* mRNA level is regulated by the circadian clock. Consistently, the

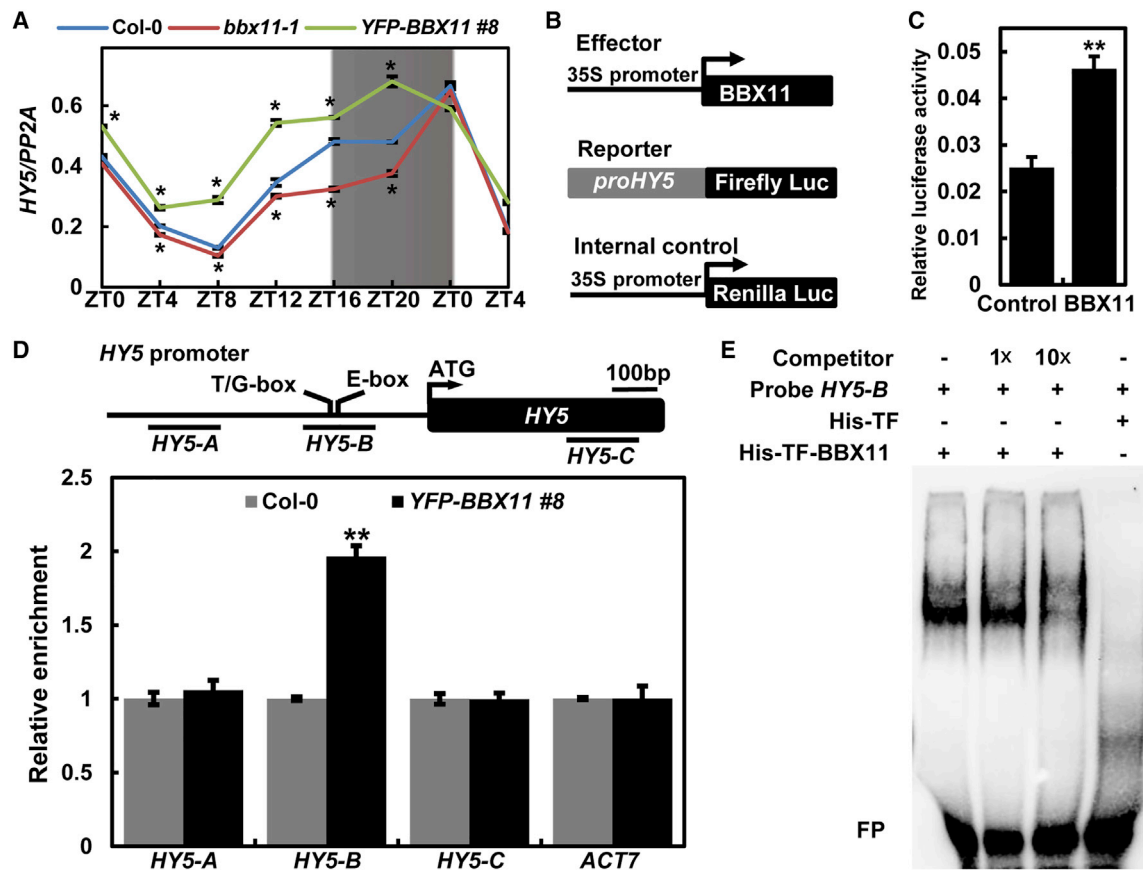


Figure 3. BBX11 Associates with the *HY5* Promoter and Upregulates Its Transcription.

(A) qRT-PCR analysis of the *HY5* transcript level in Col-0, *bbx11-1*, and YFP-BBX11 #8 seedlings grown in LD conditions (16 h light/8 h dark). ZT indicates the zeitgeber time. Data are presented as means \pm SD ($n = 3$). * $P < 0.05$, compared with Col-0, as determined by the two-tailed Student's *t*-test. The *HY5* expression level was normalized to that of *PP2A*.

(B) Schematic representation of various constructs used in transient transfection assays in *Arabidopsis* protoplasts. Arrows after the 35S promoter indicate the transcriptional start site. The *HY5* promoter was fused to firefly luciferase to create the reporter constructs.

(C) Relative luciferase activity of the *proHY5:LUC* reporter construct cotransformed with BBX11 or the control into protoplasts. Data are presented as means \pm SD ($n = 3$). ** $P < 0.01$, as determined by the two-tailed Student's *t*-test.

(D) Results of a representative ChIP-qPCR assay showing that BBX11 associates with the *HY5* promoter *in vivo*. ChIP was performed with an anti-GFP monoclonal antibody. Data are presented as means \pm SD ($n = 3$). ** $P < 0.01$, as determined by the two-tailed Student's *t*-test.

(E) Results of a representative EMSA showing that BBX11 binds to the *HY5* promoter region. “–” and “+” represent the absence or presence, respectively, of the corresponding probe or protein. For probe *HY5-B*, “+” indicates 5 pmol. For His-TF, “+” indicates 5.5 pmol. For His-TF-BBX11, “+” indicates 6.5 pmol. FP indicates the free probe.

hypocotyl length of *bbx11* mutant seedlings was significantly longer than that of Col-0 when grown in LD conditions (Figure 2C and 2D). These results suggest that BBX11 inhibits hypocotyl growth under LD conditions.

To substantiate these observations, we analyzed the phenotypes of YFP-BBX11 and *myc-BBX11* transgenic plants overexpressing BBX11 (Supplemental Figure 1). The two independent etiolated YFP-BBX11 and *myc-BBX11* overexpressing plants exhibited a similar hypocotyl length compared with Col-0; however, they developed a significantly larger apical hook angle compared with Col-0 in the dark (Supplemental Figure 6). All BBX11 transgenic lines showed markedly shortened hypocotyls when grown in various light conditions (W, B, R, and FR) (Figure 2E–2L), suggesting that the overexpression of BBX11 confers hypersensitivity in the response to various wavelength-specific light signals in *Arabidopsis*.

BBX11 Activates the Transcription of *HY5*

We have previously reported that multiple BBX proteins converge on *HY5* to regulate photomorphogenesis (Xu et al., 2016, 2018; Lin et al., 2018; Heng et al., 2019a). Thus, we examined whether BBX11 affects *HY5* at the transcriptional level. As shown in Figure 3A, the *HY5* transcript level was decreased in *bbx11-1* but increased in YFP-BBX11 at various time points under LD conditions, suggesting that BBX11 positively regulates *HY5* expression. Next, we transiently co-expressed 35S:BBX11 and *proHY5:LUC* in *Arabidopsis* protoplasts and found that BBX11 indeed activated the *proHY5:LUC* reporter in plant cells (Figure 3B and 3C), further confirming the activation of *HY5* by BBX11. To explore whether BBX11 binds to the promoter of *HY5*, we employed chromatin immunoprecipitation (ChIP)-qPCR to examine this possibility. As expected, BBX11 specifically bound to the *HY5* promoter region B (–350 to –252 bp), which contains an *E-box* and a *T/G-box* *cis*-element

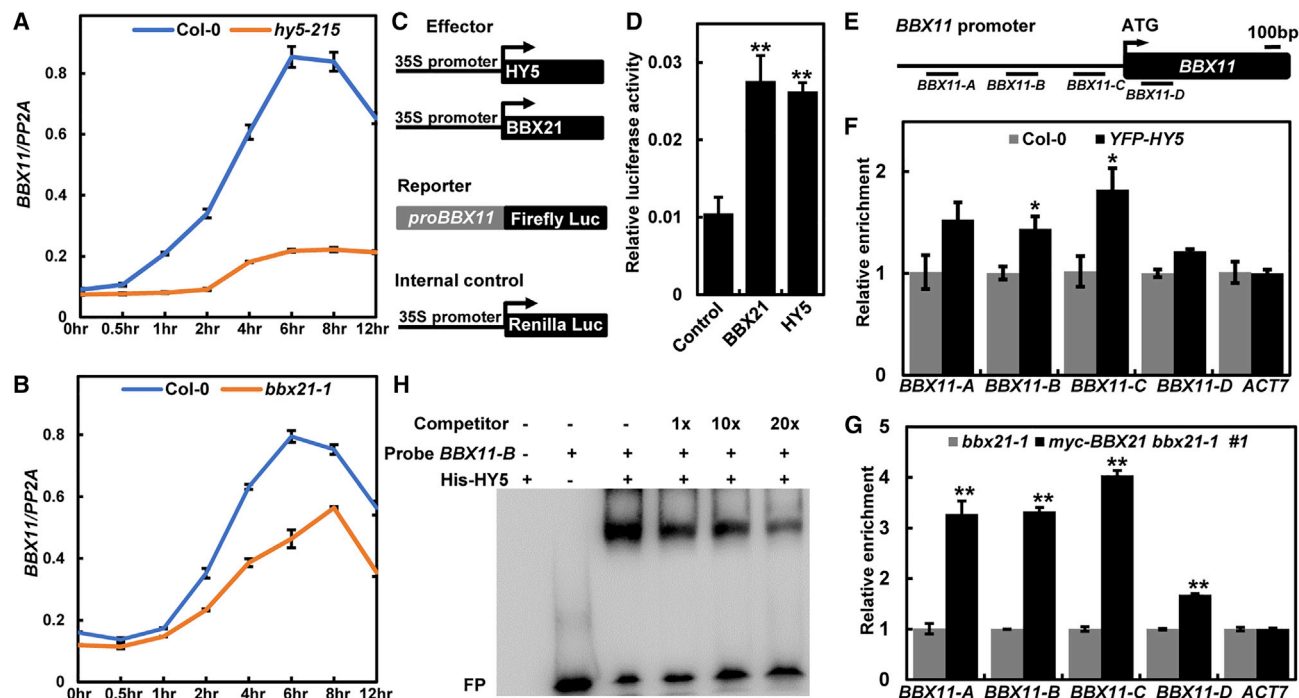


Figure 4. HY5 and BBX21 Associate with the *BBX11* Promoter and Upregulate Its Expression.

(A and B) qRT-PCR analysis of the *BBX11* transcript level during the dark-to-light transition. Four-day-old dark-grown Col-0, *hy5-215* **(A)**, and *bbx21-1* seedlings were exposed to white light (14.74 $\mu\text{mol}/\text{m}^2/\text{s}$) for up to 12 h at the indicated time points. Data are presented as means \pm SD ($n = 3$). The *BBX11* expression level was normalized to that of *PP2A*.

(C) Schematic representation of various constructs used in transient transfection assays in *Arabidopsis* protoplasts. Arrows after the 35S promoter indicate the transcriptional start site. The *BBX11* promoter was fused to firefly luciferase to create the reporter constructs.

(D) Relative luciferase activity of the *proBBX11:LUC* reporter construct cotransformed with *BBX11*, *HY5*, or the control into protoplasts. Data are presented as means \pm SD ($n = 3$). ** $P < 0.01$, as determined by the two-tailed Student's *t*-test.

(E) Schematic representation of the regions examined in ChIP-qPCR assays.

(F and G) Results of a representative ChIP-qPCR assay showing that HY5 and BBX21 associate with the *BBX11* promoter *in vivo*. ChIP was performed with anti-GFP **(F)** and anti-Myc **(G)** monoclonal antibodies. Data are presented as means \pm SD ($n = 3$). * $P < 0.05$ and ** $P < 0.01$, as determined by the two-tailed Student's *t*-test.

(H) Results of a representative EMSA showing that HY5 binds to the *BBX11-B* promoter region. “–” and “+” represent the absence or presence, respectively, of the corresponding probe or protein. For probe *BBX11-B*, “+” indicates 4 pmol. For His-HY5, “+” indicates 10 pmol. FP indicates the free probe.

(Figure 3D). In addition, the results of an *in vitro* electrophoretic mobility shift assay (EMSA) showed that His-Trigger Factor-BBX11 (His-TF-BBX11) could directly bind to the *HY5* promoter region B (–300 to –237 bp). As the amount of competitor (cold probe) increased in the reactions, the His-TF-BBX11 binding of *HY5* promoter clearly decreased. By contrast, the negative control His-TF could not bind to the same *HY5* promoter fragment (Figure 3E). Taken collectively, these results suggest that BBX11 directly binds to the *HY5* promoter to activate its transcription.

BBX21 and HY5 Activate the Transcription of *BBX11*

The results of a genome-wide ChIP-chip study indicate that HY5 can associate with the *BBX11* promoter (Lee et al., 2007). Moreover, BBX21 cannot only enhance the activity of HY5 but also activate its expression (Datta et al., 2007; Xu et al., 2016, 2018). Thus, we examined whether HY5 and BBX21 could regulate the transcription of *BBX11*. The expression of *BBX11* was markedly decreased in *hy5-215* and *bbx21-1* compared with Col-0 during the transition from dark to light at various

time points as indicated in Figure 4A and 4B. In addition, the *BBX11* transcript level was decreased in both *bbx21-1* and *hy5-215* mutants but increased in *myc-BBX21 bbx21-1* and *YFP-HY5 hy5-215* overexpressing plants grown in continuous W light (Supplemental Figure 7). In the transient activation assay, both HY5 and BBX21 activated the *proBBX11:LUC* reporter (Figure 4C and 4D). ChIP-qPCR analysis also showed that both HY5 and BBX21 associated with the *BBX11* promoter *in vivo* (Figure 4E–4G). Next, we performed EMSAs to determine whether HY5 and BBX21 could directly bind to the promoter of *BBX11* *in vitro*. His-HY5 directly bound to the subfragments of the *BBX11* promoter (–628 to –569 bp), which contains a typical *G-box* *cis*-element (CATGCG). As the amount of competitor increased, the affinity of His-HY5 binding to the *BBX11* promoter subfragments decreased (Figure 4H). However, BBX21 could not bind to the same DNA subfragments under the same experimental conditions (Supplemental Figure 8), indicating that BBX21 may indirectly associate with the *BBX11* promoter or that the binding site(s) for BBX21 may reside in other regions within the *BBX11* promoter. Taken collectively, these data suggest that both

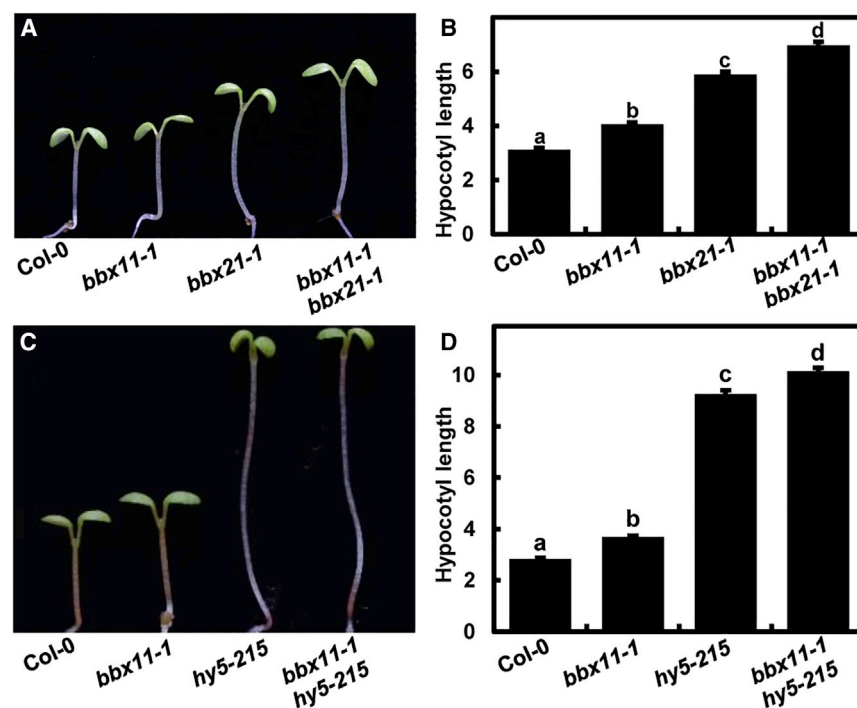


Figure 5. Hypocotyl Phenotype and Length of *bbx11-1*, *bbx21-1*, and *bbx11-1 hy5-215* Seedlings Grown in Red Light.

(A and B) Hypocotyl phenotype and length of 5-day-old Col-0, *bbx11-1*, *bbx21-1*, and *bbx11-1 bbx21-1* seedlings grown in red light ($129 \mu\text{mol}/\text{m}^2/\text{s}$).

(C and D) Hypocotyl phenotype and length of 5-day-old Col-0, *bbx11-1*, *hy5-215*, and *bbx11-1 hy5-215* seedlings grown in red light ($129 \mu\text{mol}/\text{m}^2/\text{s}$). The unit of hypocotyl length is millimeters. Data are presented as means \pm SE ($n \geq 60$) of three biological replicates. Letters above the bars indicate significant differences ($P < 0.05$), as determined by one-way ANOVA with Tukey's post hoc analysis.

BBX21 and HY5 bind to the promoter of *BBX11* to activate its expression.

Genetic Interaction between *BBX11*, *BBX21*, and *HY5*

To genetically examine functional interactions between *BBX11*, *BBX21*, and *HY5*, we generated *bbx11-1 bbx21-1* and *bbx11-1 hy5-215* double mutants by genetic crossing. Consistently, both *bbx11-1* and *bbx21-1* displayed elongated hypocotyls in R light, and the hypocotyl length of *bbx11-1 bbx21-1* was significantly longer than those of Col-0, *bbx11-1*, and *bbx21-1* when grown in R light (Figure 5A and 5B), suggesting that *BBX11* and *BBX21* may function additively in the regulation of R light-mediated hypocotyl growth. Furthermore, the hypocotyl length of *bbx11-1 hy5-215* was significantly longer than that of *hy5-215* when grown in R light (Figure 5C and 5D). Consistently, *myc-BBX11* #2 transgenic seedlings displayed shortened hypocotyls in W, B, R, and FR light, and *hy5-215 myc-BBX11* #2 seedlings were shorter than *hy5-215*, but longer than Col-0 and *myc-BBX11* #2 seedlings when grown in W and B light (Supplemental Figure 9). The hypocotyl length of *hy5-215 myc-BBX11* #2 was indistinguishable from that of *hy5-215* when grown in R and FR light. *Myc-BBX11* accumulated at comparable levels in *myc-BBX11* #2 and *hy5-215 myc-BBX11* #2 transgenic seedlings grown in various light conditions (W, B, R, and FR) (Supplemental Figure 10), suggesting that *HY5* may not affect the abundance of *BBX11* in the light. These data suggest that *BBX11* may act independently of *HY5* in W and B light, while it is likely dependent on functional *HY5* in R and FR light.

COP1 and DET1 Stabilize *BBX11*

As the E3 ubiquitin ligase COP1 promotes the degradation of *BBX21* and *HY5* (Osterlund et al., 2000; Xu et al., 2016), we examined whether COP1 could affect the stability of *BBX11*

and introduced a *cop1-4* mutation by genetic crossing into *YFP-BBX11* transgenic plants. Dark-grown *YFP-BBX11* (line #8) accumulated more *YFP-BBX11* compared with that of *YFP-BBX11 cop1-4* (Figure 6A). Moreover, the *YFP-BBX11* protein level in *YFP-BBX11* #8 was higher than that in *YFP-BBX11 cop1-4* transgenic seedlings after the transition from the dark to light for 0.5 h and 1 h, respectively (Figure 6B). Consistently, *YFP* fluorescence signals were clearly observed in the hypocotyls and roots of dark-grown *YFP-BBX11* seedlings; however, *YFP* signals were barely detectable in *YFP-BBX11 cop1-4* or *YFP-BBX11 det1-1* hypocotyls and root cells (Figure 6C–6E). The *BBX11* transcript level in *YFP-BBX11 cop1-4* was comparable to that in *YFP-BBX11* (Supplemental Figure 11), implying that *COP1* may have little effect on the transcript level of *BBX11*. Taken collectively, these data suggest that both *COP1* and *DET1* stabilize *BBX11* at the protein level in planta.

DISCUSSION

Skotomorphogenesis and photomorphogenesis are two contrasting developmental patterns of a germinated seed under conditions of dark or light. These two developmental processes are tightly controlled by light, which can rapidly change the transcriptome of young seedlings. A group of transcription factors modulates the expression of light-regulated genes in response to light (Jiao et al., 2007; Shi et al., 2018; Xu, 2019; Song et al., 2020). Here, we identify a B-box containing protein, *BBX11*, which promotes photomorphogenesis. *BBX11*, together with *BBX21* and *HY5*, forms a positive feedback loop at the transcriptional level to maintain normal seedling development.

Previous studies have shown that many positive regulators of light signaling are induced by light at transcriptional and/or protein levels (Osterlund et al., 2000; Xu et al., 2016; Heng et al., 2019a, b). The expression of *BBX11* peaks at 3–9 h after light exposure and then gradually decreases (Figure 1B). The induction of *HY5* peaks even earlier than that of *BBX11*, specifically at 1 h after light exposure (Osterlund et al., 2000). The levels of *BBX11*, *BBX21*, and *HY5* are barely detectable in

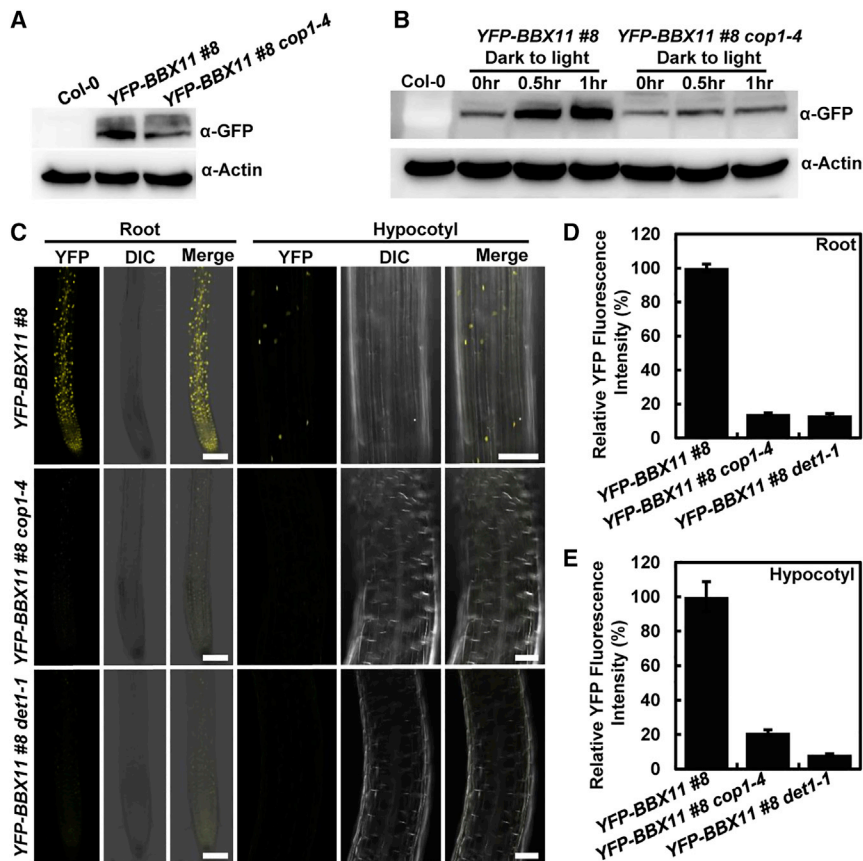


Figure 6. Abundance of BBX11 Is Stabilized by COP1 and DET1.

(A) YFP-BBX11 protein level in YFP-BBX11 #8 and YFP-BBX11 #8 *cop1-4* seedlings grown in darkness for 4 days. Four-day-old dark-grown Col-0 seedlings served as the negative control.

(B) Immunoblot analysis showing the YFP-BBX11 protein level in YFP-BBX11 #8 and YFP-BBX11 #8 *cop1-4* seedlings. Four-day-old dark-grown seedlings were transferred to white light for 0, 0.5, and 1 h as indicated. Four-day-old dark-grown Col-0 seedlings transferred to white light for 1 h served as the negative control.

(C) Relative YFP fluorescence in YFP-BBX11 #8, YFP-BBX11 #8 *cop1-4*, and YFP-BBX11 #8 *det1-1* seedlings grown in darkness for 4 days. Scale bars, 100 μ m.

(D and E) Relative YFP fluorescence in roots **(D)** and hypocotyls **(E)** of YFP-BBX11 #8, YFP-BBX11 #8 *cop1-4*, and YFP-BBX11 #8 *det1-1* seedlings grown in darkness for 4 days. Fluorescence intensity was measured using ImageJ software. Data are presented as means \pm SD ($n \geq 10$).

etiolated seedlings. However, the levels of BBX11 and BBX21 are highest at 1–4 h and 3 h after light treatment, respectively (Figure 1D; Xu et al., 2016), and that of HY5 peaks at 1 h after light exposure (Osterlund et al., 2000). These findings indicate that light can upregulate BBX11, BBX21, and HY5, which is critical for changes in gene expression and photomorphogenesis at an early stage.

A group of transcription factors converges on HY5 or the *HY5* promoter to modulate its activity and/or transcription. BBX21, CAM7, WRKY36, HYH, and HY5 itself can bind to the *HY5* promoter to activate its expression (Abbas et al., 2014; Binkert et al., 2014; Xu et al., 2016; Yang et al., 2018). In addition, BBX21 and BBX22 form heterodimers to enhance its activity (Datta et al., 2007, 2008), whereas BBX24, BBX25, and BBX28 repress its transcriptional activity through a similar molecular mechanism (Gangappa et al., 2013; Lin et al., 2018). This study revealed that BBX11 could associate with the *HY5* promoter and upregulate its transcription (Figure 3), indicating that BBX11 also acts as an activator of *HY5*. Light induces BBX11 and HY5 at both transcriptional and protein levels (Figure 1; Osterlund et al., 2000), implying that light may enhance the binding of BBX11 to the *HY5* promoter, thereby at least partially activating *HY5* transcription. Interestingly, *BBX11* is under the transcriptional control of BBX21 and HY5. Both BBX21 and HY5 bind to the *BBX11* promoter and positively regulate its expression (Figure 4), suggesting that BBX21 and HY5 are positive regulators of *BBX11*. Furthermore, both BBX21 and HY5 can bind to the *T/G-box* present in the

HY5 promoter to activate its expression (Abbas et al., 2014; Binkert et al., 2014; Xu et al., 2016). Thus, these findings suggest that BBX11, BBX21, and HY5 form a positive feedback loop for the precise control of downstream target genes. The phenotypic analysis demonstrates that BBX11, BBX21, and HY5 are positive regulators of light signaling, as *bbx11*, *bbx21*, and *hy5* mutants display elongated hypocotyls, whereas transgenic seedlings overexpressing *BBX11*, *BBX21*, or *HY5* show shortened hypocotyls in light (Figure 2; Oyama et al., 1997; Datta et al., 2007; Xu et al., 2016). These genetic observations indicate that the BBX11–BBX21–HY5-mediated transcriptional cascade promotes photomorphogenic development. These three key proteins accumulate in light, which is consistent with their respective modes of action for promoting photomorphogenesis in response to light. Taken collectively, these facts support the contention that HY5 represents a regulatory node in light-controlled transcriptional reprogramming, and multiple transcription factors regulate the expression of downstream genes at least in part by controlling the *HY5* transcript level. The BBX11–BBX21–HY5 positive feedback loop likely orchestrates a transcriptional cascade that regulates light-mediated development in plants.

BBX11, BBX21, and HY5 degrade in darkness and accumulate in light (Figure 1D–1F; Osterlund et al., 2000; Xu et al., 2016). Both BBX21 and HY5 are ubiquitinated by COP1 and subsequently degraded by the 26S proteasome system in darkness (Osterlund et al., 2000; Xu et al., 2016). However, COP1 stabilized BBX11 rather than promoting its degradation (Figure 6). This fact suggests that a yet unidentified component(s) might promote the degradation of BBX11 in etiolated seedlings. Recent studies have shown that COP1 promotes the degradation of EBF1 and EBF2, which target EIN3 and PIF3 for ubiquitination and degradation, and inhibits

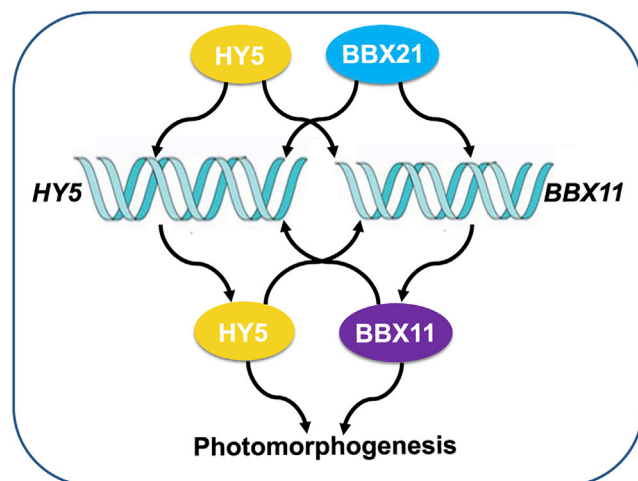


Figure 7. Proposed Working Model of the BBX11-BBX21-HY5 Positive Feedback Loop in Light Signaling.

Light promotes the accumulation of BBX11, BBX21, and HY5, which bind to the promoter of *HY5* and activate its expression. BBX21 and HY5 associate with the promoter of *BBX11* and upregulate its expression. Consequently, the BBX11-BBX21-HY5 feedback loop controls the expression of a variety of genes to promote photomorphogenic development in plants.

BIN2-mediated PIF3 phosphorylation and degradation, thereby resulting in the stabilization of EIN3 and PIF3 (Shi et al., 2016; Dong et al., 2017; Ling et al., 2017). It appears that COP1 likely promotes the degradation of a yet unknown component(s) targeting BBX11 for destabilization. Interestingly, two COP1 and two SPAs can form a stable core E3 ubiquitin ligase complex and work synergistically to control the stability of substrates in etiolated *Arabidopsis* seedlings (Zhu et al., 2008; Ordoñez-Herrera et al., 2015). Therefore, COP1 and SPAs may have similar effects on the accumulation of BBX11.

Based on previous studies and our current study, three transcription factors, BBX11, BBX21, and HY5, associate with the *HY5* promoter to activate its transcription. BBX21 and HY5 bind to the *BBX11* promoter to upregulate its expression (Figure 7). Thus, this positive feedback loop serves to orchestrate light-mediated transcriptional cascades to precisely control photomorphogenic development in plants.

METHODS

Plant Materials and Growth Conditions

Hy5-215 (Oyama et al., 1997), *phyA-211* (Reed et al., 1994), *phyB-9* (Reed et al., 1994), *bbx21-1* (Datta et al., 2007), *cry1-304* (Mockler et al., 1999), *cry2-1* (Mockler et al., 1999), *cop1-4* (McNellis et al., 1994), and *det1-1* (Chory and Peto, 1990) mutants and *myc-BBX21 bbx21-1* (Xu et al., 2016) transgenic lines were derived from the *Arabidopsis thaliana* Col-0 ecotype. *Bbx11* mutants and transgenic lines overexpressing *BBX11* were generated in this study. Multiple mutants were generated by genetic crossing and genotyped with PCR or antibiotic screening methods. Seeds were surface sterilized and sown on 1× Murashige and Skoog (MS) medium containing 1% (w/v) sucrose and 0.8% (w/v) agar. Seeds were stratified in darkness for 3 days at 4°C and then transferred to white light for 8–12 h at 22°C to induce uniform germination. To prepare seeds for phenotypic analysis, they were transferred to W light (14.74 μmol/m²/s), B light

BBX11-BBX21-HY5 Promotes Photomorphogenesis

(10.5 μmol/m²/s), R light (129 μmol/m²/s), FR light (4.5 μmol/m²/s), or LD conditions (16 h light/8 h dark, W light 14.74 μmol/m²/s) at 22°C.

Construction of Plasmids

The full-length *BBX11* coding sequence (CDS) was cloned into the *pDONR223* vector using the Gateway BP Clonase Enzyme Mix (Invitrogen). CDSs were introduced into the *pEarly Gate-104* or *pEarly Gate-203* plant binary vector using the Gateway LR Clonase Enzyme Mix (Invitrogen) to generate 35S::YFP-*BBX11* and 35S::myc-*BBX11* constructs, respectively (Earley et al., 2006). To generate constructs for transient luciferase transfection assays, *BBX11*, *HY5*, and *BBX21* CDSs were cloned into the *EcoRI/XhoI* sites of the *pGreenII 62-SK* vector (Hellens et al., 2005). The 2540-bp *BBX11* promoter upstream of ATG was cloned into the *HindIII/NcoI* sites of the *pGreen II 0800-LUC* vector. The generation of *pGreen II 0800-HY5pro-LUC* (Lin et al., 2018), *pET28a-HY5* (Heng et al., 2019a), and *pCold-TF-BBX21* (Xu et al., 2016) has been previously described. To produce the construct for prokaryotic expression, the *BBX11* CDS was cloned into the *EcoRI/HindIII* sites of the *pCold-TF* vector (Takara). Primers used for plasmid construction are listed in Supplemental Table 1.

Generation of *bbx11* Mutants Using CRISPR/Cas9

Bbx11 mutants were generated using the CRISPR/Cas9 system described by Wang et al. (2015). In brief, CRISPR-GE (<http://skl.scau.edu.cn/>) was used to identify 23-bp target sites (5'-N₂₀NGG-3') (Xie et al., 2017). Primers were synthesized, and the products were subcloned into the *pHEE401E* vector. After transforming into the *Agrobacterium tumefaciens* GV3101 strain by the freeze-thaw method, binary constructs were introduced into Col-0 using the floral-dip method. T₁ seeds were sown on MS plates containing 50 mg/l hygromycin, and the resistant seedlings (T₁) were transferred to soil. Genomic DNA was extracted and used to amplify the *BBX11* gene. PCR products were sequenced to identify mutations. Homozygous mutants were crossed with Col-0 to remove the T-DNA insertion. Seedlings carrying mutations in *BBX11* and without hygromycin resistance were selected for further studies.

Transgenic Plants

pEarly Gate-35S::YFP-BBX11 and *pEarly Gate-35S::myc-BBX11* constructs were transformed into the *A. tumefaciens* GV3101 strain by the freeze-thaw method. The floral-dip method was used to generate transgenic plants (Clough and Bent, 1998). Transgenic plants were selected on MS medium containing 20 mg/l BASTA. Homozygous lines were used for genetic and biochemical studies.

Measurement of Hypocotyl Length

Seeds were surface sterilized, sown on MS plates, stratified in darkness for 3 days at 4°C and then transferred to white light for 8 h to induce uniform germination. Thereafter, seeds were exposed to darkness or different light conditions and cultivated at 22°C. Seedling hypocotyls were scanned with a scanner, and the hypocotyl length was measured using ImageJ software (Schneider et al., 2012).

Total RNA Isolation and Quantitative RT-PCR

Total RNA was isolated from 5-day-old *Arabidopsis* seedlings using the RNeasy Plant Mini Kit (Qiagen). cDNA was synthesized using the 5× All-In-One RT MasterMix (Applied Biological Materials) according to the manufacturer's instructions. cDNA templates and primer pairs were mixed with Hieff qPCR SYBR Green Master Mix (Yeasen), and quantitative PCR was performed in a StepOnePlus Real-Time PCR System (Applied Biosystems). Each experiment was performed at least three independent times with similar results, and each sample was assayed three times within each experiment. The expression level of each target gene was normalized to that of a housekeeping gene, *PP2A*. Primers used for qRT-PCR are listed in Supplemental Table 1.

Immunoblot Analysis

Arabidopsis seedlings were homogenized in protein extraction buffer containing 100 mM NaH₂PO₄, 10 mM Tris–HCl (pH 8.0), 200 mM NaCl, 8 M urea, 1 mM phenylmethylsulfonyl fluoride, and 1× complete protease inhibitor cocktail (Roche). Primary antibodies used in this study were anti-GFP (Abmart, cat. #M20004M), anti-Myc (Sigma-Aldrich, cat. #M4439), and anti-Actin (Sigma-Aldrich, cat. #A0480).

Electrophoretic Mobility Shift Assays

Probe oligos used for EMSA are presented in [Supplemental Table 1](#). Oligos were diluted and mixed with EZ-Link Psoralen-PEG3-Biotin (Thermo Scientific). After 30 min of UV exposure, biotin-labeled probes were precipitated with potassium acetate (pH 5.2) in ethanol, air-dried, and dissolved in water, and the concentration was determined. For prokaryotic expression, the *pCold-TF-BBX11* construct was transformed into the *Escherichia coli* BL21 (DE3) strain, and His-TF-BBX11 protein was purified according to the manufacturer's instructions. The Light Shift Chemiluminescent EMSA Kit (Thermo Scientific) was used. In brief, purified proteins were incubated with biotin-labeled probes in 20-μl reaction mixtures containing 10 mM Tris–HCl (pH 7.5), 0.05% (v/v) Nonidet P-40, 10 mM MgCl₂, 5% (v/v) glycerol, and 0.1 μg/ml poly(dI-dC) at room temperature for 20 min. Thereafter, 6% (w/v) native polyacrylamide gels were used to separate the labeled probes, which were then electroblotted onto Hybond N⁺ (Millipore) nylon membranes in 0.5× Tris–Borate–EDTA buffer for 40 min. Labeled probes were detected according to the manufacturer's instructions.

Chromatin Immunoprecipitation Assays

ChIP assays were performed as previously described (Xu et al., 2016). In brief, 7-day-old seedlings grown in LD conditions (16 h light/8 h dark) were collected and treated with formaldehyde to crosslink protein–DNA complexes. After washing three times, the excess liquid was removed. Samples were frozen in liquid nitrogen and stored at –80°C or processed further. In brief, samples were ground to a fine powder with a pestle and mortar in liquid nitrogen. After isolation and sonication of chromatin, samples were centrifuged at 16 000 *g* for 5 min, and the supernatants were collected. Anti-GFP and anti-Myc antibodies were used for immunoprecipitation. The serum served as the control. Ten percent of each supernatant served as the input. Primers used for real-time qPCR are listed in [Supplemental Table 1](#).

Transient Luciferase Expression Assays

Arabidopsis plants grown in LD conditions (16 h light/8 h dark) were used for the isolation of protoplasts. Leaves were minced and digested as described by Yoo et al. (2007). Reporter and effector constructs were transformed into protoplasts. After 20 h of incubation in darkness, the protoplasts were pelleted. Firefly luciferase (LUC) and Renilla luciferase (Ren) were assayed using the Dual-Luciferase Reporter Assay System (Promega). The Ren gene driven by the cauliflower mosaic virus 35S promoter was used as the control. The relative activity was expressed as a ratio of LUC/Ren.

Statistical Analysis

Statistical analyses were performed using Microsoft Excel, GraphPad Prism 5.0, or an online program (http://astatsa.com/OneWay_Anova_with_TukeyHSD/).

ACCESSION NUMBERS

Sequence data from this article can be found in GenBank and EMBL libraries under the following accession numbers: BBX11 (TAIR: AT2G47890), BBX21 (TAIR: AT1G75540), HY5 (TAIR: AT5G11260), and COP1 (TAIR: AT2G32950).

SUPPLEMENTAL INFORMATION

Supplemental Information is available at *Plant Communications Online*.

FUNDING

This work was financially supported by the National Key R&D Program of China (2017YFA0503800), National Natural Science Foundation of China (31970258, 31330048, 31621001, and 31900210), Peking-Tsinghua Center for Life Sciences (to X.W.D.), Southern University of Science and Technology (to X.W.D.), Nanjing Agricultural University (to D.X.), Nanjing Science and Technology Innovation Program for Overseas Students (to D.X.), and Jiangsu Collaborative Innovation Center for Modern Crop Production.

AUTHOR CONTRIBUTIONS

X.Z., Y.H., X.W., and D.X. conducted the experiments. D.X. and X.W.D. designed the experiments, analyzed the data, and wrote the article.

ACKNOWLEDGMENTS

We thank all laboratory members for their valuable comments. The authors declare no conflicts of interest.

Received: November 18, 2019

Revised: January 2, 2020

Accepted: April 10, 2020

Published: April 16, 2020

REFERENCES

- Ang, L.H., Chattopadhyay, S., Wei, N., Oyama, T., Okada, K., Batschauer, A., and Deng, X.W. (1998). Molecular interaction between COP1 and HY5 defines a regulatory switch for light control of *Arabidopsis* development. *Mol. Cell* 1:213–222.
- Abbas, N., Maurya, J.P., Senapati, D., Gangappa, S.N., and Chattopadhyay, S. (2014). *Arabidopsis* CAM7 and HY5 physically interact and directly bind to the *HY5* promoter to regulate its expression and thereby promote photomorphogenesis. *Plant Cell* 26:1036–1052.
- Binkert, M., Kozma-Bognar, L., Terecskei, K., De Veylder, L., Nagy, F., and Ulm, R. (2014). UV-B-responsive association of the *Arabidopsis* bZIP transcription factor ELONGATED HYPOCOTYL5 with target genes, including its own promoter. *Plant Cell* 26:4200–4213.
- Burko, Y., Seluzicki, A., Zander, M., Pedmale, U., Ecker, J.R., and Chory, J. (2020). Chimeric activators and repressors define HY5 activity and reveal a light-regulated feedback mechanism. *Plant Cell* <https://doi.org/10.1105/tpc.19.00772>.
- Chang, C.S., Li, Y.H., Chen, L.T., Chen, W.C., Hsieh, W.P., Shin, J., Jane, W.N., Chou, S.J., Choi, G., Hu, J.M., et al. (2008). LZ1, a HY5-regulated transcriptional factor, functions in *Arabidopsis* de-etiolation. *Plant J.* 54:205–219.
- Chen, F., Li, B., Li, G., Charron, J.B., Dai, M., Shi, X., and Deng, X.W. (2014). *Arabidopsis* Phytochrome A directly targets numerous promoters for individualized modulation of genes in a wide range of pathways. *Plant Cell* 26:1949–1966.
- Chory, J., and Peto, C.A. (1990). Mutations in the DET1 gene affect cell-type-specific expression of light-regulated genes and chloroplast development in *Arabidopsis*. *Proc. Natl. Acad. Sci. U S A* 87:8776–8780.
- Clough, S.J., and Bent, A.F. (1998). Floral dip: a simplified method for *Agrobacterium*-mediated transformation of *Arabidopsis thaliana*. *Plant J.* 16:735–743.
- Datta, S., Hettiarachchi, C., Johansson, H., and Holm, M. (2007). SALT TOLERANCE HOMOLOG2, a B-box protein in *Arabidopsis* that activates transcription and positively regulates light-mediated development. *Plant Cell* 19:3242–3255.
- Datta, S., Johansson, H., Hettiarachchi, C., Irigoyen, M.L., Desai, M., Rubio, V., and Holm, M. (2008). LZ1/SALT TOLERANCE HOMOLOG3, an *Arabidopsis* B-box protein involved in light-dependent

Plant Communications

- development and gene expression, undergoes COP1-mediated ubiquitination. *Plant Cell* **20**:2324–2338.
- Dong, J., Ni, W., Yu, R., Deng, X.W., Chen, H., and Wei, N. (2017). Light-dependent degradation of PIF3 by SCFEBF1/2 promotes a photomorphogenic response in *Arabidopsis*. *Curr. Biol.* **27**:2420–2430.
- Earley, K.W., Haag, J.R., Pontes, O., Opper, K., Juehne, T., Song, K., and Pikaard, C.S. (2006). Gateway-compatible vectors for plant functional genomics and proteomics. *Plant J.* **45**:616–629.
- Gallagher, S., Short, T.W., Ray, P.M., Pratt, L.H., and Briggs, W.R. (1988). Light-mediated changes in two proteins found associated with plasma membrane fractions from pea stem sections. *Proc. Natl. Acad. Sci. U S A* **85**:8003–8007.
- Gangappa, S.N., and Botto, J.F. (2014). The BBX family of plant transcription factors. *Trends Plant Sci.* **19**:460–470.
- Gangappa, S.N., Crocco, C.D., Johansson, H., Datta, S., Hettiarachchi, C., Holm, M., and Botto, J.F. (2013). The *Arabidopsis* B-BOX protein BBX25 interacts with HY5, negatively regulating BBX22 expression to suppress seedling photomorphogenesis. *Plant Cell* **25**:1243–1257.
- Guo, H., Yang, H., Mockler, T., and Lin, C. (1998). Regulation of flowering time by *Arabidopsis* photoreceptors. *Science* **279**:1360–1363.
- Hellens, R.P., Allan, A.C., Friel, E.N., Bolitho, K., Grafton, K., Templeton, M.D., Karunairetnam, S., Gleave, A.P., and Laing, W.A. (2005). Transient expression vectors for functional genomics, quantification of promoter activity and RNA silencing in plants. *Plant Methods* **1**:13.
- Heng, Y., Lin, F., Jiang, Y., Ding, M., Yan, T., Lan, H., Zhou, H., Zhao, X., Xu, D., and Deng, X.W. (2019a). B-Box containing proteins BBX30 and BBX31, acting downstream of HY5, negatively regulate photomorphogenesis in *Arabidopsis*. *Plant Physiol.* **180**:497–508.
- Heng, Y., Jiang, Y., Zhao, X., Zhou, H., Wang, X., Deng, X.W., and Xu, D. (2019b). BBX4, a phyB-interacting and modulated regulator, directly interacts with PIF3 to fine tune red light-mediated photomorphogenesis. *Proc. Natl. Acad. Sci. U S A* **116**:26049–26056.
- Jiao, Y., Lau, O.S., and Deng, X.W. (2007). Light-regulated transcriptional networks in higher plants. *Nat. Rev. Genet.* **8**:217–230.
- Lee, J., He, K., Stolz, V., Lee, H., Figueroa, P., Gao, Y., Tongprasit, W., Zhao, H., Lee, I., and Deng, X.W. (2007). Analysis of transcription factor HY5 genomic binding sites revealed its hierarchical role in light regulation of development. *Plant Cell* **19**:731–749.
- Lin, C., Robertson, D.E., Ahmad, M., Raibekas, A.A., Jorns, M.S., Dutton, P.L., and Cashmore, A.R. (1995). Association of flavin adenine dinucleotide with the *Arabidopsis* blue light receptor CRY1. *Science* **269**:968–970.
- Lin, F., Jiang, Y., Li, J., Yan, T., Fan, L., Liang, J., Chen, Z.J., Xu, D., and Deng, X.W. (2018). B-BOX DOMAIN PROTEIN28 negatively regulates photomorphogenesis by repressing the activity of transcription factor HY5 and undergoes COP1-mediated degradation. *Plant Cell* **30**:2006–2019.
- Ling, J.J., Li, J., Zhu, D., and Deng, X.W. (2017). Noncanonical role of *Arabidopsis* COP1/SPA complex in repressing BIN2-mediated PIF3 phosphorylation and degradation in darkness. *Proc. Natl. Acad. Sci. U S A* **114**:3539–3544.
- Ma, D., Li, X., Guo, Y., Chu, J., Fang, S., Yan, C., Noel, J.P., and Liu, H. (2016). Cryptochrome 1 interacts with PIF4 to regulate high temperature-mediated hypocotyl elongation in response to blue light. *Proc. Natl. Acad. Sci. U S A* **113**:224–229.
- Ma, L., Li, J., Qu, L., Hager, J., Chen, Z., Zhao, H., and Deng, X.W. (2001). Light control of *Arabidopsis* development entails coordinated regulation of genome expression and cellular pathways. *Plant Cell* **13**:2589–2607.
- ## BBX11–BBX21–HY5 Promotes Photomorphogenesis
- Ma, L., Zhao, H., and Deng, X.W. (2003). Analysis of the mutational effects of the COP/DET/FUS loci on genome expression profiles reveals their overlapping yet not identical roles in regulating *Arabidopsis* seedling development. *Development* **130**:969–981.
- McNellis, T.W., von Arnim, A.G., Araki, T., Komeda, Y., Misera, S., and Deng, X.W. (1994). Genetic and molecular analysis of an allelic series of *cop1* mutants suggests functional roles for the multiple protein domains. *Plant Cell* **6**:487–500.
- Mockler, T.C., Guo, H., Yang, H., Duong, H., and Lin, C. (1999). Antagonistic actions of *Arabidopsis* cryptochromes and phytochrome B in the regulation of floral induction. *Development* **126**:2073–2082.
- Osterlund, M.T., Hardtke, C.S., Wei, N., and Deng, X.W. (2000). Targeted destabilization of HY5 during light-regulated development of *Arabidopsis*. *Nature* **405**:462–466.
- Ordoñez-Herrera, N., Fackendahl, P., Yu, X., Schaefer, S., Koncz, C., and Hoecker, U. (2015). A *cop1 spa* mutant deficient in COP1 and SPA proteins reveals partial co-action of COP1 and SPA during *Arabidopsis* post-embryonic development and photomorphogenesis. *Mol. Plant* **8**:479–481.
- Oyama, T., Shimura, Y., and Okada, K. (1997). The *Arabidopsis* HY5 gene encodes a bZIP protein that regulates stimulus-induced development of root and hypocotyl. *Genes Dev.* **11**:2983–2995.
- Pedmale, U.V., Huang, S.C., Zander, M., Cole, B.J., Hetzel, J., Ljung, K., Reis, P.A.B., Sridevi, P., Nito, K., Nery, J.R., et al. (2016). Cryptochromes interact directly with PIFs to control plant growth in limiting blue light. *Cell* **164**:233–245.
- Rizzini, L., Favory, J.J., Cloix, C., Faggionato, D., O'Hara, A., Kaiserli, E., Baumeister, R., Schäfer, E., Nagy, F., Jenkins, G.I., et al. (2011). Perception of UV-B by the *Arabidopsis* UVR8 protein. *Science* **332**:103–106.
- Reed, J.W., Nagatani, A., Elich, T.D., Fagan, M., and Chory, J. (1994). Phytochrome-A and Phytochrome-B have overlapping but distinct functions in *Arabidopsis* development. *Plant Physiol.* **104**:1139–1149.
- Sharrock, R.A., and Quail, P.H. (1989). Novel phytochrome sequences in *Arabidopsis thaliana*: structure, evolution, and differential expression of a plant regulatory photoreceptor family. *Genes Dev.* **3**:1745–1757.
- Schneider, C.A., Rasband, W.S., and Eliceiri, K.W. (2012). NIH Image to ImageJ: 25 years of image analysis. *Nat. Methods* **9**:671–675.
- Shi, H., Liu, R., Xue, C., Shen, X., Wei, N., Deng, X.W., and Zhong, S. (2016). Seedlings Transduce the depth and mechanical pressure of covering soil using COP1 and ethylene to regulate EBF1/EBF2 for soil emergence. *Curr. Biol.* **26**:139–149.
- Shi, H., Lyu, M., Luo, Y., Liu, S., Li, Y., He, H., Wei, N., Deng, X.W., and Zhong, S. (2018). Genome-wide regulation of light-controlled seedling morphogenesis by three families of transcription factors. *Proc. Natl. Acad. Sci. U S A* **115**:6482–6487.
- Song, Z., Bian, Y., Liu, J., Sun, Y., and Xu, D. (2020). B-box proteins: pivotal players in light-mediated development in plants. *J. Integr. Plant Biol.* <https://doi.org/10.1111/jipb.12935>.
- Wang, Z.P., Xing, H.L., Dong, L., Zhang, H.Y., Han, C.Y., Wang, X.C., and Chen, Q.J. (2015). Egg cell-specific promoter-controlled CRISPR/Cas9 efficiently generates homozygous mutants for multiple target genes in *Arabidopsis* in a single generation. *Genome Biol.* **16**:144.
- Wei, H., Kong, D., Yang, J., and Wang, H. (2020). Light regulation of stomatal development and patterning: shifting the paradigm from *Arabidopsis* to grasses. *Plant Commun.* **1**:100030.
- Xie, X., Ma, X., Zhu, Q., Zeng, D., Li, G., and Liu, Y.G. (2017). CRISPR-GE: a convenient software toolkit for CRISPR-based genome editing. *Mol. Plant* **10**:1246–1249.

- Xu, D.** (2019). COP1 and BBXs-HY5-mediated light signal transduction in plants. *New Phytol.* <https://doi.org/10.1111/nph>.
- Xu, D., Jiang, Y., Li, J., Lin, F., Holm, M., and Deng, X.W.** (2018). B-box domain protein BBX21 promotes photomorphogenesis. *Plant Physiol.* **176**:2365–2375.
- Xu, D., Jiang, Y., Li, J., Lin, F., Holm, M., and Deng, X.W.** (2016). BBX21, an *Arabidopsis* B-box protein, directly activates HY5 and is targeted by COP1 for 26S proteasome-mediated degradation. *Proc. Natl. Acad. Sci. U S A* **113**:7655–7660.
- Yadav, A., Bakshi, S., Yadukrishnan, P., Lingwan, M., Dolde, U., Wenkel, S., Masakapalli, S.K., and Datta, S.** (2019). The B-Box-containing microprotein miP1a/BBX31 regulates photomorphogenesis and UV-B protection. *Plant Physiol.* **179**:1876–1892.
- Yadav, A., Singh, D., Lingwan, M., Yadukrishnan, P., Masakapalli, S.K., and Datta, S.** (2020). Light signaling and UV-B mediated plant growth regulation. *J. Integr. Plant Biol.* <https://doi.org/10.1111/jipb.12932>.
- Yang, Y., and Liu, H.** (2020). Coordinated shoot and root responses to light signaling in *Arabidopsis*. *Plant Commun.* **1**:100026.
- Yang, Y., Liang, T., Zhang, L., Shao, K., Gu, X., Shang, R., Shi, N., Li, X., Zhang, P., and Liu, H.** (2018). UVR8 interacts with WRKY36 to regulate HY5 transcription and hypocotyl elongation in *Arabidopsis*. *Nat. Plants* **4**:98–107.
- Yoo, S.D., Cho, Y.H., and Sheen, J.** (2007). *Arabidopsis* mesophyll protoplasts: a versatile cell system for transient gene expression analysis. *Nat. Protoc.* **2**:1565–1572.
- Zhai, H., Xiong, L., Li, H., Lyu, X., Yang, G., Zhao, T., Liu, J., and Liu, B.** (2020). Cryptochrome 1 inhibits shoot branching by repressing the self-activated transcription loop of PIF4 in *Arabidopsis*. *Plant Commun.* <https://doi.org/10.1016/j.xplc.2020.100042>.
- Zhang, H., He, H., Wang, X., Wang, X., Yang, X., Li, L., and Deng, X.W.** (2011). Genome-wide mapping of the HY5-mediated gene networks in *Arabidopsis* that involve both transcriptional and post-transcriptional regulation. *Plant J.* **65**:346–358.
- Zhang, X., Shang, F., Huai, J., Xu, G., Tang, W., Jing, Y., and Lin, R.** (2017). A PIF1/PIF3-HY5-BBX23 transcription factor cascade affects photomorphogenesis. *Plant Physiol.* **174**:2487–2500.
- Zhu, D., Maier, A., Lee, J.H., Laubinger, S., Saijo, Y., Wang, H., Qu, L.J., Hoecker, U., and Deng, X.W.** (2008). Biochemical characterization of *Arabidopsis* complexes containing CONSTITUTIVELY PHOTOMORPHOGENIC1 and SUPPRESSOR OF PHYA proteins in light control of plant development. *Plant Cell* **20**:2307–2323.

荣誉证书

第九届全国大学生生命科学竞赛

(科学探究类) 广东省赛区

三等奖

项目名称：水稻茉莉酸抑制因子 JAZs 响应高温调控花时的分子机理与应用研究

学校名称：华南农业大学

参赛者：谢晓峰、刘苑菲、谭诗雅、郭若瑜、李文轩

指导老师：沈荣鑫、衡月芹

全国大学生生命科学竞赛委员会
广东省大学生生命科学竞赛委员会
2024年7月14日